

## Combustion Chemistry of Alkenes and Alkadienes

Chong-Wen Zhou<sup>\*1,2</sup>, Aamir Farooq<sup>3</sup>, Lijun Yang<sup>4</sup>, Alexander M. Mebel<sup>5</sup>

<sup>1</sup>School of Energy and Power Engineering, Beihang University, Beijing, China

<sup>2</sup>Combustion Chemistry Centre, School of Chemistry, Ryan Institute, MaREI, National University of Ireland, Galway, Galway H91TK33, Ireland

<sup>3</sup>Clean Combustion Research Center, Physical Sciences and Engineering Division, King Abdullah University of Science and Technology (KAUST), Thuwal 23955-6900, Saudi Arabia

<sup>4</sup>School of Astronautics, Beihang University, Beijing 100191, PR China

<sup>5</sup>Department of Chemistry and Biochemistry, Florida International University, 11200 SW 8<sup>th</sup> Street, Miami, Florida 33199, United States

### Abstract

Alkenes formed during refining of crude oil to gasoline by cracking the heavier fractions are present in transportation fuels, including gasoline, in significant amounts, up to as much as 15–20% in gasoline. Moreover, alkenes are also the major intermediate products for the oxidation of alkanes, which play a significant role in autoignition chemistry. This review has assessed the recent progress in gas-phase detailed kinetic model development for species with C=C double bond, mostly C2-C10 alkenes and 1,3-butadiene. This compiled knowledge on alkene combustion chemistry enabled a better understanding of influence of the number and the position of the C=C double bond on the chemical kinetics and hence combustion behavior of alkenes in engines. At first, the article gives an extensive overview of fundamental combustion experiments by considering studies of C2-C10 alkenes and 1,3-butadiene in shock tubes, rapid compression machines, laminar flames, and jet-stirred and flow reactors. The value of the data from such experiments is critically discussed. Secondly, this article highlights the important reaction classes involved in alkene oxidation over low-, intermediate- and high-temperature ranges. Combustion chemistry covering the C2 to C10 alkenes, with a special emphasis on C2 to C7 isomers is discussed by presenting a large body of experimental and modeling investigations. Detailed chemistry difference between alkene isomers and also between alkenes and alkanes is also been addressed. Thirdly, the article presents the important reaction pathways for PAH precursors formation in different alkenes. Finally, a summary of the distinguishing features of alkene combustion chemistry and an outlook toward future research in this area is presented. Note that this review is focused on linear and branched chain alkenes. The chemistry of cyclo-alkenes is not included and could be a topic of future work.

1.	Introduction .....	5
2.	Fundamental combustion experiments of alkenes .....	8
2.1	Autoignition studies in shock tubes and rapid compression machines.....	8
2.1.1	Ethylene.....	9
2.1.2	Propene/Allene.....	12
2.1.3	Butenes .....	13
2.1.4	Pentenes.....	14
2.1.5	Hexenes .....	16
2.1.6	Heptenes and higher alkenes.....	17
2.1.7	1,3-Butadiene.....	18
2.2	Laminar burning velocity.....	19
2.2.1	Ethylene.....	19
2.2.2	Propene.....	20
2.2.3	Butenes .....	21
2.2.4	Pentenes.....	22
2.2.5	Hexenes .....	23
2.2.6	Heptenes and higher alkenes.....	24
2.2.7	1,3-Butadiene.....	25
2.3	Speciation Measurements .....	26
2.3.1	Ethylene.....	26
2.3.2	Propene/Allene.....	28
2.3.3	Butenes .....	30
2.3.4	Pentenes.....	32
2.3.5	Hexenes .....	33
2.3.6	Higher alkenes .....	34
2.3.7	1,3-Butadiene.....	35

3.	Chemical kinetics of alkene combustion.....	43
3.1	The molecular structure of alkenes.....	43
3.2	Reaction mechanism, reaction classes, and rate rules .....	48
3.2.1	Reaction class 1: unimolecular decomposition of alkenes .....	51
3.2.2	Reaction class 2: H-atom abstraction from alkenes .....	51
3.2.3	Reaction classes 3 and 4: vinylic and alkenyl radical decomposition and isomerization 52	
3.2.4	Reaction class 5: H-atom addition to alkenes .....	52
3.2.5	Reaction class 6: $\ddot{O}$ -atom addition to alkenes .....	53
3.2.6	Reaction classes 7 and 8: secondary and tertiary vinylic radicals react with $O_2$ .....	55
3.2.7	Reaction classes 9-12: recombination reaction of allylic and $\dot{H}O_2$ radicals ( $\dot{R}_A + \dot{H}O_2 \rightleftharpoons R_AOOH$ , $R_A + \dot{H}O_2 \rightleftharpoons \dot{R}_A\dot{O} + \dot{O}H$ , $R_AOOH \rightleftharpoons R_A\dot{O} + \dot{O}H$ , $R_A\dot{O} \rightleftharpoons$ decomposition) .....	55
3.2.8	Reaction classes 13-14: recombination reaction of allylic and $\dot{C}H_3$ radicals and the subsequent oxidation mechanism ( $\dot{R}_A + \dot{C}H_3 \rightleftharpoons R_A\dot{C}H_3$ and $R_A\dot{C}H_3$ oxidation) .....	56
3.2.9	Reaction classes 15-16: self-recombination reaction of allylic radicals and the subsequent oxidation mechanism ( $\dot{R}_A + \dot{R}_A \rightleftharpoons R_A-R_A$ , $R_A-R_A \rightleftharpoons$ products) .....	56
3.2.10	Reaction classes 17-18: addition reaction of $\dot{H}O_2$ radicals to alkenes ( $RH + \dot{H}O_2 \rightleftharpoons R\dot{O}_2$ , $RH + \dot{H}O_2 \rightleftharpoons \dot{Q}OOH$ ).....	57
3.2.11	Reaction class 19: $R\dot{O}_2$ radical isomerization ( $R\dot{O}_2 \rightleftharpoons \dot{Q}OOH$ ).....	57
3.2.12	Reaction classes 20 – 24: reactions of the hydroperoxyalkyl radicals ( $\dot{Q}OOH$ ) ( $\dot{Q}OOH \rightleftharpoons$ products, $\dot{Q}OOH + O_2 \rightleftharpoons \dot{O}_2\dot{Q}OOH$ , $\dot{O}_2\dot{Q}OOH \rightleftharpoons$ products, $\dot{O}_2\dot{Q}OOH \rightleftharpoons HOO\dot{P}OOH$ and $HOO\dot{P}OOH \rightleftharpoons$ products).....	58
3.2.13	Reaction class 25: $\dot{R}_A + O_2 \rightleftharpoons$ dienes + $\dot{H}O_2$ .....	59
3.2.14	Reaction classes 26: $RH + \dot{O}H \rightleftharpoons \dot{R}OH$ ( $\dot{O}H$ radicals addition to both sides of the double bond).....	59
3.2.15	Reaction class 27: $\alpha$ -hydroxyalkyl + $O_2 \rightleftharpoons$ aldehyde/ketone + $\dot{H}O_2$ .....	61
3.2.16	Reaction class 28: $\dot{R}OH + O_2 \rightleftharpoons$ Waddington products .....	61
3.2.17	Reaction classes 29 and 30: $\dot{R}OH + O_2 \rightleftharpoons ROHO\dot{O}$ (first $O_2$ addition), $ROHO\dot{O} \rightleftharpoons \dot{Q}_H\dot{O}HOOH$ .....	62
3.2.18	Reaction class 31: second molecular oxygen addition ( $\dot{Q}_H\dot{O}HOOH + O_2 \rightleftharpoons \dot{O}O\dot{Q}_H\dot{O}HOOH$ ) .....	63
3.2.19	Reaction classes 32 and 33: reactions of $\dot{O}O\dot{Q}_H\dot{O}HOOH$ radicals ( $\dot{O}O\dot{Q}_H\dot{O}HOOH \rightleftharpoons HOO\dot{Q}_H=OOH + \dot{O}H$ and $HOO\dot{Q}_H=OOH \rightleftharpoons$ products).....	63

3.2.20	Reaction classes 34–38: reactions of $\dot{R}_{AEN}$ radicals (low temperature chain branching reactions for alkenyl radical) .....	63
3.3	Model validation and analysis.....	64
3.4	The combustion chemistry of ethylene.....	64
3.4.1	Low temperature chemistry of ethylene combustion .....	67
3.4.2	Intermediate temperature chemistry of ethylene combustion .....	68
3.4.3	High temperature chemistry of ethylene combustion.....	69
3.4.4	Ethylene combustion mechanism.....	71
3.5	The combustion chemistry of propene .....	72
3.5.1	High temperature chemistry of propene combustion .....	73
3.5.2	Intermediate temperature chemistry of propene combustion.....	75
3.5.3	Low temperature chemistry of propene combustion.....	76
3.5.4	Propene combustion mechanism behavior .....	76
3.5.5	Chemistry difference between propene and ethylene oxidation .....	78
3.6	The combustion chemistry of butene isomers.....	78
3.6.1	High temperature chemistry of butenes combustion.....	80
3.6.2	Intermediate temperature chemistry of butene combustion.....	82
3.6.3	Low temperature chemistry of butene combustion .....	84
3.6.4	Chemistry difference between butene isomers oxidation .....	87
3.6.5	Chemistry difference between butene and propene oxidation .....	89
3.7	The combustion chemistry of pentene isomers .....	89
3.7.1	High temperature chemistry of pentene combustion.....	91
3.7.2	Low and intermediate temperature chemistry of pentenes combustion .....	91
3.7.3	Chemistry difference between butene and pentene isomers .....	94
3.7.4	Chemistry difference between pentene isomers.....	94
3.8	The combustion chemistry of hexene isomers .....	95
3.8.1	Low and intermediate temperature chemistry of linear hexene combustion .....	96
3.8.2	High temperature chemistry of linear hexenes combustion.....	98
3.8.3	Chemistry difference between linear hexene isomers .....	98
3.8.4	Chemistry difference between pentene and hexene isomers .....	100

3.9	The combustion chemistry of heptene isomers and higher alkenes .....	100
3.10	The combustion chemistry of diolefins .....	105
3.10.1	Important reaction classes for 1,3-butadiene oxidation.....	106
3.10.2	Chemistry difference between alkenes and diolefins .....	111
3.11	Chemistry difference between alkanes and alkenes .....	112
4.	PAH and soot formation from alkenes .....	113
4.1	Alkenes as a source of RSFR – precursors of monocyclic aromatics and PAH .....	113
4.2	Direct involvement of alkenes in PAH growth reactions .....	119
4.3	Alkenes and flame sooting tendencies.....	124
5.	Conclusions and research outlook.....	127
6.	Acknowledgements.....	129
7.	References .....	130

## 1. Introduction

The combustion of fossil fuel accounts for more than 80% of global primary energy utilization [1, 2] and the related environmental issues instigate increasing concerns worldwide. Emissions from the fossil fuel combustion processes significantly influence the air quality, environment, climate, and human health [1, 2]. They cause severe air pollution and contribute to anthropogenic carbon dioxide [3, 4]. In 2019, the measured globally averaged CO<sub>2</sub> concentration at Earth's surface was 409.8 ± 0.1 ppm. The average annual growth of global mean CO<sub>2</sub> during 2009–2018 was 2.3 ppm/year, while a higher increase of 2.5 ± 0.1 ppm in global mean CO<sub>2</sub> was observed during the year 2018 [4]. From 1850 to 2018, fossil fuel combustion was responsible for 440 ± 20 Pg C (1 Pg C = 10<sup>15</sup> g C) equivalent CO<sub>2</sub> emission. Within the year 2018, global CO<sub>2</sub> emission from fossil fuel combustion reached 10 ± 0.5 Pg C/year, the highest value in history [5]. However, CO<sub>2</sub> is not the only pertinent issue regarding combustion emissions. Take black carbon for example, which is particulate soot emitted from the combustion of fossil fuels for transportation, solid fuels for industrial and residential uses, and open burning of biomass. Black carbon can impact the climate change significantly [6] and has been reported to be among the most prominent global health hazard factors [7-9] contributing notably to such risks as diseases of the respiratory and cardiovascular systems. A more detailed, fundamental understanding of the chemistry of combustion may lead to cleaner and more efficient strategies in automotive vehicle and fuel design.

Alkenes, formed during the refining of crude oil to gasoline by cracking the heavier fractions, are present in transportation fuels, up to as much as 15–20% in gasoline [10]. Typical alkene compositions in gasoline range from C5 to C8 isomers, where branched alkenes (e.g., methyl-butenes and methyl-pentenenes) prevail over linear ones [11, 12]. They contribute to determining the ignition properties of those fuels, including the octane numbers that measure resistance to knocking behavior in spark-ignition engines and build-up of pollutants [10]. Short chain alkenes have a much higher knock resistance than their saturated homologues [13], but at high concentrations they can alter the stability of the fuel and promote the formation of gums, detrimental for engine injectors. On the other hand, combustion properties of alkenes should be a concern regarding the safety against fire hazard in chemical and petrochemical industry. For example, the industrial production of a versatile chemical, ethylene oxide, through the vapor-phase epoxidation of ethylene in air or pure oxygen could present a nonnegligible fire and explosion risk due to the low explosion limit and wide flammability range of ethylene/air mixtures [14, 15].

Alkenes also serve as potential fuels or propellants for novel propulsion systems. For instance, scramjets in pursuit of hypersonic speeds can be fueled by ethylene. One of the principal issues in scramjet design is maintaining stabilized combustion in the combustion chamber, which is considerably correlated with the efficient mixing of fuel and oxidizer and the reactivity of the mixtures. Hence, the ignition properties and flame stabilization characters of ethylene under scramjet-relevant operation conditions have been investigated by a number of studies [16-19]. In the concept of rotating detonation engine (RDE), pressure gain combustion is aided by detonations in circular motion, which leads to higher efficiency compared with deflagration combustion modes. Other than hydrogen, ethylene has been utilized as the fuel for RDE in many experimental and modeling efforts [20, 21]. Feasibility of continuously rotating detonation waves is a critical research topic in RDE development. It largely depends on the operation conditions and is quite sensitive to the mass flow rate and equivalence ratio [22], and intrinsically governed by the reactions of the fuel. Therefore, thorough understandings of the detailed reaction mechanism of alkenes would be helpful in unraveling the physics behind these novel combustion technologies.

Alkenes are also the major intermediate products of the oxidation of alkanes, which play a significant role in autoignition chemistry. Alkenes are easily formed from alkanes under combustion conditions, through H-atom abstraction reactions or cleavages of  $\beta$  C–H bonds in alkyl radicals. Given that *normal*- or *iso*-alkanes are the major compounds in jet fuels [23] and diesel fuels [24], the important role of alkenes in dictating the autoignition and flame properties of these fuels should not be overlooked. Combustion kinetic studies of hydrocarbon species with C=C double bonds have been carried out extensively in the literature for ethylene [25-44], propene [37, 45-52], 1,3-butadiene [53-67], isomers of butene [68-88], pentene [13, 89-100], hexene [10, 98, 101-111], heptene [103, 112-114], octene [115-117], decene [118, 119] and 2,4,4-trimethyl-1-pentene [120-124]. However, comprehensive kinetic modeling studies of the oxidation of alkenes containing more than four carbon atoms are quite limited in the literature. The importance of allylic C–C and C–H bonds and allylic radicals, in general, is not sufficiently well understood and the practical implications are sometimes misinterpreted, with thorough understanding of important kinetic pathways still evolving.

Concerning soot formation processes, which begin with a growth of polycyclic aromatic hydrocarbons (PAHs), alkenes are believed to play a dual role. First, their pyrolysis supplies

resonantly stabilized free radicals (RSFR), in large, by cleaving the weakest allylic bonds, and small stable molecules like acetylene which then react to form PAHs. Second, they can directly participate in chemical reactions producing PAHs. Mechanistic details of these processes are still far from being well understood and their temperature- and pressure-dependent kinetic data are largely unknown.

The fossil fuels utilized for the past hundred years are mixtures of molecular components, defined by a range of physical properties. The fuels of tomorrow will have more distinct molecular structures, defined by the feedstock from which they are drawn and the chemical and physical processes to which they are subjected [125]. Understanding how specific features of molecular structure affect the energy release during the combustion of a fuel and formation of pollutants is, therefore, invaluable in aiding the design of future fuels. Biofuels have long been recognized as viable alternatives to conventional petroleum-based transportation fuels as can be produced from bio-feedstocks and are sustainable / eco-friendly. While there are a variety of potential biofuels, biodiesel and bioethanol are the major biofuels being considered globally and are at the forefront of alternative fuel technologies [126, 127]. The C=C double bond does not just exist in alkenes but also represents a very common functional group in biodiesel components. Therefore, achieving a comprehensive understanding of the combustion chemistry of the C=C double bond is helpful to understand the combustion chemistry of biodiesel and is also valuable for the future fuel design.

This article presents a wide-ranging review of the combustion chemistry of alkenes and aims to (i) reveal the essential chemistry difference between alkanes and alkenes, (ii) discuss chemical changes with the position of the C=C double bond and the increasing number of carbon atoms in the fuel molecule, (iii) describe alkenes' roles in soot formation, (iv) provide state-of-the-art reaction classes for alkenes oxidation under different temperatures and pressures. Experimental and theoretical tools for exploring combustion chemistry of fuels are highlighted to provide an understanding of the desired information and observable quantities. With the stage thus set, the article gives an extensive overview of fundamental combustion experiments by considering studies of alkenes in shock tubes, rapid compression machines, jet-stirred and flow reactors, and laminar flames. The value of the data from such experiments is critically discussed. Abbreviations are used in the following sections to denote different colleges and universities, where "NUIG" denotes National University of Ireland, Galway, "KAUST" denotes King Abdullah University of Science and Technology, "Princeton" denotes Princeton University, "TAMU" denotes Texas A&M University, "VUB" denotes Vrije Universiteit Brussel, "Nancy" denotes Université de Lorraine and "Lund" denotes Lund University. Subsequently, alkene combustion chemistry is discussed by presenting a large body of experimental and modeling investigations covering the combustion of C<sub>2</sub> to C<sub>10</sub> alkenes, with a special emphasis on C<sub>2</sub> to C<sub>7</sub> isomers. Note that this review is focused on linear and branched chain alkenes, and the chemistry of cyclo-alkenes is not included in the subsequent sections. Ignition, flame propagation, qualitative species assignment, and full quantitative speciation, depending on the specific combustion regime, are considered. The combustion kinetics and development of a comprehensive mechanism relevant to alkene combustion is presented. The article closes by presenting a summary of the distinguishing features of alkene combustion chemistry and an outlook toward future research in this area.

## 2. Fundamental combustion experiments of alkenes

### 2.1 Autoignition studies in shock tubes and rapid compression machines

Ignition delay time (IDT) is a global indicator of the overall reactivity of a fuel. IDT measurements provide highly valuable data to understand the reactivity dependence on temperature, pressure, equivalence ratio and mixture composition. IDT data are also used to compare the reactivity of various molecular structures. For model development and validation, IDTs are usually considered to be the most important validation target for chemical kinetic models.

Homogeneous ignition delay times are measured in shock tubes and rapid compression machines. These reactors provide well-defined initial boundary conditions to allow comparison of measured data with simulations. Supersonic shock waves are used to instantaneously compress and heat gaseous fuel mixtures in shock tubes. The test times in shock tube experiments are typically limited to a few milliseconds, and, therefore, shock tubes are typically used to measure high-temperature IDTs. Moreover, development of laser diagnostic technique in shock tube measurements in past years has had strong influence in the area of chemical kinetics. Measurements in shock tubes of high-temperature reaction rate coefficients using species-specific laser absorption techniques can provide new and accurate answers to questions about combustion chemical processes [128]. The capabilities of shock tubes in combustion chemistry studies as well their limitations were discussed in a detailed review by Hanson and Davidson [129]. For example, the thickness of boundary layer can be a concern for small diameter shock tubes, and this could have significant influence on the validity of one-dimensional shock equations in determining test gas conditions. Moreover, the test times in shock tube experiments are largely dictated by the lengths of the driver and driven sections, and limited by the time when the reflected shock wave reaches the interface between driver gas and driven gas or by the arrival of expansion waves. Rapid compression machines (RCMs), on the other hand, can provide test times up to a few hundred milliseconds, and, are thus suited for low-temperature IDT measurements [130]. The compression and heating in an RCM are achieved by a fast-moving piston which is locked in place at the end-of-compression to achieve constant volume conditions. Due to the relatively small volume-to-surface area ratio and longer test times, heat transfer to the walls becomes important in RCM measurements. The heat transfer is usually accounted for by measuring pressure decrease in non-reactive experiments and simulating the experiments in a variable-volume reactor. This so-called ‘adiabatic core’ assumption works well except for conditions where the first-stage ignition heat release significantly alters the heat transfer characteristics. In a recent comprehensive review about RCM facilities by Goldsborough et al. [130], difficulties in the determination of local thermal conditions were emphasized. The onset of autoignition as well as heat release rate can be altered due to the occurrence of inhomogeneities, mixing and turbulence in the RCM combustion chamber. Efforts and strategies to alleviate undesirable non-uniformities in RCM experiments were also discussed therein. Sung and Curran [131] discussed the adverse effects of roll-up vortices, induced by the high-speed motion of the piston during the compression stroke, on the interpretation of RCM data. The appearance of roll-

up vortices results in undesirable mixing of cold gas from the boundary layer with hot gases in the core region and leads to inhomogeneity of the temperature field, causing difficulties in accurately characterizing the thermodynamic state of the reacting mixture. Efforts to understand the complex fluid mechanics and alleviate unwanted inhomogeneity in RCM experiments were introduced in their review.

Ignition delay times of a variety of alkenes have been measured in shock tube and RCM experiments. These experimental data have been used to develop and validate chemical kinetic models of alkenes. Literature work on alkene IDT measurements is summarized in Table 1 and discussed here briefly.

### 2.1.1 Ethylene

Ethylene has been the subject of a number of ignition delay time experimental campaigns. One of the first IDT measurements for ethylene in the shock tube was conducted by Baker et al. in 1972 [132]. They measured IDTs for lean to rich mixtures of ethylene/O<sub>2</sub>/Ar at pressures of 3 and 12 atm and temperatures of 1058 – 1747 K. They fitted their measured data to an Arrhenius-like correlation and discussed the importance of oxygen in the chain-branching reaction. Interestingly, they described ethylene ignition process as ‘...in the first part of the induction period pyrolysis dominates, while in the second part oxidation takes over’. This is the assertion which is used in the recently published HyChem model for jet fuels [133] and is valid for the high temperature autoignition and flame chemistry of large hydrocarbon fuels.

A couple of years later (1974), Hidaka et al. [134] reported IDTs of highly diluted mixtures of ethylene/O<sub>2</sub>/Ar in a shock tube. They measured emission from CH\*, C<sub>2</sub>\* and OH\*, while describing the reactions responsible for these emission signals. They reported their IDT results based on CH\* signal as it provided the highest intensity in their experiments. About a quarter of century later (1999), the same authors [135] studied ethylene pyrolysis and oxidation with a range of new diagnostics, including IR-laser absorption near 3.39 μm and 4.24 μm, IR emission near 3.48 μm and gas chromatograph (GC). Using these new measurements, they proposed a reaction mechanism consisting of 161 reactions and 51 species, which performed well in predicting ethylene pyrolysis and IDT data. They observed that the predictions for the pyrolysis and oxidation data were very much dependent on the production and consumption of the vinyl radical.

Brown et al. [136] studied ethylene ignition in *air-like* mixtures in contrast to previous works which employed high dilution. They discussed the importance of studying non-diluted conditions which represent practical combustors better. They found that changing the diluent from argon to nitrogen can lead to significant changes in IDTs due to temperature effects.

Colket et al. [16] carried out shock tube experiments to compare IDTs of various candidate fuels for scramjet propulsion. The relative IDTs for the different fuels were found to be in the order: methane > JP-10 ≈ heptane > ethylene > hydrogen. They discussed the importance of fuel cracking and showed that fuel cracking enhances ignition. Cadman et al. [137] used schlieren imaging and chemiluminescence to study ethylene ignition over a wide range of temperatures (800 – 1600 K). They divided the ignition process in mild combustion, strong combustion and

detonation as a function of increasing temperature behind reflected shock waves. Kalitan et al. [138] studied the influence of silane ( $\text{SiH}_4$ ) on the IDTs of ethylene. They reported that by adding a small amount of  $\text{SiH}_4$  ( $< 10\%$ ), the IDTs reduced as much as 50% in some cases. They compared their measurements with various models and the IDTs agreed better with the Wang and Laskin [139] model.

Penyazkov et al. [34] measured IDTs of ethylene/air at high pressures (5.9 – 16.5 atm) in a shock tube. They observed an increase of apparent activation energy of the system while going from high to low temperatures (see Figure 1) and attributed this behavior to the underlying reaction kinetics. Saxena et al. [33] extended previous IDT works by focusing on high pressures and rich conditions ( $\phi = 3$ ) and also studied the effect of diluent concentration. They observed strong dependence of IDTs on pressure for more dilute conditions. They provided a global correlation (see Figure 2) which represented their measurements and previous data quite well over 1000 – 2300 K and 0.2 – 20 atm. Kopp et al. [32] focused on pressure dependence of ethylene/air IDTs by performing measurements over pressures of 1.1 – 24.9 atm and equivalence ratios of 0.3 – 2. They observed that fuel-lean mixtures exhibited negligible pressure dependence, while the usual trend of decreasing IDTs with increasing pressure was seen for stoichiometric and fuel-rich mixtures.

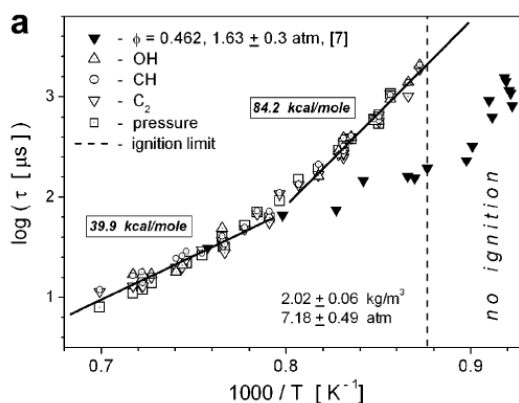


Figure 1. Ignition delay measurements for lean ethylene/air mixtures [34].

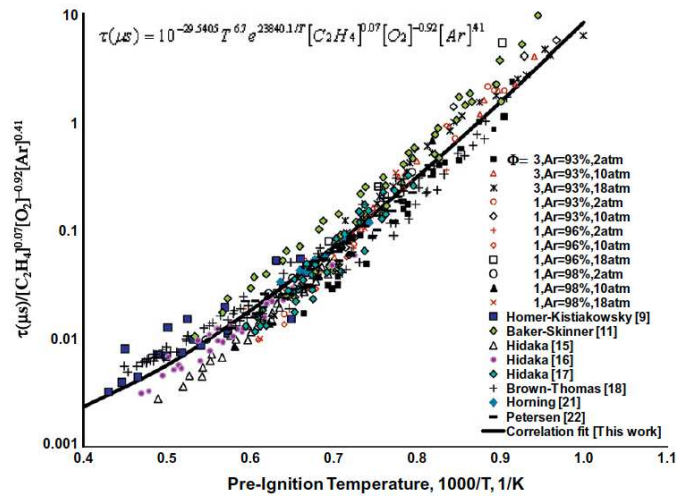


Figure 2. Shock tube IDT data of ethylene/O<sub>2</sub>/Ar mixtures [33]. The correlation is valid over  $T = 1000 - 2300$  K,  $P = 0.2 - 20$  atm and  $\phi = 0.125 - 3$ . (“This work” refers to the work of Saxena et al. [33], while other numbered citations correspond to the references therein.)

Shao et al. [140] measured the IDTs of ethylene/O<sub>2</sub>/argon mixtures at high pressures (14 – 60 atm) and high temperatures (950 – 1800 K). They were able to provide an Arrhenius-like correlation by combining their measurements with previous data (see Figure 3). They compared IDT results with two chemical kinetic models and found AramcoMech [25] to predict the measured data quite well.

The only available investigation of ethylene ignition in a rapid compression machine (RCM) was carried out by Kumar et al. [43] over 850 – 1050 K and 15 – 50 bar. Their low-pressure (15 bar) data exhibited some curvature compared to the high-pressure data. They described vinyl + O<sub>2</sub> and ethylene + HO<sub>2</sub> reactions to be important for ethylene autoignition over the range of their experimental conditions.

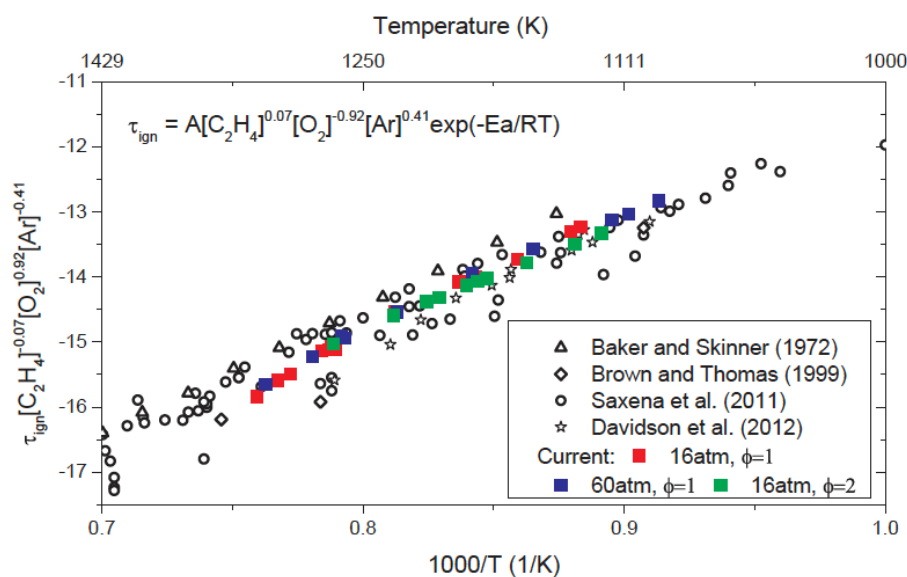


Figure 3. Shock tube ignition data of ethylene/oxygen/argon mixtures, scaled according to the given correlation [140]. (“Current” refers to the work of Shao et al. [140], while other citations correspond to the references therein.)

### 2.1.2 Propene/Allene

Burcat and Radhakrishnan [141] carried out the first measurements of IDTs of propene/ $\text{O}_2/\text{Ar}$  in a shock tube at the temperature range of 1274 – 1840 K and varying concentrations of propene and oxygen. They discussed the importance of key reactions for propene ignition, including  $\dot{\text{H}} + \text{O}_2$  chain branching reaction and H-abstraction from  $\text{C}_3\text{H}_6$  by  $\dot{\text{H}}$  atoms. They proposed a kinetic model consisting of 59 reactions which was adequate, but not complete, to predict measured IDTs. They were able to correlate their measured IDTs with an Arrhenius expression. Qin et al. [142] measured IDTs of propene in a shock tube covering similar experimental conditions as Burcat and Radhakrishnan [141]. They reported that the ignition delays measured by Burcat and Radhakrishnan [141] are too long in comparison to their data. They were able to satisfactorily predict their measured IDTs with their proposed chemical kinetic mechanism.

Burke et al. [51] carried out a very large and extensive campaign with a multi-university effort to study the ignition of propene. They measured IDTs in shock tubes and RCM covering a wide temperature range of 750 – 1750 K, three pressures (2, 10, and 40 atm) and three equivalence ratios (0.5, 1 and 2). Figure 4 shows the range of conditions studied in their work in contrast to previous literature. Although the experiments were carried out in six different shock tubes and two rapid compression machines, there is a good agreement among the measurements from various facilities at overlapping conditions. They noticed no evidence of NTC behavior over their studied conditions. They proposed a new detailed kinetic model for propene ignition which predicted the measurements very well.

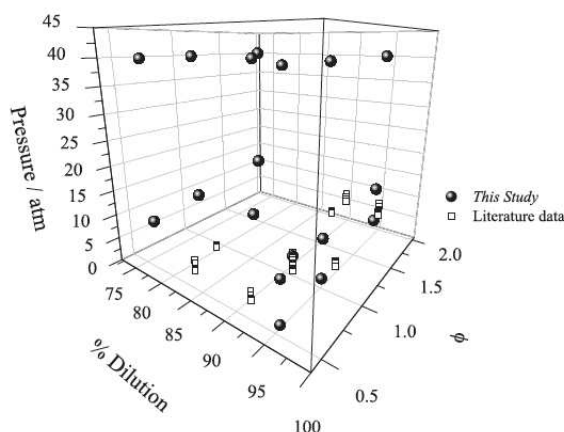


Figure 4. Comparison of condition space examined by Burke et al. [51] and previous literature work. (“This study” refers to the work of Burke et al. [51].)

Allene (propadiene,  $C_3H_4$ ) is the simplest diolefin. Curran et al. [143] measured IDTs allene/ $O_2$ /Ar behind reflected shock wave at temperature range of 1200 – 1900 K, pressures of 2 – 5 bar and equivalence ratios of 0.5 – 2. They showed that allene IDTs can be correlated using an Arrhenius expression. Their proposed model did a reasonable job of capturing the measured data. They also found that high-temperature allene ignition is quite similar to its alkyne isomer (propyne). Fournet et al. [144] measured ignition delays of allene/ $O_2$ /Ar in a shock tube at temperatures of 1190 – 1742 K and pressured of 8.5 – 10 atm. They developed a model to predict the reactivity of small unsaturated hydrocarbons, including acetylene, propyne, allene, and butadiene.

### 2.1.3 Butenes

The first ignition study of a butene isomer was carried out by Curran et al. [74] to measure shock tube IDTs of isobutene/ $O_2$ /Ar over 1100 – 1900 K, pressures of 2.2 – 4.6 atm, and equivalence ratios of 0.1 – 4. Their computed results agreed quite well with measured ignition delay times. Recently, Zhou et al. [88] performed an extensive multi-university study to provide IDTs of isobutene in four shock tubes and two rapid compression machines in the temperature range of 666 – 1650 K, pressures of 1.7 – 50 atm and equivalence ratios of 0.3 – 2. They compared their measured IDTs with their newly developed detailed kinetic model which performed nicely (see Figure 5). They described that H-abstraction from isobutene by  $\dot{O}H$  radicals inhibits overall reactivity because this reaction consumes highly reactive  $\dot{O}H$  radicals to produce unreactive 2-methylallyl radicals.

Heyberger et al. [145] measured the IDTs of lean-to-rich mixtures of 1-butene/ $O_2$ /Ar behind reflected shock waves over 1200 – 1670 K and 6.6 – 8.9 atm. Predictions by their proposed model agreed well with their measured data. They asserted that resonantly stabilized radicals play a lesser role in 1-butene chemistry in comparison to propene. Pan et al. [82] extended the pressure range of 1-butene ignition measurements by carrying out their work at 1.2, 4 and 16 atm. They compared their measurements with the prediction of different models and found AramcoMech [25] to show better agreement. In comparison to n-butane, they found that 1-

butene exhibits longer IDTs at high temperatures but shorter IDTs at lower temperatures. They also observed that 1-butene reactivity lies between that of ethylene and propene at high temperatures (see Figure 6).

Recently, Li et al. [86, 87] performed wide-ranging studies on the ignition of 1-butene and trans-2-butene in shock tubes and RCMs, covering conditions of relevance to practical combustors. They observed that 2-butene is less reactive than 1-butene but more reactive than isobutene.

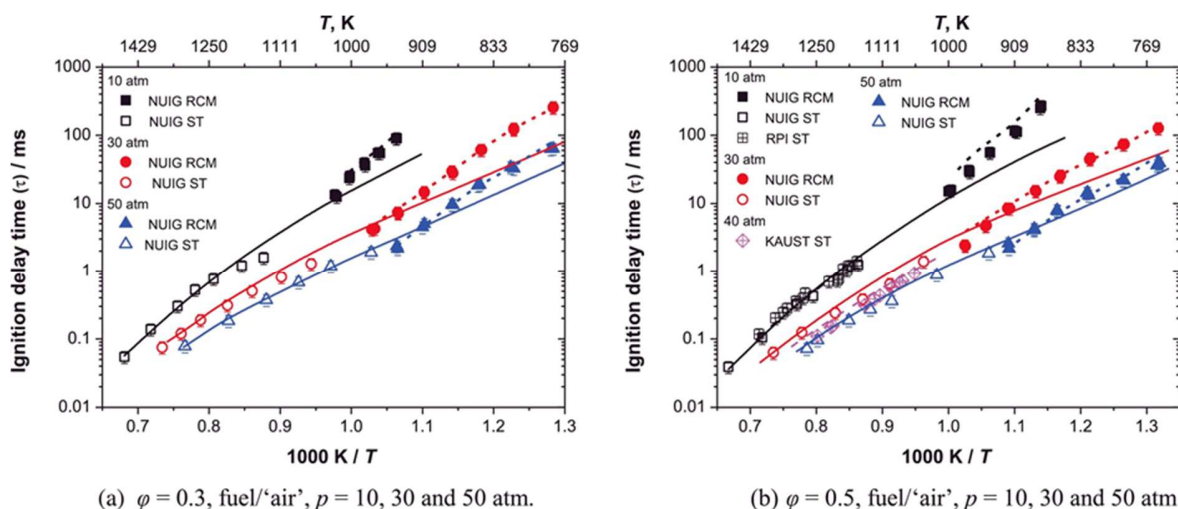


Figure 5. Comparison between measured and simulated IDTs of isobutene. Symbols: experimental data; solid lines: constant volume simulation, dashed lines: RCM simulations [88].

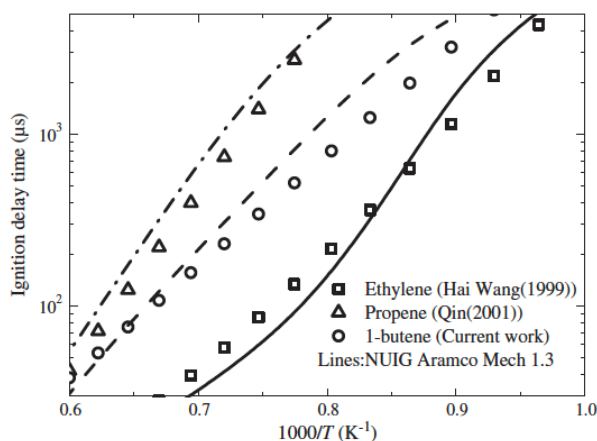


Figure 6. Comparison of IDTs of small alkenes,  $p = 4.0$  atm and  $\phi = 1.0$  [82]. (“Current work” refers to the work of Pan et al. [82], while other citations correspond to the references therein.)

#### 2.1.4 Pentenes

Ribaucour et al. [90] and Minetti et al. [89] measured IDTs of stoichiometric mixtures of 1-pentene and n-pentane in a rapid compression machine at temperatures of 600 – 900 K and pressured of 6 – 9 bar. They observed a clear NTC behavior under their studied conditions and

described the cool flame behavior. They ascribed the formation of 1,3-pentadiene to be largely responsible for the NTC region. They contrasted the reactivity of 1-pentene with n-pentane, and found 1-pentene to be less reactive due to the addition of radicals to the double bond. Cheng et al. [93] measured the ignition delay times of 1-pentene using a ST at pressures from 1.2 bar to 10 bar, at equivalence ratios from 0.5 to 2.0 with 0.5% and 1.0% fuel concentrations, in the temperature range of 1040–1880 K. They found 1-pentene to be slightly more reactive than n-pentane at the high-pressure range of their work (see Figure 7).

Kukkadapu et al. [97] added 2-pentene as a gasoline surrogate component to study its effect on the surrogate ignition in RCM and found that even a small amount of 2-pentene (5.3% by molar percentage in the LLNL surrogate) is effective in scavenging  $\dot{O}H$  radicals (almost 15% of the overall consumption rate of  $\dot{O}H$ ) in the very early stages of the first-stage ignition. About 7.5% of the  $\dot{O}H$  radicals are consumed by  $\dot{O}H$  addition to the double bond while about 7% abstract H-atoms on the allylic hydrogen atom.

Touchard et al. [99] provided high-temperature IDT measurements of 1-pentene behind reflected shock waves at temperatures of 1130 – 1620 K, pressures of 7.3 – 9.5 atm and equivalence ratios of 0.5 – 2. They developed a detailed model of 1-pentene oxidation which predicted the measured IDTs quite well. Mehl et al. [10] measured IDTs of 1-pentene and 2-pentene behind reflected shock waves over 990 – 1770 K. By combining their data with previous low-temperature measurements, they developed a model based on C1–C4 mechanism of Curran and coworkers [146, 147]. The model performed very well in predicting the reactivity of pentene isomers.

Very recently, Dong et al. [100] conducted ignition delay time measurements in both a high-pressure shock tube and an RCM for 1- and 2-pentene under engine-relevant conditions, covering a wide range of temperatures from 600 to 1300 K, pressures of 15 and 30 atm, and equivalence ratios of 0.5, 1.0 and 2.0 in ‘air’. In addition, carbon monoxide time-histories were measured at high temperature regimes and 10 atm in the shock tube for stoichiometric fuel/‘air’ mixtures of 1- and 2-pentene, respectively. It was found in their study that at temperatures above 900 K, the ignition delay times of 1- and 2-pentene are quite close regardless of pressure and equivalence ratio. However, at lower temperatures, 1-pentene exhibits NTC behavior while 2-pentene does not and is in general less reactive than 1-pentene.

As for branched pentene isomers, Westbrook et al. [91] measured high-temperature IDTs for 2-methyl-2-butene in a shock tube at temperatures from 1330 to 1730 K and equivalence ratios of 0.5, 1.0 and 2.0, under approximately 1.7, 11.2 and 31 atm.

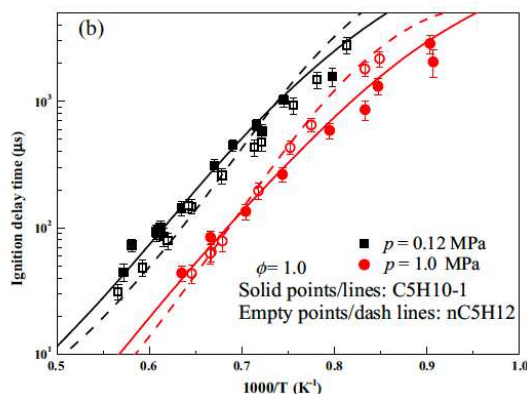


Figure 7. Comparison of IDTs of 1-pentene and n-pentane at high temperatures [93]. Lines are model predictions.

### 2.1.5 Hexenes

Vanhove et al. [102] studied the effect of the position of double bond on the reactivity of hexene isomers (1-, 2- and 3-hexene) by measuring their IDTs in a rapid compression machine over 630 – 850 K and 6.8 – 8.5 bar. For 3-hexene, they found the ignition behavior to be dominated by the properties of the double bond, whereas for 1-hexene, reactivity is dominated by the properties of the alkenyl chain. Therefore, 1-hexene behaved similar to alkanes and showed NTC behavior, while 3-hexene exhibited negligible NTC behavior. Lastly, 2-hexene showed an intermediate behavior with a weaker NTC than that of 1-hexene. Yahyaoui et al. [107] measured IDTs of 1-hexene/ $O_2$ /Ar in a shock tube at high temperatures (1270 – 1700 K), pressures of 2 – 10 bar and equivalence ratios of 0.5 – 1.5. They observed a strong decrease in the apparent activation energy for temperatures less than 1400 K.

Mehl et al. [10] measured IDTs of stoichiometric mixtures of 1-, 2- and 3-hexene/air behind reflected shock waves at temperatures of 990 – 1460 K and pressures of 8.5 - 12 atm. They also developed a model that predicted the reactivity of hexene isomers from low to high temperatures (see Figure 8). They agreed with Vanhove et al. [102] assertion that 1-hexene has the highest reactivity at low temperatures followed by 2-hexene and 3-hexene. However, they observed 2-hexene to be the fastest at high temperatures and 1-hexene to be the slowest reacting isomer at  $T > 1400$  K. They attributed this reactivity change at high temperatures to the role of decomposition reactions and  $HO_2$  chemistry. Yang et al. [111, 148] performed high-temperature (1020 – 1900 K) IDT measurements of the three hexene isomers in a shock tube at pressures of 1 – 10 atm and equivalence ratios of 0.5 – 2. By comparing the reactivity of 1- and 2-hexene, they agreed with the conclusions of Mehl et al. [10] and observed 1-hexene to have slower reactivity at high temperatures due to the formation of higher concentration of resonantly stabilized allyl radicals.

Wagon et al. [149] provided intermediate-temperature (837 – 1086 K) measurements of IDTs of stoichiometric mixtures of hexene isomers (1-, 2- and 3-hexene) in a rapid compression facility, and they supplemented their IDTs with species sampling data.

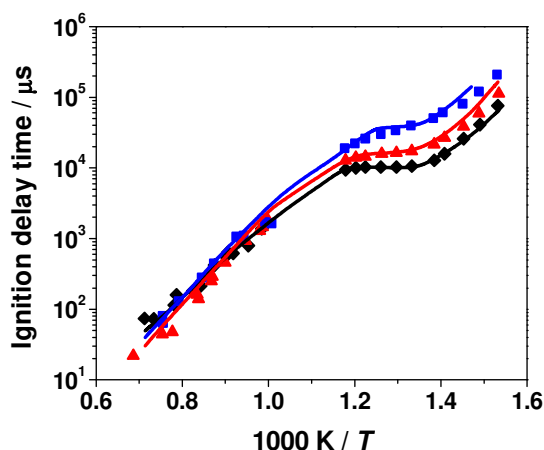


Figure 8. High-temperature IDT measurements [10] of hexene isomers at 10 atm and stoichiometric conditions. Low-temperature data from [102]. Lines are the results of the chemical kinetic model of Mehl et al. [10]. Symbols are experimental data: 1-hexene (diamonds), 2-hexene (triangles), 3-hexene (squares).

### 2.1.6 Heptenes and higher alkenes

There have been very few studies on the ignition of alkenes larger than C6. Tanaka et al. [113] studied the ignition of three linear isomers of heptene in a rapid compression machine at 827 K and 41.6 bar. Their results showed clearly that the reactivity of these heptene isomers at low temperature is affected considerably by the position of the double bond. They observed two-stage ignition for 1- and 2-heptene in RCM, while only a single stage ignition was shown by 3-heptene. These observations are thus very similar to those found for hexene isomers by Vanhove et al. [102]. In a study on biodiesel oxidation, Garner et al. [150] measured shock tube IDTs of 1-heptene as a representative of the alkyl chain of 2-octenoate. By comparing the reactivity with 1,6-heptadiene and *n*-heptane at the high temperatures of their study, they showed that *n*-heptane is most reactive, followed by 1-heptene and 1,6-heptadiene is the least reactive. This reaffirmed previous observations that increasing degree of unsaturation results in decreasing reactivity.

Recently, Wu et al. [112] investigated the auto-ignition behavior of 1-heptene and 2-heptene in the low-to-intermediate temperature range (650–950 K) at 15 and 23 bar using an RCM and compared their reactivity to that of *n*-heptane at the same conditions (see Figure 9). The reactivity comparison showed that, as expected, *n*-heptane has the highest reactivity, and both heptene isomers exhibited NTC behavior. The results showed that there is a crossing point for the reactivity of 1- and 2-heptene. At low temperatures, 1-heptene has shorter IDTs than 2-heptene, while 2-heptene is more reactive at higher temperatures. This variation in reactivity is the result of  $\text{RO}_2$  to  $\text{QOOH}$  isomerization being more likely for 1-heptene (longer alkyl chain) at low temperatures, while the high-temperature decomposition pathways for 2-heptene produce more reactive radicals.

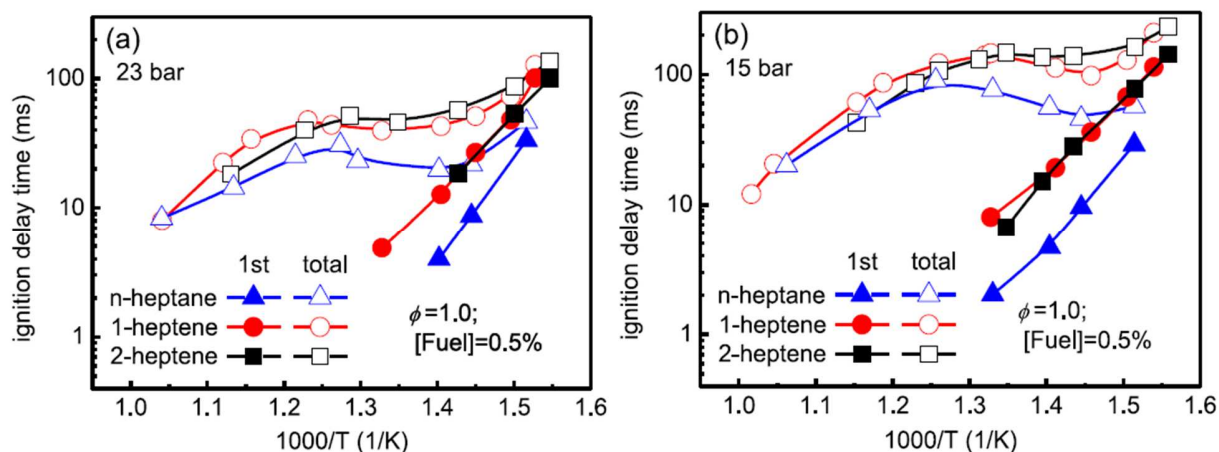


Figure 9. 1<sup>st</sup> stage and total IDTs for stoichiometric mixtures of heptene isomers and n-heptane at (a) 23 bar, and (b) 15 bar [112].

Tekawade et al. [119] examined the reactivity trends of two C<sub>10</sub> alkenes (1-decene and trans-5-decene) in a shock tube and compared the measured ignition delay times with n-decane. They found that at low temperatures, trans-5-decene is the least reactive, followed by 1-decene and n-decane being the most reactive. At high temperatures, however, the differences in ignition delay times of the three fuels are much smaller with trans-5-decene being the most reactive. These reactivity trends and the exhibited NTC behavior are consistent with previous works on C6 and C7 alkenes.

Ignition delay times of two diisobutylene isomers, 2,4,4-trimethyl-1-pentene and 2,4,4-trimethyl-2-pentene, have been investigated in two studies. Metcalfe et al. [123] measured IDTs of the two isomers in a shock tube at low pressures (1 – 4 atm) and high temperatures (1200 – 1550 K). They found that 2,4,4-trimethyl-2-pentene ignited significantly faster than 2,4,4-trimethyl-1-pentene and that the IDTs of their blend were directly dependent on the proportions of each isomer. This trend is consistent with previous works on C6, C7 and C10 linear alkenes wherein the shift of the C=C double bond to the central part of the molecule increases the reactivity at high temperatures. Metcalfe et al. [123] developed a detailed chemistry model for both isomers which captured the reactivity successfully. Hu et al. [121] measured IDTs of 2,4,4-trimethyl-1-pentene at higher pressures (2 – 10 atm) and expanded the temperatures to 1740 K. Their results agreed with Metcalfe et al. [123] data at the overlapping conditions.

### 2.1.7 1,3-Butadiene

1,3-Butadiene is the simplest conjugated diolefin and is a key intermediate species in hydrocarbon oxidation. Fournet et al. [144] measured IDTs of 1,3-butadiene/O<sub>2</sub>/Ar at conditions similar to their work on allene but their model did not do a good job in predicting 1,3-butadiene ignition for high fuel concentration data. Zhou et al. [67] performed an extensive study on 1,3-butadiene by carrying out IDT measurements in five shock tubes and a rapid compression machine, widely covering temperatures (645 – 1780 K), pressures of 1 – 40 atm and equivalence ratios of 0.3 – 2. They developed a detailed chemical kinetic model which predicted the measured IDTs very well at high temperatures but exhibited slower reactivity at low

temperatures (see Figure 10). To improve the model performance, they suggested further studies on the key elementary reactions of the addition of  $\dot{\text{O}}\text{H}$  and  $\text{H}\dot{\text{O}}_2$  radicals to the double bonds of 1,3-butadiene.

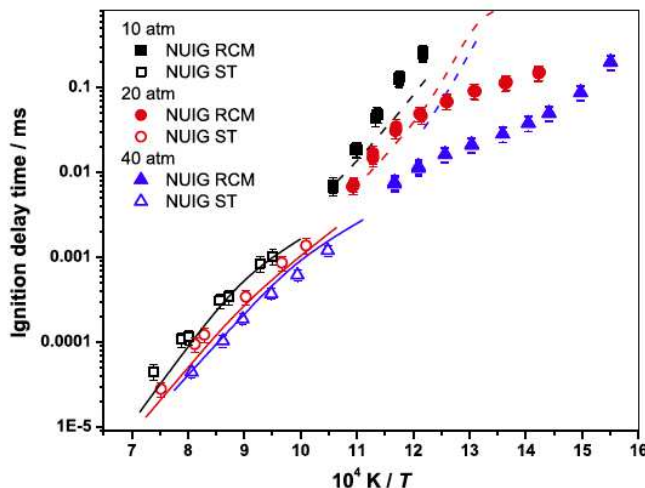


Figure 10. Measured IDTs of 1,3-butadiene/air in a shock tube and RCM [67]. Symbols: experimental data; solid lines: constant volume simulation, dashed lines: RCM simulations.

## 2.2 Laminar burning velocity

Laminar burning velocity is a very important fuel property which affects combustion in a variety of practical combustions, such as spark-ignited internal combustion engines. For a combustor designer, it is critical to know how quickly the flame is going to spread as this controls the burning rate and heat release. Therefore, laminar burning velocity is measured in idealized reactors to understand the differences among various fuels and to characterize flame speed variation as a function of equivalence ratio, initial temperature and initial pressure. Laminar burning velocity is a key validation target for the development of high-temperature chemical kinetic models. The reader is referred to reviews [151, 152] on advances and challenges of flame speed measurements. Laminar burning velocities have been measured for a variety of alkenes. Literature work on flame speed measurements is summarized in Table 1 and discussed here briefly.

### 2.2.1 Ethylene

The very first measurement of the burning velocity of ethylene was carried out by Linnett and Hoare [153] in 1948. They determined the burning velocities by measuring the shape of flame cone in a cylindrical burner tube. The shape of the cone was measured by throwing a shadow of the flame on a light-sensitive film. Due to the non-availability of pure ethylene gas, it was prepared by the reaction of ethyl alcohol with phosphoric acid at 220 °C. Figure 11 shows a shadow photograph of flame cone recorded by Linnett and Hoare [153] and their burning velocity measurements as a function of ethylene volume percent. This pioneering work was followed up by Gerstein et al. [154] who used an improved flame tube apparatus to measure burning velocities for a larger number of hydrocarbons, including ethylene. As discussed by

Egolfopoulos et al. [152], these early studies did not adequately account for aerodynamic stretch effects, which lead to somewhat uncertain determination of the laminar flame speed.

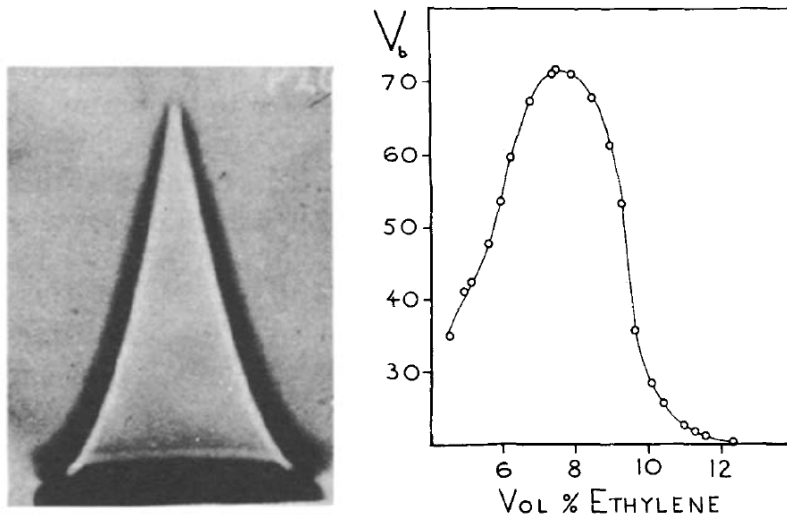


Figure 11. Shadow photograph of flame cone on cylindrical burner tube (left panel). Variation of burning velocity ( $V_b$ , cm/sec) with composition for ethylene-air mixtures (right panel) [153].

Egolfopoulos et al. [41] used the counterflow flame technique to measure laminar flame speeds for C2 hydrocarbons at room temperature and pressures ranging 0.25 to 3 atm. They also developed a C2 kinetic mechanism which predicted measured flame speeds adequately.

Various works on ethylene flame speed measurements have been summarized in a recent work by Huo et al. [155]. There is generally a good agreement among the experimental data and the kinetic models predict the flame speeds quite well. Hou et al. [155] expanded previous works by performing measurements at high pressures (up to 10 atm). They also discussed the sensitivity of flame speed to elementary reactions comprising the kinetic model. Flame speed is most sensitive to the chain branching  $\dot{H} + O_2 \rightarrow \dot{OH} + \dot{O}$  reaction followed by the key heat release reaction  $CO + \dot{OH} \rightarrow CO_2 + \dot{H}$ . At fuel-rich conditions, some C2 related reactions also become important in determining the flame speed.

### 2.2.2 Propene

Davis and Law [46] measured the laminar flame speeds of propene/air mixtures at room temperature and atmospheric pressure over an extensive range of equivalence of 0.7 to 1.7 using the counterflow twin flame configuration. Burke et al. [51] measured propene flame speeds in 5 different locations which included either a constant volume vessel (spherically expanding flame) or a heat flux burner. These data along with previous measurements are shown in Figure 12 for atmospheric pressure. The scatter in the data represents uncertainty of the flame speed measurements using different methods and facility effects, as well as inconsistencies in the flame speed extrapolation for spherical flames. The newly developed model by Burke et al. [51] did a good job in predicting the flame speed measurements except at fuel-rich conditions. The authors suggested that the chemistry model should be extended to include heavier hydrocarbons,

including aromatics, to improve the prediction for rich propene flames. The sensitivity analysis (Figure 12) shows that, in addition to the expected dependence on C0 and C1 reactions, the flame speed is affected by the formation and consumption of resonantly stabilized allyl radicals ( $\dot{C}_3H_5$ -a). Burke et al. [51] provided mass burning rate of propene for pressures as high as 20 atm and flame speed data for the temperature range of 298 – 398 K.

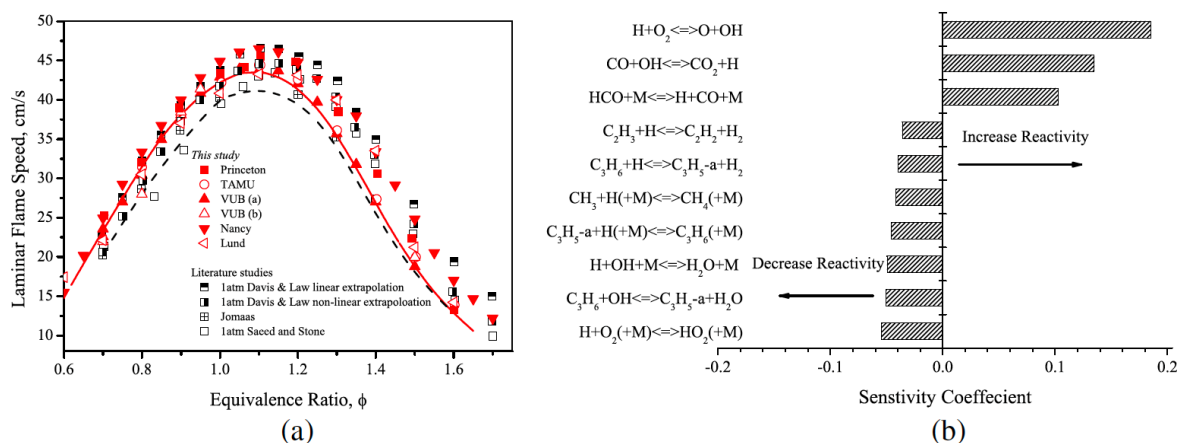


Figure 12. (a) Propene/air flame speed at  $p = 1$  atm and room temperature. Solid line is from the model by Burke et al. [51] and dash line is from AramcoMech 1.3 [25]. (b) Flame speed sensitivity at  $\phi = 0.95$ . (“This study” refers to the work by Burke et al. [51])

### 2.2.3 Butenes

Davis and Law [156] used the counterflow twin flame configuration to measure laminar flame speeds for a wide range of C1 to C8 hydrocarbons, including alkanes, alkenes, alkynes, aromatics and alcohols. They showed that alkenes have generally higher flame speeds than alkanes. They also found that flame speeds of 1-alkenes are higher than for n-butane, with propene and 1-butene having similar values, while ethylene has the largest flame speed. The higher flame speeds of ethylene are caused by a higher adiabatic flame temperature and faster oxidation kinetics at these conditions.

Fenard et al. [83, 85] measured flame speeds of 1- and 2-butene (cis and trans isomers) using a spherical combustion vessel. They observed that trans-2-butene/air mixtures have slightly lower burning velocities compared to cis-2-butene for rich conditions, though the differences are only minor. They observed that Zhao et al. [79] measurements for 1-butene are too low compared to their measurements as well as those by Davis and Law [156]. Finally, 1-butene has higher flame speeds compared to 2-butene over the range of studied conditions (see Figure 13).

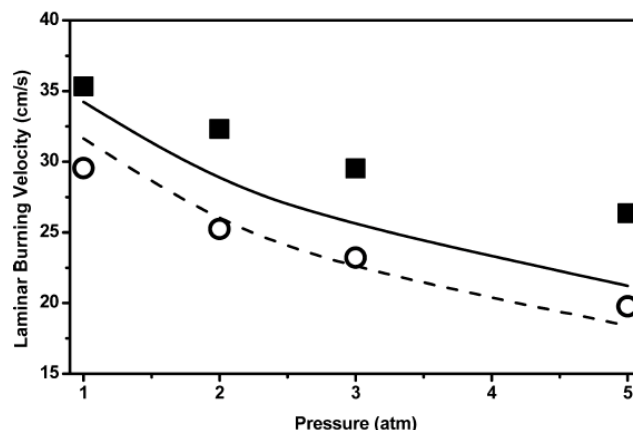


Figure 13. Laminar burning velocities of 1-butene/air and cis-2-butene/air at  $T = 300\text{ K}$ ,  $\phi = 0.8$  [83]. Squares: 1-butene; circles: cis-2-butene; lines: kinetic simulations.

Schenk et al. [78] utilized a low-pressure flame coupled to a time-of-flight MBMS and GC to carry out isomer-specific speciation of more than 30 stable molecules and radicals for three butene isomers (1-butene, *trans*-2-butene and iso-butene). They contrasted the oxidation of these three isomers with the help of experimental data as well as detailed kinetic modeling. For example, they described the pathways to the formation of propene from butene isomers and showed that propene formation is largest for 2-butene followed by 1-butene and iso-butene. On the other hand, the highest mole fraction of benzene is observed in the iso-butene flame followed by that in 1- and 2-butene and this behavior is directly correlated with the amounts of propargyl formed in these flames.

Zhou et al. [88] carried out a large experimental effort to measure laminar flame speeds of isobutene at three different facilities using the constant volume vessel and heat flux burner methods. The experiments were carried out at atmospheric pressure and initial temperatures ranging 298 – 398 K. The detailed model developed by Zhou et al. [88] underestimated isobutene flame speeds by about 5 cm/sec. Sensitivity analysis showed that the flame speed is largely sensitive to C0 and C1 chemistry and has only minor dependence on H-abstraction by  $\dot{\text{O}}\text{H}$  from isobutene. Davis and Law [156] showed in their work that the isobutene flame speed is lower than that of 1-butene, since methyl branching leads to lowering of burning velocities.

Recently, Movaghar et al. [157] conducted extensive laminar flame speed measurements for a variety of C1–C4 saturated and unsaturated hydrocarbons at high pressures from 8 to 30 atm and unburned gas temperatures ranging from 400 to 520 K, for equivalence ratios of 0.8, 1.0 and 1.3. Two butene isomers, 1-butene and isobutene, as well as ethylene and propene were included as targets in that study.

#### 2.2.4 Pentenes

Laminar flame speeds of three pentene isomers (1-pentene, 2-pentene, 2-methyl-2-butene) were investigated by Cheng et al. [92] over a range of equivalence ratios, initial pressures of 1 – 4 atm and initial temperatures of 353 – 433 K using a constant volume vessel. The results (see Figure 14) show that, similar to C4 alkenes, 1-pentene has the highest flame speed, followed by 2-

pentene and the branched pentene (2-methyl-2-butene) has the slowest flame speed. The laminar flame speeds of these fuels are largely affected by their corresponding adiabatic temperatures and, to a lesser extent, by the oxidation kinetics. As an example of kinetic effects, 2-methyl-2-butene has lower flame speed because it produces H-consuming intermediates and  $\dot{C}H_3$  radicals. The employed chemical kinetic model did a reasonable job in predicting laminar flame speeds except for 2-pentene where the model overestimated the measured value by about 6 cm/sec at stoichiometric condition. Zhong et al. [94] measured laminar flame speeds of 1-pentene/air in a constant volume combustion vessel at initial pressures of 0.1 MPa and 0.3 MPa, initial temperatures of 350 K and 450 K, and equivalence ratios ranging from 0.5 to 1.6.

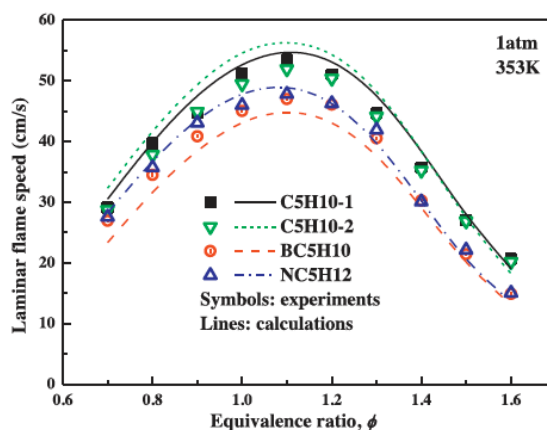


Figure 14. Laminar flame speeds of pentene isomers at 353 K and 1 atm [92].

### 2.2.5 Hexenes

Since the 1951 laminar flame measurements of Gerstein et al. [154] on a number of hydrocarbons, including 1-hexene, there has only been one more recent work on 1-hexene by Fan et al [110]. They measured laminar burning velocity of 1-hexene/air mixtures in a cylindrical combustion vessel at 373 K and a range of pressures (1 – 10 atm). The measured flame speeds (see Figure 15) were modeled quite well by their new kinetic model of 1-hexene consisting of 122 species and 919 reactions. Sensitivity analysis indicated that flame speeds are largely dependent on  $\dot{H} + O_2$  and  $CO + \dot{O}H$  reactions with minor influence from reactions involving allyl radicals.

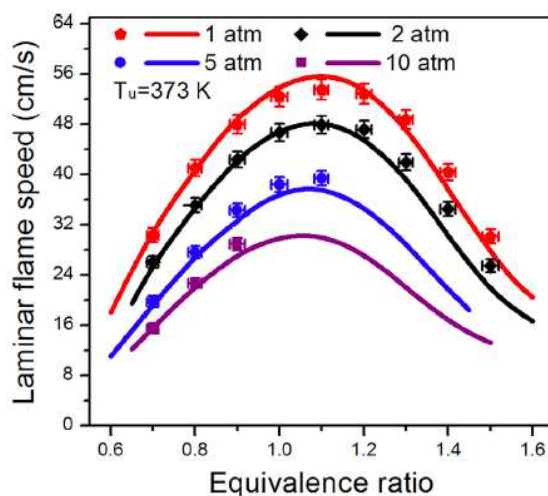


Figure 15. Experimental (symbols) and simulated (lines) laminar flame speeds of 1-hexene/air mixtures at 373 K and 1 – 10 atm [110].

### 2.2.6 Heptenes and higher alkenes

Very few studies investigated the laminar burning velocities of alkenes larger than C<sub>6</sub>. Recently, Mei et al. [114] measured flame speeds of 1-heptene/air in a constant-volume cylindrical vessel at 373 K and a range of pressures and equivalence ratios. Similar to other alkenes, the flame speeds peak near  $\phi = 1.1$ . The authors modified a previous model to improve the prediction of flame speeds of 1-heptene.

Recently, there have been three works which reported laminar flame speeds of diisobutylene isomers. Burning velocities of 2,4,4-trimethyl-1-pentene were measured by Zheng et al. [124] and Hu et al. [120], where Hu et al. [120] covered relatively wider ranges of temperature and pressure. Yin et al. [122] compared the flame speeds of the two isomers of diisobutylene, 2,4,4-trimethyl-1-pentene (JC<sub>8</sub>H<sub>16</sub>) and 2,4,4-trimethyl-2-pentene (IC<sub>8</sub>H<sub>16</sub>). The results showed that IC<sub>8</sub>H<sub>16</sub> has higher flame speed particularly at rich conditions and higher initial temperature (see Figure 16). The two isomers have very similar adiabatic flame temperatures, and, therefore, the difference in their flame speeds is mainly attributed to the different decomposition routes taken by the isomers due to the position of the double bond. The modified model by Yin et al. [122] performed quite well in prediction the experimentally measured flame speeds.

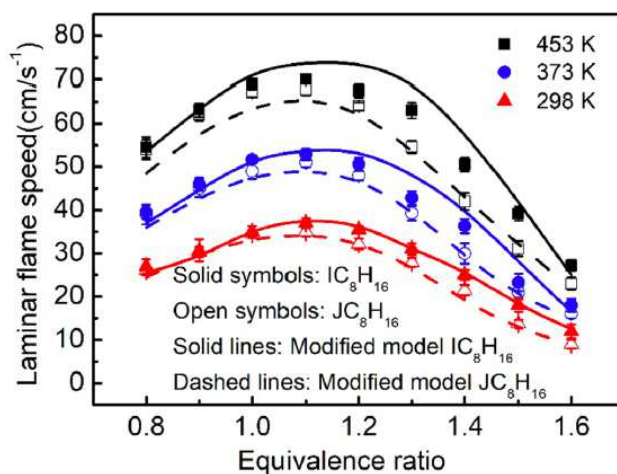


Figure 16. Comparison of laminar flame speeds of the two isomers of diisobutylene at 1 atm [122].

### 2.2.7 1,3-Butadiene

In their pioneering work, Davis and Law [156] compared laminar flame speed of 1,3-butadiene with C4 alkenes and alkanes. The results show that 1,3-butadiene has much higher flame speed compared to 1-butene, iso-butene, iso-butane, and n-butane. It is seen that the more unsaturated the molecule, the higher the flame speed. As discussed before, branching reduces the flame speed and, therefore, iso-butene has a lower flame speed compared to 1-butene.

In their extensive study on 1,3-butadiene, Zhou et al. [67] measured laminar flame speeds of 1,3-butadiene in a constant volume vessel over 295 – 399 K and pressures of 1 and 5 atm. Their detailed kinetic model captured the measured burning velocities quite well over the range of experimental conditions (see Figure 17). Sensitivity analysis revealed that, in addition to usual dependence on C0 and C1 chemistry, flame speed is affected by the reactions of  $\dot{H}$  and  $\dot{O}$  radicals with 1,3-butadiene.

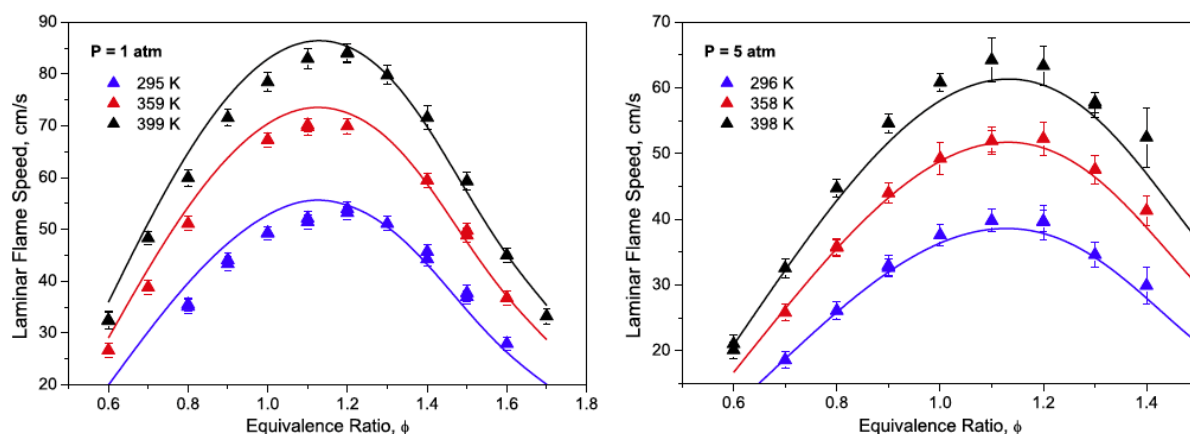


Figure 17. Laminar flame speed of 1,3-butadiene/air at 1 and 5 atm. Lines are simulations [67].

## 2.3 Speciation Measurements

Ignition delay times and laminar flame speeds are important global indicators of fuel reactivity and provide valuable targets for the development and validation of chemical kinetic models. However, these measurements do not give in-depth information about the underlying chemistry. Species measurements during fuel oxidation or pyrolysis, on the other hand, are highly desired in understanding intricacies of the chemical systems by measuring quantities such as fuel consumption rate, radical pool, production and consumption of intermediates and product formation. Such data also place much more stringent targets on the fidelity of chemical models.

Jet-stirred reactors (JSR), low-pressure flames and flow reactors may be coupled to GC-MS, FTIR or TOF-MS to measure intermediate species and products of fuel pyrolysis / oxidation. Recently, a number of groups have utilized synchrotron-based vacuum ultraviolet photon ionization mass spectrometry (SVUV-PIMS) to provide extensive speciation data which have helped tremendously in increasing our understanding of fuel chemistry and improving the fidelity of kinetic models. Literature work on alkene speciation is summarized in Table 1 and discussed here briefly.

### 2.3.1 Ethylene

A large number of speciation studies have been carried out for ethylene oxidation due to it being, perhaps, the most important intermediate of the oxidation of large hydrocarbons. In 1963, Homann et al. [158] measured 15 species in a low-pressure (34 Torr) fuel-rich ethylene flame using molecular-beam mass spectrometry (MBMS). This was followed up by works from Peeters and Mahnen [159], Peeters and Vinckier [160], Harriss et al. [161], Cool et al. [162], Marinov and Malte [163], Wilk et al. [164] and Westbrook et al. [165]. Here, we particularly mention highly detailed and pioneering works of Bhargava and Westmoreland carried out on fuel-lean ( $\phi = 0.75$ ) [166] and fuel-rich ( $\phi = 1.90$ ) [44] ethylene flames in a low-pressure flat-flame burner coupled to MBMS. The authors took special care in measuring temperature profiles and area expansion ratio, and they achieved very good elemental flux balances. They measured concentration profiles of 22 stable and radical species for the lean flame and 42 species for the rich flame. These measurements helped in mapping the ethylene flame structure and provided valuable data to build and refine ethylene kinetic mechanism. In the rich flame, they reported profiles of a number of C6 species including benzene. The authors also derived rate constants for H-abstraction reactions from ethylene by  $\dot{H}$  and  $\dot{O}H$  radicals. Profiles of some stable species are compared in Figure 18 for the fuel-lean and fuel-rich flames. As expected, rich flame results in unburnt CO and H<sub>2</sub> with a more extended reaction zone.

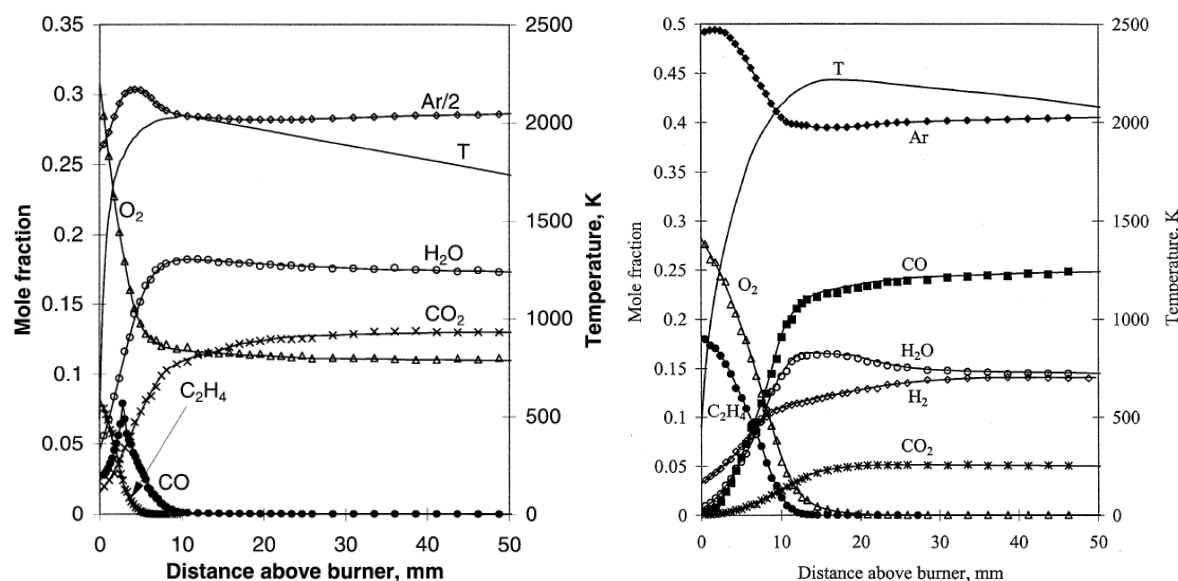


Figure 18. Mole fraction and temperature profiles for lean (left;  $\phi = 0.75$ ,  $P = 30$  Torr) and rich (right;  $\phi = 1.90$ ,  $P = 20$  Torr) ethylene flames [166] [44].

In addition to flame experiments, ethylene oxidation has also been studied extensively in jet-stirred reactors (JSR). Dagaut et al. [167] used their 4-nozzle turbulent jet design of the fused silica JSR to study ethylene oxidation over 900 – 1200 K, 1 – 10 atm and equivalence ratios of 0.15 – 4. The gaseous samples were analyzed using a multicolumn, multidetector gas chromatograph. They assembled a reaction mechanism consisting of 277 reactions and 48 species to model the measured concentration profiles. The simulated profiles did a reasonable job in predicting major species formed during ethylene oxidation. Westbrook et al. [168] used a different design of JSR to examine fuel-lean ethylene/air oxidation at atmospheric pressure and used the measurements to optimize their developed kinetic model. In other JSR speciation works, Jallais et al. [36] studied highly rich ethylene oxidation, while Le Chong et al. [37] investigated the effect of large amounts of  $\text{CO}_2$  and  $\text{H}_2\text{O}$  on ethylene oxidation kinetics.

Flow reactors coupled to GC and/or FTIR have also been used to investigate ethylene oxidation. Carriere et al. [38] studied fuel-rich ( $\phi = 2.5$ ) ethylene oxidation using a variable-pressure turbulent flow reactor over 850 – 950 K and 5 – 10 atm. They combined their data with those of Bhargava and Westmoreland [44] to test various kinetic mechanisms. They concluded that improved multi-channel calculations of the complex  $\dot{\text{C}}_2\text{H}_3 + \text{O}_2$  reaction were necessary to correctly model both low-pressure flame and high-pressure flow reactor experiments. More recently, Lopez et al. [39] extended ethylene oxidation work to very high pressures (60 bar) in a plug-flow laminar flow reactor. They included new ab initio calculations and RRKM analysis of the  $\dot{\text{C}}_2\text{H}_3 + \text{O}_2$  reaction to propose rate coefficients covering the high-pressure regime and noted that the addition reactions of  $\dot{\text{O}}\text{H}$  and  $\text{H}\dot{\text{O}}_2$  to ethylene become very important at high pressures. Their new reaction mechanism adequately modeled the measured species profiles of major species.

### 2.3.2 Propene/Allene

The first detailed study of speciation in propene ( $C_3H_6$ ) oxidation was carried out by Dagaut et al. [45] in a jet-stirred reactor over 900 – 1200 K, 1 – 8 atm and  $\phi = 0.15 - 4$ . In addition to the reactant and product profiles, they also measured intermediate compounds, such as ethylene, ethane, acetaldehyde and ethane. Their newly assembled kinetic mechanism, consisting of 277 reactions and 48 species, performed reasonably well in predicting the measured concentration profiles except for some overprediction of acetaldehyde and ethane. In later JSR investigations, Dagaut et al. [169] and Le Chong et al. [37] studied the reduction of NO by propene and the effect of  $CO_2/H_2O$  on propene oxidation, respectively.

Davis and Law [46] studied propene pyrolysis and oxidation in a flow reactor at 1 atm, 1200 K and three equivalence ratios ( $\phi = 0.7, 1, 1.4$ ). They measured intermediate compounds and species as large as benzene. Their detailed kinetic model consisting of 71 species and 469 reactions did a good job in predicting measured profiles with some deficiencies in acetylene, 1-butene and benzene prediction (see Figure 19).

Recently, Burke et al. [52] put together an extensive multi-university effort to study propene oxidation using JSR and flow reactors. They measured species profiles in JSR experiments targeted at lower dilution levels and lower temperatures (800 – 1100 K) compared to previous works, and they measured large species such as 1,5-hexadiene and benzene. Using two high-pressure flow reactors, they extended propene oxidation studies to higher pressures (6 – 15 atm). The authors used species measurements to optimize / validate rate coefficients of key reactions in the propene system. For example, Figure 20 shows the effect of the allyl +  $HO_2$  reaction rate constant on the species profiles measured in the JSR experiments. The authors proposed a comprehensive model which performed extremely well in modeling a large variety of previous and current propene oxidation experiments.

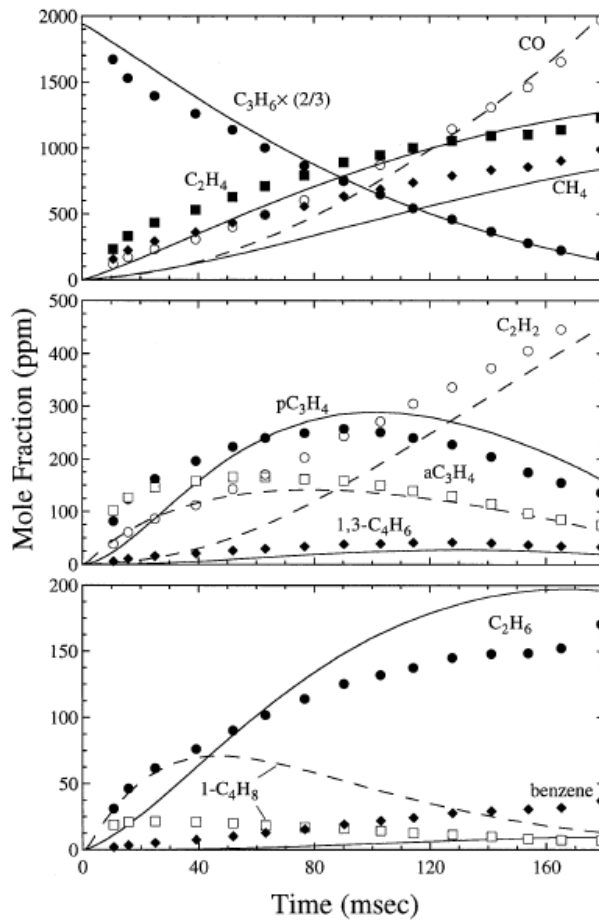


Figure 19. Experimental (symbols) and simulated (lines) mole fraction profiles during propene oxidation in a flow reactor at 1 atm, 1200 K,  $\phi = 1.4$  [46].

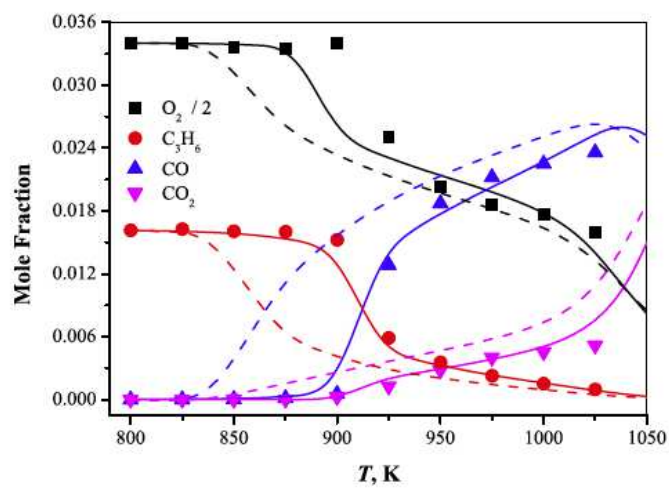


Figure 20. Effect of new (solid line) and old (dash line) rate constant of allyl +  $\text{HO}_2$  reaction rate constant on JSR species profiles at  $p = 1$  atm and  $\phi = 1.07$  [52].

A number of studies investigated the reactivity and kinetic differences of the two isomers of  $C_3H_4$ , namely allene and propyne. Here, we restrict our focus to allene. Pauwels et al. [170] added 1% allene to a low-pressure  $H_2-O_2-Ar$  flame to understand the changes in flame behavior and species formation due to the presence of allene. In addition to sampling-based mass spectrometric measurements, they used laser-induced fluorescence to measure temperature and  $\dot{O}H$  concentration. They observed significant amounts of methane and acetylene as a consequence of the recombination of propargyl which is formed by H-abstraction from allene by H radicals. Curran et al. [143] and Faravelli et al. [171] carried out JSR oxidation of allene over similar conditions and developed detailed kinetic models to describe the reactivity differences with propyne. Recently, Hansen et al. [172] performed isomer-specific speciation study in a low-pressure flame of allene by analyzing the sampled gases with SVUV-MBMS. By varying photon energy, they were able to separate species with the same mass, such as benzene and fulvene ( $m/z = 78$ ), 1-butene and 2-butene ( $m/z = 56$ ), 1,3-butadiene and 1-butyne ( $m/z = 54$ ). Their detailed model predicted the formation of radicals and aromatics quite well (see Figure 21).

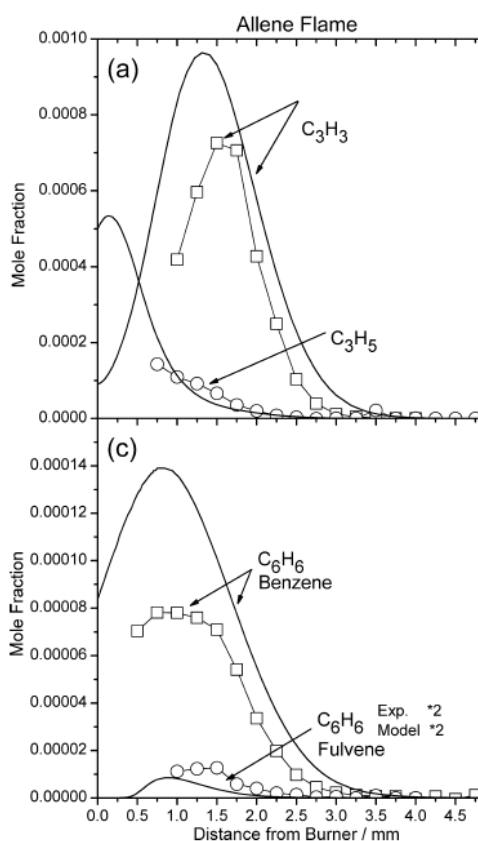


Figure 21. Experimental (symbols) and model predictions (solid lines) in stoichiometric low-pressure allene flame [172].

### 2.3.3 Butenes

The first JSR speciation work on 1-butene was carried out in 1989 by Chakir et al. [84] over 900 – 1200 K, 1 – 10 atm and equivalence ratios of 0.15 – 4. The key intermediate species detected during 1-butene oxidation were ethylene, propene, methane, 1,3-butadiene and ethane. Some

unsaturated compounds were also detected, including *cis*- and *trans*-2-butene. New reactions were added to the previously developed model of ethylene, propene and propane to model the species formed from 1-butene. In two recent works, Fenard et al. [83, 85] studied the oxidation of 1-butene, *cis*- and *trans*-2-butene in a JSR at atmospheric pressure and a range of equivalence ratios. Their newly developed kinetic model, consisting of 201 species and 1787 reactions, performed quite well in predicting their measured species profiles and literature work of Schenk et al. [78] in a low-pressure flame. Sensitivity and reaction pathway analyses showed the importance of resonantly stabilized radicals such as propenyl and butenyl in the butene oxidation system. Figure 22 shows various species measured by Fenard et al. [83] for the oxidation of *cis*-2-butene in a JSR at fuel-rich conditions. The plots show the formation of *trans*-2-butene and relatively large amounts of 1,3-butadiene.

The JSR oxidation of iso-butene was studied by Dagaut and Cathonnet [76], where they described the formation of major and minor species from iso-butene with the help of their speciation data and kinetic model. Previous to this, iso-butene ignition was also studied in a flow reactor by Brezinsky and Dryer [75] at atmospheric pressure. These two works were included in the validation of the recently developed detailed kinetic model of iso-butene by Zhou et al [88].

Recently, Zhang et al. [173] studied the low-temperature oxidation of 1-butene and iso-butene in a JSR at 790 Torr and equivalence ratio of 0.35. With dimethyl ether (DME) doped into the fuel/Ar mixtures, oxidation of the fuels was triggered at temperatures from 500 to 725 K. The SVUV-PIMS technique was employed to quantify the concentration evolutions of the oxidation intermediates.

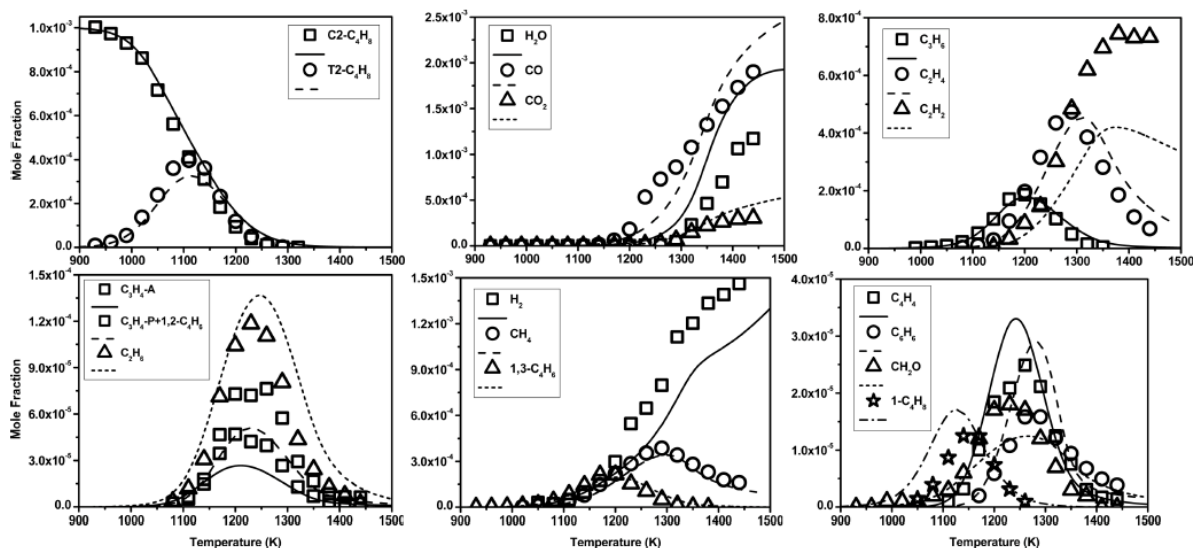


Figure 22. Experimental (symbols) and simulated (lines) concentration profiles during the oxidation of *cis*-2-butene in a JSR at  $\phi = 2$ ,  $p = 1$  atm [83].

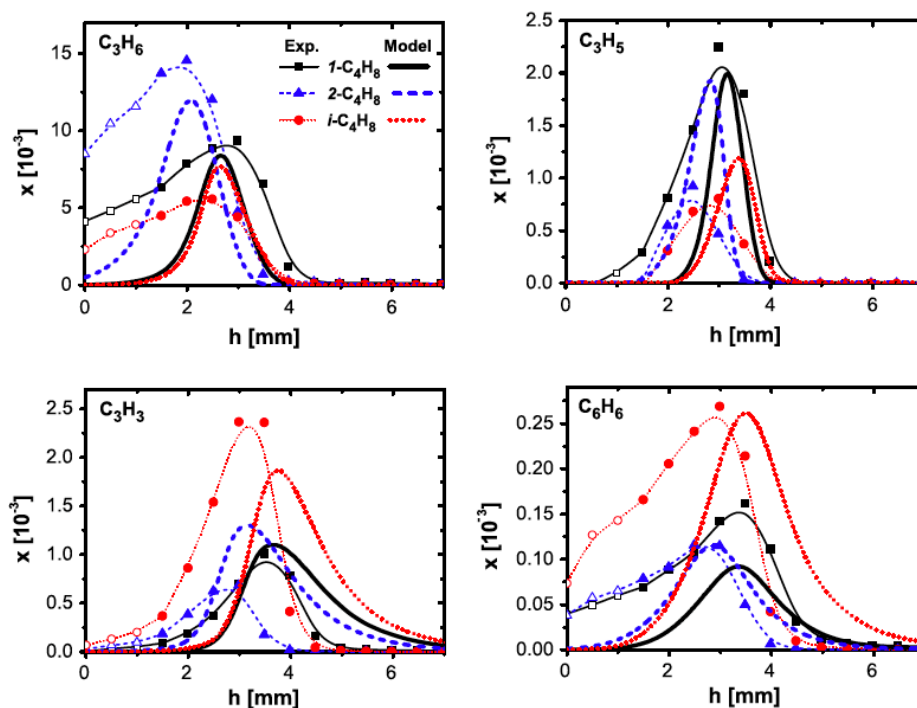


Figure 23. Formation of C3 species in butene low-pressure (40 mbar) flames at  $\phi = 1.7$ . Symbols and thin lines represent experimental data, and simulated profiles are shown as thick lines [78].

#### 2.3.4 Pentenes

The oxidation of 1-pentene was studied by Prabhu et al. [95] in a pressurized flow reactor at 6 atm and 600 – 800 K. They observed that 1-pentene exhibited alkane type behavior with low-temperature reactivity and strong NTC behavior. Their species measurements indicated that H-abstraction reactions leading to allyl radicals are more important than radical addition to the double bond, which is in contrast to smaller alkenes where addition reactions play a larger role. The authors also studied the influence of adding small amounts of nitric oxide to the oxidation behavior of 1-pentene. In another work on 1-pentene, Alatorre et al. [96] carried out speciation measurements in a fuel-rich (C/O ratio of 0.773) low-pressure (50 mbar) flame. At the high-temperatures of their work, they observed that 1-pentene behaves quite similar to propene due to the fact that 1-pentene decomposes mainly to propene and ethylene. They developed a detailed model for 1-pentene which predicted measured species profiles reasonably well. The pyrolysis of 1-pentene under 0.04 and 1 atm at temperatures in the range of 900–1300 K was investigated by Cao et al. [174] in a flow reactor coupled with SVUV-PIMS. In a recent work of Dong et al. [100], the species versus temperature profiles of the oxidations of 1- and 2-pentene at  $\phi = 1.0$ , 1 atm and temperatures in the range of 700–1000 K were measured in a JSR. Westbrook et al. [91] recently studied a branched pentene isomer, 2-methyl-2-butene in a JSR near atmospheric pressure and low to high temperatures (600 – 1100 K). In addition to the major species, they measured large amounts of isoprene, acetylene, propene, iso-butene and a few oxygenated intermediates including C5 cyclic ethers. Based on their observations, they developed a detailed kinetic model to describe the oxidation of pentene isomers from low to high temperatures.

### 2.3.5 Hexenes

There have been three detailed JSR speciation studies on hexene isomers. The first one was carried out by Yahyaoui et al. [105] on 1-hexene over 750 – 1200 K and 10 atm. Measured species profiles were modeled using their newly developed model, consisting of 177 species and 1171 reactions, for 1-hexene oxidation. Among the intermediate compounds, large fractions of ethylene, methane and propene were detected, whereas considerable amounts of 1-butene, 1,3-butadiene, acetylene and benzene were also measured. Battin-Leclerc carried out a detailed speciation study of the three hexene isomers (1-, 2- and 3-hexene) at atmospheric pressure and extended to lower temperatures down to 500 K. In addition to GC measurements, 1-hexene was also studied with tunable synchrotron vacuum ultraviolet photoionization coupled to a TOF-MS. Comparison of the reactivity of these isomers is shown in Figure 24. As observed by Vanhove et al. [102] in their RCM ignition study, JSR data also show that 1-hexene is most reactive in the NTC region followed closely by 2-hexene, whereas 3-hexene does not exhibit noticeable NTC behavior. At higher temperatures (700 – 850 K), 1-hexene is less reactive compared to the other two isomers. At further high temperatures, 1-hexene oxidation results in relatively larger formation of unsaturated compounds (ethylene, propene) and aromatics (benzene). More recently, Meng et al. [109] revisited 1-hexene oxidation in a JSR over wider range of equivalence ratios ( $\phi = 0.5 - 2$ ). In addition to the usual GC sampling, they also used single photon ionization TOF-MS and a cw-cavity-ringdown spectrometer to measure additional species. They updated their previously developed model to provide improved prediction of ignition and species profiles.

Hansen et al. [175] investigated fuel-rich ( $\phi = 2$ ) 1-hexene low-pressure (40 mbar) flat flame by analyzing sampled gases with the help of synchrotron-generated VUV radiation and TOF-MS. They measured a large number of isomer-resolved intermediate compounds and products with special emphasis on benzene and aromatic formation. They observed that benzene is dominantly formed in the 1-hexene flame via H-assisted isomerization of fulvene, whereas propargyl recombination is a minor channel for benzene formation. Fulvene is formed in this flame primarily from the reaction of allyl and propargyl radicals, because large amounts of allyl radicals are formed *via* the unimolecular dissociation of 1-hexene.

In addition to the laminar flame speeds of 1-hexene, Fan et al. [110] also studied the pyrolysis of 1-hexene at 0.04, 0.2 and 1 atm over temperatures from 800 to 1350 K in a flow reactor. SVUV-PIMS and GC-MS were both used to characterize the species concentration profiles as a function of temperature.

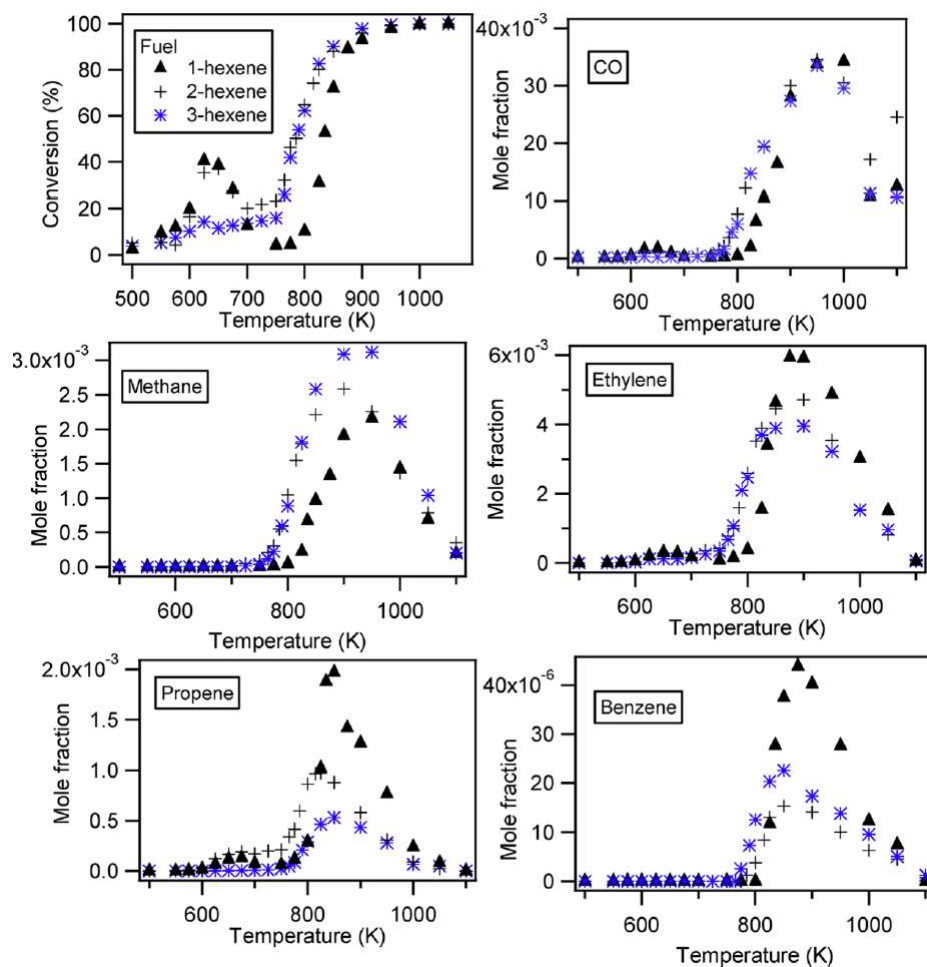


Figure 24. Comparison between three isomers of hexene for fuel conversion and species formation in a JSR at atmospheric pressure and  $\phi = 1$  [101].

### 2.3.6 Higher alkenes

There are only a handful of studies which carried out speciation measurements for alkenes larger than C6. Cao et al. [176] investigated the low-temperature oxidation of 1-heptene in a jet-stirred reactor at temperatures of 450–800 K, 770 Torr and equivalence ratios of 0.5–2.0. The SVUV-PIMS in combination with GC-MS were utilized to identify the intermediate species and quantify their concentrations. Meng et al. [117] studied the oxidation of 1-octene in a jet-stirred reactor at atmospheric pressure and a range of temperatures (500 – 1100 K) and equivalence ratios ( $\phi = 0.25 - 2$ ). A number of oxidation products, such as 1,4-pentadiene, cyclohexene, ethylcyclohexene, aldehydes, 2-octanone and octenal were measured and quantified. A clear NTC behavior was also observed for 1-octene, with the extent of NTC being largest for the fuel-lean conditions (see Figure 25). The authors developed a detailed model which captured the intermediate and high temperature chemistry quite well but underpredicted the NTC activity. They also compared their model predictions with previous speciation measurements of 1-octene oxidation by Piperel et al. [177] and Fridlyand et al. [178].

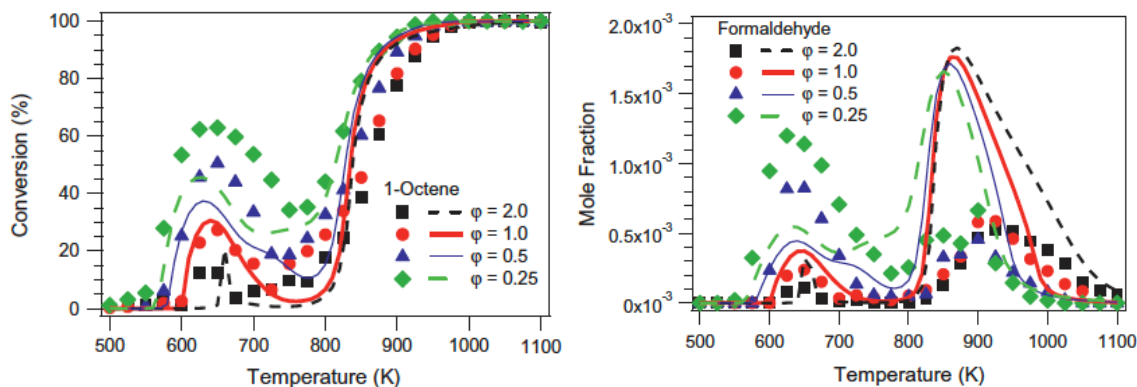


Figure 25. Oxidation of 1-octene in a JSR at atmospheric pressure [117].

In order to study the influence of double bond position on the oxidation of C10 isomers, Fridlyand et al. [118] studied four isomers of decene, namely 1-decene, cis-2-decene, cis-5-decene and trans-5-decene, in a single pulse shock tube at high pressures (40 – 66 bar) and relatively high temperatures (> 850 K). Using GC sampling, they measured few stable intermediates, including ethylene, acetylene, ethane, methane, 1-butene, propene, 1,3-butadiene and benzene. The results showed that as the double bond position moved to the center of the fuel molecule, the reactivity increased. This is consistent with previous high-temperature oxidation works on C6 – C8 alkenes. No appreciable difference was observed between the reactivity of cis and trans isomers of 5-decene.

### 2.3.7 1,3-Butadiene

Most of the studies on 1,3-butadiene have focused on the formation of aromatic species during the oxidation of this diolefin. Cole et al. [61] measured mole fraction profiles of 37 species in a rich ( $\phi = 2.4$ ) low-pressure (20 Torr) 1,3-butadiene flat-flame. The detected species included products, small intermediates and aromatics such as benzene, toluene, phenylacetylene and styrene. They hypothesized that the addition of 1,3-butadienyl radicals to acetylenic species forms aromatic compounds in their studied flame. More recently, Hansen et al. [64] studied benzene formation from a similar low-pressure 1,3-butadiene flame at relatively less fuel-rich conditions ( $\phi = 1.8$ ). This new work concluded that benzene is primarily formed via roughly equal contributions from  $\dot{C}_3H_3 + \dot{C}_3H_3$  and  $i\text{-}\dot{C}_4H_5 + C_2H_2$  reactions. The kinetic model proposed by Hansen et al. [64] performed very well to predict intermediate compounds and aromatics measured in their work as well as by Cole et al. [61]. A detailed JSR speciation study of 1,3-butadiene at high pressures (1 – 10 atm) was carried out by Dagaut and Cathonnet [179]. They measured a number of species and discussed the variation in the importance of benzene formation pathways as a function of temperature and pressure.

Table 1: Literature studies on fundamental combustion experiments of alkenes. (Note that speciation experiments of alkenes pyrolysis are not included in this table because they are rather abundant. Instead, the more reliable and recent pyrolysis data are selected to be discussed in the text)

Author	Year	Fuel Mixtures	Exp. device	Conditions
<b>Ignition delay time</b>				
<b>Ethylene</b>				
Baker et al. [132]	1972	Ethylene/O <sub>2</sub> /Ar	Shock Tube	$\phi = 0.125 - 2$ T= 1058 – 1747 K P= 3, 12 atm
Hidaka et al. [134]	1974	Ethylene/O <sub>2</sub> /Ar	Shock Tube	$\phi = 0.33 - 1$ T= 1400 – 2100 K P= 1382 – 3803 torr
Hidaka et al. [135]	1999	Ethylene/O <sub>2</sub> /Ar	Shock Tube	T= 1100 – 2100 K P= 1.5 – 4.5 atm
Brown et al. [136]	1999	Ethylene/O <sub>2</sub> /N <sub>2</sub> , Ar	Shock Tube	T= 1073 – 2211 K P= 1.3 – 5 atm
Colket et al. [16]	2001	Ethylene/O <sub>2</sub> /Ar	Shock Tube	$\phi = 0.5, 0.75, 1$ T= 1125 - 1410 K P= 5 – 8 atm
Cadman et al. [137]	2002	Ethylene/O <sub>2</sub> /N <sub>2</sub>	Shock Tube	$\phi = 1, 1.5$ T= 800 – 1620K P= 2 – 6 atm
Kalitan et al. [138]	2005	Ethylene/O <sub>2</sub> /Ar/SiH <sub>4</sub>	Shock Tube	$\phi = 0.5, 1.0$ T= 1115–1900 K P= 0.9–3.3 atm
Kumar et al. [43]	2008	Ethylene/O <sub>2</sub> /N <sub>2</sub> /Ar	RCM	$\phi = 1$ T= 580 – 1050 K P= 15 – 50 bar
Penyazkov et al. [34]	2009	Ethylene/O <sub>2</sub> /N <sub>2</sub>	Shock Tube	$\phi = 0.5, 1, 2$ T= 1060 - 1520 P= 5.9 – 16.5 atm
Saxena et al. [33]	2011	Ethylene/O <sub>2</sub> /Ar	Shock Tube	$\phi = 1, 3$ T= 1000 – 1650 K P= 2, 10, 18 atm
Kopp et al. [32]	2014	Ethylene/O <sub>2</sub> /N <sub>2</sub>	Shock Tube	$\phi = 0.3 - 2.0$ T= 1003 - 1401 K P= 1.1 – 24.9 atm
Shao et al. [140]	2018	Ethylene/O <sub>2</sub> /Ar /+ Methane	Shock Tube	$\phi = 1, 2$ T= 950 – 1800 K P= 14 – 60 atm
<b>Propene</b>				
Burcat and Radhakrishnan [141]	1985	Propene/O <sub>2</sub> /Ar	Shock Tube	T= 1274 – 1840 K P = 2.2 – 7.0 atm
Qin et al. [142]	2001	Propene/O <sub>2</sub> /Ar	Shock Tube	$\phi = 0.5 - 2$ T= 1270 – 1820 K P= 0.95 – 4.7 atm
Burke et al. [51]	2015	Propene/O <sub>2</sub> /Ar	Shock Tube, RCM	$\phi = 0.5 - 2$

				T= 722 – 1756 K P= 2, 10, 40 atm
<b>Butenes</b>				
Curran et al. [70]	1992	iso-Butene/O <sub>2</sub> / Ar	Shock Tube	$\phi = 0.1 - 4$ T = 1100 – 1900 K P = 2.2 – 4.6 atm
Zhou et al. [88]	2016	Iso-Butene/O <sub>2</sub> /N <sub>2</sub> , Ar	Shock Tube, RCM	$\phi = 0.3 - 2$ T= 666 – 1650 K P= 1.7 – 50 atm
Heyberger et al. [145]	2002	1-Butene/O <sub>2</sub> /Ar	Shock Tube	$\phi = 0.5, 1, 2$ T= 1200 - 1670 K P= 6.6 – 8.9 atm
Pan et al. [82]	2015	1-Butene/O <sub>2</sub> /Ar	Shock Tube	$\phi = 0.5, 1, 2$ T= 1000 – 1700 K P= 1.2, 4, 16 atm
Li et al. [86]	2017	1-Butene/O <sub>2</sub> /N <sub>2</sub>	Shock Tube, RCM	$\phi = 0.5 - 2$ T= 670 – 1350 K P= 10 – 50 atm
Li et al. [87]	2017	2-Butene/O <sub>2</sub> /N <sub>2</sub>	Shock Tube, RCM	$\phi = 0.5 - 2$ T= 670 – 1350 K P= 10 – 50 atm
<b>Pentenes</b>				
Ribaucour et al. [90] Minetti et al. [89]	1998 1999	1-Pentene/air	RCM	$\phi = 1$ T= 600 – 900 K P= 6 – 9 bar
Touchard et al. [99]	2005	1-Pentene/O <sub>2</sub> /Ar	Shock Tube	$\phi = 0.5 - 2$ T= 1130 – 1620 K P= 7.3 – 9.5 atm
Mehl et al. [10]	2011	1-,2-Pentene/O <sub>2</sub> /N <sub>2</sub> , Ar	Shock Tube	$\phi = 0.5, 1, 2$ T = 990 – 1770 K P = 1, 8 - 11 atm
Cheng et al. [93]	2016	1-Pentene/O <sub>2</sub> /Ar	Shock Tube	$\phi = 0.5 - 2$ T= 1040 – 1880 K P= 1.2 – 10 bar
Dong et al. [100]	2021	1-,2-Pentene/air	Shock Tube, RCM	$\phi = 0.5, 1, 2$ T= 600 – 1300 K P= 15, 30 atm
<b>Hexenes</b>				
Vanhove et al. [102]	2005	1-,2-, 3-Hexene/air	RCM	$\phi = 1$ T= 630 – 850 K P= 6.8 – 8.5 bar
Yahyaoui et al. [107] Yahyaoui et al. [105]	2005 2006	1-Hexene/O <sub>2</sub> /Ar	Shock Tube	$\phi = 0.5, 1, 1.5$ T= 1270 - 1700 P= 2 – 10 bar
Mehl et al. [10]	2011	1-,2-, 3-Hexene/O <sub>2</sub> /N <sub>2</sub>	Shock Tube	$\phi = 1$ T = 990 – 1460 K P = 8.5 – 12.1 atm
Wagnon et al. [149]	2015	1-,2-, 3-Hexene/air	RCM	$\phi = 1$ T= 837 – 1086 K

				P = 11 atm
Yang et al. [111]	2016	3-Hexene/O <sub>2</sub> /Ar	Shock Tube	$\phi = 0.5, 1, 1.5$ T = 1080 - 1640 K P = 1.2 – 10 atm
Yang et al. [148]	2016	1-, 2-Hexene/O <sub>2</sub> /Ar	Shock Tube	$\phi = 0.5 - 2$ T = 1020 – 1900 K P = 1.2 – 10 atm
<b>Heptene and higher alkenes</b>				
Tanaka et al. [113]	2003	1-,2-,3-heptene/air	RCM	$\phi = 0.4$ T = 827 K P = 10 atm
Garner et al. [150]	2011	1-heptene/O <sub>2</sub> /Ar	Shock Tube	$\phi = 0.5 - 1.5$ T = 1250 – 1700 K P = 41.6 bar
Wu et al. [112]	2018	1-, 2-heptene/air	RCM	$\phi = 0.5 - 2$ T = 650 – 950 K P = 15, 23 bar
Tekawade et al. [119]	2017	1-, 5-decene/air	Shock Tube	$\phi = 0.25 - 1$ T = 686 - 1199 K P = 20, 40 bar
Metcalf et al. [123]	2007	Diisobutylene/O <sub>2</sub> /Ar	Shock Tube	$\phi = 0.5 - 1.5$ T = 1200 - 1550 K P = 1, 4 atm
Hu et al. [121]	2017	Diisobutylene/O <sub>2</sub> /Ar	Shock Tube	$\phi = 0.5 - 2$ T = 1350 - 1750 K P = 2 – 10 atm
<b>Allene</b>				
Curran et al. [143]	1996	Allene/O <sub>2</sub> /Ar	Shock Tube	$\phi = 0.5 - 2$ T = 1200 - 1900 P = 2 – 5 bar
Fournet et al. [144]	1999	Allene/O <sub>2</sub> /Ar	Shock Tube	T = 1196 – 1742 K P = 8.5 – 10 atm
<b>Butadiene</b>				
Fournet et al. [144]	1999	1,3-Butadiene/O <sub>2</sub> /Ar	Shock Tube	T = 1180 – 1646 K P = 8.5 – 10 atm
Zhou et al. [67]	2018	1,3-Butadiene/O <sub>2</sub> /Ar,N <sub>2</sub>	Shock Tube, RCM	$\phi = 0.3 - 2$ T = 645 – 1780 K P = 1 – 40 atm
<b>Flame Speed</b>				
<b>Ethylene</b>				
Linnett and Hoare [153]	1948	Ethylene/O <sub>2</sub> /N <sub>2</sub>	Flame tube	
Gerstein et al. [154]	1951	Ethylene /O <sub>2</sub> / N <sub>2</sub>	Flame tube	
Egolfopoulos et al. [41]	1991	Ethylene /O <sub>2</sub> / N <sub>2</sub>	Counterflow burner	$\phi = 0.5 - 2$ T = 298 K P = 0.25 – 3 atm
Davis and Law [156]	1998	Ethylene /O <sub>2</sub> / N <sub>2</sub>	Counterflow burner	$\phi = 0.7 - 1.7$ T = 298 K P = 1 atm

Hirasawa et al. [180]	2002	Ethylene /O <sub>2</sub> / N <sub>2</sub>	Counterflow burner	$\phi = 0.5 - 1.9$ T = 298.
Jomaas et al. [42]	2005	Ethylene /O <sub>2</sub> / N <sub>2</sub>	Dual-chamber	$\phi = 0.6 - 1.8$ P = 1, 2, 5 atm
Kumar et al. [43]	2008	Ethylene /O <sub>2</sub> / N <sub>2</sub>	Counterflow burner	$\phi = 0.5 - 1.4$ T = 298, 360, 400, and 470.
Ravi et al. [181]	2015	Ethylene /O <sub>2</sub> / N <sub>2</sub>	Constant volume vessel	
Huo et al. [155]	2018	Ethylene /O <sub>2</sub> / N <sub>2</sub>	Dual-chamber	$\phi = 0.6 - 1.8$ P = 10 atm
Movaghar et al. [157]	2020	Ethylene/O <sub>2</sub> /N <sub>2</sub>	Spherically expanding flames under constant pressure, Spherically expanding flames under constant volume	$\phi = 0.8, 1, 1.3$ T = 400 – 520 K P = 8 – 30 atm
<b>Propene</b>				
Gerstein et al. [154]	1951	Propene /O <sub>2</sub> / N <sub>2</sub>	Flame Tube	
Davis and Law [156]	1998	Propene /O <sub>2</sub> / N <sub>2</sub>	Counterflow burner	$\phi = 0.7 - 1.7$ T = 298 K P = 1 atm
Davis et al. [46]	1999	Propene /O <sub>2</sub> / N <sub>2</sub>	Counterflow burner	$\phi = 0.7 - 1.7$ T = 298. P = 1 atm
Jomaas et al. [42]	2005	Propene /O <sub>2</sub> / N <sub>2</sub>	Dual-chamber	$\phi = 0.7 - 1.4$ P = 1, 2, 5 atm
Burke et al. [51]	2015	Propene /O <sub>2</sub> / N <sub>2</sub>	Constant volume vessel, Heat flux burner,	$\phi = 0.6 - 1.7$ T = 298 – 398 K P = 1 – 20 atm
Movaghar et al. [157]	2020	Propene/O <sub>2</sub> /N <sub>2</sub>	Spherically expanding flames under constant pressure, Spherically expanding flames under constant volume	$\phi = 0.8, 1, 1.3$ T = 400 – 520 K P = 8 – 30 atm
<b>Butenes</b>				
Gerstein et al. [154]	1951	1-Butene /O <sub>2</sub> / N <sub>2</sub>	Flame tube	
Davis and Law [156]	1998	1-Butene /O <sub>2</sub> / N <sub>2</sub>	Counterflow burner	$\phi = 0.7 - 1.7$ T = 298 K P = 1 atm
Fenard et al. [85]	2015	2-Butene /O <sub>2</sub> / N <sub>2</sub>	Constant volume vessel	$\phi = 0.8 - 1.4$ T = 300 K P = 1 atm
Fenard et al. [83]	2015	1-, 2-Butene/O <sub>2</sub> /Ar	Constant volume vessel	$\phi = 0.8 - 1.4$ T = 300 – 450 K P = 1- 5 atm
Zhao et al. [79]	2015	1-Butene /O <sub>2</sub> / N <sub>2</sub>	Dual-chamber	$\phi = 0.7 - 1.8$ P = 1 – 10 atm
Zhou et al. [88]	2016	Iso-Butene/O <sub>2</sub> /N <sub>2</sub>	Constant volume vessel, Heat flux burner	$\phi = 0.6 - 1.9$ T = 298 – 398 K

				P= 1 atm
Movaghar et al. [157]	2020	1-Butene/O <sub>2</sub> /N <sub>2</sub> Iso-Butene/O <sub>2</sub> /N <sub>2</sub>	Spherically expanding flames under constant pressure, Spherically expanding flames under constant volume	$\phi = 0.8, 1, 1.3$ T = 400 – 520 K P= 8 – 30 atm
<b>Pentenes</b>				
Gerstein et al. [154]	1951	1-Pentene /O <sub>2</sub> / N <sub>2</sub>	Flame tube	
Cheng et al. [92]	2017	1-, 2-Pentene /O <sub>2</sub> / N <sub>2</sub>	Constant volume vessel	$\phi = 0.7 - 1.6$ T= 353 – 433 K P= 1 – 4 atm
<b>Hexenes</b>				
Gerstein et al. [154]	1951	1-Hexene /O <sub>2</sub> / N <sub>2</sub>	Flame tube	
Fan et al. [110]	2016	1-Hexene /O <sub>2</sub> / N <sub>2</sub>	Constant volume vessel	$\phi = 0.7 - 1.5$ T= 373K P= 1 – 10 atm
<b>Heptene and higher alkenes</b>				
Mei et al. [114]	2019	1-Heptene/Air	Constant volume vessel	$\phi = 0.7 - 1.5$ T = 373 K P = 1 – 10 atm
Zheng et al. [124]	2018	Diisobutylene/air	Constant volume vessel	$\phi = 0.6 - 1.5$ T = 400, 450 K P = 1, 3 atm
Hu et al. [120]	2019	Diisobutylene/air	Constant volume vessel	$\phi = 0.7 - 1.6$ T = 298 – 453 K P = 1 – 5 atm
Yin et al. [122]	2019	Diisobutylene/air	Constant volume vessel	$\phi = 0.8 - 1.6$ T = 298 – 453 K P = 1 atm
<b>Butadiene</b>				
		1,3-Butadiene /O <sub>2</sub> / N <sub>2</sub>		
Davis and Law [156]	1998	1 3-Butadiene /O <sub>2</sub> / N <sub>2</sub>	Counterflow burner	$\phi = 0.7 - 1.7$ T = 298 K P = 1 atm
Zhou et al. [67]	2018	1,3-Butadiene /O <sub>2</sub> / N <sub>2</sub>	Constant volume vessel	$\phi = 0.6 - 1.7$ T= 295 – 399 K P= 1 – 5 atm
<b>Speciation Measurements</b>				
<b>Ethylene</b>				
Dagaut et al. [167]	1988	Ethylene/O <sub>2</sub> /N <sub>2</sub>	JSR	$\phi = 0.15 - 4$ T= 900 – 1200 K P= 1 – 10 atm
Westbrook et al. [168]	1988	Ethylene/O <sub>2</sub> /N <sub>2</sub>	JSR	$\phi = 0.36 - 0.48$ T= 1003 – 1253 K P= 1 atm
Marinov and Malte [163]	1995	Ethylene/O <sub>2</sub> /N <sub>2</sub>	JSR	$\phi = 0.086 - 0.103$ T= 1003 – 1253 K P= 1 atm

Wilk et al. [164]	1990	Ethylene/O <sub>2</sub> /N <sub>2</sub>	PFR	$\phi = 2.0$ T= 696 – 718 K P= 0.8 atm
Westbrook et al. [165]	1982	Ethylene/O <sub>2</sub> /N <sub>2</sub>	PFR	$\phi = 0.19, 1.8$ T= 980 – 1120 K P= 1.0 atm
Bhargava and Westmoreland [166]	1998	Ethylene/O <sub>2</sub> /Ar	Flat-flame burner	$\phi = 0.75$ P = 30 Torr
Bhargava and Westmoreland [44]	1998	Ethylene/O <sub>2</sub> /Ar	Flat-flame burner	$\phi = 1.90$ P = 20 Torr
Jallais et al. [36]	2002	Ethylene/O <sub>2</sub> /N <sub>2</sub>	JSR	$\phi = 3 - 10$ T= 773 – 900 K P= 1 atm
Carriere et al. [38]	2002	Ethylene/O <sub>2</sub> /N <sub>2</sub>	Flow reactor	$\phi = 2.5$ T= 850 - 950 K P= 5 – 10 atm
Lopez et al. [39]	2009	Ethylene/O <sub>2</sub> /N <sub>2</sub>	Flow reactor	T= 600 – 900 K P= 60 bar
Le Cong et al. [37]	2010	Ethylene/O <sub>2</sub> /N <sub>2</sub> / , CO <sub>2</sub> , H <sub>2</sub> O	JSR	$\phi = 0.5 - 2$ T= 950 – 1450 K P= 1 atm
<b>Propene</b>				
Dagaut et al. [45]	1988	Propene/O <sub>2</sub> /N <sub>2</sub>	JSR	$\phi = 0.15 - 4$ T= 900 – 1200 K P=1 – 8 atm
Davis and Law [46]	1999	Propene/O <sub>2</sub> /N <sub>2</sub>	Flow Reactor	$\phi = 0.7, 1, 1.4$ T= 1200 K P= 1 atm
Dagaut et al. [169]	2000	Propene/O <sub>2</sub> /N <sub>2</sub>	JSR	$\phi = 0.75 - 2$ T= 1100 – 1450 K P= 1 atm
Le Cong et al. [37]	2010	Propene/O <sub>2</sub> /N <sub>2</sub> / , CO <sub>2</sub> , H <sub>2</sub> O	JSR	$\phi = 0.5 - 2$ T= 950 – 1450 K P= 1 atm
Burke et al. [52]	2014	Propene/O <sub>2</sub> /N <sub>2</sub>	JSR Flow Reactor	$\phi = 0.64 - 2.19$ T= 800 – 1100 K P= 1 – 15 atm
<b>Butenes</b>				
Chakir et al. [84]	1989	1-Butene/O <sub>2</sub> /N <sub>2</sub>	JSR	$\phi = 0.15 - 4$ T= 900 – 1200 K P= 1 – 10 atm
Schenk et al. [78]	2013	1-, 2-Butene, iso-butene/O <sub>2</sub> /Ar	Flat-flame burner	$\phi = 1.7$ P = 40 mbar
Fenard et al. [85]	2015	Trans-2-Butene/O <sub>2</sub> /N <sub>2</sub>	JSR	$\phi = 0.5 - 2$ T= 900 – 1450 K P= 1 atm
Fenard et al. [83]	2015	1-, cis-2-Butene/O <sub>2</sub> /Ar	JSR	$\phi = 0.25 - 2$ T= 900 – 1440 K P= 1 atm
Brezinsky and Dryer	1986	iso-Butene/O <sub>2</sub> /N <sub>2</sub>	Flow reactor	$\phi = 0.47$

[75]				T= 1085 K P= 1 atm
Dagaut and Cathonnet [76]	1998	iso-Butene/O <sub>2</sub> /N <sub>2</sub>	JSR	$\phi$ = 0.2 – 2 T= 800 – 1230 K P= 1 – 10 atm
Zhang et al. [173]	2021	1-, iso-Butene/DME/O <sub>2</sub> /Ar	JSR	$\phi$ = 0.35 T= 500 – 725 K P= 790 Torr
<b>Pentenes</b>				
Prabhu et al. [95]	1996	1-Pentene /O <sub>2</sub> /N <sub>2</sub>	Flow reactor	$\phi$ = 0.4 T= 600 – 800 K P= 6 atm
Alatorre et al. [96]	2001	1-Pentene /O <sub>2</sub> /Ar	Flat-flame burner	P = 50 mbar
Westbrook et al. [91]	2015	2-methyl-2-butene/O <sub>2</sub> /He	JSR	T= 600 – 1100 K P= 800 Torr
Dong et al. [100]	2021	1-, 2-Pentene/O <sub>2</sub> /N <sub>2</sub>	JSR	$\phi$ = 1 T= 700 – 1100 K P= 1 atm
<b>Hexenes</b>				
Yahyaoui et al. [105]	2006	1-Hexene /O <sub>2</sub> /Ar	JSR	$\phi$ = 0.5, 1, 1.5 T= 750 – 1200 K P= 10 bar
Hansen et al. [175]	2010	1-Hexene /O <sub>2</sub> /Ar	Flat-flame burner	$\phi$ = 2 P = 40 mbar
Battin-Leclerc et al. [101]	2014	1-, 2-, 3-Hexene /O <sub>2</sub> /Ar, He	JSR	$\phi$ = 1 T= 500 – 1100 K P= 1.07 bar
Meng et al. [109]	2017	1-Hexene /O <sub>2</sub> /He	JSR	$\phi$ = 0.5 - 2 T= 500 – 1100 K P= 1 atm
<b>Higher alkenes</b>				
Cao et al. [176]	2021	1-Heptene/O <sub>2</sub> /Ar	JSR	$\phi$ = 0.5, 1, 2 T= 450 – 800 K P= 770 Torr
Meng et al. [117]	2017	1-Octene/O <sub>2</sub> /He	JSR	$\phi$ = 0.25 – 2 T = 500 – 1100 K P = 1 atm
Fridlyand et al. [118]	2015	1-,cis-2-,cis-5, trans-5 decene /O <sub>2</sub> /Ar	Shock Tube	$\phi$ = 1 T = 850 - 1500 K P = 40 – 66 bar
<b>Allene</b>				
Pauwels et al. [170]	1995	Allene /H <sub>2</sub> /O <sub>2</sub> /Ar	Flat-flame burner	$\phi$ = 1.5 P = 25 Torr
Curran et al. [143]	1996	Allene/O <sub>2</sub> /N <sub>2</sub>	JSR	$\phi$ = 0.2 - 2 T= 800 – 1260 K P= 1 – 10 bar
Faravelli et al. [171]	2000	Allene /O <sub>2</sub> /N <sub>2</sub>	JSR	$\phi$ = 0.2 - 2 T= 800 – 1200 K P= 1 – 10 bar
Hansen et al. [172]	2009	Allene /O <sub>2</sub> /Ar	Flat-flame burner	$\phi$ = 1

				P = 25 Torr
<b>Butadiene</b>				
Cole et al. [61]	1984	1,3-Butadiene /O <sub>2</sub> /Ar	Flat-flame burner	$\phi = 2.4$ P = 20 Torr
Dagaut and Cathonnet [179]	1998	1,3-Butadiene /O <sub>2</sub> /N <sub>2</sub>	JSR	$\phi = 0.25 - 2$ T = 750 – 1250 K P = 1 – 10 atm
Hansen et al. [64]	2009	1,3-Butadiene /O <sub>2</sub> /Ar	Flat-flame burner	$\phi = 1.8$ P = 30 Torr

### 3. Chemical kinetics of alkene combustion

#### 3.1 The molecular structure of alkenes

Before considering important reaction classes and comprehensive chemical kinetic models for alkenes oxidation, we should first look at the structural features of alkenes that distinguish them from other fuels and how those features in turn affect their kinetic behavior during combustion. Alkenes contain a C=C double bond which results in different thermochemical and reaction kinetic properties as compared to alkanes. The following effects need to be paid special attention to when we discuss the kinetics of alkenes oxidation. *First*, addition reactions to the double bond with different radicals and atoms at different temperatures are crucial in determining the reactivity of alkenes. *Second*, the presence of weak allylic C–H or C–C bonds makes the formation of allylic radicals in alkenes dominant through the entire temperature range and hence their chemistry needs to be carefully considered. *Third*, the number and type of allylic radicals changes along with the position of the C=C double bond, therefore, the subsequent chemistry needs to be distinguished. These unique features provide interesting discussion points with regard to the combustion chemistry of alkenes.

The molecular structures of alkenes are routinely determined at the chemically-accurate G4 [182] and CBS-QB3 [183] levels of electronic structure theory using Gaussian 09 [184] to identify the most stable conformers and then to calculate bond dissociation energies (BDEs). The G4 [182] and CBS-QB3 [183] composite methods are computationally less expensive but still able to predict 0 K formation enthalpies in reasonable accuracy [185-188], hence they were employed in the extensive BDE calculations for the C–H and C–C bonds in a series of C<sub>2</sub>–C<sub>8</sub> alkenes as shown in Figure 29. Taking the comparison between *n*-pentane and *l*-pentene, shown in Figure 26 as an example, it can be seen that the bond dissociation energy for the secondary allylic C–H bond is about 13.0 kcal mol<sup>-1</sup> lower than that for the normal secondary C–H bond, which makes the formation of allylic radicals in *l*-pentene oxidation very competitive. Moreover, the subsequent chemistry for the formed allylic radical in *l*-pentene oxidation and alkyl radical in *n*-pentane is also quite different. It is well known that in alkane oxidation, the first and second molecular oxygen addition to the alkyl radicals and related isomerization reactions are the main chain branching reaction pathways providing the low temperature radical pools, whilst this is not the same for alkenes. As shown in Figure 26, the stabilization energy for the formed C–OO bond

in *n*-pentane is 36.1 kcal mol<sup>-1</sup> at the G4 level, which makes the R $\dot{O}_2$  radical strong enough to proceed to the subsequent isomerization and second O<sub>2</sub> addition reactions. Alternatively, the bond for *1*-pentene is only 20.4 kcal mol<sup>-1</sup>, not strong enough to undergo the subsequent low temperature chemistry as in alkanes, and the R<sub>A</sub> $\dot{O}_2$  radical is likely to dissociate back to  $\dot{R}_A + O_2$ .

Detailed potential energy surfaces for the formation of R $\dot{O}_2$  radicals in both 1-pentene and *n*-pentane and their subsequent isomerization reaction pathways are shown in Figure 27 (a) and (b), respectively. As shown in Figure 27 (a), the formed R<sub>A</sub> $\dot{O}_2$  lies only 20.4 kcal mol<sup>-1</sup> lower in energy than the reactants and the isomerization of R<sub>A</sub> $\dot{O}_2$  through a six-membered ring transition state to form the Q<sub>A</sub>OOH radical holds the lowest energy barrier which lies 4.5 kcal mol<sup>-1</sup> higher than the reactants. Apart from the higher energy, the formed six-membered ring structure in the transition state locks the rotation of three hindered rotors, hence decreasing the entropy of the reaction process which ultimately decreases the rate constant of this reaction channel. Taking these two effects into consideration, the formed R<sub>A</sub> $\dot{O}_2$  intermediate in alkene oxidation would more likely dissociate back to the allylic radical + O<sub>2</sub> rather than take the isomerization pathways of alkanes. Therefore, the reactions of  $\dot{R}_A$  radicals with molecular oxygen are not found to be of particular importance in determining the fuel reactivity. However, as shown in Figure 27 (b), the formed R $\dot{O}_2$  intermediate lies 36.1 kcal mol<sup>-1</sup> lower than the reactants and the subsequent isomerization products of R $\dot{O}_2$  produced through six- and five-membered ring transition states lie 11.4 and 3.0 kcal mol<sup>-1</sup> lower than the reactants, respectively. Therefore, the system will follow the low temperature chain branching pathways known for alkanes. This is one of the major differences between alkanes and alkenes originating from the effect of the C=C double bond functional group.

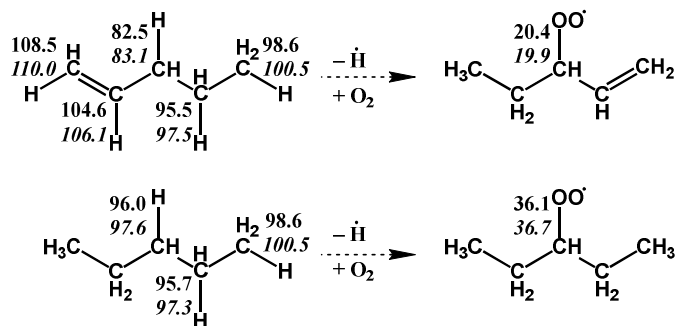


Figure 26. C-H bond dissociation energy for 1-pentene and *n*-pentane and that for C-OO in their ROO radicals calculated at G4 and CBS-QB3 (in *italic*) levels of theory calculated in this work.

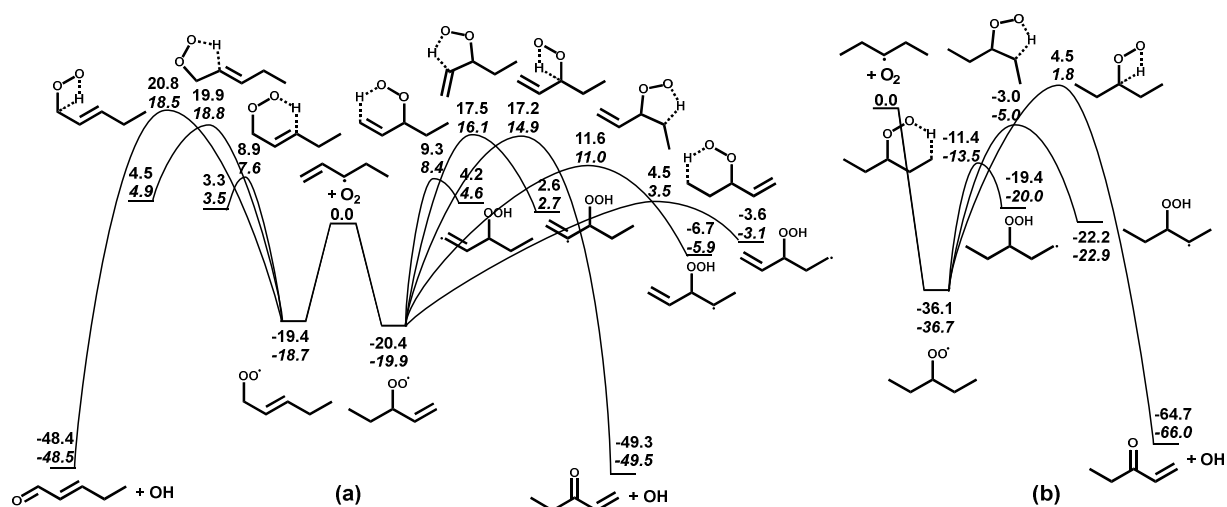


Figure 27. Potential energy surface for the isomerization reactions of  $R\dot{O}_2$  radicals in (a) 1-pentene representing alkenes and (b) 1-pentane representing alkanes. Energy barriers are obtained at the G4 and CBS-QB3 (in *italic*) levels of theory calculated in this work.

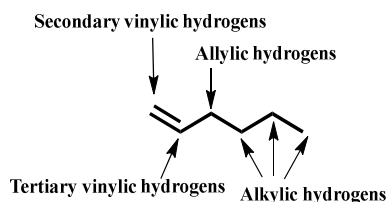
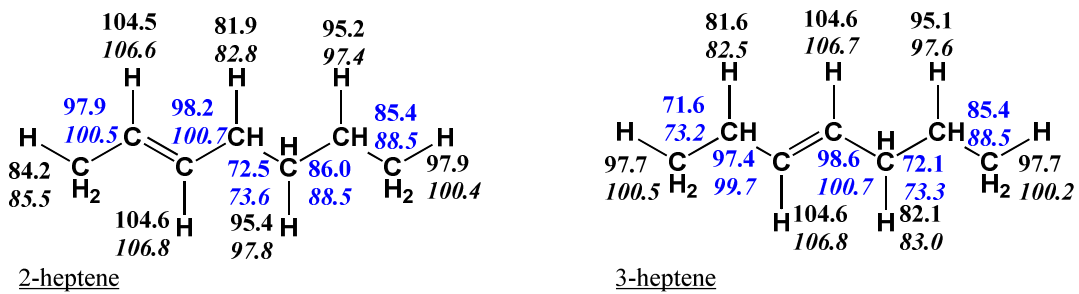
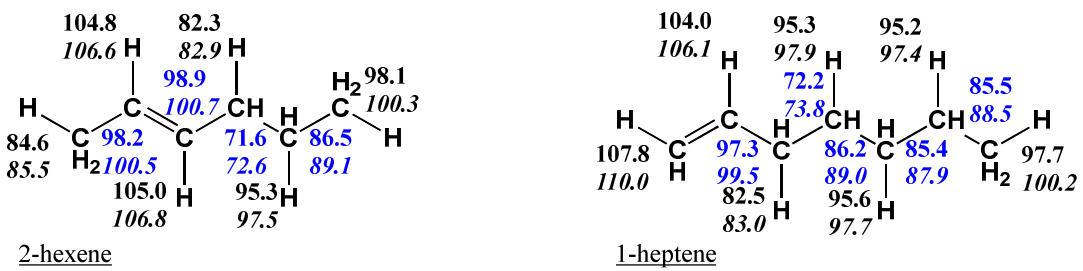
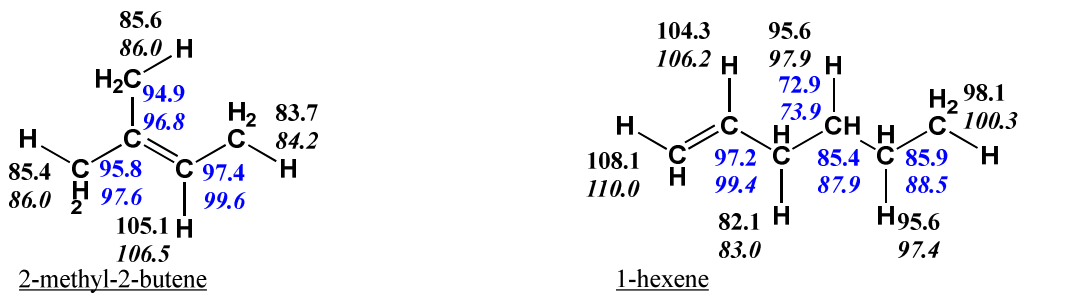
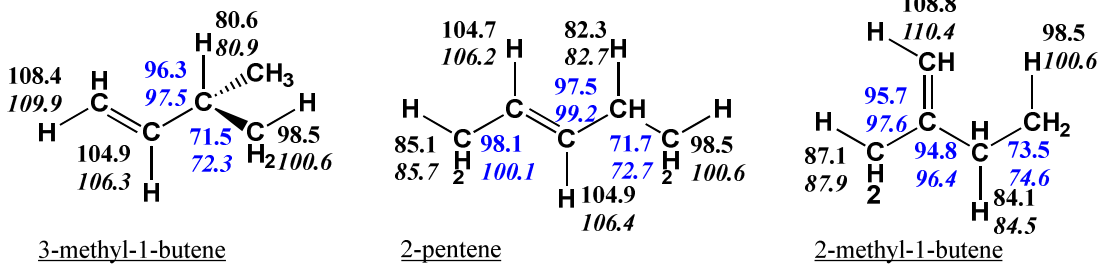
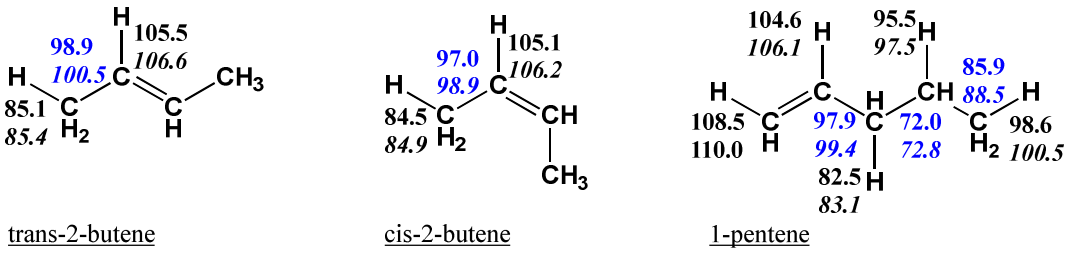
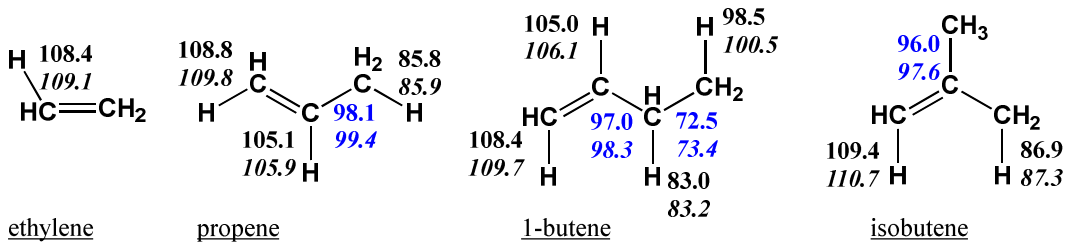


Figure 28. Hydrogen types in alkenes, taking 1-hexene as an example.

Hydrogen types in alkenes are defined in Figure 28 which takes 1-hexene as an example. Extensive calculations for the bond dissociation energies of the C–H and C–C bonds in alkenes, including C2 to C8 species discussed in the subsequent sections, have been carried out at both G4 and CBS-QB3 levels of theory and the results are shown in Figure 29. The results calculated here are in reasonable agreement with the available measured values collected by Luo [189], with BDEs for the C–H bonds all within  $\sim 2.0$  kcal/mol, and BDEs for the C–C bonds all within  $\sim 2.5$  kcal/mol except for a very few cases up to 3.0 kcal/mol. The allylic C–C bonds always hold the lowest BDE of  $\sim 72.0$  kcal/mol, and consistently weaker than the alkylic C–C bonds by  $\sim 13.0$  kcal/mol and the vinylic C–C bonds by  $\sim 23.5$  kcal/mol. This indicates that among the C–C bonds in alkenes, the allylic ones have the highest tendency to be broken during the high temperature pyrolysis regimes. Secondary vinylic C–H bond holding the strongest BDE of  $\sim 108.5$  kcal mol $^{-1}$  is the most difficult one to be cleaved, followed by the tertiary vinylic C–H bond with BDE of  $\sim 104.8$  kcal mol $^{-1}$ . Allylic C–H bonds having the weakest BDEs are the easiest to be cleaved. BDEs for the allylic C–H bonds follow the order of primary ( $\sim 85.1$  kcal mol $^{-1}$ ), secondary ( $\sim 82.2$  kcal mol $^{-1}$ ), and then the weakest tertiary C–H bonds ( $\sim 80.6$  kcal mol $^{-1}$ ). It should be noted that BDEs of allylic C–H bonds are consistently weaker than their corresponding C–H bond types in alkanes by  $\sim 13.0$  kcal mol $^{-1}$ . The presence of the functional group with a C=C double bond influences only BDE of the allylic C–C and C–H bonds. The C–H bonds next to the allylic carbon in the opposite position from the C=C double have BDE typical for alkylic hydrogen. It also needs to be highlighted that the BDEs of the two types of vinylic C–H bonds in 1,3-

butadiene are all very high such that hydrogen atom abstraction reactions are less likely to occur as compared to alkenes with allylic hydrogen atoms. Therefore, addition reactions of different radicals and atoms onto the C=C double bond in 1,3-butadiene are more favored. This is also one of the main differences between mono-alkenes and dienes which do not have allylic hydrogen atom.

Furthermore, the presence of C=C double bond in alkenes can have several other interesting effects. In the allylic alkenyl radicals,  $\dot{R}_A$ , produced from H-atom abstraction reactions, the radical site is delocalized among the two carbon atoms adjacent to the  $\beta$  carbon atom which leads to a multiplication of products in subsequent radical recombination reactions. For example, in the oxidation of 1- and 2-butene [86, 87], the recombination reactions of hydroperoxyl ( $\dot{H}O_2$ ) and 1-methylallyl ( $\dot{C}_4H_7$ ) radicals significantly govern fuel reactivity at low to intermediate temperatures, where two possible  $R_AOOH$  adducts with  $\dot{H}O_2$  either adding to the central or terminal carbon atom should be considered, as a result of the mesomerism of  $\dot{C}_4H_7$  radical (Figure 36). For higher alkenes ( $\geq C_5$ ), it is possible that fuel molecules directly split into two smaller alkenes through retro-ene elimination pathways, surmounting a pericyclic transition state. For example, 1-hexene can undergo retro-ene reaction to form two propene molecules, which was found to be the major consumption pathway for 1-hexene at low temperature oxidation conditions [105, 107].



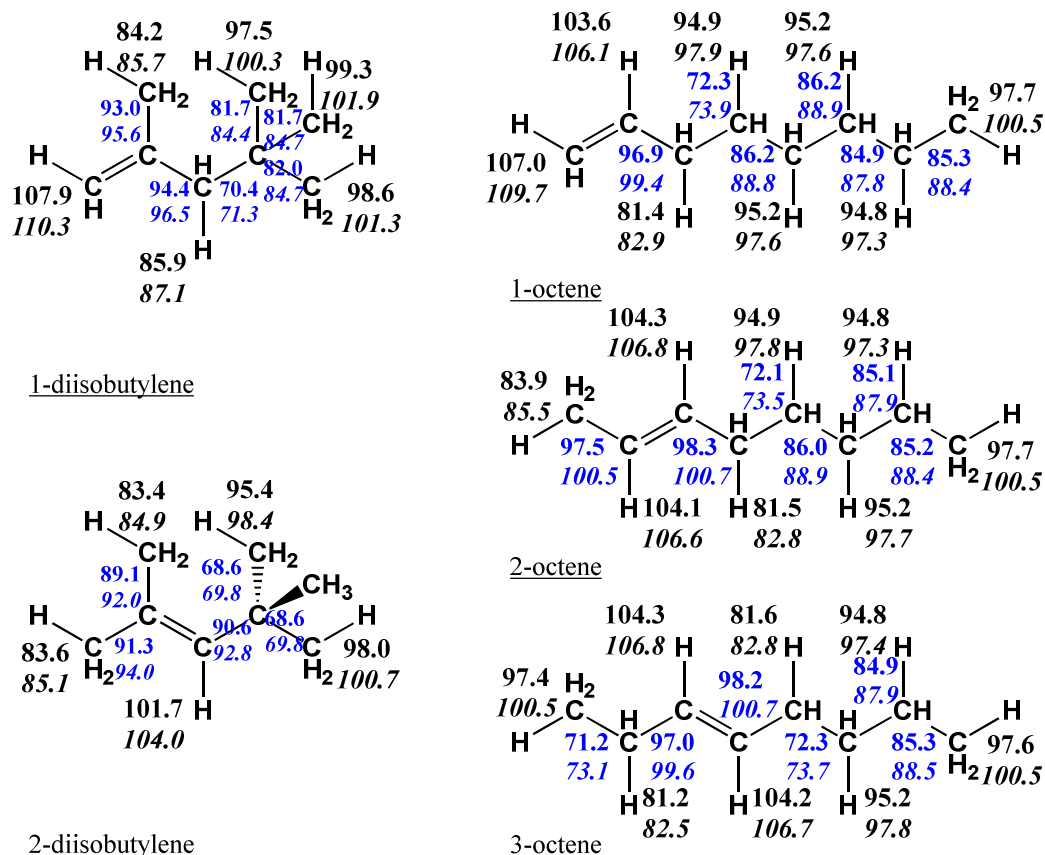


Figure 29. Bond dissociation energies for C-H (in black) and C-C bonds (in blue) in C<sub>2</sub>-C<sub>8</sub> alkenes (kcal mol<sup>-1</sup>) calculated at G4 and CBS-QB3 (in *italic*) levels of theory calculated in this work.

### 3.2 Reaction mechanism, reaction classes, and rate rules

Facilitated by the appearance of stiff kinetic equation solvers in 1970s, numerical simulations of the combustion system were able to deal with larger reaction mechanisms including varied time scales [190]. Since 1980s when Westbrook and Dryer [191, 192] put forward the concept of the hierarchical development of kinetic mechanism for hydrocarbon fuels, the combustion research community has seen dramatic advances in chemical kinetic modeling during the last several decades. In the reviews of Westbrook et al. [190] and Simmie [193], as well as a more recent review by Curran [194], brief history of the development of chemical kinetic mechanisms and the massive previous efforts in chemical kinetic modeling for hydrocarbon fuels were presented.

Experimental measurements and mechanism studies for C<sub>2</sub>-C<sub>10</sub> alkenes, including both low and high temperature kinetic schemes, covering ethylene [25-44], propene [37, 45-52], 1,3-butadiene [53-67], isomers of butene [68-88], pentene [13, 89-100], hexene [10, 98, 101-111], heptene [103, 112-114], octene [115-117], decene [118, 119] and 2,4,4-trimethyl-1-pentene [120-124] have been taken into consideration in the following discussion. The detailed reaction mechanism for C<sub>2</sub>-C<sub>4</sub> alkenes is compiled in a hierarchical way which starts from the oxidation of small hydrocarbons and then continues by sequentially adding reaction mechanisms for larger alkenes. The 1,3-butadiene mechanism used here is the recently published AramcoMech 3.0 [67] with base C<sub>3</sub>-C<sub>4</sub> alkenes oxidation mechanism of AramcoMech 2.0 [51, 52, 87, 88, 195]. The base

C0-C2 hydrocarbon oxidation mechanism used here is from the published AramcoMech 1.3 [25], with the H<sub>2</sub>/CO/O<sub>2</sub> sub-mechanism based on the work of K eromn es et al. [196]. All of those mechanisms were developed at the Combustion Chemistry Centre of National University of Ireland Galway (NUIG). For higher alkenes, few combustion models are available for the two pentene isomers [92-94, 99, 100] of 1-pentene and 2-methyl-2-butene [91, 93] at high temperatures to simulate their high temperature ignition delay time and laminar flame speeds and also for three hexene isomers [10, 98, 101-111], 1-hexene, 2-hexene and 3-hexene, at both low-temperature (NTC reactivity) and high-temperature ranges (laminar flame speeds), which can be used to simulate their combustion phenomena under those conditions. Thus, the mechanism for C2-C4 alkenes from AramcoMechs [25, 51, 52, 67, 87, 88, 195], 1-pentene by Touchard et al. [98, 99], 2-methyl-2-butene by Westbrook et al. [91], and linear hexene isomers by Battin-Leclerc et al. [101, 109] at low and intermediate temperatures and from Mehl et al. [10] at high temperatures are chosen for the present analysis and discussion.

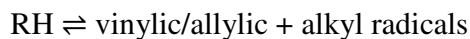
The important reaction classes for alkenes oxidation are discussed below in detail. Figure 30 presents a generalized scheme for the primary mechanism in the oxidation of alkenes including important reaction classes over different temperature ranges, where temperature ranges for low-, intermediate- and high-temperature chemistry can be roughly defined as 600–850 K, 850–1200 K and >1200 K [194]. Important reaction classes determining the reactivity of alkene oxidation under different temperatures are assembled in Scheme 1, in sequence along the oxidation reaction from fuel to fully oxidized products.

The most important point here is that all of these fuel consumption reaction pathways contribute significantly to oxidation of alkenes in some or all of the temperature ranges relevant for practical combustion systems. Omitting any of these will severely limit the predictive capability of the kinetic mechanism. In addition to the completeness of possible reaction pathways, assigning rate parameters to each elementary reaction pathway with sufficient accuracy is also crucial. The underlying uncertainty in rate constants, which may be determined from experimental measurements, theoretical kinetics or estimations on the basis of rate rules, is one of the major obstacles to the *a priori* prediction for combustion properties of a fuel [197]. Due to improved algorithms and increased computational resources, theoretical reaction kinetics calculation has been routinely employed in the quantitative determinations of elementary reaction rate constants in the last few decades, with the accuracy of high-level *ab initio* calculations often rivals that of direct measurements [185, 198]. The global uncertainties in the predicted phenomenological rate constants arise from the propagation of parametric uncertainties. Several case studies gave some qualitative and quantitative insights into the uncertainties in theoretical kinetic calculations. Goldsmith et al. [199] carried out uncertainty analysis for the master equation calculation of *n*-propyl + O<sub>2</sub> reaction system using a random sampling high-dimensional model representation (HDMR) approach. The fundamental parameters, including reaction barriers, vibrational frequencies, collisional energy transfer parameters and tunneling corrections, were quasi-randomly sampled within their uncertainty range to obtain the frequency distributions of the predicted rate constants. They found that rate constant values distributed at 3 $\sigma$  variance limits typically differ from the most frequent ones by a factor of 4–6, as a result of the pre-set uncertainties in the underlying parameters. Generally, the predicted rate constants for



### 3.2.1 Reaction class 1: unimolecular decomposition of alkenes

Bond dissociation reactions can happen in the alkenes pyrolysis. Depending on the different types of C–H and C–C bonds present in alkenes, the pyrolysis reaction process can be composed of the following reaction classes



This reaction class may be important in determining the laminar flame speeds for alkene/air mixtures. Theoretical or experimental investigations on the rate constants of this reaction class are quite limited in the literature, and Tsang [202] recommended the rate constants for propene pyrolysis in the recombination direction. A retro-ene/molecular elimination reaction which involves an intramolecular hydrogen shift reaction coupled with dissociation is also one of the reaction classes likely to happen in alkenes pyrolysis [98, 104]. For instance, Touchard et al. [98] stated such reaction pathway for 1-hexene pyrolysis leads to two propene molecules.

### 3.2.2 Reaction class 2: H-atom abstraction from alkenes

In alkenes, H atoms can be characterized as allylic, secondary and tertiary vinylic, as well as primary, secondary, and tertiary hydrogens. The rate constant for H-atom abstraction depends on the radical species and the type of H atom being abstracted. As shown previously, C–H bond in the secondary vinylic moiety is the most difficult to abstract, followed by the tertiary vinylic H atoms, while the allylic H atoms have the weakest bonds and are most easily abstracted. The rest of the hydrogen atoms follow the same order as in alkanes, so that the primary C–H bond is the strongest followed by the secondary one, and the tertiary C–H bond is the weakest.

Hydrogen atom abstraction reactions are one of the primary means by which alkenes are consumed in combustion environments. A variety of small radical species (*e.g.*,  $\dot{\text{H}}$ ,  $\dot{\text{O}}\text{H}$ ,  $\text{H}\dot{\text{O}}_2$ ,  $\ddot{\text{O}}$ ,  $\text{CH}_3\dot{\text{O}}_2$ ,  $\text{CH}_3\dot{\text{O}}$ ,  $\dot{\text{C}}\text{H}_3$ ,  $\dot{\text{C}}_2\text{H}_5$ ) and stable molecule (*e.g.*,  $\text{O}_2$ ) can abstract hydrogen atoms from alkenes. As the allylic C–H bonds are the weakest C–H bonds in alkenes, the formation of the resonantly stabilized radicals is generally dominant and they play a very important role in the entire combustion temperature range.

With relatively low barriers, H-atom abstraction by  $\dot{\text{O}}\text{H}$  radical from the allylic sites consumes the reactive  $\dot{\text{O}}\text{H}$  radical to form a resonance stabilized radical, and thus inhibits the reactivity through the entire combustion temperature range. Because of this, the rate constant for this reaction is particularly important for simulating alkenes reactivity from 500 to 2000 K. Farooq and his group has carried out a series of measurements on the kinetics of this important reaction class [203-205].

H-atom abstraction by molecular oxygen also plays an important role in high temperature oxidation of alkenes which forms allylic and  $\text{H}\dot{\text{O}}_2$  radicals as a chain branching pathway to promote reactivity. H-atom abstraction reactions by molecular oxygen have been measured for propene [206] and isobutene [207] in a relatively narrow temperature range. The lack of direct measurements across the entire combustion temperatures range thus requires application of computational theory and estimation methods to determine the appropriate rate coefficients for these reactions. Very recently, Zhou et al. [208] carried out a series of investigations on H atom

abstraction by molecular oxygen from alkene, furan, and alkylbenzene families covering the primary, secondary, tertiary, and super secondary allylic hydrogen atoms. Conventional transition state theory with Eckart tunneling corrections was used to calculate the rate constants. The implications of the rate constants for combustion modeling of oxidation of different fuels have also been considered in this work and it provides a first systematic study of one of the key initiation reactions for compounds containing allylic hydrogen atoms.

### 3.2.3 Reaction classes 3 and 4: vinylic and alkenyl radical decomposition and isomerization

At high temperatures (e.g., above 1000 K) the radicals formed including allylic, secondary, tertiary vinylic and alkenyl radicals can undergo unimolecular decomposition through  $\beta$ -scission reactions. In these reactions, the bond in  $\beta$  position with respect to the radical site breaks to form unsaturated species with two double bonds (e.g., allene, 1,3-butadiene, 1,2-butadiene, 1,3-pentadiene, 1,2-pentadiene, *etc.*) or one triple bond (e.g., acetylene, 1-butyne, 1-pentyne, *etc.*) and another alkyl radical or hydrogen atom. Isomerization reaction of the allylic fuel radical can also happen through the H-atom transfer from any carbon site to the radical site. The rate coefficient for these reactions depends on the nature of the broken and formed C–H bonds (*i.e.*, secondary and tertiary vinylic, as well as primary, secondary, and tertiary) and the structure of the transition states involved, which ultimately determine the potential energy barrier.

### 3.2.4 Reaction class 5: H-atom addition to alkenes

Hydrogen atom addition to alkenes is one of the key reactions that open the double bond in alkenes oxidation chemistry at high temperatures and this reaction has a significant influence on the reactivity prediction of propene [51, 52], butene isomers [86-88], pentene isomers [92, 93, 98, 106], hexene isomers [104, 109-111] and 1,3-butadiene [54, 67] oxidation. At high temperatures ( $> 1200$  K), hydrogen atom will add to the double bond in alkenes followed by  $\beta$ -scission reactions which mostly produce smaller alkenes and primary alkyl radicals. This reaction inhibits reactivity, as it competes with the main chain branching and reactivity promoting reaction,  $\dot{\text{H}} + \text{O}_2 \rightleftharpoons \ddot{\text{O}} + \dot{\text{O}}\text{H}$ . The exception is the central addition of hydrogen atom to 1-butene [86], which can form  $\text{C}_2\text{H}_4 + \dot{\text{C}}_2\text{H}_5$  products and ultimately generate two vinyl radicals and three hydrogen atoms to promote the reactivity of 1-butene oxidation. The hydrogen atom addition to the central carbon atom of 1,3-butadiene [67] forming two vinyl radicals and one hydrogen atom also promotes reactivity. In summary, for the hydrogen atom addition reactions, if the products are smaller alkenes (other than ethylene) and primary alkyl radicals, that reaction will inhibit reactivity; whilst if the products are ethylene and hydrogen atom, that reaction will promote reactivity.

As temperatures decrease, the addition reactions of hydrogen atom to alkenes can form an alkyl radical which promotes reactivity. The alkyl radical formed can undergo typical low-temperature chemistry via reaction with molecular oxygen to form  $\text{R}\dot{\text{O}}_2$  radicals, which can undergo isomerization reactions to form  $\dot{\text{Q}}\text{OOH}$  radicals. Those are mainly consumed by a second molecular oxygen addition reaction, leading to the formation of ketohydroperoxides (KHP), the decomposition of which is also a major branching step and promotes the low-temperature reactivity. Noteworthy, the concentration of hydrogen atoms at lower temperature is relatively

low and, therefore, the reactivity effect from the  $\dot{\text{H}}$  atom addition and its subsequent reactions is quite limited and less important than that from the  $\dot{\text{O}}\text{H}$  additions.

### 3.2.5 Reaction class 6: $\dot{\text{O}}$ -atom addition to alkenes

The reaction of atomic oxygen with alkenes is a fundamental oxidation step in combustion and is prototypical for reactions in which oxygen adds to double bonds. It is also another important reaction that opens the double bond in alkenes oxidation chemistry at high temperatures. For this class of reactions generally, decomposition of the initial adduct via spin-allowed reaction channels on the triplet surface competes with intersystem crossing (ISC) and a set of spin-forbidden reaction channels on the ground-state singlet surface. The two surfaces share some bimolecular products but feature different intermediates, pathways, and transition states. The overall product branching is, therefore, a sensitive function of the ISC between the triplet and the singlet potentials.

Recently, Li et al. [209] presented a comprehensive study on the kinetics of  ${}^3\dot{\text{O}} + \text{C}_2\text{H}_4$  using ab initio transition state theory based master equation (AITSTME) approach that included an *a priori* description of ISC, and also reviewed much of the previous experimental and theoretical studies on this reaction. Casavecchia and Cavallotti [210, 211] investigated the kinetics of  $\dot{\text{O}}({}^3\text{P}) + \text{C}_3\text{H}_6$  both theoretically and experimentally in crossed molecular beams. They generated a comprehensive detailed mechanism of  ${}^3\dot{\text{O}} +$  unsaturated hydrocarbon reactions that are complicated by the existence of many possible channels and ISC between triplet and singlet PESs. Branching ratios between multiple important reaction channels have also been provided in their work and they proposed that the BRs cannot be extrapolated from room-temperature kinetics studies. Very recently, Bedjanian and Morin [212] has reviewed the reaction of  $\dot{\text{O}}({}^3\text{P}) + \text{C}_3\text{H}_6$  both experimentally and theoretically, and they also investigated the products of the reaction over an extended temperature range (298 - 905 K) by using a low pressure flow reactor combined with a quadrupole mass spectrometer. It is very interesting to find out that their products branching ratios are quite different from the experimental and theoretical work carried out by Casavecchia and Cavallotti [210, 211]. Large difference can be found for the products of  $\dot{\text{C}}_2\text{H}_5$  radical and formaldehyde, for which Bedjanian and Morin proposed 0.26 and 0.15 at 298 K, however, that values from Casavecchia and co-workers are 0.09 and 0.44. Clear reason for this discrepancy is unknown, however it should be noted that branching ratio between different products are quite important in determining the final reactivity of propene oxidation [52], hence these influence to the reactivity prediction of propene oxidation needs to be investigated in the future.

Scheme 1. Important reaction classes for alkenes oxidation with unique chemistry for alkenes are highlighted in bold.

High-temperature reaction classes

1. Unimolecular alkene decomposition
2. H-atom abstraction from alkenes
3. **Vinyl radical decomposition and isomerization**
4. **Alkenyl radical decomposition and isomerization**
5. **H-atom addition to alkenes**
6. **O-atom addition to alkenes**
7. **Secondary vinyl radical reacts with O<sub>2</sub>**
8. **Tertiary vinyl radical reacts with O<sub>2</sub>**

Intermediate-temperature reaction classes (RH refers to alkene, R<sub>A</sub> refers to allylic radical)

9. **R<sub>A</sub>+H $\dot{O}_2$ ⇌R<sub>A</sub>OOH**
10. **R<sub>A</sub>+H $\dot{O}_2$ ⇌R<sub>A</sub> $\dot{O}$ + $\dot{O}H$**
11. **R<sub>A</sub>OOH⇌R<sub>A</sub> $\dot{O}$ + $\dot{O}H$**
12. **R<sub>A</sub> $\dot{O}$  decomposition**
13. **R<sub>A</sub>+ $\dot{C}H_3$ ⇌R<sub>A</sub>CH<sub>3</sub>**
14. **R<sub>A</sub>CH<sub>3</sub> oxidation**
15. **R<sub>A</sub>+R<sub>A</sub>⇌R<sub>A</sub>-R<sub>A</sub> (larger dienes)**
16. **R<sub>A</sub>-R<sub>A</sub> oxidation**
17. **RH+H $\dot{O}_2$ ⇌R $\dot{O}_2$**
18. **RH+H $\dot{O}_2$ ⇌ $\dot{Q}OOH$**
19. **R $\dot{O}_2$ ⇌ $\dot{Q}OOH$**
20. **QOOH ⇌products**
21. **QOOH+O<sub>2</sub>⇌ $\dot{O}_2$ QOOH**
22.  **$\dot{O}_2$ QOOH ⇌ products**
23.  **$\dot{O}_2$ QOOH⇌HOO $\dot{P}OOH$**
24. **HOO $\dot{P}OOH$  ⇌ products**
25. **R<sub>A</sub>+O<sub>2</sub>⇌dienes + H $\dot{O}_2$**

Low-temperature reaction classes

26. **RH+ $\dot{O}H$ ⇌ $\dot{R}OH$  ( $\dot{O}H$  radical addition to both sides of the double bond)**
27.  **$\alpha$ -hydroxyalkyl + O<sub>2</sub> ⇌ aldehyde/ketone + H $\dot{O}_2$**
28.  **$\dot{R}OH+O_2$ ⇌Waddington products**
29.  **$\dot{R}OH+O_2$ ⇌ROHO $\dot{O}$  (first O<sub>2</sub> addition)**
30. **ROHO $\dot{O}$ ⇌ $\dot{Q}_H$ OHO $\dot{O}H$  (hydroxyl-RO<sub>2</sub> isomerization)**
31.  **$\dot{Q}_H$ OHO $\dot{O}H+O_2$ ⇌ $\dot{O}O\dot{Q}_H$ OHO $\dot{O}H$  (second O<sub>2</sub> addition)**
32.  **$\dot{O}O\dot{Q}_H$ OHO $\dot{O}H$ ⇌HOO $\dot{Q}_{-H}$ =OOH +  $\dot{O}H$  (isomerization to form hydroxyl-KTP)**
33. **HOO $\dot{Q}_{-H}$ =OOH decomposition**

(The following reaction classes are only important for C<sub>≥</sub>6, R<sub>AEN</sub> refers to alkenyl radical)

34. **R<sub>AEN</sub>+O<sub>2</sub>⇌R<sub>AEN</sub>O $\dot{O}$**
35. **R<sub>AEN</sub>O $\dot{O}$ ⇌ $\dot{Q}_{HAEN}$ OOH**
36.  **$\dot{Q}_{HAEN}$ OOH+O<sub>2</sub>⇌ $\dot{O}O\dot{Q}_{HAEN}$ OOH**
37.  **$\dot{O}O\dot{Q}_{HAEN}$ OOH⇌HOO $\dot{P}_{AEN}$ OOH (isomerization to form alkenyl-KTP)**
38. **HOO $\dot{P}_{AEN}$ OOH⇌decomposition**

### 3.2.6 Reaction classes 7 and 8: secondary and tertiary vinylic radicals react with O<sub>2</sub>

Even though the vinylic C–H bond strength (~108 kcal mol<sup>-1</sup>) is much higher than that of the primary allylic C–H bond (~86 kcal mol<sup>-1</sup>), the vinylic radical can still be formed at high temperatures through H-atom abstraction reactions, and its subsequent reactions with molecular oxygen can form  $\ddot{O}$  atom which is a chain branching reaction pathway. In the combustion chemistry of ethylene, it was shown that the vinyl radical is consumed almost entirely by reactions with molecular oxygen [25, 31]. The formed C<sub>2</sub>H<sub>3</sub>O<sub>2</sub> adduct lies 43.4 kcal mol<sup>-1</sup> below the reactants [213] which means this addition reaction is highly favored and dissociation back to vinyl + O<sub>2</sub> is unlikely. Similarity has been found in the high temperature oxidation of propene [52] which shows that under JSR and flow reactor conditions the secondary ( $\dot{C}_3H_5-s$ ) and tertiary ( $\dot{C}_3H_5-t$ ) vinylic radicals are almost exclusively consumed by the reaction with molecular oxygen. For the oxidation of isobutene [88], 2-butene [87], and 1-butene [86], we found the same trends that the vinylic radical reactions with molecular oxygen play a very important role in the high temperature oxidation of those fuels. This reaction class has not been mentioned in the oxidation mechanism of pentene isomers [92-94, 99, 100] and hexene isomers [98, 104, 105, 109-111], and this should be included as an important reaction class for vinylic radicals oxidation.

Apart from the comprehensive investigation on the reaction of vinyl + O<sub>2</sub> both experimentally [214-224] and by theoretical calculations [39, 213, 225-229], to the best of our knowledge, the reactions of secondary and tertiary vinylic radicals formed from propene, butene isomers, pentene isomers, and hexene isomers with molecular oxygen in combustion process have not been investigated either experimentally or theoretically. Rate constants used in the propene model is taken by analogy from the high-level ab initio study of Klippenstein et al. [230] and those for butene isomers are also taken by analogy from the high-level ab initio calculation of Goldsmith et al. [213]. As this reaction class is of great importance in high temperature oxidation of alkenes, we recommend that further studies of the total rate constants, the product channels and the branching ratios need to be carried out.

### 3.2.7 Reaction classes 9-12: recombination reaction of allylic and HO<sub>2</sub> radicals ( $\dot{R}_A + HO_2 \rightleftharpoons R_AOOH$ , $R_A + HO_2 \rightleftharpoons \dot{R}_A\dot{O} + \dot{O}H$ , $R_AOOH \rightleftharpoons R_A\dot{O} + \dot{O}H$ , $R_A\dot{O} \rightleftharpoons$ decomposition)

The radical-radical recombination reaction between allylic and hydroperoxyl radicals and the subsequent dissociation reactions play a very important role in determining the reactivity of alkenes oxidation across a range of conditions, especially at low to intermediate temperatures [51, 52, 86-88, 106, 109]. Taking propene oxidation for example, at approximately 875 K and 1 atm in a JSR, the reaction of allyl and hydroperoxyl radicals accounts for approximately half of the entire allyl radical consumption [52] and that number can be 47% for isobutene [88]. This reaction process involves chemical activation and includes the bimolecular recombination between the allylic and HO<sub>2</sub> radical to form allylic hydroperoxide ( $\dot{R}_A + HO_2 \rightleftharpoons R_AOOH$ ), the decomposition of allylic hydroperoxide ( $R_AOOH \rightleftharpoons R_A\dot{O} + \dot{O}H$ ), the chemically activated reaction between allylic and HO<sub>2</sub> radical to form alkyl-allyloxy and hydroxyl radicals directly ( $R_A + HO_2 \rightleftharpoons R_A\dot{O} + \dot{O}H$ ), and the unimolecular reaction of alkyl-allyloxy radical ( $R_A\dot{O} \rightleftharpoons$  decomposition).

At elevated temperatures and low-pressures, the chemically activated process of allylic radical reacting with hydroperoxyl radical to form alkyl-allyloxy and hydroxyl radicals is favored. However, as temperature decreases and pressure increases, the formation of the stabilized adduct, allylic hydroperoxide of  $R_AOOH$ , becomes dominant. Allylic hydroperoxide subsequently decomposes to give alkyl-allyloxy and hydroxyl radicals. At combustion relevant conditions, both of the major channels for the reaction of allylic radical and hydroperoxyl radical act to promote reactivity as they ultimately convert a stable allylic radical to a reactive hydroxyl radical.

The alkyl-allyloxy radical can undergo both decomposition and isomerization reactions to produce different types of products. The decomposition reaction can give bi-molecular products such as vinylic radical and aldehydes, allylic-aldehydes and atomic hydrogen, and formyl and alkyl radicals. The isomerization reaction can produce allylic-ether radicals which can ultimately form vinylic radicals and aldehydes. The comprehensive investigation of this reaction class has only been carried out by Goldsmith et al. [231] for the allyl radical plus hydroperoxyl radical system, which has been used in the propene [51, 52] and analogously for butenes [86-88] oxidation mechanisms. Due to the importance of this reaction class in alkenes oxidation, we recommend further theoretical and experimental work.

### 3.2.8 Reaction classes 13-14: recombination reaction of allylic and $\dot{C}H_3$ radicals and the subsequent oxidation mechanism ( $\dot{R}_A + \dot{C}H_3 \rightleftharpoons R_A\dot{C}H_3$ and $R_A\dot{C}H_3$ oxidation)

The recombination reaction of allylic and methyl radicals to give a larger alkene is an important inhibiting reaction for alkene combustion, especially at intermediate temperatures [52, 88]. This chain termination reaction acts to inhibit reactivity for ignition delay time determination. The larger alkenes formed will also undergo the important reaction classes listed in Scheme 1 for alkenes oxidation.

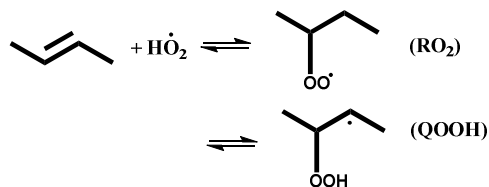
### 3.2.9 Reaction classes 15-16: self-recombination reaction of allylic radicals and the subsequent oxidation mechanism ( $\dot{R}_A + \dot{R}_A \rightleftharpoons R_A-R_A$ , $R_A-R_A \rightleftharpoons$ products)

Allylic radicals can undergo self-recombination to form larger diene  $R_A-R_A$  molecules. This chain termination reaction inhibits reactivity at low and intermediate temperatures [52, 88]. Hydrogen atom abstraction can also happen between the two allylic radicals to form alkenes and dienes. However, the contribution from this reaction channel is quite limited and can be neglected.

As shown in Figure 30, the formed larger dienes can go through hydrogen atom abstraction reactions to form fuel radicals, among which the allylic radicals are dominant and should be paid special attention to. Hydrogen atom abstraction by  $\dot{O}H$  and  $\dot{C}H_3$  radicals,  $\dot{O}$  and  $\dot{H}$  atoms, and molecular oxygen are important reactions for the oxidation of these larger dienes. Rate constants of these reactions can be estimated based on their BDE and the number of hydrogen atoms available for abstraction by analogy with alkenes. The formation of larger dienes is important at intermediate temperatures at which the  $\dot{H}O_2$  radical reacting with the allylic diene radicals should be taken into consideration, as shown in Figure 30. The allylic diene radicals formed can also undergo  $\beta$ -scission to yield smaller dienes and allylic radicals. These reactions will slow down the ignition delay times of alkene oxidation and give a pronounced contribution in the allylic radical consumption.

### 3.2.10 Reaction classes 17-18: addition reaction of $\dot{\text{H}}\text{O}_2$ radicals to alkenes ( $\text{RH} + \dot{\text{H}}\text{O}_2 \rightleftharpoons \text{R}\dot{\text{O}}_2$ , $\text{RH} + \dot{\text{H}}\text{O}_2 \rightleftharpoons \dot{\text{Q}}\text{OOH}$ )

When we take 2-butene as an example, the initial reaction process can be described as:

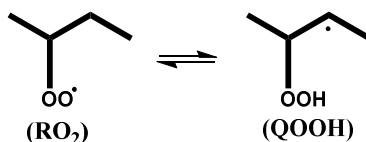


The addition reactions of  $\dot{\text{H}}\text{O}_2$  radical to alkenes are of importance in determining the reactivity of alkenes oxidation at intermediate temperatures. The most important products of the addition reaction of alkene +  $\dot{\text{H}}\text{O}_2$  are alkylperoxy radical ( $\text{R}\dot{\text{O}}_2$ ), hydroxyl radical + cyclic ether, and the corresponding hydroperoxyalkyl ( $\dot{\text{Q}}\text{OOH}$ ) species. Barrier heights for alkene +  $\dot{\text{H}}\text{O}_2 \rightleftharpoons \text{R}\dot{\text{O}}_2$  and alkene +  $\dot{\text{H}}\text{O}_2 \rightleftharpoons \dot{\text{Q}}\text{OOH}$  are typically close to each other and, therefore, these two channels are competing with each other. It is interesting to note that the alkene +  $\dot{\text{H}}\text{O}_2$  reaction takes place on the same potential energy surface as the alkyl +  $\text{O}_2$  one, which makes the alkenes chemistry linked with alkanes chemistry. At low temperatures, the formation of the alkylperoxy radical is favored due to the lower barrier height, while at higher temperatures the hydroperoxyalkyl and/or oxirane +  $\dot{\text{O}}\text{H}$  formation is faster because of the looser transition state structure.

However, the direct experimental investigation of alkene +  $\dot{\text{H}}\text{O}_2$  reactions is difficult, because these reactions are slow and not all reaction products are easily detectable with standard experimental techniques. Zádor *et al.* [232] have thoroughly investigated the comprehensive pressure and temperature dependent rate constants for reactions of seven alkenes (i.e., ethylene, propene, 1-butene, trans-2-butene, isobutene, cis-cyclo- $\text{C}_6\text{H}_{10}$  and ethenol) with  $\dot{\text{H}}\text{O}_2$ . RRKM/ME analysis was used to calculate the temperature and pressure dependent rate constants based on the PES obtained at the QCISD(T)/cc-pV $\infty$ Z//B3LYP/6-311++G(d,p) level of theory. They proposed that  $\dot{\text{H}}\text{O}_2$  adds almost exclusively to the  $\text{sp}^2$  carbon atom with more alkyl groups attached in non-conjugated alkenes, and this finding is qualitatively in accordance with the calculated differences in charge transfer in the transition states. Due to the importance of this reaction class, we recommend that further theoretical work on other alkenes with hydroperoxyl radical is necessary.

### 3.2.11 Reaction class 19: $\text{R}\dot{\text{O}}_2$ radical isomerization ( $\text{R}\dot{\text{O}}_2 \rightleftharpoons \dot{\text{Q}}\text{OOH}$ )

When we take 2-butene as an example, one of the reaction steps can be shown as:

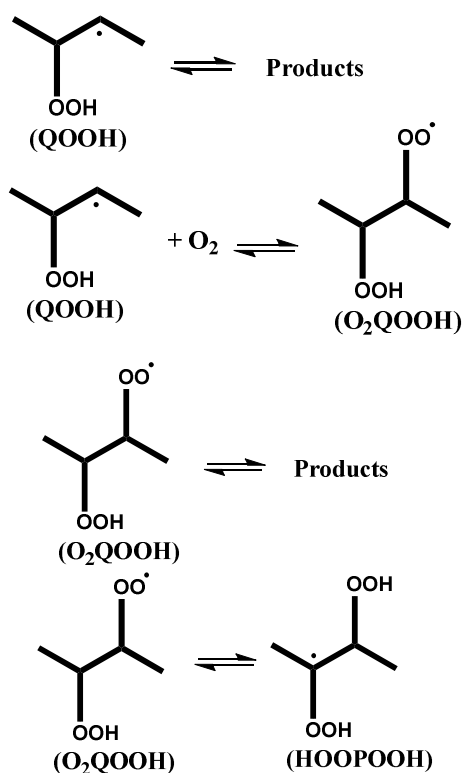


In the low-temperature oxidation regime (i.e., 500 to 900 K), isomerization of  $\text{R}\dot{\text{O}}_2$  becomes rapid, resulting in substantial flux through  $\dot{\text{Q}}\text{OOH}$ . However, rapid decomposition, isomerization, and reaction with  $\text{O}_2$  typically remove  $\dot{\text{Q}}\text{OOH}$  faster than it is formed. It is well established that isomerization of the  $\text{R}\dot{\text{O}}_2$  radicals to form the hydroperoxyalkyl radicals  $\dot{\text{Q}}\text{OOH}$  proceeds through the intramolecular H-atom transfer involving ring-shaped transition states. The isomerizations in alkyl radicals can be categorized according to the positions of the heavy atoms

between which the H atom is transferred and the type of C - H bond being broken. The barrier heights for these isomerizations depend on the size of the ring and on the strength of the C - H bond broken in the isomerization. Zádor et al. [233] have discussed the kinetics and thermodynamics of this reaction class comprehensively, hence further discussion on this reaction class will not be provided here.

3.2.12 Reaction classes 20 – 24: reactions of the hydroperoxyalkyl radicals ( $\dot{Q}OOH$ ) ( $\dot{Q}OOH \rightleftharpoons$  products,  $\dot{Q}OOH + O_2 \rightleftharpoons \dot{O}_2QOOH$ ,  $\dot{O}_2QOOH \rightleftharpoons$  products,  $\dot{O}_2QOOH \rightleftharpoons HO\dot{O}POOH$  and  $HO\dot{O}POOH \rightleftharpoons$  products)

When we take 2-butene as an example, the reaction classes discussed here can be shown as:



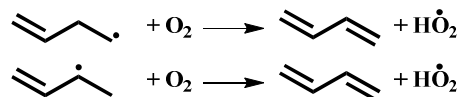
The fate of hydroperoxyalkyl radicals  $\dot{Q}OOH$  is central to the modeling of autoignition. Unimolecular decomposition of  $\dot{Q}OOH$  can produce a reactive  $\dot{O}H$  radical and, therefore, it plays an important role in radical chain propagation. Alternatively, a second molecular oxygen can add to  $\dot{Q}OOH$  to form a hydroperoxyalkylperoxy radical,  $\dot{O}_2QOOH$  which can rapidly isomerize and dissociate to form either  $\dot{O}H$  + keto-hydroperoxide or  $H\dot{O}_2$  + alkenyl hydroperoxide. These bimolecular products can also be formed directly from the  $O_2 + \dot{Q}OOH$  reactants via chemical activation. Furthermore, the O–OH bonds in the keto-hydroperoxides and alkenyl hydroperoxides are relatively weak, and these intermediates can further decompose to oxy-radicals +  $\dot{O}H$  at low temperatures. Consequently, the addition of a second molecular oxygen to  $\dot{Q}OOH$  can produce three radicals from every radical consumption which is the important chain-branching pathway to promote the reactivity below  $\sim 900$  K. A thorough review of experimental and theoretical work on this reaction can be found in Zádor et al. [233].

Although these chemistry pathways can explain the low temperature reactivity of hydrocarbon oxidation quite well, these mechanisms were still considered hypothetical until recently. Savee et al. [234] characterized  $\dot{Q}OOH$  spectroscopically and performed direct kinetics measurements of its reaction with  $O_2$  at 400 K and 10 Torr using photoionization mass spectrometry with synchrotron-generated tunable vacuum ultraviolet ionizing radiation which gave experimental benchmarks for the reactivity of resonance stabilized  $\dot{Q}OOH$  and suggested that such radicals may be relatively long-lived in combustion systems. Goldsmith et al. [235] selected the smallest hydrocarbon, propane, which has the NTC behavior as a target molecule to investigate the low temperature oxidation mechanisms. They examined the role of  $O_2 + \dot{Q}OOH$  chemistry in low-temperature alkyl autoignition, employing ab initio transition-state theory based master-equation calculations to determine many of the key rate constants for the propane oxidation system.

### 3.2.13 Reaction class 25: $\dot{R}_A + O_2 \rightleftharpoons \text{dienes} + \dot{H}O_2$

The addition of  $O_2$  to alkyl radical and subsequent reaction pathways are the main low temperature branching pathways for alkane oxidation. On the contrary, for alkenes, the addition of  $O_2$  to allylic radicals does not play an important role in the alkene low temperature oxidation. For alkanes, the heat release of the entrance channel ( $\dot{R} + O_2 \rightleftharpoons \dot{R}O_2$ ) is  $\sim 35 \text{ kcal mol}^{-1}$ , whilst that for alkenes ( $\dot{R}_A + O_2 \rightleftharpoons \dot{R}_A O_2$ ) is only  $\sim 20 \text{ kcal mol}^{-1}$  or specifically  $21.5 \text{ kcal mol}^{-1}$  for  $i\dot{C}_4H_7 + O_2 \rightleftharpoons iC_4H_7\dot{O}_2$  in isobutene oxidation [88] and  $19.9 \text{ kcal mol}^{-1}$  for the similar reaction of 1-butene [86]. The forward concerted elimination of  $\dot{R}_A O_2$  to form diene and hydroperoxyl radical needs to overcome the barrier of  $\sim 27 \text{ kcal mol}^{-1}$  which is higher than that for the reverse dissociation reaction back to form allylic radical and molecular oxygen. Thus, dissociation back to  $\dot{R}_A + O_2$  is favored over the higher barrier isomerization/elimination reaction processes.

Rather than the addition reaction to happen between allylic radical and molecular oxygen, hydrogen-atom abstraction from the  $\beta$ -site of the allylic radical by molecular oxygen is more likely to happen and this reaction promotes reactivity, as it consumes a stabilized allylic radical to generate a more reactive hydroperoxy radical. Considerable amount of the allylic fuel radicals were found to be consumed by H-atom abstraction reaction by  $O_2$  in, for example, the oxidation of 1- and 2-butene [86, 87]. It is worth noting that the reaction  $\dot{R}_A + O_2 \rightleftharpoons \text{dienes} + \dot{H}O_2$  is not chemically activated via the reaction pathway of  $\dot{R}_A + O_2 \rightleftharpoons \dot{R}_A O_2 \rightleftharpoons \text{dienes} + \dot{H}O_2$ , but is a direct abstraction reaction instead.



### 3.2.14 Reaction classes 26: $\text{RH} + \dot{O}H \rightleftharpoons \dot{R}OH$ ( $\dot{O}H$ radicals addition to both sides of the double bond)

Low temperature chemistry for alkenes oxidation is illustrated in Figure 31. The addition reactions of hydroxyl radical to the double bond in alkenes plays a very important role in determining the reactivity of alkenes oxidation when temperature is lower than 850 K. Depending on the position of the double bond in alkenes, the hydroxyl radical can add to either the terminal or central carbon atom. For this specific reaction, branching ratios between these

two additions, along with temperature changes, is far more important than the total rate constants in determining the alkenes reactivity. That is because the formed hydroxyl adducts can undergo different reaction pathways which have different impact on determining the reactivity of alkenes oxidation. Taking the addition reaction of  $\dot{\text{O}}\text{H}$  radical to propene as an example, Zádor et al. [236] have carried out high-level ab initio calculations on this reaction system and found a 50:50 branching ratio for hydroxyl radical addition to propene to form the two  $\dot{\text{C}}_3\text{H}_7\text{O}$  radicals via addition to the terminal or central carbon atom. However, in their propene oxidation model, Burke et al. [52] kept the total rate coefficient constant while changing the branching ratio to 75:25 in favor of addition to the terminal carbon to give a good reactivity prediction. The same trends have also been found in butene isomers oxidation [86-88]. This adjustment is also consistent with the experimental study carried out by Loison et al. [237] who found  $72 \pm 16\%$  of hydroxyl radical addition to propene and  $71 \pm 16\%$  to 1-butene, with both favoring the terminal carbon addition. On the other hand, for 1-hexene oxidation, Battin-Leclerc et al. [109] reported that the use of the 50:50 branching ratio for the addition to the terminal or central carbon atom as suggested by Zádor et al. [236] for propene is appropriate, which is quite different from smaller alkenes oxidation [52, 87, 88].

The obtained adducts of hydroxyalkyl radicals can undergo isomerization and decomposition reactions to form smaller molecules such as aldehydes and alkyl radicals. Detailed reaction mechanism can be found in the works of Zádor et al. [236] and Zhou et al. [238] for the addition reaction of hydroxyl radical to propene. Due to the importance of the branching ratios for the entrance channel in the alkenes reactivity prediction, further theoretical or calculation studies on this topic will be valuable for understanding the fuel chemistry.

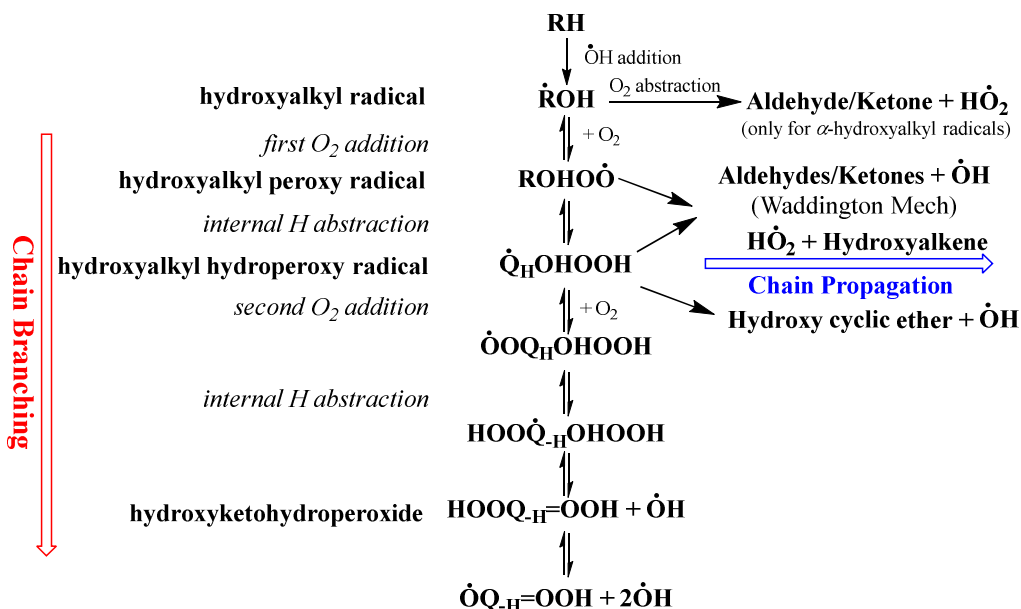


Figure 31. Scheme of low-temperature chemistry for hydroxyalkyl radicals in alkenes oxidation.

### 3.2.15 Reaction class 27: $\alpha$ -hydroxyalkyl + O<sub>2</sub> $\rightleftharpoons$ aldehyde/ketone + HO<sub>2</sub>

The addition of hydroxyl radical to the double bond is a major consumption pathway at low temperatures and the hydroxyl adducts can isomerize to  $\alpha$ -hydroxyalkyl radicals. Molecular oxygen will react with the  $\alpha$ -hydroxyalkyl radicals to directly form an aldehyde/ketone and HO<sub>2</sub> radical rapidly in the atmosphere. Theoretical studies on the elementary reactions of hydroxyalkyl radicals with O<sub>2</sub> are quite limited and mainly focus on small reaction systems of hydroxymethyl [239-241],  $\alpha$ -hydroxyethyl, [240, 242, 243],  $\beta$ -hydroxyethyl, [242] 2-hydroxy-1,1-dimethylethyl [244] and 2-hydroxy-2-methylpropyl [244]. Experimental studies of the reaction of hydroxyalkyl radical with molecular oxygen reactions at engine relevant conditions have been carried out only for hydroxymethyl [241] and  $\alpha$ - and  $\beta$ -hydroxyethyl [242]. The study from Zádor et al. [242] and Silva et al. [243] showed that the reaction of  $\alpha$ -hydroxyethyl + O<sub>2</sub> proceeds through an activated  $\alpha$ -hydroxy-ethylperoxy adduct that rapidly decomposes to acetaldehyde + HO<sub>2</sub> radical. These reactions have been included in the mechanism of n-butanol [245, 246] and isobutanol [247] oxidation.

### 3.2.16 Reaction class 28: $\dot{R}OH + O_2 \rightleftharpoons$ Waddington products

The  $\dot{O}H$  radical addition to the double bond in alkenes produces hydroxyalkyl radicals which can also be formed in the low temperature oxidation of alcohols, which links the low temperature chemistry of alkenes and alcohols. The hydroxyalkyl radical will further react with molecular oxygen to form the hydroxyalkyl peroxy radical (ROHO $\dot{O}$ ) [248]. Rate constants for this first O<sub>2</sub> addition depends on whether the radical carbon is in an  $\alpha$  position to the hydroxyl group or at the primary, secondary, or tertiary site.

The ROHO $\dot{O}$  radical can isomerize to form hydroxyalkyl hydroperoxyl radicals ( $\dot{Q}_H OHOOH$ ) through the 5-member, 6-member, and 7-member transition state rings. Rate constants for those reactions have not been studied extensively and the estimation of the kinetics has been used in the model development for alcohols [249, 250] and alkenes [52, 86-88, 98, 109, 111]. The rate constants for the isomerization depend on the nature of the broken C–H bond (*i.e.*, primary, secondary and tertiary) and the number of atoms in the ring structure of the transition state. The charge transfers from oxygen lone pairs to the  $\alpha$   $\sigma^*_{CH}$  orbital will make the  $\alpha$  C–H bond much weaker than a normal C–H bond in alkane [251] and this effect should be taken into consideration when the barriers for the H-atom transfer are estimated. Waddington and co-workers [252, 253] proposed the mechanism involving the  $\beta$ -RO $\dot{O}$  radical undergoing a six-membered ring isomerization to abstract an H atom from the hydroxyl moiety and decompose rapidly afterwards. This reaction process is called the Waddington mechanism which involves chain propagating reaction pathways and competes directly with low-temperature chain branching pathways and hence inhibits low-temperature reactivity. Apart from the six-membered ring transition state structure, Welz et al. [254-256] investigated the low temperature chemistry of butanol isomers and isopentanol oxidation and stated that the Waddington mechanism can also happen for the  $\gamma$ -RO $\dot{O}$  and  $\delta$ -RO $\dot{O}$  radicals abstracting the hydrogen atom from the OH group through 7- and 8-membered ring transition states.

### 3.2.17 Reaction classes 29 and 30: $\dot{\text{R}}\text{OH}+\text{O}_2\rightleftharpoons\text{ROHO}\dot{\text{O}}$ (first $\text{O}_2$ addition), $\text{ROHO}\dot{\text{O}}\rightleftharpoons\dot{\text{Q}}_{\text{H}}\text{OHOOH}$

The Waddington mechanism involving the hydrogen atom from the OH moiety transferring to the radical site of the hydroxyalkyl peroxy radical (ROHO $\dot{\text{O}}$ ) has been discussed above. Besides the Waddington reaction pathways, the internal hydrogen atom transfer in ROHO $\dot{\text{O}}$  can also occur between the radical site and the alkylic hydrogen atom. Isomerization rate constant not only depend on the type of hydrogen being transferred (whether it is an  $\alpha$  to the hydroxyl group or primary, secondary, or tertiary) but also depend on the ring structure of the transition states whether it is a 4-, 5-, 6-, 7-, or 8- membered ring.

This reaction class is an important initiation step for determining the formation of the chain branching radical pool precursor of hydroxyketohydroperoxide and is competitive with the chain propagation Waddington reaction pathways. Hence, branching ratio between this reaction class and the Waddington reaction pathway is crucially important in determining the low temperature reactivity of alkenes oxidation. In order to give an initial picture of the competition between these reaction channels, the potential energy surface for the involved reaction channels has been calculated in this work at G4 and CBS-QB3 levels of theory, as shown in Figure 32, taking 1-pentene oxidation as an example. As can be seen in the PES, even though the Waddington mechanism is very well known and considered as the most dominant reaction pathway for those reaction processes, the isomerization reaction pathway abstracting the secondary hydrogen atom via the six-member transition state holds an even lower energy barrier than the Waddington reaction pathways by 0.8 kcal mol<sup>-1</sup> at the G4 level of theory. Nevertheless, other isomerization reaction pathways forming seven- and five-membered ring structures in the transition states are also competitive which should be taken into consideration in model development.

Theoretical studies have been carried out by Olivella et al. [257] and Kuwata et al. [258] to investigate the unimolecular reactions of  $\beta$ -hydroxyethylperoxy radical, with the highest level of theory in potential energy surface characterization were both CCSD(T)/6-311+G(3df,2p)//B3LYP/6-31G(d,p) in the two studies. The Waddington pathway was found to be the most important unimolecular reaction channel for  $\beta$ -hydroxyethylperoxy, while peroxy group abstracting the  $\alpha$ -H atom traversing a five-membered-ring TS and HO<sub>2</sub> concerted elimination pathway for  $\beta$ -hydroxyethylperoxy radical are less competitive. Lizardo-Huerta et al. [259] employed the CBS-QB3 method and conventional TST theory to systematically investigate the unimolecular reactions of 50  $\beta$ -HORO $\dot{\text{O}}$  radicals, where internal H-transfer (through a five, six or seven membered cyclic TS, and Waddington mechanism) and HO<sub>2</sub> elimination pathways were taken into consideration for the  $\beta$ -HORO $\dot{\text{O}}$  radicals. Special attention was placed on the intramolecular effects, such as the location of the hydroxyl or methyl groups in the cyclic TSs, or the substitution of H atom by alkyl groups on the carbon atom bonded to the peroxy group.

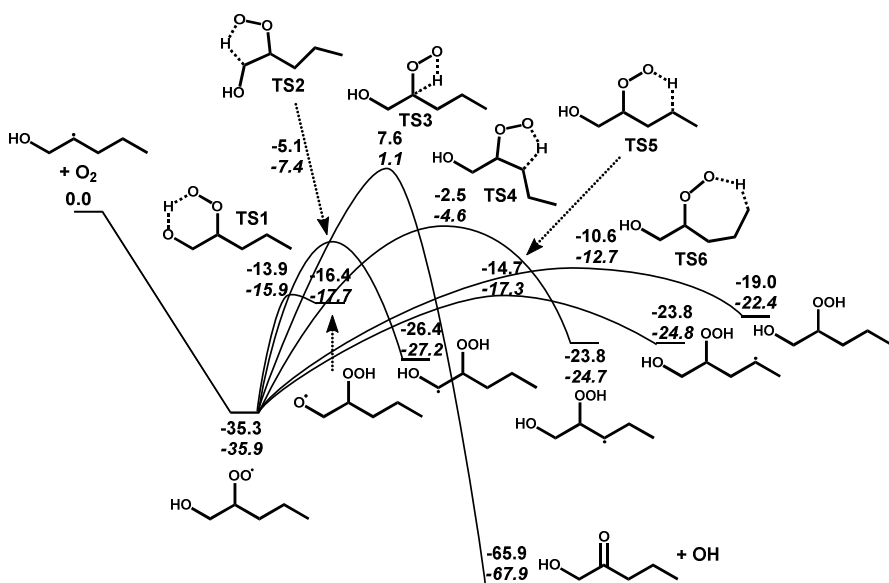


Figure 32. PES for the competition between Waddington mechanism and other isomerization reaction channels leading to low temperature chain branching reaction pathways. Electronic energy barriers are calculated at the G4 and *CBS-QB3* levels of theory. Energies are shown in kcal/mol.

### 3.2.18 Reaction class 31: second molecular oxygen addition ( $\dot{Q}_H\text{OHO}OH + \text{O}_2 \rightleftharpoons \dot{O}OQ_H\text{OHO}OH$ )

The addition of molecular oxygen to hydroxyalkyl hydroperoxy radical (*i.e.*,  $\dot{Q}_H\text{OHO}OH$ ) is recognized as the second  $\text{O}_2$  addition and is a very important reaction pathway for the chain branching process. Rate constants for this second  $\text{O}_2$  addition depends on whether the radical carbon is an  $\alpha$  to the hydroxyl group or at a primary, secondary, or tertiary site.

### 3.2.19 Reaction classes 32 and 33: reactions of $\dot{O}OQ_H\text{OHO}OH$ radicals ( $\dot{O}OQ_H\text{OHO}OH \rightleftharpoons \text{HOO}Q_{-H}=\text{OOH} + \dot{O}H$ and $\text{HOO}Q_{-H}=\text{OOH} \rightleftharpoons \text{products}$ )

The isomerization reaction of  $\dot{O}OQ_H\text{OHO}OH$  radical can form hydroxyketohydroperoxide ( $\text{HOO}Q_{-H}=\text{OOH}$ ) and release one  $\dot{O}H$  radical. Rate constants for this reaction process can be estimated by analogy with alkanes' low temperature oxidation and taking the influence of OH moiety into consideration. Sarathy et al. [250] stated that the hydrogen atom being abstracted bound to the  $\alpha$ -carbon of the hydroperoxide group (OOH) has a lower C–H bond strength than a normal C–H bond, which makes it easier to abstract.

The decomposition of hydroxyketohydroperoxide is the final chain branching pathway for the alkenes oxidation which produces two radicals from one stable intermediate species. This reaction process can form an  $\dot{O}H$  radical, a smaller oxygenated radical and a stable oxygenate (aldehyde or ketone).

### 3.2.20 Reaction classes 34–38: reactions of $\dot{R}_{AEN}$ radicals (low temperature chain branching reactions for alkenyl radical)

The alkenyl radical can be formed in the alkenes oxidation via hydrogen atom abstraction by various reactive radicals of  $\dot{O}H$ ,  $\text{HO}_2$ ,  $\dot{C}H_3$ ,  $\text{CH}_3\dot{O}_2$ ,  $\text{CH}_3\dot{O}$ , etc. Apart from  $\beta$ -scission to form smaller unsaturated hydrocarbon and radicals, and the reaction with  $\text{O}_2$  to form  $\text{HO}_2$  and

conjugated dienes at low temperatures, those alkenyl radicals can add molecular oxygen which is followed by isomerization and second O<sub>2</sub> addition, leading to the formation of unsaturated cyclic ethers and alkenylketohydroperoxides, similar to the well-known low temperature chemistry of alkanes [233]. These reaction classes are important for alkenes when the number of carbons is larger than five ( $C \geq 6$ ).

It should be noted that the low temperature reactivity of a fuel is controlled by the ability to form ketohydroperoxides which can lead to the chain branching radical pool. In contrast to alkanes in which the alkyl radicals are the source for the formation of ketohydroperoxides, for alkene low temperature chemistry, the formation of hydroxyalkyl radical from OH radical addition to the C=C double bond and the formation of alkenyl radical are the sources of hydroxyketohydroperoxides and alkenylketohydroperoxides, respectively. The hydroxyketohydroperoxides and alkenylketohydroperoxides can be formed when the number of carbon atoms in the fuel molecule is larger than two and five, respectively. Reaction channels forming Waddington products are very competitive with the ones forming hydroxyketohydroperoxides and the formation of allylic radical is more favored than that of alkenyl radicals, and hence, even though there are two sources for the formation of ketohydroperoxides in alkenes. They are less reactive than their saturated counterparts at low temperatures.

### 3.3 Model validation and analysis

Ignition delay time and laminar flame burning velocity are crucial characteristics of fuel combustion from both fundamental and practical considerations and are often used as key parameters for chemical kinetic mechanisms validation and optimization. Simulating the concentrations of intermediates and product species is important for analyzing reaction pathways and emissions. Experimental studies of alkenes' ignition delay times, laminar flame speeds and speciation were described in detail in Section 2. Here, we will discuss those studies in the context of model validation. Experimental data from newer studies are favored over older data for discussion and analysis. For the combustion chemistry for each alkene, important elementary reactions involved in determining the reactivity of the fuel will also be fully discussed.

All simulations were conducted with CHEMKIN-PRO [260] using appropriate reactor modules. Premixed laminar flame simulations accounted for thermal diffusion, assumed mixture-averaged transport, and the solutions were grid-independent by assigning GRAD and CURV values of 0.02. The mixed-averaged diffusion method for calculating the transport coefficients was used. Burner-stabilized premixed flames were simulated using the experimentally measured temperature profile as boundary condition.

### 3.4 The combustion chemistry of ethylene

Ethylene is the simplest alkene and is one of the key intermediates in the oxidation of higher hydrocarbons. Therefore, it plays an important role in the combustion chemistry of most practical fuels. Moreover, ethylene itself is a very reactive fuel and can be formed easily from JP-type fuel cracking and decomposition for high-speed air-breathing propulsion applications of pulse detonation engines and scramjet [16]. Notable comprehensive reaction mechanisms described for ethylene oxidation capable to reproduce available experimental data are those by Konnov [27], Xu and Konnov [26], AramchMech 1.3 [25], San Diego mechanism (UCSD) [28]

and USC mechanism [29]. The ethylene mechanism of USC [29] has been validated extensively against experimental measurements of ignition delays in shock tubes, laminar flame speeds, and species profiles in flames. The UCSD mechanism [28] has also been validated against laminar flame speed and ignition delay time. Mechanism from Konnov [26, 27] has been validated against ignition and flame propagation. The ethylene mechanism of AramchMech 1.3 [25] has been validated extensively against experimental measurements of ignition delay time in shock tubes, laminar flame speeds, speciation profiles in flame, flow reactor, and jet-stirred reactor. Very recently, Kikui et al. [30] investigated the combustion and ignition characteristics of four alkenes (ethylene, propylene, 1-butene and 1-pentene) using a micro-flow reactor. They also conducted reaction path analysis to examine the high reactivity of ethylene and stated that the formation of HCO radical is a key factor in determining the reactivity of ethylene oxidation. H-atom addition reaction of ethylene where the reaction occurs at the double bond of ethylene is a unique reaction compared with alkanes and consumes a significant amount of ethylene. Table 2 presents experimentally measured and theoretically calculated reaction rate constants available in the literature for ethylene-related reactions.

Table 2. Overview of experimental studies of elementary reaction kinetics relevant to ignition and combustion of ethylene.

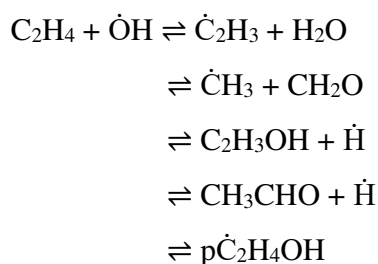
Reference	Reaction system	Experimental method	Detection technique	$T, P$ range
Eskola et al. 2003[222]	$\dot{C}_2H_3 + O_2$	Laser photolysis	Time-resolved FTIR emission spectroscopy	200-362 K 0.13-0.53 kPa
Oguchi et al. 2009 [223]	$\dot{C}_2H_3 + O_2$	Laser photolysis	Laser-induced fluorescence	298.15 K 10-100 Torr
Chishima et al. 2009 [224]	$\dot{C}_2H_3 + O_2$	Laser photolysis	Cavity ring-down spectroscopy technique (CRDS)	298 K 10-120 Torr
Matsugi et al. 2014 [221]	$\dot{C}_2H_3 + O_2$	Laser photolysis	PLP/CRDS	298.15 K 10-100 Torr
Slagle et al. 1984 [261]	$\dot{C}_2H_3 + O_2$	Laser photolysis	Photoionization mass spectrometry	297-602 K 0.48-3.6 Torr
Park et al. 1984 [219]	$\dot{C}_2H_3 + O_2$	Laser photolysis	Photoionization mass spectrometry	296 K 0.4-4.04 Torr
Hanning-Lee et al. 1993 [262]	$C_2H_4 + \dot{H}$	Exciplex laser flash photolysis	Time-resolved resonance fluorescence	800 K 97-600 Torr
Brouard et al. 1986 [263]	$C_2H_4 + \dot{H}$	Excimer laser flash photolysis	Time-resolved resonance fluorescence	775-825 K 200 Torr
Lightfoot et al. 1987 [264]	$C_2H_4 + \dot{H}$	Laser flash photolysis	Resonance fluorescence	285-604 K 50-600 Torr

Kurylo et al. 1970 [265]	$C_2H_4+\dot{H}$	Flash photolysis	Resonance fluorescence	298 K 5-500 Torr
Michael et al. 1973 [266]	$C_2H_4+\dot{H}$	Sensitized photolysis	Lyman $\alpha$ photometry	Room temperature 2.09-600 Torr
Sugawara et al. 1981 [267]	$C_2H_4+\dot{H}$	Pulse radiolysis	Resonance absorption	211-461 K 200 Torr
Lee et al. 1978 [268]	$C_2H_4+\dot{H}$	Flash photolysis	Resonance fluorescence	198-320 K 300-760 Torr
Bott and Cohen 1991 [269]	$C_2H_4+\dot{OH}$	Reflected shock tube (ST)	UV absorption	1197 K 1 atm
Smith 1987 [270]	$C_2H_4+\dot{OH}$	Laser pyrolysis	Laser induced fluorescence (LIF)	1220 K 20 Torr
Bradley et al. 1976 [271]	$C_2H_4+\dot{OH}$	Incident shock tube	UV absorption	~1300 K 1.5 Torr
Baldwin et al. 1966 [272]	$C_2H_4+\dot{OH}$	Method similar to gas chromatograph		813 K
Bhargava and Westmoreland 1998 [166]	$C_2H_4+\dot{OH}$	Laminar flames	Molecular-beam mass spectrometry (MBMS)	1455-1740 K 30 Torr
Westenberg and Fristrom 1965 [273]	$C_2H_4+\dot{OH}$	Flames	Electron spin resonance (ESR) spectroscopy	1250-1400 K 0.1 atm
Tully 1983 [274]	$C_2H_4+\dot{OH}$	Flash photolysis	Laser induced fluorescence (LIF)	291-591 K 600 Torr
Tully 1988 [275]	$C_2H_4+\dot{OH}$	Laser photolysis	Laser induced fluorescence (LIF)	650-901 K
Liu et al. 1987, 1988 [276, 277]	$C_2H_4+\dot{OH}$	Pulse radiolysis	Resonance absorption	343-1173 K 1.01 bar
Westbrook et al. 1988 [168]	$C_2H_4+\dot{OH}$	Jet-stirred reactor (JSR)	Direct measurement	1003-1253 K atmospheric pressure
Greiner 1970 [278]	$C_2H_4+\dot{OH}$	Flash photolysis	Kinetic spectrograph	299-497 K
Fulle et al. 1997 [279]	$C_2H_4+\dot{OH}$	Laser flash photolysis	Saturated laser induced fluorescence	300-814 K 1-130 bar
Srinivasan et al. 2007 [280]	$C_2H_4+\dot{OH}$	Reflected shock tube	Multi-pass absorption spectrometry	1463-1931 K 5.93-15.99

				Torr
Diau and Lee 1992 [281]	$C_2H_4 + \dot{O}H$	Laser photolysis	Laser induced fluorescence (LIF)	544-673 K 278-616 Torr
Zellner and Lorenz 1984 [282]	$C_2H_4 + \dot{O}H$	Laser photolysis	Resonance fluorescence	296-524 K 4-130 mbar
Hoare and Patel 1969 [283]	$C_2H_4 + \dot{O}H$	Conventional static reactor	Gas chromatograph	734-798 K 200 Torr
Avramenko and Lorentso 1949 [284]	$C_2H_4 + \dot{O}H$	Discharge flow system		350-451 K

### 3.4.1 Low temperature chemistry of ethylene combustion

$C_2H_4 + \dot{O}H \rightleftharpoons Products$ . Hydrogen atom abstraction by hydroxyl radical from ethylene is a very important reaction promoting the reactivity of ethylene oxidation as it produces a very reactive vinyl radical which can continue to react with molecular oxygen to chain branching pathways. This reaction has been studied extensively by experimental measurements and documented by Vasu et al. [285]. Vasu et al. [285] measured the reaction rates of hydroxyl radicals with ethylene behind reflected shock wave in the temperature range 973–1438 K for pressure from 2 to 10 atm. Their total rate constants are in good agreement with previous experimental measurements and the theoretical calculation results provided by Senosiain et al. [286] are 40% higher for the hydrogen atom abstraction reaction channel. Senosiain et al. [286] performed theoretical calculations for the abstraction and total rate constants with electronic energy barriers and vibrational frequencies calculated at the RQCISD(T)/cc-pV $\infty$ Z//UQCISD/6-311++G(d,p) level of theory, with potential energy surface shown in Figure 33. Rate constants of the following reaction channels have been investigated extensively.



Theoretical calculation results from Senosiain et al. [286] were adopted by Metcalfe et al. [25] in the AramcoMech 1.3 development, and they also documented the comparison of the rate constants from Vasu et al. [285] and Senosiain et al. [286]. Theoretical calculations from Senosiain et al. [286] confirm that when temperature is higher than 850 K, hydrogen abstraction channel becomes more important. Branching ratio analysis carried out by Metcalfe et al. [25] found that the importance of the stabilization to 2-ethylhydroxyl radical increases at higher pressures, with its formation being dominant from low temperatures to  $\approx$  900 K at atmospheric pressure but persisting to almost 1250 K at 1000 atm. Recently, Khaled et al. [287] has measured

the rate constants for the reaction of  $\dot{\text{O}}\text{H}$  radicals with ethylene and also found that the association pathways becomes negligible for  $T > 700$  K.

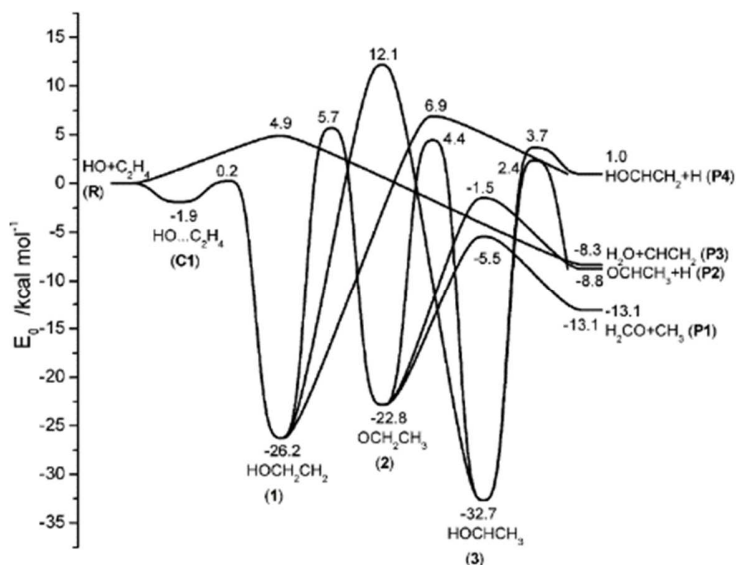


Figure 33. Simplified  $\text{C}_2\text{H}_5\text{O}$  potential energy surface using the RQCIT/QCI theoretical model chemistry [286].

### 3.4.2 Intermediate temperature chemistry of ethylene combustion

$\text{C}_2\text{H}_4 + \text{H}\dot{\text{O}}_2 \rightleftharpoons \text{Products}$ . Chen and Bozzelli [288] carried out thermochemical kinetic analysis for the reaction of  $\text{H}\dot{\text{O}}_2$  radical addition to the primary, secondary, and tertiary carbon-carbon double bonds of ethylene, propene, and isobutene using canonical transition state theory. Thermochemical properties of reactants, alkyl hydroperoxides, hydroperoxy alkyl radicals were determined by ab initio and density functional calculations. The authors only provided the rate constants for the entrance addition channels and no information was given for the subsequent isomerization or decomposition reactions. It is interesting to note that ethylene +  $\text{H}\dot{\text{O}}_2$  reaction takes place on the same potential energy surface as ethyl +  $\text{O}_2$ . Miller et al. [289] used a combination of electronic structure theory, variational transition-state theory, and solved a time-dependent master equation to study the kinetics of the reaction between ethyl and molecular oxygen over wide ranges of temperature and pressure. They stated that above  $\approx 700$  K, the reaction can be written as an elementary step of  $\dot{\text{C}}_2\text{H}_5 + \text{O}_2 \rightleftharpoons \text{C}_2\text{H}_4 + \text{H}\dot{\text{O}}_2$  which is consistent with the experimental results by Baldwin, Walker, and their co-workers [290, 291] indicating that the major bimolecular product from the alkyl +  $\text{O}_2$  reaction is alkene +  $\text{H}\dot{\text{O}}_2$ . However, from Figure 34, we can see that for the reaction of ethylene +  $\text{H}\dot{\text{O}}_2$ , the formation of the ethylperoxy radical is favored at low temperatures due to the lower barrier height, while at higher temperatures, the hydroperoxyalkyl and/or oxirane +  $\dot{\text{O}}\text{H}$  formation is faster because of the looser transition state structure.

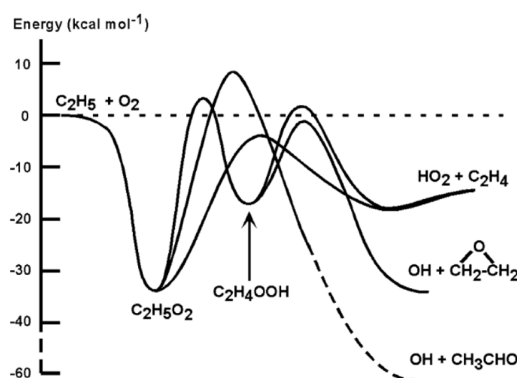


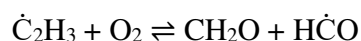
Figure 34. Schematic potential energy surface for the reaction of  $\dot{\text{C}}_2\text{H}_5$  with  $\text{O}_2$  [292].

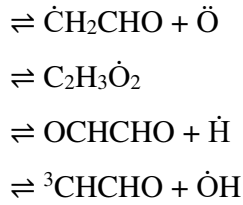
### 3.4.3 High temperature chemistry of ethylene combustion

#### $\text{C}_2\text{H}_4 (+\text{M}) \rightleftharpoons \text{Products}$ .

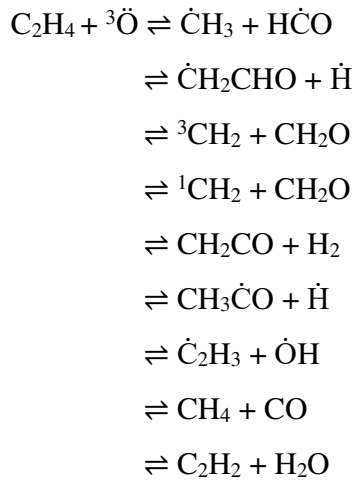
The C–H bond dissociation reaction is the one most likely to happen for ethylene decomposition. Alternatively,  $\text{H}_2$  elimination reaction to form acetylene is also a favored reaction channel at high temperatures. Farooq and co-workers [293] undertook time-resolved measurements of acetylene behind reflected shock waves at temperatures of 1600–2200 K and pressures of 3–5 bar for ethylene pyrolysis. They measured time histories of acetylene mole fraction from the absorption of a quantum cascade laser operating around 13.6  $\mu\text{m}$  without providing rate constants for the  $\text{H}_2$  elimination reaction. Georgievskii and Klippenstein [294] has investigated the kinetics of  $\dot{\text{C}}_2\text{H}_3 + \dot{\text{H}} \rightleftharpoons \text{C}_2\text{H}_4$  by Variable Reaction Coordinate–Transition State Theory (VRC-TST) which is recommended to be used for ethylene pyrolysis.

$\dot{\text{C}}_2\text{H}_3 + \text{O}_2 \rightleftharpoons \text{Products}$ . The vinyl radical reaction with molecular oxygen is of crucial importance to ethylene oxidation. It also plays a significant role in the reactivity of larger hydrocarbon fuels as ethylene can be formed in significant concentrations via hydrogen abstraction followed by  $\beta$ -scission. Sensitivity analysis for ethylene/air oxidation under shock tube conditions carried out by Metcalfe et al. [25] shows that when temperature goes to above 1100 K, the channel forming  $\dot{\text{C}}\text{H}_2\text{CHO} + \ddot{\text{O}}$  promoting the reactivity the most, however, the channel forming  $\text{CH}_2\text{O} + \text{H}\dot{\text{C}}\text{O}$  inhibiting the reactivity the most. Vinyl radical reacting with molecular oxygen and forming different products dominates the reactivity of ethylene oxidation. This key reaction having numerous product channels, some of which are chain branching and some of which are chain propagating, has been investigated extensively by both experiments [214–224] and theoretical calculations [39, 213, 225–229] in the literature. Results from the prior literature have been discussed in detail by Goldsmith et al. [213] and Metcalfe et al. [25]. The temperature- and pressure dependent rate constants calculations using VRC-TST, and conventional transition state theory as implemented in the RRKM/ME approach in the MESS code have been carried out by Goldsmith et al. [213]. They proposed that the main bimolecular products are  $\text{CH}_2\text{O} + \text{H}\dot{\text{C}}\text{O}$  (inhibit reactivity) at lower temperatures and  $\dot{\text{C}}\text{H}_2\text{CHO} + \ddot{\text{O}}$  (promote reactivity) at higher temperatures. Above 10 atm, the collisional stabilization of  $\text{C}_2\text{H}_3\dot{\text{O}}_2$  directly competes with these two product channels and the adduct decomposes primarily to  $\text{CH}_2\text{O} + \text{H}\dot{\text{C}}\text{O}$ . The next two most significant bimolecular products are  $\text{OCHCHO} + \dot{\text{H}}$  and  ${}^3\text{CHCHO} + \dot{\text{O}}\text{H}$ .





$\text{C}_2\text{H}_4 + {}^3\ddot{\text{O}} \rightleftharpoons \text{Products}$ . The reaction between ethylene and atomic oxygen is also important in promoting the reactivity of ethylene oxidation as it is a chain-branching pathway. This reaction has received much attention and has been investigated extensively in the literature both by theoretical calculations [209, 295] and experiments [296-302]. A weakly bound complex on a triplet surface is formed first and this is followed by rearrangement or dissociation to form several sets of products. The system can also change its electron spin and transition non-adiabatically to the singlet surface, where it can undergo a completely different set of rearrangements and dissociations. The total rate constant of this reaction appears to be reasonably well established experimentally over a wide range of temperatures but not the product distribution. Recently, Li et al. [209] applied the AITSTME approach that includes an *a priori* description of intersystem crossing, to study the kinetics of  ${}^3\ddot{\text{O}} + \text{C}_2\text{H}_4$  comprehensively and determined the branching ratios of different product sets at different temperatures and pressures.



They found that at elevated temperatures, the reaction channels forming  $\dot{\text{C}}\text{H}_2\text{CHO} + \dot{\text{H}}$  and  $\text{CH}_2 + \text{CH}_2\text{O}$  are dominant which differs from the room temperature preference for the  $\dot{\text{C}}\text{H}_3 + \text{H}\dot{\text{C}}\text{O}$  channel from the results of Nguyen *et al.* [295].

$\text{C}_2\text{H}_2 (+\text{M}) + \dot{\text{H}} \rightleftharpoons \dot{\text{C}}_2\text{H}_3 (+\text{M})$  and  $\text{C}_2\text{H}_4 (+\text{M}) + \dot{\text{H}} \rightleftharpoons \dot{\text{C}}_2\text{H}_5 (+\text{M})$ . After hydrogen atom addition to acetylene and ethylene, the bond energies are relatively low and the radical tends to dissociate rapidly back to the reactants. This is particularly significant at elevated temperatures as the  $\dot{\text{H}}$  atom produced is free to undergo chain branching with molecular oxygen. The reverse of this reaction is also the decomposition of vinyl and ethyl radicals. The rate constants of these reactions are important in determining such global combustion properties as laminar flame speed,

extinction, and ignition limit. Rate constants of the addition reaction have been investigated extensively by experiments at temperatures below 1000 K, as reviewed by Miller and Klippenstein [303] who highlighted the lack of experimental studies at combustion-relevant conditions. The most complete theoretical treatments of the reactions of interest here are those of Knyazev and Slagle [304] for  $\dot{\text{H}} + \text{C}_2\text{H}_2$  and Feng et al. [305] for  $\dot{\text{H}} + \text{C}_2\text{H}_4$ . The theoretical work from Miller and Klippenstein [303] improved on these studies by using variational transition-state theory, high-level electronic-structure calculations to characterize the stationary-point regions of the PES, and used a two-dimensional master equation in calculating the number of states for both  $E$  and  $J$  which is more accurate than the one dimensional ME used by Feng et al. [305]. The ethylene mechanism provided by Metcalfe et al. [25] in AramchMech 1.3 adopted the theoretical results from Miller and Klippenstein [303] by reducing both the high-pressure and low-pressure limits of the addition reaction by 30% to achieve a better agreement with high temperature ignition delay measurements. This adjustment is reasonable and within the uncertainty of the theoretical calculation.

Yang and Tranter [306] investigated the high-temperature dissociation of ethyl radicals behind incident shock waves in a diaphragmless shock tube by laser schlieren densitometry in the temperature range of 1150–1870 K and pressures of  $55 \pm 2$  Torr. Their measurement results are in very good agreement with the calculations from Miller and Klippenstein [303].

#### 3.4.4 Ethylene combustion mechanism

The ethylene mechanism utilized here is from AramcoMech 1.3 which was developed by Metcalfe et al. [25]. Rate constants of vinyl radical +  $\text{O}_2$  in AramcoMech 1.3 were estimated by Metcalfe based on comprehensive comparison and review of previous theoretical calculations and also the model behavior on the ignition delay times of ethylene oxidation at different temperatures and pressures. By taking the rate constants from the recent theoretical work of Goldsmith et al. [213] for vinyl radical +  $\text{O}_2$  and substituting it for the estimated values used by Metcalfe et al., and after making few changes in the rate constants (increasing the rate constants for  $\dot{\text{C}}_2\text{H}_3 + \text{O}_2 \rightleftharpoons \dot{\text{C}}\text{H}_2\text{CHO} + \ddot{\text{O}}$  by 10% and decreasing the rate constants for  $\dot{\text{C}}_2\text{H}_3 + \text{O}_2 \rightleftharpoons \text{CH}_2\text{O} + \dot{\text{H}}\text{CO}$  by 10%) the revised model can capture all the targets related to ethylene oxidation provided by Metcalfe et al. [25]. We utilize AramcoMech 1.3 in this work for its comprehensive development and testing for ethylene, as well as hydrogen [196], hydrogen/CO mixtures [196], methane, ethane, formaldehyde, which are all relevant to ethylene combustion. The chemistry of key radicals related with ethylene oxidation, such as  $\dot{\text{C}}\text{H}_2\text{CHO}$ ,  $\dot{\text{H}}\text{CCO}$ ,  $\dot{\text{H}}\text{CO}$ , etc., has also been included and extensively validated in AramcoMech 1.3.

The ethylene mechanism in AramcoMech 1.3 has been validated against comprehensive shock tube ignition delay time measurements from Kopp et al. [32] ( $\text{C}_2\text{H}_4/\text{Air}$ , 1003–1401 K, 1.1–24.9 atm,  $\phi = 0.3$ –2.0), Saxena et al. [33] ( $\text{C}_2\text{H}_4/\text{O}_2/\text{Ar}$ , 1000–1650 K, 2.0–18.0 atm,  $\phi = 1, 3$ ), and Penyazkov et al. [34] ( $\text{C}_2\text{H}_4/\text{Air}$ , 1060–1520 K, 5.9–16.5 atm,  $\phi = 0.5$ –2.0), jet-stirred reactor species profiles from Dagaut et al. [35] ( $\text{C}_2\text{H}_4/\text{O}_2/\text{N}_2$ , 880–1253 K, 1–10 atm,  $\phi = 0.1, 4.0$ ), Jallais et al. [36] ( $\text{C}_2\text{H}_4/\text{O}_2/\text{N}_2$ , 773–900 K, 1 atm,  $\phi = 3.0$ –10.0), and Le Cong et al. [37] ( $\text{C}_2\text{H}_4/\text{O}_2/\text{N}_2$ , 950–1450 K, 1 atm,  $\phi = 0.5$ –2.0), flow reactor species profiles from Carriere [38]

(C<sub>2</sub>H<sub>4</sub>/O<sub>2</sub>/N<sub>2</sub>, 850–950 K, 5–10 atm,  $\phi = 2.5$ ) and Lopez [39] (C<sub>2</sub>H<sub>4</sub>/O<sub>2</sub>/N<sub>2</sub>, 600–900 K, 60 atm,  $\phi = 1.0, 5.0$ ), laminar flame speeds from Hassan et al. [40] (C<sub>2</sub>H<sub>4</sub>/Air, 298 K, 1 and 2 atm,  $\phi = 0.5$ –1.4), Egolfopoulos et al. [41] (C<sub>2</sub>H<sub>4</sub>/Air, 298 K, 1 atm,  $\phi = 0.5$ –2.2), Jomaas et al. [42] (C<sub>2</sub>H<sub>4</sub>/Air, 298 K, 1, 2 and 5 atm,  $\phi = 0.7$ –1.4), and Kumar et al. [43] (C<sub>2</sub>H<sub>4</sub>/Air, 298, 360 and 470 K, 1 atm,  $\phi = 0.9$ –1.6), and flame species profiles from Bhargava and Westmoreland [44] (C<sub>2</sub>H<sub>4</sub>/O<sub>2</sub>/Ar, 300 K, 20 Torr,  $\phi = 1.9$ ). AramcoMech 1.3 can capture the above-mentioned experimental measurements of IDT quite well.

Shao et al. [140] measured ignition delay time of small hydrocarbons including methane, ethylene, propene and their blends at elevated pressures, and provided a valuable constraint for the refinement of the core small-hydrocarbon sub-mechanisms used in all combustion kinetics. They found that both the AramcoMech 1.3 and USC Mech2 over predicted the reactivity at 16 atm and  $T > 1200$  K. However, AramcoMech 1.3 showed a very low equivalence ratio dependence which was in good agreement with their measurements. Moreover, the AramcoMech 1.3 also predicted the high pressure (60 atm) IDT data very closely. On the other hand, the USC Mech2 did not capture the equivalence ratio dependence at 16 atm and also pronouncedly over predicted the ethylene reactivity at 60 atm. Apart from the vinyl + O<sub>2</sub> reaction, pressure-dependent rate constants for the  $\ddot{O}$  atom addition to ethylene calculated by Li et al. [209] needs to be updated in the ethylene mechanism of AramcoMech.

### 3.5 The combustion chemistry of propene

Propene is a significant component of liquefied petroleum gas (LPG) and a key intermediate in the combustion of higher paraffins (*e.g.*, propane, n-butane, n-heptane, and iso-octane), cycloparaffins, or from the side chain of alkylbenzenes [307]. It can be formed either through the pyrolysis of fuel molecules or  $\beta$ -scission of fuel radicals. As a key hierarchical component, it is very important to understand the combustion characteristics of propene. Apart from the importance of propene itself, the resonance stabilized allyl radical can easily be formed through H-atom abstraction by  $\dot{O}H$ ,  $H\dot{O}_2$ ,  $CH_3\dot{O}_2$ ,  $CH_3\dot{O}$ , O<sub>2</sub>,  $\ddot{O}$ , etc., from the allylic hydrogen atom. The allyl radical is also relevant to the formation of aromatics via allene, propyne, and the propargyl radical, the key PAH precursor.

The mechanism development and experimental measurements of propene oxidation using different facilities have been reported extensively in the literature [37, 45-52] and have been documented by Burke et al. [52]. Westbrook and Pitz [47] developed a comprehensive chemical kinetic model for oxidation and pyrolysis of propane and propene. Based on this work, five years later, Wilk et al. [48] developed a detailed chemical kinetic mechanism for propene oxidation at low and intermediate temperatures to simulate the static reactor data. They highlighted the importance of the addition of  $\dot{O}H$  to propene and H-atom abstraction by  $\dot{O}H$  from propene in determining the subsequent distributions of intermediate products, such as acetaldehyde, acrolein, and formaldehyde. They measured the NTC behavior and also predicted it by their model. The occurrence of multiple cool flames was also predicted in the model at the same temperatures as recorded in the experiment.

Dagaut et al. [45] developed a comprehensive mechanism to reproduce their JSR speciation data. Le Cong [37] investigated the propene oxidation in the presence of CO<sub>2</sub> and H<sub>2</sub>O in a jet-stirred reactor, and an updated reaction mechanism based on the one published by Dagaut et al. [45]

was used to simulate the experimental results. Braun-Unkloff et al. [50] developed a propene model and validated it against the laminar flame speed and ignition delay time of different propene-oxygen mixtures. Davis and Law [46] also proposed a detailed chemical kinetic mechanism for propene oxidation. Their mechanism has been validated against experimental measurements taken in flow reactor as well as flame speed data.

Heyberger et al. [49] generated the detailed mechanism for the oxidation and combustion of propene by their EXGAS code. The mechanism was validated against the data obtained in a static vessel and jet-stirred reactor. The mechanism reproduced correctly both the NTC observed at ~ 630 K and the variations of the concentrations with residence time of  $C_3H_6$ , CO,  $CO_2$ ,  $CH_4$ ,  $C_2H_2$ ,  $C_2H_4$ , etc. They also carried out flux and sensitivity analyses to get insight into the kinetic structure of the mechanism, e.g., NTC behavior of the mechanism. They stated that at low temperatures, the NTC is mainly due to the reversibility of the molecular oxygen addition to the adduct,  $\dot{C}_3H_6OH$ , which yields degenerate branching agents via a mechanism similar to that of alkyl radicals and two additions of oxygen.

Very recently, Burke et al. [51, 52] developed the comprehensive model for propene oxidation and pyrolysis. The model has been validated against new experimental data for ignition delay time, laminar flame speed, and speciation profiles from jet-stirred and flow reactors over a wide range of temperature and pressures. As the mechanism developed by Burke et al. [51, 52] has been extensively validated over a wide range of experimental measurements, it will be used in the following discussion. The important reaction classes have also been highlighted by Burke et al. [52] and here we focus on the ones updated recently.

### 3.5.1 High temperature chemistry of propene combustion

$C_3H_6 (+M) \rightleftharpoons Products$ . The detailed model for propene oxidation developed by Burke et al. [52] shows that the propene/air laminar flame speeds are sensitive to propene decomposition to allyl radical and a hydrogen atom. Unimolecular decomposition of propene has received much attention both theoretically and experimentally in the literature which has been documented by Wang et al. [308] and Ye et al. [309]. Recently, Wang et al. [308] developed a mechanism that describes the molecular weight growth kinetics observed during propene pyrolysis. They carried out propene pyrolysis experiments at 848–1148 K with nominal residence times of ~ 2.4, 1.2 and 0.5 s at ~ 0.83 atm. Ye et al. [309] performed high-level ab initio calculations on unimolecular decomposition of propene using the VRC-TST to treat the radical-radical recombination reaction processes. Their results show that the reaction channels forming allyl +  $\dot{H}$  and  $\dot{C}_2H_3 + \dot{C}H_3$  are the two main competitors. Hung et al. [310] also studied this reaction system both theoretically and experimentally. The potential energy surface for possible reaction channels was investigated at the CBS-QB3 level of theory, coupled with RRKM/ME calculations for the main reaction pathways. Experimental measurement has also been carried out by using a highly sensitive detection technique behind reflected shock waves at 2 atm and 1450–1710 K. They found that the product channel forming allyl +  $\dot{H}$  is much more competitive than that forming vinyl +  $\dot{C}H_3$  and the branching ratio between these two channels is approximately 0.8:0.2.

*Hydrogen atom abstraction by  $\dot{O}H$ ,  $\dot{H}O_2$ ,  $\dot{C}H_3$ ,  $CH_3\dot{O}_2$ ,  $CH_3\dot{O}$ ,  $O_2$  etc.* Three radicals can be formed from propene after hydrogen atom abstraction from three sites: the methyl site forming the resonance stabilized allyl radical, the other terminal carbon site forming the vinylic radical and the central carbon forming secondary vinylic radical. Hydrogen atom abstraction by radicals of  $\dot{O}H$ ,  $\dot{H}O_2$ ,  $\dot{C}H_3$ ,  $CH_3\dot{O}_2$  and  $CH_3\dot{O}$  from the allylic site inhibits the reactivity of fuel oxidation

because those reactions consume relatively highly reactive radicals and form the resonance stabilized allyl radical. From the BDE comparison of the three C-H bonds in propene, it is clear that hydrogen atom abstraction from the allylic site is the most dominant and competitive reaction channel.

Hydrogen atom abstraction by  $\dot{\text{O}}\text{H}$  radical from propene has been extensively studied experimentally for the total rate constants, whereas theoretical investigations provided comprehensive results on the PES [203, 236, 238, 311-316]. The product channel forming allyl radical +  $\text{H}_2\text{O}$  is dominant over the other two abstraction reaction channels which form propen-1-yl +  $\text{H}_2\text{O}$  and propen-2-yl +  $\text{H}_2\text{O}$  when temperature is higher than 1000 K at 760 Torr, whilst the contribution of these three channels to the propene oxidation reactivity is quite different. The channel forming allyl +  $\text{H}_2\text{O}$  inhibits the reactivity through the entire temperature range of 700–1500 K, but the other two abstraction channels forming propen-1-yl and propen-2-yl radicals did not show any significant contribution to the reactivity of propene oxidation. Even though the branching ratios for the formation of propen-1-yl and propen-2-yl radicals are low even at high temperatures, their subsequent reactions with molecular oxygen forming oxygen atom and the corresponding radical promote the reactivity pronouncedly.

Allylic hydrogen atom abstraction by  $\text{H}\dot{\text{O}}_2$  radical has been investigated by Zádor et al. [232] who found that this reaction channel is non-negligible and competes with the addition reactions. This influences the role of propene +  $\text{H}\dot{\text{O}}_2$  reaction on the autoignition property of propene. Allylic hydrogen atom abstraction by  $\dot{\text{C}}\text{H}_3$  radical has been found to play a significant role in the methane formation detected in JSR[52].

Allylic hydrogen atom abstraction by molecular oxygen plays a significant role in promoting the reactivity of propene oxidation at high temperatures (e.g.,  $T = 1250$  K,  $p = 10$  atm and  $\phi = 2.0$ ) [52]. Rate constants for this reaction channel have been studied both experimentally and theoretically in the literature. Burke et al. [52] gave a very detailed comparison and discussion of this reaction for the propene oxidation model. Rate constants used in their model are close to the one for toluene +  $\text{O}_2$  system. Very recently, Zhou et al. [208] performed a very comprehensive high level ab initio study on a series of rate constants of the hydrogen atom abstraction from the allylic site by molecular oxygen. Their calculated rate constant for propene +  $\text{O}_2$  is in good agreement with the experimental measurements of Stothard and Walker [206].

*$\text{C}_3\text{H}_6 + \dot{\text{H}} \rightleftharpoons \text{Products}$ .* The addition of  $\dot{\text{H}}$  atom to propene is one of the important reaction that opens the double bond in propene oxidation chemistry at high temperatures and this reaction can form n- $\dot{\text{C}}_3\text{H}_7$  radical through central addition and iso- $\dot{\text{C}}_3\text{H}_7$  through terminal addition. It can also form ethylene +  $\dot{\text{C}}\text{H}_3$  radical through a chemically activated reaction process and this inhibits reactivity at high temperatures as it is in competition with the chain branching reaction pathway of  $\dot{\text{H}} + \text{O}_2 \rightleftharpoons \dot{\text{O}}\text{H} + \dot{\text{O}}$ . Miller and Klippenstein employed high-level electronic structure methods to characterize the PES, RRKM theory to calculate microcanonical E,J-resolved rate constants for the dissociation processes, and master-equation methods to determine phenomenological rate constants  $k(T,p)$ , for all of the non-abstraction reaction. [317]

*$\text{C}_3\text{H}_6 + \dot{\text{O}} \rightleftharpoons \text{Products}$ .* The addition of  $\dot{\text{O}}$  atom to propene is another important reaction that opens the double bond in propene oxidation chemistry at high temperatures. Cavallotti and collaborators [210, 211] reported experimental/theoretical studies of this reaction by combining crossed molecular beam mass spectrometry experiments with high-level ab initio electronic

structure calculations of the triplet and singlet potential energy surfaces together with the intersystem crossing between these two PESs and solved the RRKM/ME.

$\dot{C}_3H_5-s+O_2 \rightleftharpoons \text{Products}$  and  $\dot{C}_3H_5-t+O_2 \rightleftharpoons \text{Products}$ . Even though the formation of  $\dot{C}_3H_5-s$  and  $\dot{C}_3H_5-t$  radicals is not competitive with that of  $\dot{C}_3H_5-a$ , the formation of the two vinylic radicals should be considered at high temperatures. Their subsequent reaction with molecular oxygen can form vinoxyl radicals and oxygen atom which promote reactivity. Detailed investigations on the kinetics of those reactions are quite limited and so far no theoretical or experimental results on these specific reaction systems are available. Analogy to the high-level calculations carried out for vinyl radical with molecular oxygen by Goldsmith et al. [213] is normally used for the kinetics of the vinylic radicals reactions with molecular oxygen.

### 3.5.2 Intermediate temperature chemistry of propene combustion

$C_3H_6 + HO_2 \rightleftharpoons \text{Products}$ . Addition reaction of  $HO_2$  radical to the double bond in propene is one of the major reactions in the propene oxidation mechanism at intermediate temperatures of 800 K to 1200 K. Zádor et al. [232] has studied the addition reaction between propene and  $HO_2$  radical over wide temperature and pressure ranges. The alkylhydroperoxy-formation ( $\dot{Q}OOH$ ) is the major pathway at higher temperatures and the alkylperoxy-formation ( $RO\dot{O}$ ) is dominant at the lower end of the temperature range with the crossing temperature being near 600 K. At higher pressures, the  $\dot{Q}OOH$  radicals are much more stable which can lead to chain branching when reacting with a second oxygen molecule. They also found that  $HO_2$  mostly adds to the carbon atom with more C–C bonds, following a quasi-Markovnikov's rule and at ~900 K, and the branching ratio of allylic abstraction by  $HO_2$  becomes equal to that of the addition channel.

$\dot{C}_3H_5-a+HO_2 \rightleftharpoons \text{Products}$ . Rather than reacting with molecular oxygen like the vinylic radicals, the allyl radical prefers reacting with  $HO_2$  radical and the well depth for this radical-radical recombination can reach 55.2 kcal mol<sup>-1</sup> [231]. This reaction promotes the reactivity at low to intermediate temperatures and can consume half of the allyl radicals at approximately 875 K and 1 atm [52] and its influence on propene oxidation has been fully documented by Burke et al. [52]. The PES for the radical-radical recombination reaction of allyl with hydroperoxyl radicals, the thermal decomposition of allyl hydroperoxide, and the unimolecular reactions of allyloxy radical computed at a high-level of theory was coupled with RRKM/ME calculations by Goldsmith et al. [231] to evaluate the temperature- and pressure-dependence of the rate constants. So far, this is the only theoretical investigation on this reaction class and rate constants provided in this work have been adopted in the propene oxidation mechanism [52] as well for butene isomers using their analogy with propene [86-88].

$\dot{C}_3H_5-a+\dot{C}H_3 \rightleftharpoons C_4H_8-1$ . The radical-radical recombination of allyl and methyl radicals forming 1-butene is an important chain terminating reaction which inhibits reactivity of the propene oxidation system. Detailed discussion on the impact of this reaction on propene ignition delay time predictions has been given by Burke et al [52].

$\dot{C}_3H_5-a + \dot{C}_3H_5-a \rightleftharpoons C_6H_{10}$ , and  $C_6H_{10}$  sub-mechanism. The radical-radical self-recombination reaction of allyl radicals can form 1,5-hexadiene and this reaction inhibits reactivity at low and intermediate temperatures. Tranter and co-workers [318, 319] measured the rate constant of this reaction in a single pulse shock tube with gas chromatographic measurements at 1–10 bar and 650–1300 K. Georgievskii et al. [320] have carried out variable reaction coordinate transition state theory to calculate the self-recombination reaction of allyl radicals and high pressure limiting rate constants has been provided. There is no theoretical or experimental investigation

on the oxidation of 1,5-hexadiene in the literature and the reaction class of propene oxidation can be used as an analogy for the sub-mechanism of 1,5-hexadiene oxidation, by considering the BDE difference between the primary and secondary allylic hydrogen atoms.

### 3.5.3 Low temperature chemistry of propene combustion

$C_3H_6 + \dot{O}H \rightleftharpoons Products$ . Addition reaction of  $\dot{O}H$  radical to the double bond in propene is one of the major reactions in the propene oxidation mechanism when temperature is lower than 850 K. This reaction has been studied extensively in the literature. From modeling development point of view, even though the total rate constants of this reaction is important in determining the consumption of propene at low temperatures, the branching ratio between the terminal addition and the central addition is more important in determining the reactivity of propene oxidation. That is because the subsequent reaction channels for the terminal and central adducts are different, with the terminal adducts preferring chain propagation reaction channels and the central adducts favoring chain branching reaction channels. In the model development of propene, Burke et al. [52] have taken the total addition reaction rate constants of  $\dot{O}H$  addition to propene the same as the one provided by the calculated results of Zádor et al. [236] with branching ratio adjustment taken into consideration to match the propene oxidation reactivity. A systematic investigation on the branching ratio of the  $\dot{O}H$  radical addition to the double bond along with the position change of the double bond will be valuable in the model development of alkenes low temperature chemistry.

### 3.5.4 Propene combustion mechanism behavior

Homogeneous ignition delay times of propene/air have been studied over wide ranges of temperatures and pressures of relevance to internal combustion engines using shock tubes and RCMs. Very recently, Burke et al. [51] carried out a series of IDT experiments in six different shock tubes and two rapid compression machines. This is the first study of its kind to directly compare ignition in several different shock tubes over a wide range of conditions. The cross-comparison of shock tubes suggests 20-30% reproducibility for the IDT measurements. The combination of shock tube and RCM data greatly expanded the data available for validation of propene oxidation models to higher pressures (2-40 atm) and lower temperatures (750-1750 K). Moreover, species profiles from JSR experiments obtained at near-atmospheric pressure over a temperature range of 800–1100 K and for equivalence ratios from  $\phi = 0.64$  to 2.19 have also been obtained and used in their model validation. Species profiles from two high-pressure flow reactor facilities, the VPFR ( $p=6-12.5$  atm,  $T= 843-1020$  K,  $\phi= 0.7-1.3$ ) and HPLFR ( $p=15$  atm,  $T= 800$  K,  $\phi= 0.35-1.25$ ), were also measured and used for model validation. The model developed in that work captured the wide-ranging experimental results quite well. Detailed model behavior for propene oxidation has been documented by Burke et al. [51, 52] and will not be discussed here.

One interesting point to highlight is that the model developed by Burke et al. [51, 52] is validated above 750 K and there is no NTC behavior reported in both the experimental measurements and the model prediction. However, the experimental measurements carried out by Wilk et al. [48] in a static reactor covering lower temperatures of 530–740 K, equivalence ratios of 0.8–2.0, and a pressure of 600 Torr show pronounced NTC behavior for propene oxidation, especially when the equivalence ratio equals 2, as shown in Figure 35. Heyberger et al. [49] also observed NTC behavior of propene oxidation experimentally at  $\approx 630$  K in a static vessel and the mechanism developed along with their experimental results reproduces the NTC correctly. Even though both

groups reported the NTC behavior of propene oxidation at lower temperatures, they have different explanation for this phenomenon. Wilk et al. [48] reported that the position of the NTC region is determined by the shift in the equilibrium of reactions involving the addition of molecular oxygen to hydrocarbon radicals,  $\dot{R} + O_2 (+M) \rightleftharpoons \dot{R}O_2 (+M)$ , and in propene oxidation, the most important hydrocarbon radicals that participate in these reactions are  $\dot{C}_3H_5$ ,  $\dot{C}H_3$ ,  $\dot{C}_2H_5$ ,  $i\dot{C}_3H_7$ ,  $CH_3\dot{C}O$  and  $C_2H_3\dot{C}O$ . The peroxy radicals ( $\dot{R}O_2$ ) can further react with the fuel through H-atom abstraction,  $\dot{R}O_2 + C_3H_6 \rightleftharpoons RO_2H + \dot{C}_3H_5$ , to produce hydroperoxides which thermally decompose to form  $\dot{R}O + \dot{O}H$  resulting in chain branching. As the temperature is raised, the equilibrium of the  $\dot{R} + O_2 (+M) \rightleftharpoons \dot{R}O_2 (+M)$  reactions is shifted to the left. The overall rate of chain branching decreases significantly and the region of NTC behavior is reached. The addition reaction of hydroxyl radical to propene has also been included in their mechanism followed by the first molecular oxygen addition reaction to produce acetaldehyde via Waddington mechanism. No specific reaction accounting for the NTC behavior has been reported in that work.

Alternatively, Heyberger et al. [49] stated that at low temperatures, the NTC is mainly due to the reversibility of the addition to oxygen of the adducts,  $\dot{C}_3H_6OH$ , which yields degenerate branching via a mechanism similar to that of alkyl radicals and involving two oxygen additions. Few important reactions have been proposed for the NTC behavior, including (1)  $C_3H_6OHO\dot{O} + C_3H_6 \rightleftharpoons \dot{C}_3H_5 + C_3H_6OHOOH$ , (2)  $\dot{C}_3H_5OHO\dot{O}H + O_2 \rightleftharpoons \dot{O}_2C_3H_5OHO\dot{O}H$ , (3)  $\dot{C}_3H_6OOH + O_2 \rightleftharpoons \dot{O}_2C_3H_6OOH$ , (4)  $\dot{C}_3H_5 + HO_2 \rightleftharpoons C_3H_5OOH$ , and (5) addition of  $\dot{O}H$  radicals to propene. Considering the reaction barrier and the concentration of  $HO_2$  radical at low temperatures, the reaction (5) involving the addition of  $\dot{O}H$  radical to propene should be the main reaction accounting for the NTC behavior. Heyberger et al. [49] proposed that the formed adduct  $\dot{C}_3H_6OH$  can add to oxygen to form  $\dot{O}OC_3H_6OH$  radicals which can isomerize to form  $\dot{C}_3H_5OHO\dot{O}H$ , and further oxygen addition to  $\dot{C}_3H_5OHO\dot{O}H$  radical followed by isomerization / decomposition leads to the formation of  $\dot{O}H$  radicals and  $C_2H_4OHCOOOH$ , which are degenerate branching agents and easily decompose by breaking of the O–OH bond. This is consistent with what we found in the low temperature oxidation of butene isomers [86-88] where the NTC behavior was attributed to the addition reaction of hydroxyl radical to the double bond followed by first and second  $O_2$  additions leading to the chain branching reactions.

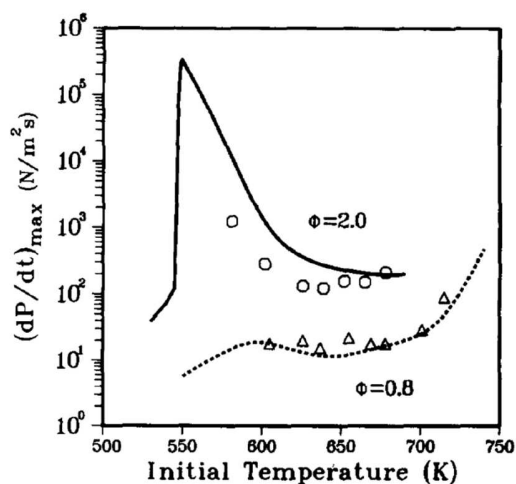


Figure 35. The variation of maximum rate of pressure rise,  $(dP/dt)_{\max}$ , with initial temperature for propene oxidation. The curves represent the computed results using the detailed mechanism developed by Wilk et al. [48], and the symbols represent the experimental results that have not been previously reported.

### 3.5.5 Chemistry difference between propene and ethylene oxidation

The important reaction classes for propene oxidation over the entire temperature range are consistent with the ones categorized in Figure 30, and those for ethylene oxidation also fall into the scheme shown in Figure 30 mainly focusing on the high temperature chemistry.

There are three major differences in the chemistry of propene and ethylene. *Firstly*, the differences arise from the allylic radical chemistry. The resonance stabilized allyl radical plays a significant role in propene oxidation at intermediate temperatures while it is obvious that ethylene does not have that type of radicals and the corresponding chemistry. *Secondly*, the different chemistry is from the low temperature chemistry with propene having an NTC behavior and ethylene not having NTC. That is because the addition of hydroxyl radical to ethylene is followed by molecular oxygen addition to finally produce formaldehyde and  $\dot{O}H$  radical through Waddington mechanism. No second molecular oxygen addition can happen for the ethylene low temperature chemistry and hence no NTC behavior can be observed experimentally and/or from simulations. *Thirdly*, the different chemistry can be from the addition reactions of  $H\dot{O}_2$  radicals. For the reaction of ethylene +  $H\dot{O}_2$ , the formation of the ethylperoxy radical is favored at low temperatures, while at higher temperatures the hydroperoxyalkyl and/or oxirane +  $\dot{O}H$  formation is faster. Alternatively, for propene,  $H\dot{O}_2$  radical adds to the central carbon to form  $\dot{Q}OOH$  radical and this  $\dot{Q}OOH$  radical is much more stable at higher pressures, and can thus lead to chain branching when reacting with a second oxygen molecule.

### 3.6 The combustion chemistry of butene isomers

Butene isomers are known as important intermediates in the pyrolysis and oxidation of high-order hydrocarbons and they are also known as the shortest alkene with structural isomers including isobutene, 1-butene, cis-2-butene, and trans-2-butene. Moreover, they are also key pyrolysis products for conventional petroleum-derived fuels [321]. 1-Butene is the smallest unsaturated hydrocarbon having a secondary allylic carbon group and primary carbon groups which exhibit both alkane- and alkene-type chemistry. Understanding the oxidation chemistry of butene isomers is important in revealing the consumption process of jet and rocket fuels [307, 321].

The mechanism development and experimental measurements using different facilities have been carried out extensively for isobutene, 1- and 2-butene and reported in the literature [68-88]. Detailed discussion on the experiment and mechanism development for butene isomers has been documented in the recent work published by Zhou et al. [88] and Li et al. [86, 87]. Therefore, here we only address the important reaction classes and their variation with temperature according to the modeling and experimental measurements of these three species.

Dagaut and Cathonnet [76] investigated the oxidation of isobutene for the first time in a jet-stirred reactor at high temperature (~ 800–1230 K) at 1, 5 and 10 atm. They also developed a detailed kinetic reaction mechanism (110 species and 743 reactions, most of them reversible) to simulate the oxidation of isobutene in these conditions and the ignition of isobutene-oxygen-argon mixtures in a shock tube. Their model predictions showed that the oxidation of isobutene under the investigated conditions proceeds mainly through the following reaction paths: (a) at atmospheric pressure,  $iC_4H_8 (-H) \rightarrow i\dot{C}_4H_7 \rightarrow \text{allene} + \dot{C}H_3$ , followed by oxidation routes of these intermediates; and (b) at high pressure,  $iC_4H_8 (-H) \rightarrow i\dot{C}_4H_7 \rightarrow \text{allene} + \dot{C}H_3$  and  $iC_4H_8 + \dot{O}H \rightarrow iC_4H_8OH (+O_2) \rightarrow \text{acetone} + CH_2O + \dot{O}H$ , followed by oxidation routes of these intermediates.

Zhao et al. [79] measured laminar flame speeds and ignition temperatures in nonpremixed counterflow experiments for the butene isomers at normal and elevated pressures of 2, 5 and 10 atm. Isobutene exhibited the highest ignition temperature, while those of trans-2-butene and cis-2-butene were quite similar to each other and slightly higher than that of 1-butene. These results showed that the reactivities of the butene isomers increase in the order of isobutene, 2-butene, and 1-butene.

Dagaut and co-workers developed a detailed chemical kinetic mechanism (201 species involved in 1787 reactions) to reproduce the experimental data for 1-butene [83] and 2-butene [85] obtained from a JSR and a combustion vessel. The model showed the importance of resonance stabilized radicals such as propenyl and butenyl radicals and they also mentioned that more data would help clarifying the ignition of 1-butene under fuel-lean conditions where the two reactions  $C_4H_8-1(+M) \rightleftharpoons \dot{C}_3H_5-a + \dot{C}H_3 (+M)$  and  $C_4H_8-1+O_2 \rightleftharpoons \dot{C}_4H_7-13 + HO_2$  influence the modeling particularly. Moreover, the model showed that the isomerization reaction of trans-2-butene  $\rightleftharpoons$  cis-2-butene represents an important initial step of trans-2-butene oxidation.

Zhang et al. [80] studied the pyrolysis of these three butene isomers in a flow reactor focusing on the decomposition reactions of fuel and recombination reactions to produce cyclic and aromatic species from 900 to 1900 K at 3 Torr. They proposed that the major decomposition pathways of 1-butene, 2-butene and isobutene are  $1-C_4H_8 \rightarrow a\dot{C}_3H_5 \rightarrow aC_3H_4 \rightarrow pC_3H_4 \rightarrow C_2H_2$ ,  $2-C_4H_8 \rightarrow sax\dot{C}_4H_7 \rightarrow 1,3-C_4H_6 \rightarrow \dot{C}_2H_3 \rightarrow C_2H_2$  and  $i-C_4H_8 \rightarrow i\dot{C}_4H_7 \rightarrow aC_3H_4 \rightarrow pC_3H_4 \rightarrow C_2H_2$ , respectively.

Recently, Zhou et al. [88] and Li et al. [86, 87] developed comprehensive chemical kinetic models for the oxidation of the three butene isomers and validated their models against new experimental measurements of ignition delay times, laminar flame speeds and literature experimental data related to the oxidation of butene isomers. The mechanism [87, 88] included in AramcoMech 2.0 for the oxidation of the three butene isomers is the most comprehensive one so far and has been extensively validated against a wide range of experimental data, hence this mechanism is adopted in the following discussions.

### 3.6.1 High temperature chemistry of butenes combustion

$C_4H_8(+M) \rightleftharpoons Products$ . Speciation measurements for the pyrolysis of isobutene in the PU flow reactor [322] and 1-butene [80] in a flow reactor are sensitive to the decomposition of the two species. In the case of isobutene, two important reaction channels highlighted are the allylic C–H bond fission reaction channel which has the lowest bond dissociation energy (forming 2-methylallyl ( $i\dot{C}_4H_7$ ) radical and an  $\dot{H}$  atom) and the C–C bond fission reaction channel (forming  $\dot{C}_3H_5-t$  and  $\dot{C}H_3$  radicals). The high pressure limit rate constant has been adopted by analogy with propene [202] and with further QRRK calculations to estimate the pressure fall off. However, in order to improve the agreement with flow reactor speciation measurements from [322], the rate constant for the formation of methylallyl radical and atomic hydrogen has been increased by a factor of two in the model developed by Zhou et al. [88].

Important reactions involving C–C and C–H bond breaking in 1- and 2-butene were included in the model developed by Li et al. [86, 87]. The pressure dependent rate constants for the C–C bond fission reactions were adapted from the study of Tsang et al [202, 323]. The allylic site C–H bond fission reaction was found to be the most favored channel, and the rate constants were estimated to match those validated in the 1-butene pyrolysis experiments of Zhang et al [80].

#### *Hydrogen atom abstraction by $\dot{O}H$ , $H\dot{O}_2$ , $O_2$ , $\dot{C}H_3$ , $CH_3\dot{O}_2$ , $CH_3\dot{O}$ , etc.*

For all of the hydrogen atom abstractions by different radicals from butene isomers, we find that abstraction from the allylic site is the fastest followed by the primary carbon site, with the vinylic site being the slowest which is in line with the C–H bond dissociation energies.

Ignition delay times of the butene isomers are highly sensitive to the H-atom abstraction reaction by  $\dot{O}H$  radicals from the allylic site over the entire range of temperatures and pressures. This reaction inhibits reactivity throughout the entire temperature range of the ignition delay time measurements because it consumes a highly reactive  $\dot{O}H$  radical and forms an unreactive resonance stabilized  $\dot{C}_4H_7$  radical. Rate constants for the H-atom abstraction from isobutene by  $\dot{O}H$  radicals has been investigated by both Sun et al. [324] based on the PES obtained at the CCSD(T)/6-311++G(d,p)//BH&HLYP/6-311G(d,p) level of theory and Zhou et al. [88] based on the PES obtained at the QCISD(T)/CBS//M062X/6-311++G(d,p) level of theory. Rate constants from these two calculations are within 40% from one another, but with different curvatures. The rate constants for the H-atom abstraction from 1-butene by  $\dot{O}H$  radical were adopted in the experimental and theoretical study carried out by Vasu et al. [325] with PES obtained at the CCSD(T)/6-311++G(d,p)//QCISD/6-31G(d,p) level of theory, and they were decreased by a factor of 2.6 which is the uncertainty provided by Vasu et al. [325]. Khaled et al. [205] measured the H-atom abstraction rate constants from isobutene by  $\dot{O}H$  radical behind reflected shock waves over the temperature range of 830 – 1289 K and pressures near 1.5 atm. Branching ratio between the two abstraction channels have also been measured in this study and their results are in very good agreement with the calculations carried out by Zhou et al. [88].

Rate constants for the H-atom abstraction reactions from isobutene by hydroperoxyl radical forming 2-methylallyl radical ( $i\dot{C}_4H_7$ ) have been investigated theoretically by Zádor et al. [232] and the other H-abstraction channel forming the vinylic radical have been studied by Zhou et al. [88]. Rate constants for that in 1-butene are taken from the theoretical results provided for propene by Zádor et al. [232] using the analogy between 1-butene and propene.

Hydrogen atom abstraction by molecular oxygen from the allylic site in butene isomers plays an important role in determining the oxidation reactivity of butene isomers over the entire temperature range of 666–1650 K. In the oxidation of butene isomers, this reaction inhibits reactivity at temperatures below 900 K and promotes reactivity at temperatures above 900 K. That is because when temperature is lower than 900 K, the  $C_4H_8 + O_2 \rightleftharpoons \dot{C}_4H_7 + HO_2$  reaction occurs in the reverse direction which consumes the two radicals to form two stable molecules. When temperature is higher than 900 K, the reaction happens in the forward direction which consumes the two stable molecules and forms the two radicals. H-atom abstraction from the allylic carbon site on 1- and 2-butene results in the formation of the same products, and in this way both 1- and 2-butene oxidation mechanisms are intrinsically linked and a mechanism for one must contain the other. The reaction between isobutene and molecular oxygen has been investigated in the literature both experimentally [207] and theoretically [326]. Very recently, Zhou et al. [208] studied the rate constants of hydrogen atom abstraction from allylic C–H bonds by molecular oxygen from alkenes, furan, and alkylbenzene. Ignition delay times for 1-butene, 2-butene, isobutene, 2-methylfuran, 2,5-dimethylfuran, and toluene were increased by 50% to 2.0 times by using the new calculated rate constants provided by Zhou et al. [208]. This work provided the first systematic study of this key initiation reaction for compounds containing allylic hydrogen atoms.

Hydrogen atom abstraction by  $\dot{C}H_3$  radical mainly occurs on the allylic site of butene isomers. This reaction producing 1- and 2-methylallyl radicals and methane is predicted to be an important source of methane detected in the JSR. Rate constants for the 1-butene reaction with  $\dot{C}H_3$  radical are recommended using the estimated results taken from Tsang [202] and that for isobutene from Yasunaga et al. [73]. Hydrogen-atom abstraction by other important radicals, such as  $CH_3\dot{O}_2$ ,  $CH_3\dot{O}$  are also significant in the oxidation of butene isomers and have been taken into consideration in the respective model development works.

#### *$C_4H_8 + \dot{H} \rightleftharpoons Products$ .*

Sensitivity analysis for the ignition delay time of isobutene oxidation shows that the formation of propene and a  $\dot{C}H_3$  radical through the reaction of  $iC_4H_8 + \dot{H} \rightleftharpoons C_3H_6 + \dot{C}H_3$  inhibits reactivity at higher temperatures as it forms an unreactive  $\dot{C}H_3$  radical from a very reactive hydrogen atom, and this reaction also competes with the main chain branching reaction,  $\dot{H} + O_2 \rightleftharpoons \dot{O} + \dot{O}H$ . Accurate characterization of this propene formation channel is also important for predicting  $C_3H_6$  profiles in species-resolved experiments. In the model developed by Zhou et al. [88], the analogous rate constants for  $\dot{H}$  atom addition to and abstraction from propene calculated by Miller and Klippenstein [317] using a high level of theory were used to describe the kinetics of the isobutene reaction with  $\dot{H}$  atom. In the mechanism, the rate constant for the reaction channel forming  $C_3H_6$  and  $\dot{C}H_3$  radicals was decreased by a factor of three to better predict propene formation in the flow reactor data reported by Held et al. [322].

The H-atom addition to 1-butene is slightly different from that in isobutene. There are two carbon sites where the  $\dot{H}$  atom can add to via terminal and central additions. When  $\dot{H}$  atom adds to the terminal carbon atom, the reaction through chemical activation can form propene and  $\dot{C}H_3$  which will inhibit the reactivity for the same reason as that for isobutene. On the other hand, when  $\dot{H}$  atom adds to the central carbon atom, this will result in the formation of  $C_2H_4 + \dot{C}_2H_5$ , which will generate two vinyl radicals and three  $\dot{H}$  atoms thus ultimately promoting reactivity. Rate constants in the model of 1- and 2-butene oxidation were calculated using RRKM/ME to get pressure dependent values based on the  $\dot{C}_4H_9$  reactive PES obtained at the CCSD(T)/cc-

pVXZ//M06/6-311++G(d,p) level of theory (where  $X = D, T$  and  $Q$ ) extrapolated to the complete basis set limit [327, 328].

#### $C_4H_8 + \ddot{O} \rightleftharpoons Products.$

Oxygen atom addition to the C=C bond is one of the important reaction classes to break the double bond in alkene oxidation. Three important reaction channels of  $iC_4H_8 + \ddot{O} \rightleftharpoons i\dot{C}_3H_7 + H\dot{C}O$ ,  $iC_4H_8 + \ddot{O} \rightleftharpoons \dot{C}H_2CO + \dot{C}H_3 + \dot{C}H_3$ , and  $iC_4H_8 + \ddot{O} \rightleftharpoons iC_3H_6CO + \dot{H} + \dot{H}$  have been included in the mechanism of isobutene oxidation and these are chain branching reactions. It is a bit surprising to find out that in the mechanism of 1-butene oxidation, this  $\ddot{O}$  atom addition reaction did not show any significant sensitivity to any of the data sets presented in the model [86]. One possibility is that this reaction class has not been studied previously either experimentally or theoretically, thus the kinetics data used in the model need to be refined. Further investigation on this reaction class in butene isomers oxidation under combustion conditions will be helpful in improving the accuracy of the model.

#### $\dot{C}_4H_7-s + O_2 \rightleftharpoons Products$ and $\dot{C}_4H_7-t + O_2 \rightleftharpoons Products.$

Concentrations of the vinylic radicals are relatively small at low temperatures but increase with temperature. At high temperatures, vinylic radical reaction with molecular oxygen is the main pathway to consume these radicals. The reaction can generate alkenylperoxy radicals followed by O-O bond fission resulting in the formation of  $\ddot{O}$  atoms, which pronouncedly promote reactivity. In the combustion of ethylene [25, 31, 32] and propene [51, 52], it was found that the vinyl, 2-propenyl ( $\dot{C}_3H_5-t$ ) and 1-propenyl ( $\dot{C}_3H_5-s$ ) radicals were consumed almost entirely by reactions with molecular oxygen. To the best of our knowledge, there have been no previous studies on the reactions of vinylic radicals involved in butene isomers (1-buten-2-yl, 1-buten-1-yl, 2-buten-2-yl, isobuten-1-yl) with molecular oxygen. The rate constants of isobuten-1-yl radical with molecular oxygen have been adopted by analogy with propene [52] in the mechanism. In 1- and 2-butene oxidation, the total rate constants for the reactions of both 1-buten-2-yl ( $\dot{C}_4H_7-2$ ) and 1-buten-1-yl ( $\dot{C}_4H_7-1$ ) radicals with molecular oxygen and the subsequent O-O bond fission reactions are estimated by analogy to the reaction of vinyl radical with molecular oxygen from the high-level ab initio study of Goldsmith et al. [213]. Further theoretical or experimental investigations on this reaction class in the oxidation of butene isomers will be helpful to improve the accuracy of the model.

#### $i\dot{C}_4H_7 \rightleftharpoons Products$ , $\dot{C}_4H_7-s \rightleftharpoons Products$ and $\dot{C}_4H_7-t \rightleftharpoons Products.$

The decomposition of 2-methylallyl ( $i\dot{C}_4H_7$ ) radicals,  $i\dot{C}_4H_7 \rightleftharpoons C_3H_4-a + \dot{C}H_3$ , is competitive with its recombination reactions with other radicals such as  $\dot{C}H_3$ ,  $H\dot{O}_2$ ,  $i\dot{C}_4H_7$ , etc., in the intermediate temperature range. The rate constants for this reaction have been calculated by Zhou et al. [88] when developing the model. Sensitivity analysis for the ignition delay time of 1-butene oxidation at 1250 K shows that the isomerization of 1-methylallyl ( $\dot{C}_4H_7-3$ ) radical to 3-buten-1yl ( $\dot{C}_4H_7-4$ ) radical and vice versa, and the related  $\beta$ -scission reaction of 3-buten-1yl radical are sensitive reactions. The high-pressure limit rate constants for this reaction class were calculated on the  $\dot{C}_4H_7$  PES at the CCSD(T)/cc-pVXZ//M062X/6-311++G(d,p) (where  $X=D, T$ , and  $Q$ ) level of theory.

### 3.6.2 Intermediate temperature chemistry of butene combustion

#### $C_4H_8 + H\dot{O}_2 \rightleftharpoons Products.$

Detailed reaction pathways for the addition reactions of hydroperoxyl radicals to isobutene [88] and 1-butene [86] have been discussed in detail. Here, we mainly focus on the kinetic part. The rate constants for the addition reactions of hydroperoxyl radicals to 1-butene and the related reactions on the  $C_4H_9O_2$  PES have been investigated by different groups [232, 329-334]. High level ab initio calculations have been carried out by Zádor et al. [232] to investigate the rate constants for  $\dot{H}O_2$  radical addition to the non-terminal unsaturated carbon atom in 1-butene to form a hydroperoxyl-alkyl radical and its following reaction to form a cyclic ether and a hydroxyl radical and their calculated rate constants were adopted in the model development. Villano et al. performed a systematic investigation of alkylperoxyl radical decomposition to alkenes and hydroperoxyl radicals [332], and  $\dot{H}O_2 + \text{olefin}$  addition channels [330] using electronic structure calculations performed at the CBS-QB3 level of theory. The rate constants for the dissociation reactions were obtained from calculated equilibrium constants and literature review of experimental rate constants for the reverse association reactions. Rate constants from these calculations are used in the model development for the butene isomers.

*$i\dot{C}_4H_7 + \dot{H}O_2 \rightleftharpoons \text{Products}$ .*

Similar to propene oxidation where the allyl radical reaction with hydroperoxyl radical plays a significant role in determining the consumption of allyl radical in the oxidation reactivity of propene at intermediate temperatures [52], the reaction of 2-methylallyl and hydroperoxyl radicals is observed to be very important across a range of conditions, especially at low-to-intermediate temperatures, for butene oxidation. A rate of production analysis shows that at approximately 730 K, 30 atm, and  $\phi = 1.0$ , this reaction can consume approximately 47.1% of all 2-methylallyl radicals. Pressure dependent rate constants for this reaction have been taken from their analogs for the allyl +  $\dot{H}O_2$  reaction, which has been extensively studied by Goldsmith et al. [213]. The formed important intermediate methyl-allyloxy radicals can undergo both decomposition and isomerization reactions to produce different type of products. Rate constants for these reactions were also taken by analogy from the study of Goldsmith et al. [213] for propene.

*$\dot{C}_4H_7(1-3) + O_2 \rightleftharpoons C_4H_6 + \dot{H}O_2$ .*

The 1-methylallyl radical can be formed by H-atom abstraction from the secondary allylic carbon in 1-butene or the primary allylic carbon in 2-butene, see Figure 36. The reaction of 1-methylallyl radical with molecular oxygen promotes reactivity, as it consumes a stabilized allylic radical to generate a more reactive hydroperoxy radical. This reaction can only happen in 1- and 2-butene oxidation but not for isobutene. It is worth noting that this is not a chemical activation but rather a direct hydrogen abstraction reaction process. The well depth of the association reaction process of  $\dot{C}_4H_7(1-3) + O_2 \rightleftharpoons \dot{C}_4H_7(1-3)O_2$  is 19.9 kcal mol<sup>-1</sup> at the CBS-QB3 level of theory and the barrier for the subsequent concerted elimination to form 1,3-butadiene +  $\dot{H}O_2$  is 27.2 kcal mol<sup>-1</sup>, and hence, once the associated intermediate is formed, it will still dissociate back to  $\dot{C}_4H_7(1-3) + O_2$ . Alternatively, this reaction can happen through the H-atom abstraction from the primary carbon site and the rate constant is adopted from the theoretical work of DeSain et al. [292].

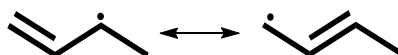


Figure 36. Stabilization of 1-methylallyl ( $\dot{C}_4H_7(1-3)$ ) radical.

*$\dot{C}_4H_7 + \dot{C}H_3 \rightleftharpoons C_5H_{10}$ .*

The recombination reaction of 2-methylallyl and methyl radicals to form 2-methyl-1-butene ( $i\dot{C}_4H_7 + \dot{C}H_3 \rightleftharpoons aC_5H_{10}$ ) represents the pathway which inhibits reactivity at intermediate and higher temperatures. This is the main reaction to form the 2-methyl-1-butene species which can be detected in JSR measurements. Similar reaction processes can also be found for 1- and 2-butene ( $\dot{C}_4H_7_{1-3} + \dot{C}H_3 \rightleftharpoons C_5H_{10-2}$  and  $\dot{C}_4H_7_{1-3} + \dot{C}H_3 \rightleftharpoons cC_5H_{10}$ ) and those also inhibit the reactivity of the system. Rate constants for these reactions are taken from Tsang [202] by analogy with allyl + methyl radical recombination.

$\dot{C}_4H_7 + \dot{C}_4H_7 \rightleftharpoons C_8H_{14}$ , and  $C_8H_{14}$  sub-mechanism.

The chain terminating self-recombination reaction of the resonance stabilized radicals formed in butene isomers inhibit reactivity significantly at low- and intermediate- temperatures because this reaction is competitive with the chain branching reaction between the resonance stabilized radical and hydroperoxyl radical. The radical recombination reaction between 2-methylallyl ( $i\dot{C}_4H_7$ ) radicals can form 2,5-dimethyl,1-5-hexadiene which will be consumed through further oxidation reaction via reaction classes similar to the ones we highlighted for alkenes in Figure 30. 1-Methylallyl ( $\dot{C}_4H_7_{1-3}$ ) radical can also undergo self-recombination to form 2,6-octadiene, 3-methyl,1-5-heptadiene and 3,4-dimethyl,1-5-hexadiene; branching ratios for these three reaction channels were recommended as 1:2:1 by Li et al. [86]. There are no theoretical or experimental measurements available for these reaction systems, thus rate constants are taken from Tranter and co-workers [318] for the allyl radical self-recombination. Rate constants for the 2,5-dimethyl,1-5-hexadiene formation were divided by a factor of 2.3 to match the low temperature ignition delay time measurement in the model developed by Zhou et al. [88]. This reaction class is crucial in determining the oxidation reactivity of butene isomers at low to intermediate temperatures and, therefore, future theoretical or experimental investigations on this reaction class are important and recommended.

### 3.6.3 Low temperature chemistry of butene combustion

$C_4H_8 + \dot{O}H \rightleftharpoons Products$ .

The addition reaction of  $\dot{O}H$  radical to butene isomers is one of the most important reaction classes for butene oxidation at temperatures lower than  $\sim 850$  K. In the oxidation of isobutene and 1-butene, branching ratio between the addition to the terminal and central carbon plays a significant role in determining the reactivity because the subsequent oxidation reaction pathways of the adducts are significantly different. As shown in Figure 37, taking the increased steric hindrance from the methyl group in isobutene into consideration, the branching ratio of these channels are treated as 75:25 keeping the total rate constant the same as that for  $\dot{O}H$  addition to propene calculated by Zádor et al. [236]. For the terminal addition, the formed adduct ( $i\dot{C}_4H_8OH$ -ti) will react with molecular oxygen and ultimately form acetone, formaldehyde and hydroxyl radical through Waddington mechanism which is a chain propagation reaction pathway. On the other hand, the adduct of  $i\dot{C}_4H_8OH$ -ti formed from the central addition can react with molecular oxygen to form acetone, formaldehyde and hydroxyl radicals through Waddington mechanism, and it can further react with the second molecular oxygen to get the low temperature chain branching products which promote the reactivity. At 730 K, even though only 4.4% of isobutene forms  $i\dot{C}_4H_8OH$ -ti, its subsequent chain branching reaction with molecular oxygen pronouncedly promotes low temperature reactivity, as shown in Figure 38.

Flux analysis carried out by Zhou et al. [88] shows that the importance of this  $\dot{O}H$  addition reaction in butene oxidation depends on the temperature. At 730 K and 30 atm,  $\dot{O}H$  radical

addition reaction consumes 21.7% of the fuel with 17.3% forming  $i\text{C}_4\text{H}_8\text{OH}$ -it through terminal addition and 4.4% forming  $i\text{C}_4\text{H}_8\text{OH}$ -ti radicals through central addition. When temperature increases to 850 K, only 7.9% of isobutene is consumed through the terminal addition and central addition no longer contributes at all. As the temperature goes up to 950 K, the addition reaction does not contribute to fuel consumption.

The same trend has also been found for the reaction of  $\dot{\text{O}}\text{H}$  radical addition to 1-butene. This is the most important reaction promoting reactivity at low temperatures ( $T = 700$  K) for 1-butene oxidation because low temperature chain branching reaction pathway can subsequently occur, as shown in Figure 39. Rate constants for the entrance addition reactions were estimated by analogy with the propene +  $\dot{\text{O}}\text{H}$  radical system as calculated by Zádor et al. [236]. Moreover, a branching ratio of 75:25 in favor of addition to the terminal carbon was adopted based on the experimental study by Loison et al. [237]. The influence of this branching ratio on ignition delay times at low temperatures can be seen in Figure 40.

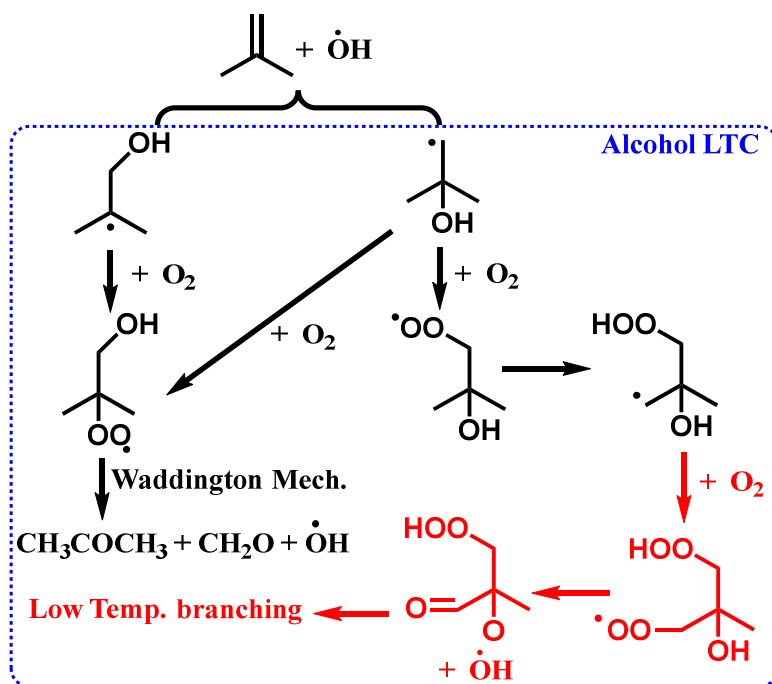


Figure 37. The addition reaction of  $\dot{\text{O}}\text{H}$  radical to isobutene and subsequent oxidation reaction pathways at  $\phi = 1.0$ , 730 K. Chain branching pathways promoting the reactivity are highlighted in red.

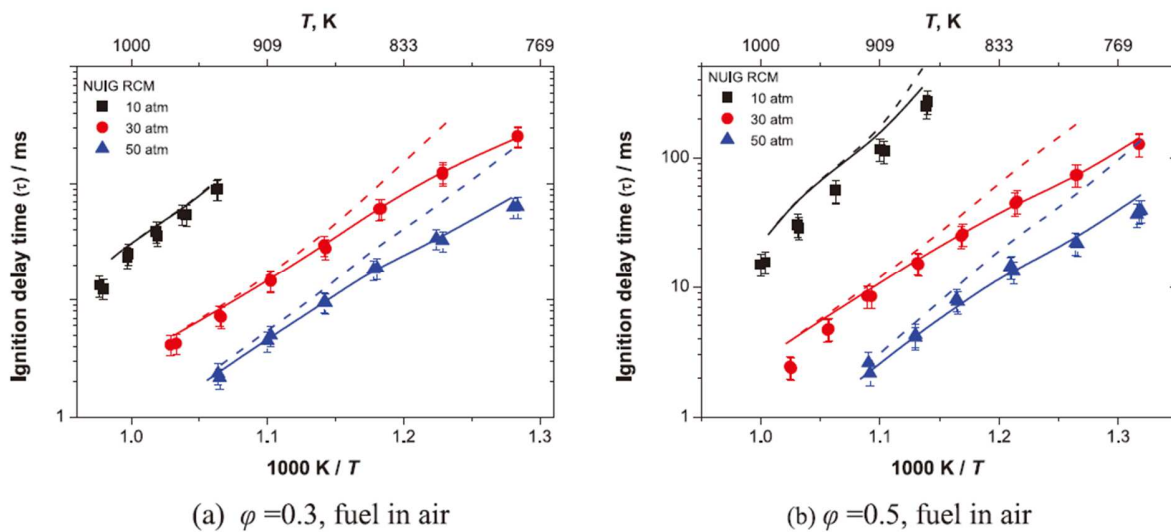


Figure 38. Model prediction by including (solid line) and excluding (dashed line) the second molecular oxygen addition reaction class in IDT [88].

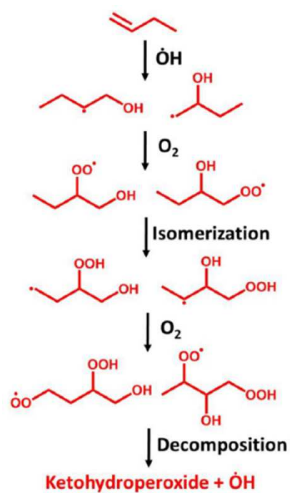


Figure 39. Low temperature chain branching reaction pathways for 1-butene oxidation [86].

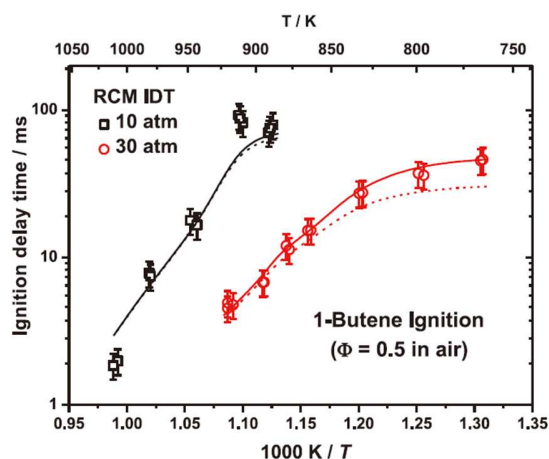


Figure 40. Branching ratio effects from the  $\dot{\text{O}}\text{H}$  terminal and central addition to 1-butene to IDTs at  $\phi = 0.5$ , fuel in air,  $p = 10$  and 30 atm. Terminal vs. central: solid line (75:25); dashed line (50:50) [86].

It is worth noting that the formed adducts from the addition of  $\dot{\text{O}}\text{H}$  radical to butene isomers are also alcohol radicals. Hence, the low temperature chemistry of butene overlaps with that of butanol oxidation at the same temperature. This treatment captures the low temperature reactivity of butene isomers oxidation quite well. However, further theoretical or experimental research providing accurate pressure and temperature dependent rate constants for the first and second radical addition to molecular oxygen will be necessary to achieve a better understanding of the low temperature chemistry of alkene oxidation.

### 3.6.4 Chemistry difference between butene isomers oxidation

Even with the same chemical formula, reactivity of the three butene isomers are quite different. As shown in Figure 41, 1-butene is the most reactive species followed by 2-butene and isobutene is the most un-reactive species at 30 atm for stoichiometric fuel/air mixtures. In order to explain the differences in reactivity due to the isomeric structure, sensitivity analyses for 1-, 2-butene and isobutene oxidation have been carried out by Li et al. [87] at identical conditions:  $\phi = 1.0$ ,  $T = 700$  K, 950 K, and 1250 K, and  $p = 30$  atm. Here, we highlight the chemistry difference among these three species as a function of temperature.

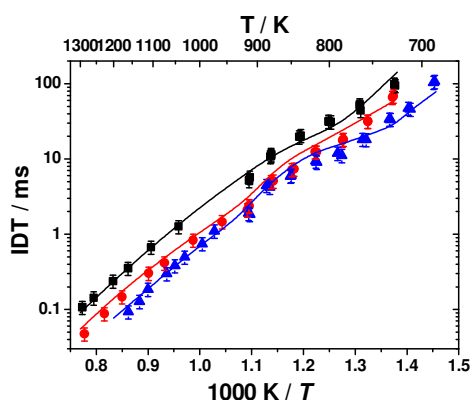


Figure 41. Ignition delay times comparison between the three butene isomers ( $\blacksquare$  isobutene,  $\bullet$  2-butene,  $\blacktriangle$  1-butene) at 30 atm with  $\phi = 1.0$  in air. Symbols are experimental measurements and lines are model predictions.

Hydrogen atom abstraction reactions by hydroxyl radical from an allylic carbon atom inhibit reactivity for all three isomers at all temperatures. Rate constants of  $C_4H_8-1 + \dot{O}H$  and  $C_4H_8-2 + \dot{O}H$  are adopted from the theoretical results from Vasu et al. [325] based on the PES obtained at the CCSD(T)/6-311++G(d,p)//QCISD/6-31G(d) level of theory, while the rate constant of  $iC_4H_8 + \dot{O}H$  is calculated based on the PES obtained at the QCISD(T)/CBS//M062X/6-311++G(d,p) level of theory [88]. Rate constants for the three reactions follow the order of  $iC_4H_8 + \dot{O}H > C_4H_8-2 + \dot{O}H > C_4H_8-1 + \dot{O}H$  which is consistent with the reactivity of these three isomers.

When temperature is higher than 1000 K, the most promoting reactions are H-atom abstractions by molecular oxygen from allylic carbon atom which result in the generation of methyl-allyl radicals ( $i\dot{C}_4H_7$  and  $\dot{C}_4H_7-3$ ). The rate constants of  $iC_4H_8 + O_2$  are adopted from Yasunaga et al. [73], while the rate constants of  $C_4H_8-1 + O_2$  and  $C_4H_8-2 + O_2$  are determined by the Evans-Polanyi relationship developed by Somers et al. [335]. Rate constants for the three reactions follow the order of  $C_4H_8-2 + O_2 \approx C_4H_8-1 + O_2 > iC_4H_8 + O_2$  which means that this reaction class in 1- and 2-butene promotes the reactivity of these two isomers more than that for isobutene and this is consistent with the reactivity of these three isomers. Moreover, the subsequent reaction  $\dot{C}_4H_7-3 + O_2 \rightleftharpoons C_4H_6 + H\dot{O}_2$  further promotes reactivity for 1- and 2-butene but this reaction does not exist for isobutene.

At high temperatures, the most inhibiting reactions for 1- and 2-butene oxidation are  $\dot{H}$  atom addition reactions to the two isomers on the same potential energy surface. Addition to 2-butene and the terminal carbon atom in 1-butene will both generate propene and a methyl radical with rate constants in the order  $C_4H_8-2 + \dot{H} > C_4H_8-1 + \dot{H}$ , which means that this reaction inhibits the reactivity of 2-butene more than that for 1-butene and this is also consistent with the reactivity comparison. Moreover,  $\dot{H}$  atom addition to the central carbon in 1-butene results in the formation of  $C_2H_4 + \dot{C}_2H_5$  and ultimately generates two vinyl radicals and three  $\dot{H}$  atoms which will promote the reactivity pronouncedly.

At intermediate temperatures ( $\sim 800$ – $1000$  K), both 1- and 2-butene can undergo H-atom abstraction by hydroxyl radicals from secondary vinylic carbon atom resulting in the generation of vinylic radicals of 1-buten-2-yl ( $\dot{C}_4H_7-2$ ) and 2-buten-2-yl ( $\dot{C}_4H_7-2$ ), and their subsequent reactions with molecular oxygen generate alkenylperoxy radicals,  $C_4H_7-2\dot{O}_2$  and  $C_4H_7-2\dot{O}_2$ , followed by O–O bond fission resulting in  $\dot{O}$  atoms, which promotes reactivity pronouncedly. However, the  $\beta$ -scission of the 2-butanone-3-yl ( $C_4H_7\dot{O}-2$ ) radical, generated via O–O bond fission in a  $C_4H_7-2\dot{O}_2$  radical, generates methyl radicals which can recombine with  $\dot{C}_4H_7-3$  radicals to produce 2-pentene and 3-methyl-1-butene, which slightly inhibits reactivity.

At low temperatures ( $< 800$  K), the promoting reactions for the three isomers are hydroxyl radical addition to the C=C double bond. Rate constants for the entrance channels of the three isomers are all estimated by analogy to the propene +  $\dot{O}H$  calculations of Zádor et al. [236] (with 75:25 branching ratio for terminal versus central addition for both isobutene and 1-butene). The total rate constant of the reaction  $2-C_4H_8 + \dot{O}H$  is 2.5 times slower than that of isobutene and 1-butene. Furthermore, the adduct radicals ( $S\dot{C}_4H_8OH-3$ ,  $P\dot{C}_4H_8OH-2$ ,  $S\dot{C}_4H_8OH-1$ ,  $I\dot{C}_4H_8OH-it$  and  $I\dot{C}_4H_8OH-ti$ ) can react with molecular oxygen followed by an isomerization reaction to form hydroxyalkyl hydroperoxyl radicals ( $\dot{Q}_H OHOH$ ). This species can add to the second molecular oxygen followed by isomerization to form hydroxyketohydroperoxide and  $\dot{O}H$  leading to the low temperature chain branching pathways. All of the three isomers follow similar reaction classes shown here for the low temperature chemistry, however, because of the isomeric structural difference between these three species, the formed products from the branching pathways are

different, ultimately leading to the different reactivity of these species. We found that the more branched the molecule is, the lower the reactivity at low temperatures. Thus, when comparing the reactivity of 1-butene and isobutene, there are more chain branching reactions in 1-butene than in isobutene which lead to faster chain branching in 1-butene.

### 3.6.5 Chemistry difference between butene and propene oxidation

Important reaction classes for the oxidation of propene and butene isomers over the entire temperature range are similar and have been included in Figure 30. Reactivity difference between propene and butene isomers originates from the rate constant differences between specific elementary reactions and also from the different type of hydrogen atoms involved in the reactions. Taking propene and 1-butene as examples, even though the important reaction classes for both are the same, the different kinetic behavior of the secondary allylic hydrogen atom in 1-butene and primary allylic hydrogen in propene makes the reactivity of these two species quite different.

At low temperatures (700-950K), one of the main differences between butene and propene oxidation is the temperature range for the  $\dot{\text{O}}\text{H}$  addition reaction and the subsequent first and second molecular oxygen addition reactions. This reaction class is important for propene oxidation when temperature is lower than 750 K. The experimental measurements by Heyberger et al. [49] along with the model they developed predict NTC behavior of propene oxidation at  $\approx$  630 K. Nevertheless, Wilk et al. [48] first measured the NTC behavior of propene oxidation and also predicted it by their model in the temperature range of 530-740 K. However, as discussed previously, the comprehensive model for propene oxidation developed by Burke et al. [51, 52], validated above 750 K, did not show this NTC behavior and at this temperature range, chemistry shows that after  $\dot{\text{O}}\text{H}$  addition to propene, the formed adducts will react with molecular oxygen followed by the formation of acetone, formaldehyde and  $\dot{\text{O}}\text{H}$  radical via Waddington mechanism. The model does not include the second molecular oxygen addition reactions but still predicts the ignition delay times quite well. Hence, the low temperature chemistry shown in Figure 30 is important for propene at temperatures lower than 750 K. Alternatively, for butene isomers, the chemistry shown in Figure 30 is important in the temperature range of 700 - 850 K. Precise reason for this shift is unknown so far and further theoretical work on this topic will be helpful to understand the difference.

### 3.7 The combustion chemistry of pentene isomers

Combustion chemistry of pentene isomers has been investigated comprehensively in the literature [13, 89-100] especially for 1-pentene, which is considered as a surrogate component of unsaturated hydrocarbons in gasoline.

Minetti et al. [89] measured the pre-autoignition chemistry of 1-pentene in a rapid compression at the low temperature range (600 – 900 K). They measured pressure traces, light emissions, intensities of cool flames, autoignition delays and hydrocarbon conversions before final ignition for both 1-pentene and n-pentane, and found that 1-pentene has a lower reactivity than n-pentane over the entire temperature range. They did not develop a detailed kinetic model to explain the phenomenon and just proposed that by taking the higher reactivity of the allylic hydrogens and direct addition of  $\dot{\text{O}}\text{H}$  and  $\text{H}\dot{\text{O}}_2$  radicals into account, the classical low temperature oxidation scheme of alkanes can be applied to 1-pentene.

Mehl et al. [13] used the RCM experiments of Minetti et al. [89] and new high temperature shock tube experimental results of their own to compare ignition delay times of n-pentane and 1-pentene, concluding that n-pentane is faster to ignite at low temperatures because it has stronger NTC behavior than 1-pentene. Mehl et al. suggested that the C=C double bond in 1-pentene scavenges radical species at low temperatures via their addition reactions to the double bond, thereby delaying its ignition. Mehl et al. also discussed the implications of their work on octane sensitivity of alkanes and alkenes, suggesting that there are two major differences that should be highlighted between the oxidation chemistry of alkenes and alkanes. The first is the formation of very stable allyl or allyl-like radicals, whilst the second relates to the possible addition of propagating radicals, with a scavenging effect due to the presence of double bonds. They found the allylic radical is more likely reacting with molecular oxygen rather with hydroperoxyl radicals.

Ribaucour et al. [90] have studied the autoignitions of 1-pentene by rapid compression machine at high pressure and they observed two-stage ignition and NTC behavior for 1-pentene oxidation. They also developed a detailed mechanism based on a common skeleton scheme to simulate the experimental results including ignition delay times, cool flame intensities, and cyclic ether distributions. Sensitivity analysis of the low-temperature scheme for 1-pentene showed that the total ignition delay time is dependent on the competition between the decomposition channels of hydroperoxyalkyl radical into the branching sequence and into alkenes. The cool flame delay time is less sensitive but depends mainly on the decomposition rate of unsaturated ketohydroperoxides. Their model behaved well only when they (1) included the addition reaction channels of  $\dot{\text{O}}\text{H}$  and  $\text{H}\dot{\text{O}}_2$  to the double bond and (2) if a higher rate constant for the decomposition of the hydroperoxyalkyl radicals into cyclic ethers was used when this radical is formed by direct  $\text{H}\dot{\text{O}}_2$  addition instead of isomerization of alkylperoxy radicals. Some of the important reaction classes were not included in the mechanism, for instance, abstractions of alkylic H-atoms, isomerizations of the peroxy radicals following successive additions of hydroxyl radicals and oxygen molecules, and formations of unsaturated cyclic ethers were not considered.

Zhong et al. [94] has developed a detailed chemical model which includes 83 species and 560 reactions to describe 1-pentene oxidation against the measured the laminar flame speeds of 1-pentene/air mixtures. Alatorre et al. [96] studied a fuel-rich non-sooting 1-pentene/oxygen/argon flame at low pressures both experimentally and computationally. Special emphasis was directed towards the formation of the first aromatic ring and the further growth of small aromatic hydrocarbons. By the reaction flow analysis, they found that the major reaction channel for benzene formation results from the recombination of propargyl radicals.

Touchard et al. [98, 99] developed a detailed kinetic mechanism for the oxidation of 1-pentene at both high and low temperatures by using EXGAS system for the automatic generation of mechanisms. Their mechanism was validated against their experimental measurements of ignition delay times from ST and RCM and speciation data from a plug flow reactor. They also detailed the changes or additions necessary for the definition of the specific generic reactions involving alkenes and their free radicals, as well as the correlations to estimate the related rate constants. They found the addition of hydroxyl radicals to the double bond and some specific reactivity of the allylic radical played a significant role in autoignition delays. The reactions of allylic and alkenyl radicals with  $\text{O}_2$  to produce dienes are also important in predicting the fuel reactivity.

Very recently, Dong et al. [100] put forward a detailed chemical kinetic mechanism for the oxidations of 1- and 2-pentene, which was developed based on a published pentane mechanism [336]. The pentene mechanism was validated against their newly measured data for 1- and 2-pentene combustion, including ignition delay times in ST and RCM under engine-relevant conditions and species profiles during the oxidation in JSR, as well as those experimental data from the previous studies [10, 90, 93, 99]. Since the mechanism is able to capture all aforementioned experimental data quite well, both for 1- and 2-pentene, flux and sensitivity analyses were performed to unravel the differences in chemistry of the two isomers. They found that 2-pentene is in general less reactive than 1-pentene at low to intermediate temperatures (650–800 K), mainly because the adducts of OH addition reactions to 2-pentene are more likely consumed through chain-propagating rather than chain-branching reaction pathways.

An excellent review by Westbrook et al. [91] summarized the detailed model development for linear hexene and pentene isomers and highlighted the important reaction pathways for the oxidation of 2-methyl-2-butene (2M2B). A comprehensive chemical kinetic reaction mechanism was developed to describe the oxidation of 2M2B with particular attention on the role played by allylic C–H bonds and allylic pentenyl radicals. Experimental measurements of ignition delay times behind reflected shock waves in a shock tube and species mole fractions for fuel, intermediate, and products in a jet-stirred reactor were also carried out in their work for model validation. Their results showed that, at high temperatures, 2M2B reacts rapidly, similar to related alkane fuels, but the pronounced thermal stability of the allylic pentenyl species inhibits low temperature reactivity, so 2M2B does not produce “cool flames” or negative temperature coefficient behavior. They also analyzed the connections between olefin hydrocarbon fuels, resulting allylic fuel radicals, the resulting lack of low-temperature reactivity, and the gasoline engine concept of octane sensitivity.

The combustion chemistry of 1-pentene, which is considered as a gasoline surrogate component, has been investigated extensively in the literature and there are very few experiments or model developments for 2-pentene. Hence, the model put forward by Westbrook et al. [91] for 2-methyl-2-butene oxidation and by Touchard et al. [98, 99] for 1-pentene oxidation is used in the subsequent discussion.

### 3.7.1 High temperature chemistry of pentene combustion

Detailed model of 1-pentene oxidation developed by Touchard et al. [99] shows that at a high temperature of 1222 K, 1-pentene is mainly consumed by H-abstractions reactions by hydrogen atoms and hydroxyl radicals, unimolecular decomposition giving allyl and ethyl radicals, and additions of hydrogen atoms. The reactions of hydrogen atom abstraction by O<sub>2</sub> and the addition of O atom to the C=C double bond which are found to be important in the oxidation of butene isomers at high temperatures have not been reported in their work. In the model developed by Westbrook et al. [91] for the oxidation of 2M2B, a sensitivity analysis at shock tube experimental temperatures of 1330–1730 K does not recognize the importance of the radical addition reactions to 2M2B or to its allylic pentenyl radicals, whilst the decomposition reaction of allylic radicals contributes to the main consumption of 2M2B during oxidation.

### 3.7.2 Low and intermediate temperature chemistry of pentenes combustion

It is interesting to find that at low temperatures, both the autoignition delay time between 600 and 900 K of 1-pentene from Ribaucour et al. [90] and speciation measurements from a plug flow reactor between 654 and 716 K by Prabhu et al. [95] show NTC behavior. Touchard et al.

[98] developed a comprehensive model to try to capture the low temperature experimental data of 1-pentene oxidation, as shown in Figure 42. The reaction pathway analysis of 1-pentene oxidation at 800 K from their model shows that, apart from the Waddington mechanism, the  $\dot{\text{O}}\text{H}$  addition reaction to form the hydroxyalkyl radical followed by molecular oxygen oxidation, isomerization and second  $\text{O}_2$  addition reactions which can ultimately form hydroxyketohydroperoxides to give chain branching pathways, promote the reactivity at low temperatures, as shown in Figure 43. This is the first study in the literature clearly stating the low temperature chain branching pathways for alkenes through the formation of hydroxyketohydroperoxides. In addition to the formation of ketohydroperoxides from  $\dot{\text{O}}\text{H}$  addition reactions, molecular oxygen addition to the alkenyl radical followed by isomerization and second  $\text{O}_2$  addition can also produce alkenylketohydroperoxides promoting the low temperature reactivity. Even though the model does not capture the reactivity of the fuel quite well, it shows the importance of the low temperature chain branching reaction pathways in predicting the fuel reactivity. Future theoretical or experimental measurements on those reactions will be valuable for improving the model prediction.

Besides the  $\dot{\text{O}}\text{H}$  addition reactions, Touchard et al. [98] also highlighted the important reaction classes of  $\text{H}\dot{\text{O}}_2$  addition to the  $\text{C}=\text{C}$  double bond, the radical-radical recombination of allylic radical with  $\text{H}\dot{\text{O}}_2$ , hydrogen atom abstraction by molecular oxygen from the  $\beta$ -position of the double bond in allylic radicals forming dienes +  $\text{H}\dot{\text{O}}_2$ , which are consistent with the ones mentioned above for butene isomers. It should also be noted that at 800 K, the model predicts 14% of the allylic radicals to react with molecular oxygen followed by isomerization and cyclization reactions to ultimately form cyclic ether. This is inconsistent with the previous finding that the formed weak allylic  $\text{C}-\text{OO}$  bonds in allylperoxy radical cannot maintain levels high enough to initiate low-temperature chemistry and most likely dissociate back to the allylic radical and  $\text{O}_2$ .

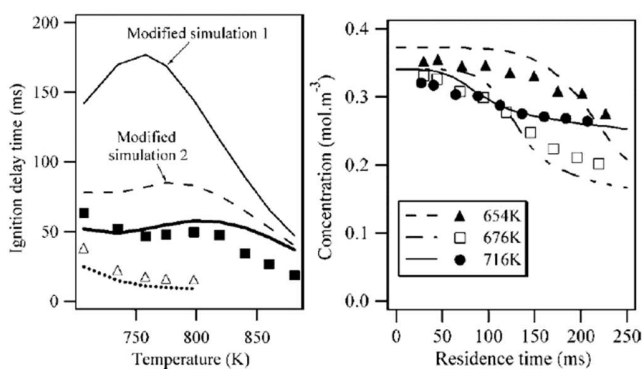


Figure 42. (a) Cool flame ( $\Delta$ ) and autoignition ( $\blacksquare$ ) delay times of 1-pentene in a rapid compression machine (from Ribaucour et al. [90]); (b) 1-pentene oxidation in a flow reactor (from Prabhu et al. [95]). Lines are modeling results from Touchard et al. [98]

Westbrook et al. [91] discussed the important reaction classes for 2-methyl-2-butene oxidation over a wide range of temperatures. They proposed five reaction classes which are important for 2M2B oxidation, including H-atom abstraction reactions from the fuel by small radical species, unimolecular decomposition of the fuel into two radical species, and the addition reactions, particularly, of  $\dot{\text{H}}$  atoms,  $\dot{\text{O}}\text{H}$  and  $\text{H}\dot{\text{O}}_2$  radicals which can lead to unique product species distribution in olefin fuel consumption. The important addition reaction classes highlighted here are consistent with the ones discussed above for the oxidation of butenes apart from the addition reaction of  $\dot{\text{O}}$  atoms to the  $\text{C}=\text{C}$  double bond in pentene isomers.

The importance of  $\dot{\text{O}}\text{H}$  and  $\text{H}\dot{\text{O}}_2$  addition to the  $\text{C}=\text{C}$  in 2M2B has also been highlighted. No NTC behavior was found in their JSR measurements over the temperature range of 600 – 1150 K at atmospheric pressure. The main reaction pathway for the hydroxylalkyl radical formed from the  $\dot{\text{O}}\text{H}$  addition is the Waddington mechanism to produce acetone and acetaldehyde which is the main source for the formation of these two species. Addition of  $\text{H}\dot{\text{O}}_2$  to the  $\text{C}=\text{C}$  bond can produce  $\dot{\text{O}}\text{H}$  radical and cyclic ether which can be detected in the JSR experiments.

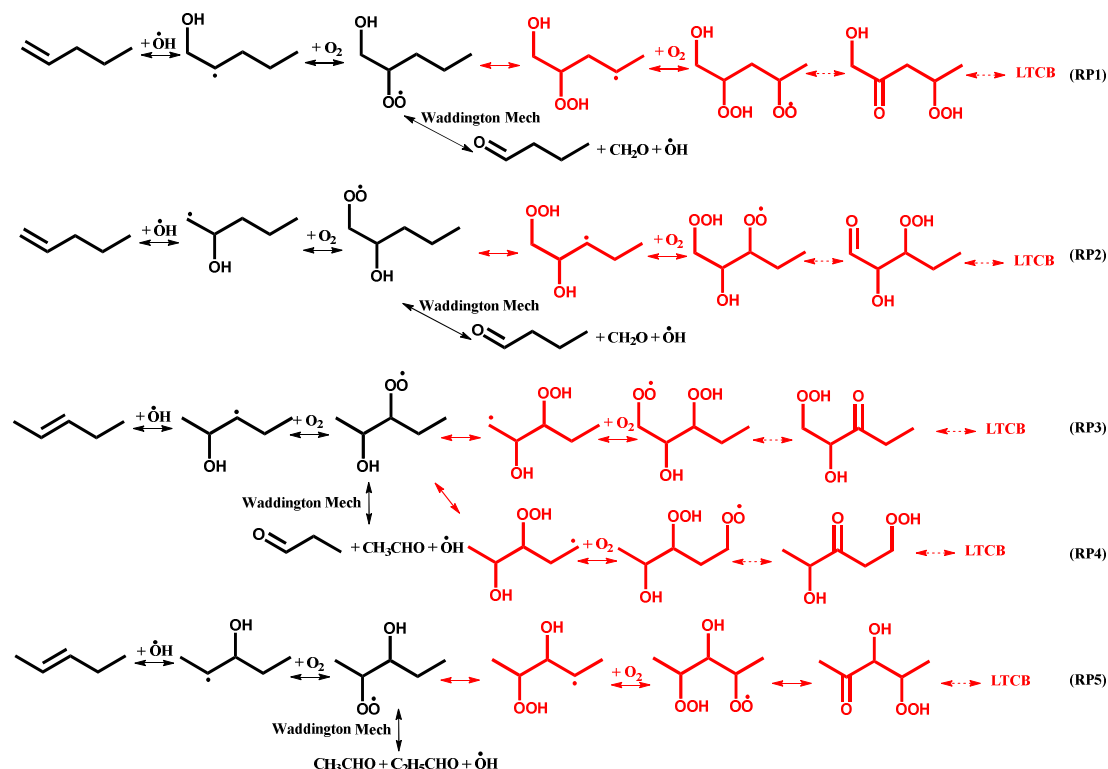


Figure 43. Scheme of the low temperature oxidation of 1- and 2-pentene reaction pathways. Reactions shown in red promote reactivity.

It is worth noting that the produced resonantly stabilized radicals have a pair of equivalent allylic species with the same thermochemistry parameters, which should be treated as one species, but the subsequent reactions with other molecules/radicals need to be treated separately. In the model development, reactions initiating from the same equivalent allylic species can go through different channels to form different products, and these reaction channels compete with each other. For example, by taking the allylic radical formed in 2M2B, the two equivalent forms, possessing the same thermochemistry parameters, can produce different and quite distinct species when reacting with important radicals such as  $\text{H}\dot{\text{O}}_2$ . Hence, the subsequent reactions for these two species should be included in the chemical kinetic model development. The JSR measurements carried out in the work of Westbrook et al. [91] have distinguished the intermediate products from the different reaction pathways of the equivalent resonantly stabilized radicals.

At intermediate temperatures, the formed resonantly stabilized radical can react with molecular oxygen to give dienes +  $\text{H}\dot{\text{O}}_2$  through H-atom abstraction reactions, which is an important reaction pathway for the consumption of allylic radicals. Apart from that, the recombination reaction between allylic radical and  $\text{H}\dot{\text{O}}_2$  radicals is also one of the key reaction classes in

determining the oxidation reactivity of pentenes. The formed stable pentenyl hydroperoxide species,  $\dot{C}_5H_9OOH$ , decomposes by breaking the O–O bond to produce unsaturated versions of alkoxy radicals, with an activation energy of 43 kcal mol<sup>-1</sup>, which is the same as the activation energy for the decomposition of the ketohydroperoxide intermediates in the low temperature chemistry for saturated hydrocarbon fuels. This is a chain termination reaction pathway when the temperature is not high enough to break the O–O bond, but once the species reaches a temperature where the O–O bond can break rapidly to form  $\dot{O}H$  radical and unsaturated alkoxy radicals, then this becomes a chain branching reaction pathway, which can promote the oxidation reactivity of pentenes. The unsaturated alkoxy radicals can decompose rapidly through  $\beta$ -scission reactions to form smaller radicals.

Westbrook et al. [91] also investigated the addition of molecular oxygen to the resonantly stabilized radical followed by the isomerization and second O<sub>2</sub> addition reaction, which represent the typical low temperature chain branching chemistry for saturated hydrocarbon oxidation. No low temperature reactivity for 2M2B oxidation was observed and it was proposed that the formed weak allylic C–OO bonds cannot maintain allylperoxy radical levels high enough to initiate low-temperature NTC reactivity and these radicals dissociate back to the allylic radical and O<sub>2</sub>. This is consistent with what has been observed for the allylic butenyl radicals which react with  $\dot{H}O_2$  radicals rather than with O<sub>2</sub>.

### 3.7.3 Chemistry difference between butene and pentene isomers

Touchard et al. [99] compared the autoignition delay time obtained in a shock tube for 1-butene [145] and 1-pentene oxidation at the same conditions of 1300 – 1620 K, equivalence ratio of 2.0 and initial fuel concentration of 1%. They found that 1-pentene has a higher reactivity, which may be due to its decomposition to ethyl radicals, and rapidly yields very reactive hydrogen atoms, whilst the decomposition of 1-butene leads to less reactive methyl radicals. However, it should be noted that apart from the unimolecular decomposition of the fuel molecules directly, other reaction classes such as  $\dot{H}$  and  $\dot{O}$  atoms addition to the double bond, and their subsequent reactions producing distinct products are also important in predicting the reactivity of the fuels in this temperature range. At low temperatures, the important reaction classes shown in Scheme 1 can be important for both butene and pentene isomers. However, for the linear isomers, the difference between them mainly arise from the difference between the alkyl group within the molecule. The more alkyl group in the molecule, the higher of the reactivity. A comprehensive, adequate and comparable model for pentenes will be necessary and important to give a clear picture for the reactivity comparison with butenes.

### 3.7.4 Chemistry difference between pentene isomers

The combustion chemistry of 1-pentene has been studied extensively in the literature; however, this is not so for 2-pentene. Cheng et al. [92] measured the laminar flame speeds of three pentene isomers (1-pentene, 2-pentene, and 2-methyl-2-butene) and n-pentane using a constant volume combustion bomb. A modified reaction mechanism based on n-pentane oxidation published by Bugler et al. [336] was used to simulate their experimental data. Laminar flame speeds from the experiments show that 1-pentene burns faster than 2-pentene but their model predicts the opposite, hence the model of 2-pentene was ignored in their reactivity analysis. Their experiment shows that the laminar flame speeds increase in the order of 2-methyl-2-butene (2M2B), n-pentane, 2-pentene, and 1-pentene. They proposed that the generation and consumption of the  $\dot{H}$

atoms is a key factor controlling the fuel reactivity at high temperatures. The important reactions for 1-pentene oxidation included in their reactivity analysis are unimolecular decomposition and  $\beta$ -scission of various pentenyl radicals.  $\dot{\text{H}}$  atom addition reactions to 2M2B have been included in the oxidation of 2M2B but not for 1-pentene. Hence, a more comprehensive model which includes the important high temperature reactions of  $\dot{\text{H}}$  and  $\dot{\text{O}}$  atom additions is crucial to have a concrete explanation of the differences between pentene isomers.

As shown in Figure 42, at low temperatures, the RCM data from Ribaucour et al. [90] and the flow reactor data from Prabhu et al. [95] for 1-pentene oxidation show a curvature of the low temperature reactivity which is attributed to the formation of hydroxyketohydroperoxides, as shown in detail for reaction channels RP1 and RP2 in Figure 43. The isomerization reactions for hydroxyalkyl peroxy radicals can also occur through five- and seven-membered ring transition state structures, which are not included in Figure 43. Those transition states were proven to be not dominant in the low temperature oxidation of alkanes and hence only the reactions via six-membered ring transition states are taken into consideration. Even though there are no low temperature reactivity measurements or chemistry models developed for 2-pentene oxidation, by analogy with the reaction classes occurring in the oxidation of 1-pentene, we can predict that the reactivity of 2-pentene at low temperatures will also have a similar curvature as in 1-pentene. The position of the curvature depends on the reactivity competition between the low temperature chain branching reaction pathways and the Waddington mechanism.

Comparing the isomerization reaction of hydroxyalkyl peroxy radical ( $\text{ROHO}\dot{\text{O}}$ ) for 1-, and 2-pentenes, shown in Figure 43, we can predict that the reactivity of 1-pentene is higher than that of 2-pentene at low temperatures. As shown in RP1 and RP2, both of these two isomerization reactions occur to abstract a secondary hydrogen atom, whilst that process in RP3 and RP4 abstracts a primary hydrogen atom whose bond strength is  $\sim 4 \text{ kcal mol}^{-1}$  higher than that for the secondary hydrogen bond. Even though the reaction process for RP5 also abstracts a secondary hydrogen, the importance of its products depends on the branching ratio of the initial  $\dot{\text{O}}\text{H}$  addition reaction to the  $\text{C}=\text{C}$  double bond. It is interesting to note that the low temperature chemistry of the hydroxyalkyl radical oxidation shown in Figure 43 also represents important reaction classes for pentanol low temperature oxidation.

In summary, the curvature of the reactivity for linear pentene originates from the formation of the hydroxyketohydroperoxides, and the formation of alkenylketohydroperoxides is not favorable for alkenes  $< \text{C}_5$ . Branching ratio of the  $\dot{\text{O}}\text{H}$  radical addition to the two sides of the  $\text{C}=\text{C}$  bond is crucial in determining the final reactivity of pentenes oxidation, since the ultimately formed hydroxyketohydroperoxides from the adducts are quite different.

### 3.8 The combustion chemistry of hexene isomers

The concept of the “influence of the position of the double bond” in determining oxidation and ignition of olefins has been addressed in several papers in the literature. These studies discuss relative rates of combustion of isomers in a particular family of linear alkenes, most often hexenes [10, 98, 101-109], but also including families of linear heptenes, [103] decenes, [337] as well as methyl nonenoates [338]. Experimental measurements from RCM, JSR, plug flow reactors, shock tubes, and motored engines have been used to investigate the combustion behavior of double-bond containing long molecules. In these studies, it has been found that the isomers where the  $\text{C}=\text{C}$  double bond is located in the terminal carbon site (1-olefins) are the most reactive, followed by isomers with the  $\text{C}=\text{C}$  double bond located at the 2-site in the carbon chain;

the C=C double bond located in the middle part of the fuel molecule react slowest. This shows that as the C=C double bond moves toward the center of the olefin, the low-temperature NTC behavior decreases. This is because the strong NTC behavior in alkenes depends on the length of the saturated carbon atom chain available to support alkylperoxy ( $\text{RO}_2$ ) radical isomerization reaction sequences, as discussed in the commonly accepted alkane ignition mechanisms [106, 339]. A centrally located C=C double bond interrupts such a saturated chain and the addition reaction classes, which do not show strong NTC behavior, become important.

Experimental studies have been carried out behind reflected shock waves, in stirred reactors, and rapid compression machines for 1-hexene [105, 107, 108] and for all three linear isomers of hexene [101-103]. Most of these experimental studies also included either detailed kinetic modeling or kinetics-based interpretation of their results, while others [98, 103, 104] are primarily kinetic modeling studies that provide analyses of these olefin experiments.

Mehl et al. [10] investigated the autoignition behavior of pentene and hexene linear isomers in low and high temperature regions, and developed a wide-ranging chemical kinetic model. Their mechanism was validated against ignition delay time measured in a RCM at low temperatures of 630–850 K by Vanhove et al. [102], and new shock tube experiments were performed in the work of Mehl et al. [10] to validate the model in the temperature region of 990 – 1770 K. Reactivity changes at different temperatures for three hexene isomers were discussed in their work.

Yahyaoui et al. [105] studied the high temperature oxidation of 1-hexene in a jet-stirred reactor (JSR) between 750 and 1200 K at 10 atm and in a shock tube at higher temperatures [105, 107]. The EXGAS program was used to develop the detailed chemical mechanism of the 1-hexene oxidation and the modeling results proposed that at low temperatures, 1-hexene is mainly consumed by retro-ene reaction to give propene and, with a smaller ratio, by unimolecular decomposition to give allyl and 1-propyl radicals. Alternatively, at high temperatures, unimolecular decomposition becomes more important than the retro-ene reaction. No addition reactions of  $\dot{\text{O}}\text{H}$ ,  $\text{H}\dot{\text{O}}_2$ ,  $\ddot{\text{O}}$  and  $\dot{\text{H}}$  to the C=C double bond were proposed to be important in their model. The model underestimates the reactivity of 1-hexene oxidation at temperatures lower than 1400 K.

An important work of Battin-Leclerc et al. [101, 109] reports a study of oxidation of the three linear isomers of hexene in a jet-stirred reactor at temperatures ranging from 500 to 1100 K. Varying reactivity of the three fuels with temperature was observed and discussed according to the changes in the reaction pathways with the position of double bond. Along with the experimental results, comprehensive analyses were carried out for the oxidation of three hexene isomers over different temperature ranges and a detailed chemical kinetic model was developed for 1-hexene oxidation [109]. Hence, the experimental and modeling results from Battin-Leclerc et al. [101, 109] at low to intermediate temperatures and from Mehl et al. [10] at high temperatures for linear hexene isomers have been used in the following discussion.

### 3.8.1 Low and intermediate temperature chemistry of linear hexene combustion

The main reactions that occur during linear hexene isomers oxidation at low and intermediate temperatures have been proposed by Battin-Leclerc et al. [101]. As discussed for other alkenes,

the addition of hydroxyl radical to the C=C forming hydroxylhexyl radical plays a significant role in determining the reactivity of hexene oxidation at lower temperatures. Molecular oxygen can add to the hydroxylhexyl radical to form hydroxyhexyl peroxy radical which can undergo the Waddington mechanism to form saturated aldehydes or proceed through the typical low temperature chain branching pathway to hydroxyketohydroperoxides or hydroxyl cyclic ethers. As the size of the alkene molecule increases, the Waddington mechanism becomes less important and the isomerization of the hydroxyhexyl peroxy radical followed by the cyclic ether formation and low temperature chain branching reaction pathways as shown in Figure 31 becomes more important for hexenes.

As the chain of the alkene elongates, H-atom abstraction from the alkylic hydrogens, as shown in Figure 28, in hexene can form the alkenyl radical. Three main reaction classes can occur with this alkenyl radical. Firstly, it can undergo  $\beta$ -scission to form smaller unsaturated hydrocarbons and radicals; secondly, it can react with molecular oxygen to form HO<sub>2</sub> radicals and conjugated dienes through the abstraction of an H-atom either from  $\beta$  position of the alkenyl radical or allylic radicals; thirdly, it can add to molecular oxygen, followed by isomerization and second O<sub>2</sub> addition leading to the formation of unsaturated cyclic ethers and ketohydroperoxides which is similar to the well-known low temperature chemistry of alkanes [233].

Summarizing the low temperature chemistry of hydrocarbons, the radicals formed in all cases react mainly by addition to an oxygen molecule and can ultimately form ketohydroperoxides. Ketohydroperoxides are the branching agents leading to the formation of a number of radicals, which accumulate to the radical pool and ultimately promote the system reactivity. In saturated hydrocarbons, the radicals can be the fuel radicals directly formed through H-atom abstraction from fuel molecules. In unsaturated hydrocarbons, the radicals can include hydroxylalkyl radical formed from OH radical addition to the C=C double bond followed by subsequent first and second molecular oxygen addition reactions to the formation of hydroxyketohydroperoxides ultimately, as shown in Figure 31. Additionally, alkenylketohydroperoxides can also be formed from alkenyl fuel radicals during alkene oxidation. Therefore, the reactivity of alkenes at low temperature is controlled by its ability to form both the hydroxyketohydroperoxides and alkenylketohydroperoxides.

At intermediate temperatures, the HO<sub>2</sub> radical reacts with hexene and the allylic radical plays an important role in determining the reactivity of hexene oxidation. The HO<sub>2</sub> radical can add to the C=C double bond directly, followed by the formation of three-membered ring cyclic ethers and OH radical. On the other hand, HO<sub>2</sub> radical can also react with the allylic radical through a barrierless reaction process to form alkoxy and OH radicals, thus promoting reactivity.

Even though the important reaction classes for the low and intermediate temperature oxidation of linear hexene isomers are consistent with what we found for butene isomers and pentene isomers, it is still difficult to develop accurate kinetics models for hexene oxidation. The main problem is that so far there are quite limited experimental and theoretical investigations available on the important reaction classes for hexene oxidation. Taking the detailed model developed by Battin-Leclerc [109] for 1-hexene oxidation as an example, rate constants for the reaction of OH radical addition to the C=C double bond were taken by analogy from the rate constants and branching ratio calculated by Zádor et al. [236] on propene. The branching ratio between the terminal and

central addition plays a significant role in determining the reactivity of hexene oxidation because the two formed hydroxyl adducts can undergo different reaction pathways, which have different impacts on the reactivity. Therefore, the branching ratio for these two channels needs to be thoroughly examined. As the chain grows longer from propene to hexene, the substitute effect should also be taken into consideration. Similar to the oxidation of butene isomers [87, 88], this branching ratio may need to be adjusted to 75:25 for improved prediction, hence further theoretical analysis on this reaction needs to be carried out to provide an accurate branching ratio. Moreover, the secondary allylic hydrogen atom in 1-hexene with the weakest C-H bond should be the easiest one to be abstracted by important radicals such as  $\dot{\text{O}}\text{H}$ ; the branching ratio for the formation of secondary alkenyl radical should be larger than for the other channels, but the model shows that the formation of alkenyl radicals is dominant over the formation of allylic radicals. This will affect the model prediction significantly as it gives an incorrect prediction of one of the most important allylic radical formation routes. Therefore, further theoretical studies on those reaction classes are of significant importance for detailed model development for larger alkenes oxidation.

### 3.8.2 High temperature chemistry of linear hexenes combustion

Very limited kinetic models in the literature are available for hexene isomers oxidation at high temperatures. Yahyaoui et al. [105] proposed that at high temperatures, 1-hexene is mainly consumed by monomolecular initiation via C-C and C-H scissions, bimolecular initiation involving H-atom abstraction reactions to form hexenyl radicals, and retro-ene decomposition yielding two molecules of propene. Yang et al. [111] mentioned that the trans-3-hexenyl radicals decompose rapidly through  $\beta$ -scission reactions. Mehl et al. [10] stated that at about 1000 K, the reactivity is determined by the radicals formed from the  $\beta$ -decompositions of the most abundant resonantly stabilized radicals in the system, and the more  $\dot{\text{H}}$  atoms are produced, the higher the reactivity. When temperature is higher than 1400 K, the C-C bond fission becomes dominant and the reactivity is again determined by the formation of  $\dot{\text{H}}$  atoms in the system. It should be noted that none of the important reaction classes proposed in smaller alkenes of butene isomers, such as  $\dot{\text{H}}$  and  $\dot{\text{O}}$  atom addition to the C=C double bond and subsequent reactions were mentioned in the model development for hexene isomers. This will severely limit the predictive capabilities of the kinetic models. Future studies on those important reaction classes will be important to improve the model predictions for hexene isomers.

### 3.8.3 Chemistry difference between linear hexene isomers

Ignition delay times of linear hexenes by Vanhove et al. [102] in an RCM and from Mehl et al. [10] in a shock tube are shown in Figure 8. Detailed kinetic models developed by Mehl et al. [10] for hexene isomers match the experimental results quite well. As can be seen at low temperatures, 1-hexene has a strong NTC behavior which is close to the typical features of alkanes and it shows a two-stage ignition, whilst 3-hexene only shows a single stage ignition and 2-hexene has an intermediate behavior. Ignition delays for all three isomers became approximately equal at about 850 K in the RCM measurements of Vanhove et al. [102]; however, the reactivity of hexene isomers in the study of Battin-Leclerc et al. [101], shown in Figure 44, was fastest for 1-hexene between 500 and 700 K but appeared to converge at about 700 K. Battin-Leclerc et al.

discussed the role of pressure on the reactivity of hexene isomers, mentioned that the influence of pressure on the equilibrium of the addition reactions can shift the temperature zones in which some specific reactions are of importance, and explained differences in the reactivity ranking between the hexene isomers. The work of Battin-Leclerc et al., carried out at atmospheric pressure in a JSR, is the only study to date in which the reversal in the reactivity of the three hexene isomers ordering has been observed in a single family of experiments. The same reversal from other experimental measurements was seen at much higher pressures, such as in the work by Vanhove et al. [102], where it was beyond not possible to extend the reaction temperature above 850 K in the RCM. From the two experimental investigations at different pressures, we identify the reversal of reaction pathways for linear hexene isomers occurring at about 700 K, as observed by Battin-Leclerc et al. [101] at atmospheric pressure and at a higher temperature of around 850 K at 10 atm, as seen by Vanhove et al. [102].

As discussed above, the low temperature chemistry of a fuel is mainly determined by the formation of ketohydroperoxides. In alkenes, the ketohydroperoxides are composed of hydroxyketohydroperoxide formed from  $\dot{\text{O}}\text{H}$  radical addition to the  $\text{C}=\text{C}$  double bond initially, and alkenylketohydroperoxides formed from the alkenyl radical *via* typical low temperature chemistry of alkanes. Thus, the longer the saturated carbon atom chain available in alkenes, the stronger the NTC behavior, such as in 1-hexene. On the other hand, when the  $\text{C}=\text{C}$  double bond moves from the terminal position (1-hexene) to the central one (3-hexene), the formation of alkenylketohydroperoxides significantly weakens, but the low temperature chemistry of 3-hexene still shows a weak NTC behavior, which is from the formation of hydroxyketohydroperoxide through  $\dot{\text{O}}\text{H}$  radical addition to the  $\text{C}=\text{C}$  double bond.

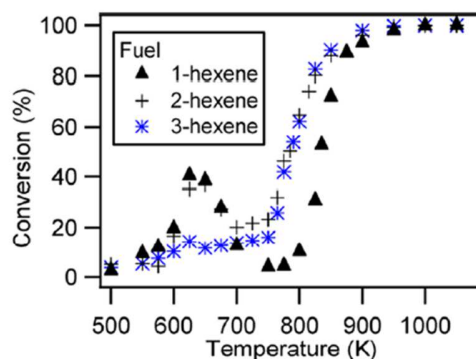


Figure 44. Comparison between the three isomers of hexene for the fuel conversion from JSR data obtained at 1.07 bar, at a residence time of 2 s, under stoichiometric conditions. (Battin-Leclerc et al. [101])

When temperature is higher than 1400 K, the reactivity of 1-hexene becomes the slowest while 2-hexene becomes the fastest and 3-hexene lies in between. Mehl et al. [10] discussed that the important reaction pathways in hexene isomers are  $\beta$ -scissions in resonantly stabilized radicals and unimolecular decomposition through  $\text{C}-\text{C}$  bond cleavage. Fragments leading to the formation of  $\dot{\text{H}}$  atoms, such as ethyl radicals, promote the high temperature radical branching more than methyl radicals. Apart from those reaction pathways, the addition reactions of  $\dot{\text{H}}$  and  $\dot{\text{O}}$  atoms to the  $\text{C}=\text{C}$  double bond which were crucially important for smaller alkenes oxidation

were not taken into consideration in those models, hence detailed explanation of the high temperature difference between the three isomers needs to be revisited.

### 3.8.4 Chemistry difference between pentene and hexene isomers

The important reaction classes for pentene and hexene isomers oxidation are quite similar, as shown in Figure 30. Vanhove et al. [102] compared the ignition delay times for 1-pentene and 1-hexene in a rapid compression machine between 600 and 900 K and their results showed that 1-hexene was more reactive than 1-pentene, which was consistent with their respective octane numbers (RON = 90.9 for 1-pentene and 76.4 for 1-hexene). This inversion of relative reactivity between the two compounds reflects important differences in the chemical mechanisms involved in the low temperature range. As mentioned above, the low temperature reactivity of a fuel is controlled by the formation of ketohydroperoxides. In addition to the reaction pathways shown in Figure 43 for 1-pentene that can also occur for 1-hexene to form the hydroxyketohydroperoxides, the formation of alkenylketohydroperoxides in 1-hexene also promotes the low temperature reactivity, which is unlikely to happen for 1-pentene. As shown in Figure 45, the formation of the alkenylketohydroperoxides from hexenyl radical oxidation is likely to occur and their subsequent low temperature chain branching reactions will contribute to the reactivity of hexene oxidation.

It should be noted that the reaction pathways shown in Figure 45 are likely to occur for alkenyl radicals but not for the allylic radicals in hexenes and higher alkenes, as the formed C–OO bonds from allylic radicals are not strong enough to proceed to subsequent reactions and are favored to dissociate back to the allylic radical and molecular oxygen. This is also the main reason which causes reactivity difference between hexenes and pentenes. As the double bond moves to the central part of the molecule, the reactivity benefit from the formation of alkenylketohydroperoxides reduces, and the formation of hydroxyketohydroperoxides becomes more dominant.

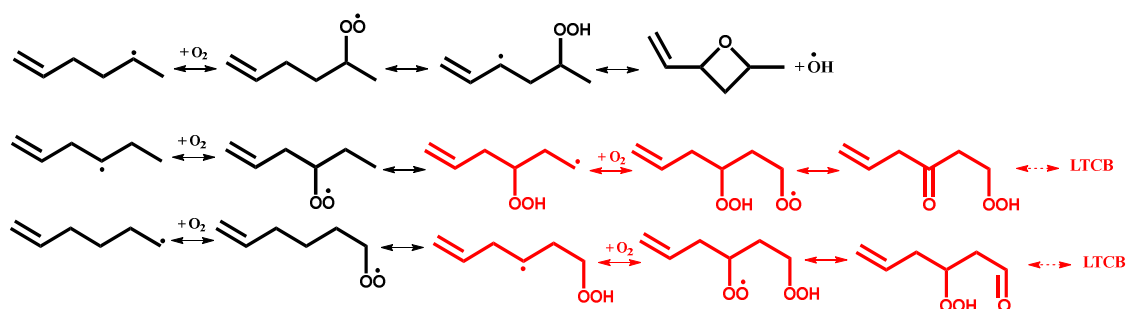


Figure 45. Reaction pathways for the formation of alkenylketohydroperoxides at low temperature oxidation of 1-hexene. Reaction pathways labeled in red promote the reactivity.

### 3.9 The combustion chemistry of heptene isomers and higher alkenes

The combustion chemistry of heptene isomers and higher alkenes (*i.e.*, C<sub>7</sub> and larger) has not been studied extensively. A few studies have been carried out on the isomers of heptene [103, 112-114], octene [115-117], decene [118, 119] and 2,4,4-trimethyl-1-pentene [120-124], mainly in the recent 5 years. Tanaka et al. [113] measured pressure profiles during the combustion of three linear isomers of heptene in a rapid compression machine at 827 K, which showed clearly

that the reactivity of alkenes at low temperature is considerably affected by the position of the double bond. They observed a two stage ignition in the oxidation of 1- and 2-heptene in RCM, while only a single stage ignition was shown by 3-heptene. Bounaceur et al. [103] performed kinetic modeling analysis for the linear isomers of heptene in addition to the linear isomers of hexene, using RCM experimental data for the heptene isomers from Tanaka et al. [113]. Their model can well predict the occurrence of cool flame for 1- and 2-heptene and the fact that such a phenomenon is not observed for 3-heptene.

Westbrook et al. [340] carried out a detailed chemical kinetic modeling study on the effects of C=C double bonds on the ignition of biodiesel fuels. Their experimental data and kinetic modeling analysis show that the C=C double bond in biodiesel fuels have a very significant impact on their rates of ignition that is reflected in their cetane numbers in diesel engines. While C=C double bonds accelerate the reactivity in the high temperature regime, the double bonds reduce the overall rate of reaction at low temperatures, thereby reducing the CN number. This is consistent with what we have discussed above.

As mentioned in the previous section about the reactivity of hexene isomers, the low temperature reactivity of fuels is determined by the ability to form ketohydroperoxides. In the case of 1- and 2-heptenes, both hydroxyketohydro-peroxides and alkenylketohydroperoxides can be formed and contribute to the reactivity of these two fuels at low temperatures. Similar reaction pathways can be found in Figure 43 and Figure 45 for pentene and hexene isomers, respectively. When the double bond moves to the central part of the fuel, like in 3-heptene, the formation of alkenylketohydroperoxides is unlikely to happen and the formation of hydroxyketohydroperoxides is the main source of the chain branching pathways for low temperature oxidation of 3-heptene. This is the reason why the low temperature reactivity of 3-heptene is much lower than for the other two isomers.

Meng et al. [117] developed a detailed model for 1-octene oxidation based on the kinetic rules for 1-hexene by the same group [109] and their model has been validated against the speciation results obtained in a JSR over 500 to 1100 K. Their experimental results for 1-octene oxidation show a very strong NTC behavior over the range of equivalence ratios investigated when temperature is lower than 800 K, but the model failed to capture the trends. When we have a closer look on the rate of production of the model at 650 K, we can find that the kinetics of few reactions needs to be revisited to improve the model prediction. First, bond dissociation energy of the allylic C-H bond is  $\sim 87.7$  kcal mol<sup>-1</sup> and that for the secondary C-H bond is  $\sim 98$  kcal mol<sup>-1</sup>, thus, the hydrogen abstraction reaction from the allylic hydrogen atom is much favored over the other channels. In the model developed by Meng et al., the branching ratio of allylic radical formation is only 9.3% and that for the secondary alkenyl radical formation is 12.0%, which is among the reasons affecting the model prediction. Secondly, the model predicts the formed allylic radical to react with molecular oxygen through isomerization reactions and form alkenylketohydroperoxides. However, from our previous analysis of pentene and hexene oxidation, we concluded that the C-OO bond in the allylic peroxide radical is not strong enough to proceed along the low temperature chain branching reaction pathways. Thus, the alkenylketohydroperoxides cannot be formed via this reaction pathway. Thirdly, the branching ratio of the terminal addition and central addition of  $\dot{O}H$  radical to the C=C double bond are set the same in the model, which is not consistent with what we found for the oxidation of propene [51, 52] and butene isomers [86-88]. Difference in the branching ratios of this very important reactions is crucially important as the subsequent reactions of the formed two hydroxyalkyl

radicals are different, which adversely affects the reactivity predicted by the model. Fourthly, as stated above, the low temperature reactivity of alkenes is controlled by the formation of hydroxyketohydroperoxides originating from OH addition to the C=C double bond and of alkenylketohydroperoxides formed through the molecular oxygen addition to the alkenyl radical, whilst the model does not include these important reaction classes. Those reaction classes need to be revisited to improve the model prediction of 1-octene oxidation at low temperatures.

Hellier et al. [116] performed engine experiments to measure the ignition properties of four octene isomers to investigate the effect of double bond position and *cis* versus *trans* conformation on diesel combustion and emissions. To observe the impact of moving the position of the double bond towards the centre of the alkyl chain, 1-octene, *trans*-2-octene, and *trans*-3-octene were selected. To allow a comparison of *cis* and *trans* isomers, *cis*-3-octene was also chosen. The order of the ignition delay (shortest first) was found to be the following: 1-octene, *cis*-3-octene, *trans*-3-octene and *trans*-2-octene; this is not consistent with what we found in the combustion kinetics of butene, pentene, hexene and heptene isomers oxidation, from which we concluded that when the position of the double bond moves progressively towards the centre of the molecule the ignition delay consistently increases. Hellier et al. did not develop a detailed kinetic model to explain the experimental results and stated that the phenomena of *cis*-3-octene possessing a shorter ignition delay than *trans*-3-octene, and *trans*-3-octene possessing a shorter ignition delay than *trans*-2-octene, can be attributed to the need for alkenyl and alkenyl peroxy radicals to be in the *cis* arrangement prior to internal isomerization across the double bond. This is not consistent with what we found for the low temperature chemistry of alkene oxidation. The alkenylketohydroperoxides control the low temperature reactivity for alkenes oxidation, but their formation depends on the saturated side of the alkene, the longer the -CH<sub>2</sub>-CH<sub>2</sub>-CH<sub>2</sub>- group in alkenes, the higher the reactivity of that fuel. This group cannot be formed across the C=C double bond and that is why the shift of the C=C double to the central part of the molecule shortens this group and hence decreases the reactivity of the fuel. The experimental results of Hellier et al. [116] need to be revisited to give a clearer picture of octene isomers ignition in engines.

Recently, Fridlyand et al. [118] conducted high pressure, high temperature single pulse shock tube oxidation experiments to investigate the chemical kinetics effects of the double bond position in long chain alkenes including 1-decene, *cis*-2-decene, *cis*-5-decene, and *trans*-5-decene. Their experimental measurements of stable important intermediates indicated increased reactivity for the isomers with more centrally located double bonds, with no influence from the *cis*-*trans* configuration. The high temperature reactivity trend is opposite to the low temperature reactivity which is consistent with the experimental results for 1- and 2-heptene measured in an RCM by Wu et al. [112]. Even though RCM cannot measure the reactivity of heptene isomers at high temperatures over 950 K, the crossing point of the reactivity for the two isomers at 800 K and 23 bar shows that when temperature is higher, the reactivity of 2-heptene is higher than that of 1-heptene. Fridlyand et al. also reported the first high-temperature kinetic model for decenes, largely capturing their high-temperature speciation measurements. Reaction classes included in their model are mainly decomposition of decene isomers and fuel related allylic and alkenyl radicals. At the high temperature, they found that the unimolecular decomposition of each decene fuel molecule and the rapid decomposition of the resonantly stabilized radicals into reactive intermediates are the two most important reaction classes. The reactivity of the decene isomers is in the order of 5-decene igniting fastest, followed by 2-decene, with 1-decene being the slowest to ignite.

Very recently, Tekawade et al. [119] examined the high- and low-temperature reactivity trends of alkenes and a corresponding n-alkane by studying the influence of double bond placement on the ignition of C<sub>10</sub> species at high-pressure conditions. A combination of spray and gas-phase ignition delay studies was performed to produce ignition delay data at a wide range of temperatures (650–1200 K) and pressures (1–4 MPa). They found that at low temperatures, the order of reactivity is trans-5-decene being the least reactive (longest ignition delay), followed by 1-decene and n-decane being the most reactive. However, at high temperatures, the reactivity trends reverse, with trans-5-decene being the most reactive and n-decane being the least reactive, although the differences in the ignition delay at high temperatures are much smaller than those at low temperatures and only slightly larger than the experimental uncertainties ( $\pm 20\%$ ), see *Figure 46*. This trend is consistent with the low temperature reactivity measurements for isomers of hexene [101, 102], heptene [112], and high temperature chemistry of decene isomers published by Fridlyand et al. [118]. The model developed by Fridlyand et al. [118] can capture ignition delay times from 1100 to 1200 K and the slight reactivity difference between 1-decene and trans-5-decene at these conditions. The model only considers high-temperature chemistry and, therefore, does not capture the departure from Arrhenius behavior for temperatures above 1055 K where the intermediate and low temperature chemistry is important. Based on the model developed by Fridlyand et al., [118], Tekawade et al. [119] discussed the reasons for the high temperature reactivity trend and they highlighted that the more allylic hydrogen atoms are present in the molecule, the higher the reactivity, and the different intermediate pools ( $\dot{\text{H}}$  atoms,  $\dot{\text{C}}\text{H}_3$ ,  $\text{C}_2\text{H}_4$ ,  $\text{C}_3\text{H}_6$ , larger olefins, and resonantly stable radicals) that result from different n-decenes affect the reactivity as well. However, it should be noted that the more allylic hydrogens in the molecule, the more resonance stabilized allylic radicals will be formed, and this inhibits the reactivity of the fuel. Including important high temperature reactions, such as addition of  $\dot{\text{H}}$  and  $\dot{\text{O}}$  to the C=C double bond and subsequent reactions, hydrogen-atom abstraction reactions of O<sub>2</sub> from allylic sites, and vinylic radical reactions with O<sub>2</sub>, in the model for decene isomers will be helpful to give us a global picture of their high temperature reactivity. As shown in *Figure 46*, pressure also has a much stronger influence on ignition delays in the NTC regime than at high temperatures, which is due to a strong dependence of the competition between low- and moderate-temperature radical branching and propagation on the pressure and concentration of fuel radicals.

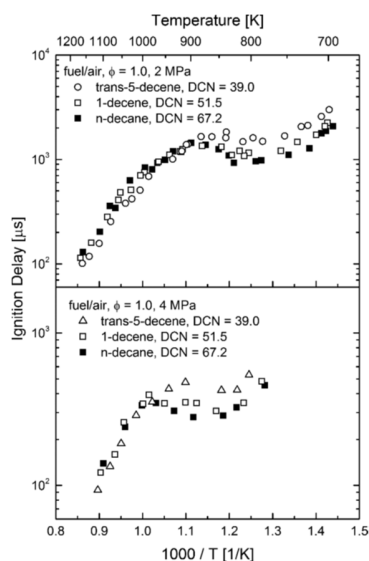


Figure 46. Shock-tube ignition delay measurements: fuel comparisons. (Tekawade et al. [119])

Ignition delay times and laminar flame speeds for the oxidation of two diisobutylene isomers, 2,4,4-trimethyl-1-pentene and 2,4,4-trimethyl-2-pentene, which were treated as alkene components in a surrogate diesel, have been investigated in the literature [120-124]. Metcalfe et al. [123] has measured ignition delay times of the two isomers behind reflected shock wave at 1 and 4 atm between 1200 and 1550 K with equivalence ratios ranging from 1.0 to 0.25. They found that 2,4,4-trimethyl-2-pentene ignited significantly faster under shock tube conditions than 2,4,4-trimethyl-1-pentene and that the ignition delay times for the blend were directly dependent on the proportions of each isomer. A comprehensive chemistry model was developed for both isomers which can capture the reactivity successfully, as shown in Figure 47.

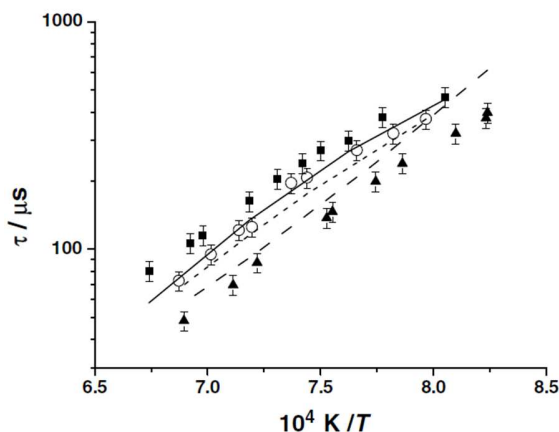


Figure 47. Experimental (points) and model predicted (lines) ignition delay times for 0.75% fuel oxidation behind reflected shock waves at  $\phi = 0.5$ , 4.0 atm in Ar, (■—) 2,4,4-trimethyl-1-pentene, (○- - -) 2,4,4-trimethyl-1-pentene: 2,4,4-trimethyl-2-pentene (3:1), (▲—) 2,4,4-trimethyl-2-pentene. 10% error bars on experimental data, from Metcalfe et al. [123]

The trend shown in Figure 47 is consistent with previous high temperature experimental results for decene isomers by Fridlyand et al. [118] and Tekawade et al. [119], which reveals that at high temperatures the shift of the C=C double bond to the central part of the molecule increases the

reactivity of the fuel. The model from Metcalfe et al. [123] highlights the importance of the isobutene chemistry in the decomposition of 2,4,4-trimethyl-1-pentene, but not for 2,4,4-trimethyl-2-pentene.

Based on the model developed by Metcalfe et al. [123], Hu et al. [121] carried out ignition delay times measurements of 2,4,4-trimethyl-1-pentene in a shock tube. By updating the core mechanism from AramcoMech 2.0 [25, 51, 52, 87, 88, 196] and also the isobutene oxidation part from Zhou et al. [88], their model gives a better prediction of the ignition delay time at high temperatures. Laminar flame speeds for 2,4,4-trimethyl-1-pentene and 2,4,4-trimethyl-2-pentene have also been investigated by Hu and co-authors [120, 122], who showed that 2,4,4-trimethyl-2-pentene has a higher flame speed than 2,4,4-trimethyl-1-pentene.

Summarizing the larger alkenes discussed in this section, the shift of the C=C double bond from terminal to the central part interrupts the formation of a chain branching precursor of alkenylketohydroperoxides and hence decreases the reactivity at low temperatures but accelerates the reactivity at high temperatures.

### 3.10 The combustion chemistry of diolefins

Here, we will discuss the combustion chemistry of 1,3-butadiene ( $\text{CH}_2=\text{CHCH}=\text{CH}_2$ ). With two conjugated C=C double bonds, 1,3-butadiene is a crucially important intermediate which can be formed during the combustion of olefins and larger dienes. It is a good source of  $\dot{\text{C}}_4\text{H}_5$  radicals which are involved in the formation of aromatic species [341], particularly in benzene formation through the addition of  $i\text{-}\dot{\text{C}}_4\text{H}_5$  ( $\text{CH}_2=\text{CH}-\text{C}=\text{CH}_2$ ) to  $\text{C}_2\text{H}_2$  [64]. Moreover, as the smallest diene, its detailed combustion chemistry model investigation is helpful to understand the chemistry of species with two double bonds. The pyrolysis and oxidation mechanism of 1,3-butadiene has been studied previously [53-60] with some works focusing on the PAH formation kinetics [61-66] and the interaction chemistry when 1,3-butadiene blended with other important fuels.

BDEs of the two C - H bonds in 1,3-butadiene as well as those in isobutene and propene were determined using the more sophisticated QCISD(T)/CBS method, which has been employed in the 0 K formation enthalpy calculations for 219 small molecules and radicals relevant in combustion chemistry by Goldsmith et al. [342], in combination with density functional M062X/6-311++G(d,p) [343] for geometry optimizations. The results are shown in Figure 48 for comparison. We can see that BDEs of the secondary vinylic C - H in the three species is within 1.7 kcal/mol, while the tertiary vinylic C - H bond in 1,3- $\text{C}_4\text{H}_6$  is 6.2 kcal/mol weaker than that in propene. This is because the C2 - H bond in 1,3- $\text{C}_4\text{H}_6$  in Figure 48 is a combination of vinylic and allylic C - H bonds closer to a vinylic bond. Hence, H - atom abstraction by  $\dot{\text{O}}\text{H}$ ,  $\text{H}\dot{\text{O}}_2$ ,  $\dot{\text{C}}\text{H}_3$  radicals and  $\dot{\text{H}}$  and  $\ddot{\text{O}}$  atoms from the tertiary C - H bond in 1,3- $\text{C}_4\text{H}_6$  is easier than that from the secondary C - H bond but much more difficult than from the allylic C-H bond in propene. This causes the main difference between alkenes discussed above and 1,3- $\text{C}_4\text{H}_6$ . In alkenes, the chemistry of resonance stabilized radicals plays a key role in determining their reactivity over different temperature and pressure ranges, while in 1,3- $\text{C}_4\text{H}_6$ , rather than the abstraction reactions, addition reactions of  $\dot{\text{H}}$  and  $\ddot{\text{O}}$  atoms as well as  $\dot{\text{O}}\text{H}$  and  $\text{H}\dot{\text{O}}_2$  radicals to the double

bond play an important role in determining the reactivity. We will now discuss important reaction classes for 1,3-butadiene.

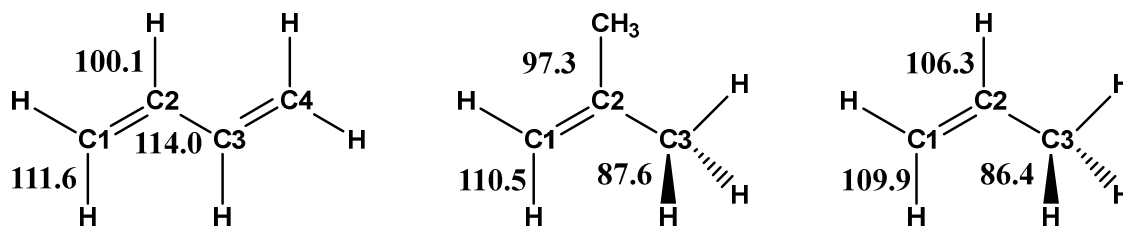
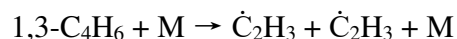
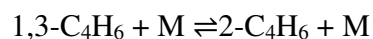
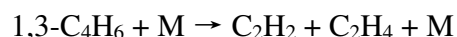
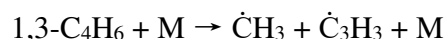


Figure 48. BDEs (in kcal/mol) of different types of C–H bonds in 1,3- $C_4H_6$ , isobutene and propene obtained at the QCISD(T)/CBS//M062X/6-311++G(d,p) level of theory.

### 3.10.1 Important reaction classes for 1,3-butadiene oxidation

$1,3-C_4H_6 + M \rightleftharpoons Products$ . Pyrolysis of 1,3-butadiene has been investigated extensively in the literature [56, 57, 60, 344, 345] and has been reviewed comprehensively by both Laskin [54] and Lockhart et al. [346]. Detailed discussion will not be provided here. Here, we just mention the very recent work carried out by Lockhart et al. [346] both theoretically and experimentally. The measurements have been taken in a diaphragmless shock tube, at postshock total pressures of 26–261 Torr and temperatures ranging from 1428 to 2354 K, using laser schlieren densitometry.



Four reaction pathways of 1,3-butadiene pyrolysis have been identified and the direct dissociation path to form the  $\dot{C}H_3 + \dot{C}_3H_3$  radicals is found to be the important reaction channel at temperatures ranging from 1739 to 2354 K with branching ratios ranging from 0.62 to 0.78, with greatest yields at the lowest temperatures, independent of pressure. Molecular fragmentation of 1,3- $C_4H_6$  to  $C_2H_2 + C_2H_4$  is a relatively minor loss channel with branching fractions ranging from 0.04 to 0.15, with greatest yields at the highest temperature independent of pressure. Isomerization from 1,3- $C_4H_6$  to 2- $C_4H_6$  is the most significant isomerization channel with a branching fraction of 0.12 independent of temperature and pressure. The contributions of direct dissociation to vinyl radicals and H-atom elimination from the terminal carbons are negligible under all experimental conditions. This finding is different from previous results [54] which state that the initial step was the C–C bond rupture to form two vinyl radicals, followed by the concerted unimolecular process to proceed in two steps via the formation of vinylidene;  $1,3-C_4H_6 \rightarrow C_2H_4 + H_2CC:$  and  $H_2CC: + M \rightarrow C_2H_2 + M$ . A simplified potential energy surface for the isomerization and dissociation pathways of 1,3- $C_4H_6$  has also been given and rate constants calculations for those reaction channels have also been presented by Lockhart et al. [346].

$1,3\text{-C}_4\text{H}_6 + \dot{\text{H}} \rightleftharpoons \dot{\text{C}}_2\text{H}_3 + \text{C}_2\text{H}_4 / \dot{\text{C}}_4\text{H}_7 1\text{-}3$ . Hydrogen atom addition to 1,3-C<sub>4</sub>H<sub>6</sub> is one of the key reactions that can determine the reactivity of 1,3 - C<sub>4</sub>H<sub>6</sub> oxidation at high temperatures [54, 67]. Sensitivity analysis in Figure 49, taken from Zhou et al. [67] for flame speed and ignition delay times, shows that the reaction channel forming the reactive vinyl radical and ethylene molecule plays an important role in promoting the reactivity, while the reaction channel forming the resonance stabilized  $\dot{\text{C}}_4\text{H}_7 1\text{-}3$  radical inhibits the reactivity.

Investigations of various reactions on the  $\dot{\text{C}}_4\text{H}_7$  PES have received much attention in the literature both theoretically [347-350] and experimentally [351-353]. Potential energy surfaces of  $\dot{\text{C}}_4\text{H}_7$  decomposition and isomerization have been reported by Miller [347] at the G3//B3LYP level of theory. Unimolecular decomposition and isomerization of the 3-butenyl ( $\dot{\text{C}}\text{H}_2\text{CH}_2\text{CH}=\text{CH}_2$ ) has also been investigated by Miyoshi [348] with potential energy surface obtained at the CBS-QB3 level of theory and solving the RRKM/ME to get the pressure dependent rate constants for the reactions studied. Xu et al. [349] has investigated the potential energy surface of the  $\dot{\text{C}}_4\text{H}_7$  radical at the CBS-QB3 level of theory to better characterize the radical addition reactions that lead to the molecular weight growth. Pressure dependent rate constants for this reaction have also been achieved by QRRK/modified strong collider analyses and the authors stated that the  $\dot{\text{H}}$  atom addition to olefins was found to inhibit the molecular weight growth by leading to the production of a lower olefin and methyl radicals. Recently, Huang et al. [350] investigated the pressure-dependent kinetics on the  $\dot{\text{C}}_4\text{H}_7$  potential energy surface and its effect on the combustion model predictions. The CCSD(T)-F12/cc-pVTZ-F12//QCISD/6-311++G(2df,2p) level of theory was used to explore the detailed reaction potential energy surface coupled with the RRKM/ME method to calculate the temperature and pressure dependent rate coefficients. Very recently, rate constants for  $\dot{\text{C}}_4\text{H}_7$  radical decomposition were calculated by Li et al. [354] using RRKM/ME theory based on the potential energy surface obtained at the ROCCSD(T)/cc-pV $\infty$ Z//M062X/6-311++G(d,p) level of theory, provided in Figure 50. The important reaction channels calculated in this work are shown below. The calculation results from Huang et al. [350] and Li et al. [354] gave good agreement in the temperature range of 800 to 2000 K. The high pressure limit rate constants provided by Li et al. [354] for the reaction  $\text{C}_2\text{H}_4 + \text{C}_2\text{H}_3 \rightarrow$  products agree quite well with the ones from the experimental measurements by Shestov et al. [351], Ismail et al. [352] and Fahr et al. [353].

- $1,3\text{-C}_4\text{H}_6 + \dot{\text{H}} \leftrightarrow \dot{\text{C}}_4\text{H}_7 1\text{-}3$
- $1,3\text{-C}_4\text{H}_6 + \dot{\text{H}} \leftrightarrow \text{C}_2\text{H}_4 + \dot{\text{C}}_2\text{H}_3$
- $1,3\text{-C}_4\text{H}_6 + \dot{\text{H}} \leftrightarrow \text{C}_3\text{H}_4\text{-a} + \dot{\text{C}}\text{H}_3$
- $1,3\text{-C}_4\text{H}_6 + \dot{\text{H}} \leftrightarrow \text{C}_3\text{H}_4\text{-p} + \dot{\text{C}}\text{H}_3$
- $1,3\text{-C}_4\text{H}_6 + \dot{\text{H}} \leftrightarrow 1,2\text{-C}_4\text{H}_6 + \dot{\text{H}}$
- $1,3\text{-C}_4\text{H}_6 + \dot{\text{H}} \leftrightarrow 1\text{-C}_4\text{H}_6 + \dot{\text{H}}$

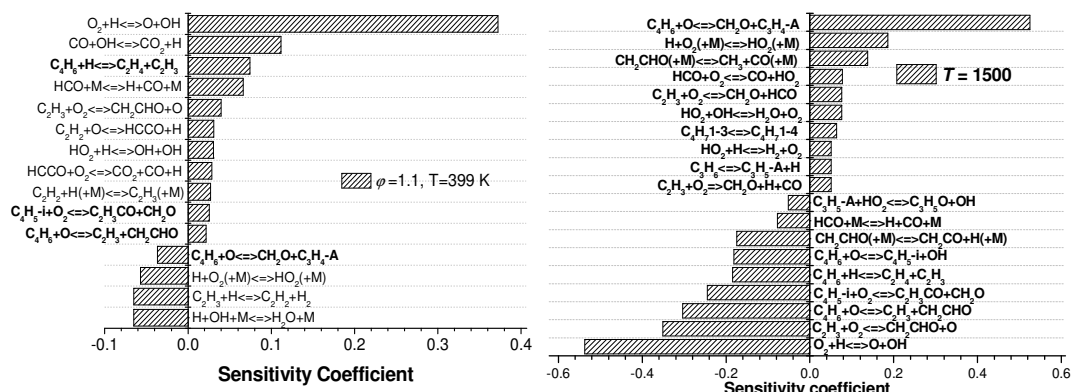


Figure 49. Sensitivity analysis of the flame speed at  $\phi = 1.1$ ,  $T = 399$  K,  $p = 5$  atm (left) and ignition delay time at  $\phi = 0.5$ ,  $T = 1500$  K,  $p = 20$  atm (right) for 1,3- $C_4H_6$  oxidation.

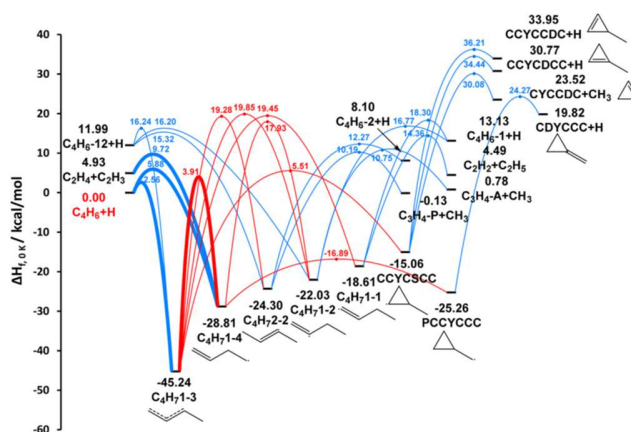
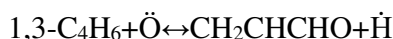
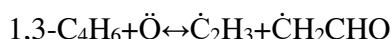
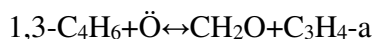


Figure 50. Comprehensive potential energy surface for  $\dot{C}_4H_7$  radical decomposition.

$1,3-C_4H_6 + \ddot{O} \rightleftharpoons CH_2O + C_3H_4-a / \dot{C}_2H_3 + \dot{C}_2HCHO$ . Brezinsky et al. [53] examined 1,3- $C_4H_6$  oxidation in an atmospheric flow reactor at temperature near 1100 K and equivalence ratio of 0.55, 1.18, and 1.65. They found that the concentration of crotonaldehyde ( $CH_3-CH=CH-CHO$ ) was high at the initial oxidation stage of 1,3- $C_4H_6$  and they proposed that the addition of oxygen atom to the double bond in 1,3- $C_4H_6$  plays an important role with the reaction pathway shown as  $1,3-C_4H_6 + \ddot{O} \rightarrow CH_2=CH-CH-CH_2-O \rightarrow CH_2=CH-CH_2-CHO \rightarrow CH_2=CH-CH_2-CO + \dot{H}$ ,  $CH_2=CH-CH_2-CO \rightarrow a\dot{C}_3H_5 + CO$ . Dagaut and Cathonnet [179] investigated the oxidation of 1,3- $C_4H_6$  in a jet-stirred reactor and they found vinyloxirane in the postreaction mixture. Based on this finding, the authors proposed that the addition of the  $\ddot{O}$  atom onto the double bond in 1,3- $C_4H_6$  leads to the formation of vinyloxirane through the reaction of  $1,3-C_4H_6 + \ddot{O} \rightarrow$  vinyloxirane. Vinyloxirane can be consumed through the unimolecular decomposition pathways, vinyloxirane  $\rightarrow C_3H_6 + CO$  and vinyloxirane  $\rightarrow C_2H_4 + CH_2CO$ . The reaction pathway proposed by Dagaut and Cathonnet [179] is a chain termination reaction which is significantly different from that of Brezinsky et al. [53], which is, effectively, a chain branching reaction. Both studies emphasized the importance of the reaction between 1,3-butadiene and the  $\ddot{O}$  atom. By using the analogy between the product channels of the reaction between propene and the  $\ddot{O}$  atom investigated by

Cavallotti et al. [210, 211], Zhou et al. [67] proposed two dominant product channels for the addition reaction of 1,3-C<sub>4</sub>H<sub>6</sub> with  $\ddot{O}$  atom which include the formation of  $\dot{C}_2H_3 + \dot{C}H_2CHO$  and  $CH_2O$  and C<sub>3</sub>H<sub>4</sub>-a. Sensitivity analysis for 1,3-C<sub>4</sub>H<sub>6</sub> oxidation at  $\phi = 0.5$ , pressure = 20 atm and temperatures of 950 K and 1200 K, carried out by Zhou et al. [67], is presented in Figure 51. It shows that the reaction leading to the formation of the two reactive radicals  $\dot{C}_2H_3$  and  $\dot{C}H_2CHO$  is the most promoting reaction channel while that leading to the formation of the two stable molecules of  $CH_2O$  and C<sub>3</sub>H<sub>4</sub>-a is the most inhibiting reaction channel. The branching ratio between the two main product channels of  $\dot{C}_2H_3 + \dot{C}H_2CHO$  and  $CH_2O + C_3H_4$ -a determines the fuel reactivity. The main reaction channels for  $\ddot{O}$  atom adding to 1,3-C<sub>4</sub>H<sub>6</sub> proposed by Zhou et al. [67] are as follows



For the reactivity prediction of 1,3-butadiene oxidation, this is a key reaction and it is important to either have experimental measurements or high-level *ab initio* electronic structure calculations of the underlying triplet/singlet potential energy surfaces and statistical (RRKM/ME) computations of branching ratios including inter-system crossing.

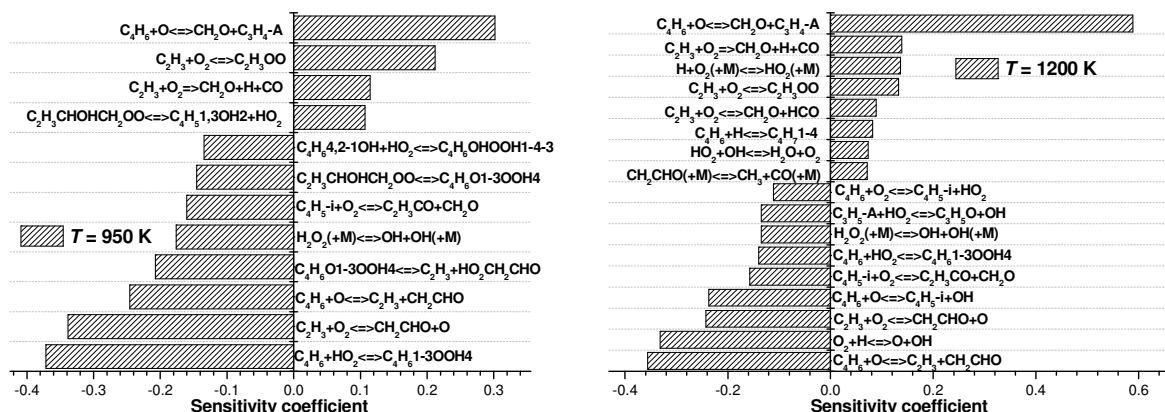


Figure 51. Sensitivity analysis of 1,3-butadiene oxidation at  $\phi = 0.5$ , 20 atm, 950 K and 1200 K.

### 1,3-C<sub>4</sub>H<sub>6</sub> + $\dot{H}O_2 \rightleftharpoons$ Products.

It is expected that for conjugated alkenes, the branching fractions for various  $\dot{H}O_2$  addition channels are influenced by the partial resonance stabilization at the transition state. As shown in Figure 48, the dissociation energy of the C–H bond in 1,3-butadiene is much higher than that in alkenes. Therefore, addition reactions of important radicals onto the double bond of 1,3-butadiene is much more important at intermediate temperatures than the abstraction reactions. Laskin et al. [54] assumed that the addition reaction between  $\dot{H}O_2$  radical and 1,3-C<sub>4</sub>H<sub>6</sub> can lead to the formation of vinyloxirane and 2,5-dihydrofuran through the reactions of  $1,3-C_4H_6 + \dot{H}O_2 \rightarrow$  vinyloxirane +  $\dot{O}H$  and  $1,3-C_4H_6 + \dot{H}O_2 \rightarrow$  2,5-dihydrofuran +  $\dot{O}H$ . However, apart from the decomposition of the formed intermediates, Zhou et al. [67] also proposed the resonance stabilized radical reactions shown in Figure 52. Rate constants for those reaction pathways have been taken from the analogy with alkenes with reasonable adjustment based on the difference of the reactants. Future *ab initio* calculations or experimental measurements on those important

reaction pathways will be helpful to fully understand the intermediate temperature chemistry of 1,3-butadiene oxidation.

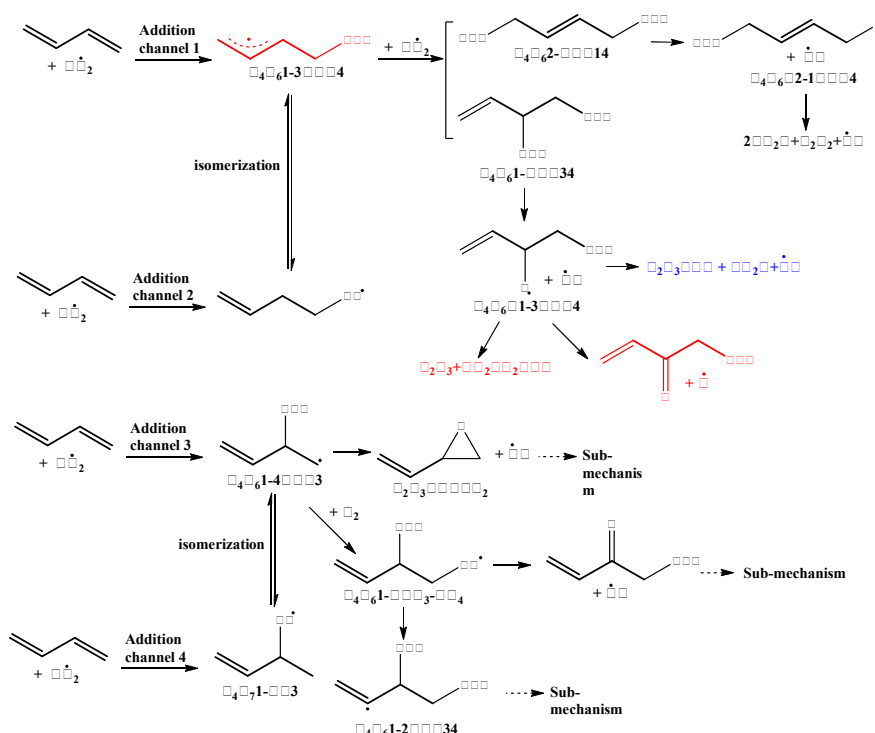


Figure 52. Important reaction channels for the addition reaction  $1,3\text{-C}_4\text{H}_6 + \text{HO}_2$  and the subsequent reactions. Formation of the species highlighted in red: promotes reactivity, in blue: inhibits reactivity.

### $1,3\text{-C}_4\text{H}_6 + \dot{\text{O}}\text{H} \rightleftharpoons \text{Products}$ .

Hydrogen atom abstraction by  $\dot{\text{O}}\text{H}$  radicals from 1,3-butadiene has been studied by Vasu et al. [355] and Khaled et al. [287] both experimentally and theoretically. The experiments were carried out over the temperature range 1011–1406 K and pressure near 2.2 atm. The rate coefficients were also calculated over the temperature range 250 – 2500 K using variation transition state theory based on the QCISD(T)/cc-pV $\infty$ Z//B3LYP/6-311++G(d,p) level of theory. The calculations are in good agreement with the experimental results above 1200 K. Consistent with what we found for the alkenes chemistry [86-88] at lower temperatures, the reactions of  $\dot{\text{O}}\text{H}$  radicals adding to the double bond play a more important role than the H-atom abstraction reactions. Sensitivity analysis for 1,3-butadiene oxidation for  $\phi = 0.5$  and 20 atm at 770 K and 870 K, respectively, is shown in Figure 53. It indicates that the addition reaction of the reactive  $\dot{\text{O}}\text{H}$  radical onto the double bond of 1,3-butadiene and the subsequent reactions determine the reactivity of 1,3-butadiene oxidation under those conditions. Detailed reaction pathways for the oxidation process are shown in Figure 54, as proposed by Zhou et al. [67], and their rate constants were taken from analogy with alkenes chemistry with a certain adjustment based on the BDEs of different bonds in 1,3-butadiene. Future *ab initio* calculations and/or experimental measurements on those important reaction pathways will be helpful to fully understand the low temperature chemistry of 1,3-butadiene oxidation. It is worth to highlight that in the mechanism

proposed by Laskin et al. [54], only H-atom abstraction reactions by  $\dot{\text{O}}\text{H}$  radicals are taken into consideration while  $\dot{\text{O}}\text{H}$  addition pathways are not included.

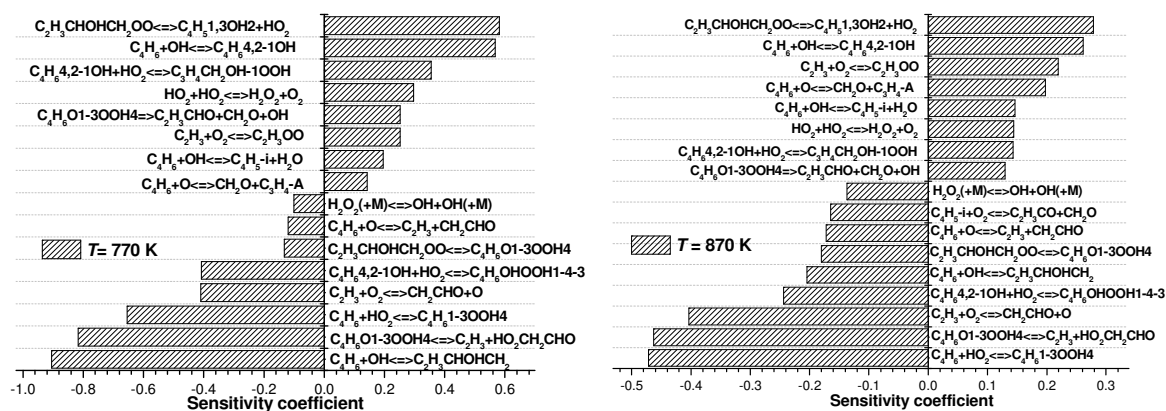


Figure 53. Brute-force sensitivity analysis of 1,3-butadiene ignition delay times at 20 atm,  $\phi = 0.5$  for  $T = 770$  K and  $870$  K.

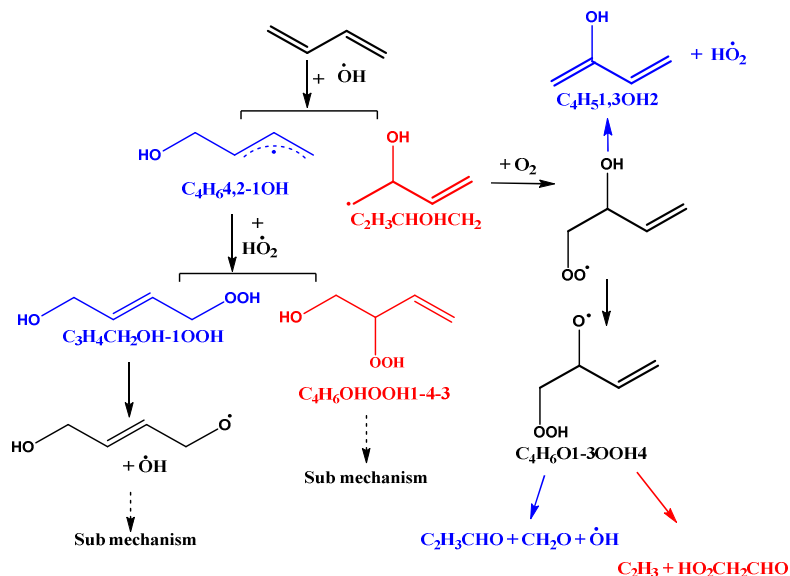


Figure 54. Important reaction channels for 1,3- $\text{C}_4\text{H}_6 + \dot{\text{O}}\text{H}$  addition reaction and their subsequent reactions. Formation of the species highlighted in red: promotes reactivity, in blue: inhibits reactivity.

$n\text{-}\dot{\text{C}}_4\text{H}_5 + \text{O}_2 \rightleftharpoons \text{Products}$ . The kinetics of  $\dot{\text{C}}_4\text{H}_5$  ( $\dot{\text{C}}\text{HCHCHCH}_2$  radical) with  $\text{O}_2$  were investigated from 296 to 900 K in a tubular reactor coupled to a photoionization mass spectrometer by Slagle et al. [356]. They assigned the reaction products to be  $\text{CH}_2\text{CO} + \text{CH}_2\text{CHO}$ , based on a similar channel for the  $\dot{\text{C}}_2\text{H}_3 + \text{O}_2$  reaction. Pressure dependent rate constants for this reaction, recommended by Zhou et al. [67] in 1,3-butadiene oxidation model, are obtained based on analogy with those calculated by Goldsmith et al. [213] for  $\dot{\text{C}}_2\text{H}_3 + \text{O}_2$ .

### 3.10.2 Chemistry difference between alkenes and diolefins

As discussed, BDEs for the C–H bonds in 1,3-butadiene are much higher than those in alkenes, in particular, in comparison with the allylic C–H bond. Therefore, the addition reactions of

radicals and atoms onto the C=C double bond in 1,3-butadiene are more favored than the abstraction reactions. At lower temperatures, the reaction initially starts from  $\dot{\text{O}}\text{H}$  radical addition to the C=C double bond in 1,3-butadiene followed by isomerization and decomposition reactions. At intermediate temperatures, however, the reaction initially starts from  $\text{H}\dot{\text{O}}_2$  radical addition to the C=C double bond by forming the allylic- $\dot{\text{Q}}\text{OOH}$  which will further react with another  $\text{H}\dot{\text{O}}_2$  radical to lead to chain propagation or branching reaction pathways. When temperature rises, addition reactions of  $\dot{\text{H}}$  and  $\dot{\text{O}}$  atom to 1,3-butadiene are the main reaction channels which break the C=C double bond. When the fuel molecule changes to larger dienes, the allylic hydrogen atom will be involved and hence the allylic hydrogen chemistry should also be included.

### 3.11 Chemistry difference between alkanes and alkenes

Chemistry differences between alkanes and alkenes mainly arise from the influence of the C=C double bond on the kinetics, including addition reactions to the double bond and the allylic radical related reactions. The dominant addition reactions change with temperature. At low temperatures,  $\dot{\text{O}}\text{H}$  radical addition to the double bond is dominant and is followed by molecular oxygen addition reactions. At intermediate temperatures,  $\text{H}\dot{\text{O}}_2$  radical addition to the double bond becomes more important with favored formation of a cyclic ether and  $\dot{\text{O}}\text{H}$  radical. As temperature further increases, additions of  $\dot{\text{H}}$  and  $\dot{\text{O}}$  atoms to the double bond represent the main source for breaking the C=C bond.

The low temperature reactivity of different types of fuels is governed by the formation of ketohydroperoxides (KHP). In saturated hydrocarbons, KHP can be formed through fuel radical reacting with molecular oxygen followed by isomerization and second  $\text{O}_2$  addition reactions. However, KHP formation pathways in unsaturated hydrocarbons are different. There are two types of KHPs that can be formed in the low temperature oxidation of unsaturated hydrocarbons which are hydroxyketohydroperoxides and alkenylketohydroperoxides. The formation of hydroxyketohydroperoxides initially starts from the molecular oxygen addition to the hydroxylalkyl radical, and competes with the chain propagation reaction of Waddington mechanism. The formation of alkenylketohydroperoxides initially starts from the molecular oxygen addition to alkenyl radical followed by isomerization and second molecular oxygen addition. When the number of the chain carbon atoms in the molecular is larger than five, the formation of alkenylketohydroperoxides can be competitive.

At intermediate temperatures, the allylic radical chemistry controls the reactivity of unsaturated hydrocarbon oxidation. The dominant reaction pathways are the radical-radical recombination reactions between the allylic radical and  $\text{H}\dot{\text{O}}_2$ ,  $\dot{\text{C}}\text{H}_3$ , and self-recombination reaction of allylic radicals. These reaction classes are also different from saturated hydrocarbon chemistry at intermediate temperatures. In contrast, at high temperatures, the C=C double bond will absorb the reactive  $\dot{\text{H}}$  and  $\dot{\text{O}}$  atoms which will decrease the reactivity as compared to saturated hydrocarbons.

## 4. PAH and soot formation from alkenes

Alkenes can play a dual role in PAH growth processes leading eventually to soot formation: first, they supply resonantly stabilized free radicals (RSFR) and small stable molecules like acetylene which then react to form monocyclic aromatics and PAHs and second, directly participate in chemical reactions producing PAHs. The review below is organized around these two roles; in the beginning, we discuss experimental flame studies and corresponding chemical mechanisms deduced from them based on the cracking patterns of the participating alkenes and then, consider various mechanisms of PAH growth involving additions of alkenes to aryl radicals inferred either from theory or experiment, or both.

### 4.1 Alkenes as a source of RSFR – precursors of monocyclic aromatics and PAH

Few research groups considered PAH formation and sooting trends of various fuels containing different alkenes in flames and tried to correlate these trends with the structure of the particular alkenes present. For instance, Dagaut and Cathonnet [76], while studying oxidation of isobutene in a jet-stirred reactor at combustion temperatures and pressures, observed the formation of the first aromatic ring, benzene, and their kinetic modeling identified two reactions, addition of propargyl radical  $\dot{C}_3H_3$  to allene  $C_3H_4$  and recombination of two propargyl radicals, to be responsible for this process. The same authors considered benzene formation from propene [357] and concluded that the propargyl recombination is not important and propene itself is not involved in the reaction pathways leading to benzene. They invoked as a possible source recombination of two allyl radicals leading to 1,3-cyclohexadiene followed by its dehydrogenation but detected a correlation between the concentration of 1,3-cyclohexadiene and benzene only at low fuel conversions. Instead, they found a good correlation of the concentrations of cyclopentadiene and acetylene with that of benzene. Based on this they proposed the  $\dot{C}_4H_5 + C_2H_2$  reaction as the main source, with  $\dot{C}_4H_5$  being produced from cyclopentadienyl radical  $c-C_5H_5$ . This however contradicts to the chemistry of  $c-C_5H_5$  decomposition, which is well-established [358-360], which gives  $\dot{C}_3H_3 + C_2H_2$  as the main product. Most recently, Dagaut and co-workers [83] used the same jet-stirred reactor technique (but with more extensive detection of various molecules formed including gas chromatography and infrared spectrometry) to investigate oxidation of 1- and 2-butene and detected benzene, which was attributed to propargyl recombination according to kinetic modeling.

The most detailed investigation of PAH growth and soot formation in a variety of pure 1-alkene fuels from propene to 1-octene was recently published by Wang et al. [361]. They studied counterflow diffusion flames at atmospheric pressure and diagnosed PAH and soot formation employing laser-induced fluorescence (LIF) with a detection wavelength of 500 nm and laser induced-incandescence (LII) techniques, respectively. Based on the LIF data, the largest amount of PAH was produced in the 1-butene flame, followed by 1-pentene and 1-hexene, propene, 1-octene, and ethylene:  $1-C_4H_8 > 1-C_5H_{10} \sim 1-C_6H_{12} > C_3H_6 > 1-C_8H_{16} > C_2H_4$ . Interestingly, the trend for soot formation deduced from the LII results was somewhat different:  $1-C_4H_8 > C_3H_6 > 1-C_5H_{10} > 1-C_6H_{12} > 1-C_8H_{16} > C_2H_4$  (Fig. 55). In order to account for the observed trends and to reveal the aromatic formation pathways, the authors carried out numerical simulations with a comprehensive chemical kinetic model including PAH growth chemistry for the 1-alkene fuels.

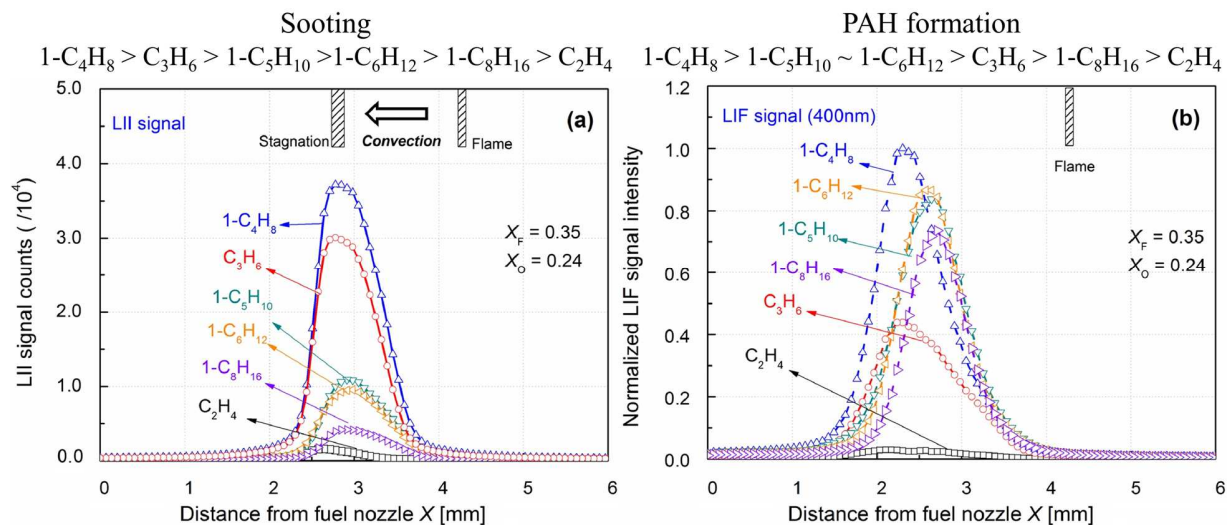
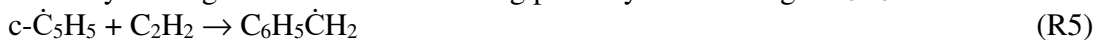


Figure 55. Soot formation and PAH growth observed in flames of pure 1-alkene fuels [361] based on LII (a) and LIF (b) signals, respectively.

The model used was initially based upon KAUST-Aramco PAH Mech 1.0 [362] for ethylene flames, comprising AramcoMech 1.3 high-temperature chemistry [51, 52] as the base mechanism with additional oxidation reactions for hydrocarbons up to benzene [363], PAH growth reaction pathways up to coronene (A7) from KAUST PAH Mechanisms (KM1, KM2) [364, 365], and the LLNL gasoline surrogate mechanism [366] containing high-temperature submechanisms for C4 to C7 1-alkenes. Additionally, the high-temperature combustion submechanism for 1-octene and PAH growth reactions initiated by propargyl radical addition to naphthalene leading to the formation of pyrene were included [367]. This extended mechanism was denoted as KAUST-Aramco PAH Mech 1.0-alkenes and included 575 species and 3395 reactions. The results of modeling showed a great importance of intermediate RSFR species with odd carbon numbers in the formation of aromatics, in particular propargyl  $\dot{C}_3H_3$ , allyl  $\dot{C}_3H_5$ , cyclopentadienyl  $c-\dot{C}_5H_5$ , benzyl  $\dot{C}_7H_7$  ( $C_6H_5\dot{C}H_2$ ), and indenyl  $\dot{C}_9H_7$  produced from fuel decomposition. For instance, the authors compared the  $C_2H_4$ ,  $C_3H_6$  and  $1-C_4H_8$  fuels in terms of the reaction pathways producing the aromatic ring (benzene, A1), which in turn can grow to larger PAH via the HACA mechanism [368, 369]. Propargyl and cyclopentadienyl were deduced not only be responsible for benzene formation but also to contribute significantly to the growth of larger PAHs. Wang et al. found that the flame of the  $C_2H_4$  fuel exhibits the lowest concentrations of  $\dot{C}_3H_3$  and  $c-\dot{C}_5H_5$ , orders of magnitude lower than those with the  $1-C_4H_8$  and  $C_3H_6$  fuels. In addition, the decomposition of 1-butene fuel produced much more  $\dot{C}_3H_5$  radicals than the decomposition of propene. Very low concentrations of the  $C_3$  and  $C_5$  RSFR in the ethylene flame lead to the very low benzene concentration. Propargyl and allyl radicals are particularly important for benzene formation:



Cyclopentadiene can undergo direct H abstraction from the CH<sub>2</sub> group forming cyclopentadienyl. Wang et al. used the following pathways connecting c-C<sub>5</sub>H<sub>5</sub> with benzene:



In the meantime, it is well established now that benzene can be readily produced via methylation of cyclopentadienyl [370-373]:

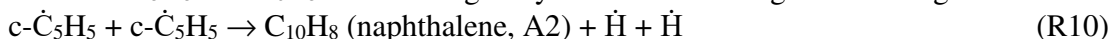


One more pathway, not listed above, contributes significantly to benzene formation in the C<sub>2</sub>H<sub>4</sub> flame:



but in all other considered flames, the contribution of R2, i.e., the recombination of two propargyl radicals, to benzene formation is dominant. The rate of R9 is orders of magnitude slower than R2 in all flames except the C<sub>2</sub>H<sub>4</sub> flame, but the latter is lacking C<sub>3</sub> species and hence R2 is only of secondary importance in benzene formation there.

How the propargyl and allyl radicals are produced from the fuel pyrolysis? Their formation requires dehydrogenation reactions of C<sub>3</sub> species or bimolecular reactions between C<sub>2</sub> and C<sub>1</sub> species [374, 375]. Both C<sub>3</sub> and C<sub>1</sub> species are formed more easily in the C<sub>3</sub>H<sub>6</sub> and 1-C<sub>4</sub>H<sub>8</sub> flames than in the C<sub>2</sub>H<sub>4</sub> flame, which results in much higher  $\dot{\text{C}}_3\text{H}_3$  concentrations, in particular. The c-C<sub>5</sub>H<sub>5</sub> and C<sub>6</sub>H<sub>5</sub> $\dot{\text{C}}\text{H}_2$  RSFR greatly contribute to the growth of larger PAH:



(It should be noted here that thermal decomposition of  $\dot{\text{C}}_{10}\text{H}_9$  to naphthalene +  $\dot{\text{H}}$  is also quite fast under combustion conditions and hence needs to be included in the mechanism. Theoretical rate for R10 and R12 are available in the literature, but up-to-date high-level calculations for R11 are necessary to update this mechanism).

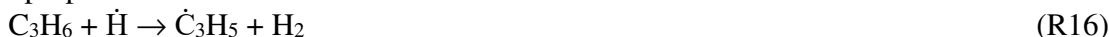


(Here, although the reaction R14 is included in the model, its mechanism is not well understood and is questionable. Quantum chemical calculations for R13 and R14 have not been reported so far and are necessary to accurately evaluate their rate constants and to improve this mechanism).

The C<sub>2</sub>H<sub>4</sub> flame has the lowest PAH concentrations because it produces low concentrations of the C<sub>3</sub> and C<sub>5</sub> RSFR. The C<sub>3</sub>H<sub>6</sub> flame has similar  $\dot{\text{C}}_3\text{H}_3$  concentrations with the 1-C<sub>4</sub>H<sub>8</sub> flame, but its c-C<sub>5</sub>H<sub>5</sub> concentration is much lower. Also, the mole fraction of allyl in the 1-C<sub>4</sub>H<sub>8</sub> flame is about 4 times higher than that in the C<sub>3</sub>H<sub>6</sub> flame. 1-butene can produce allyl directly through unimolecular decomposition cleaving the weakest C-C allylic bond:



whereas propene can form this radical via a bimolecular H abstraction reaction:



and thus requires  $\dot{\text{H}}$  atoms to be present, which exhibit high concentrations near the high temperature flame zone. The allyl radical is important for the formation of c-C<sub>5</sub>H<sub>5</sub> via R4, and cyclopentadienyl in turn plays a critical role in the subsequent PAH through R5–R14. Therefore, the lower yield of allyl rationalizes the lower sooting tendency of C<sub>3</sub>H<sub>6</sub> compared to 1-C<sub>4</sub>H<sub>8</sub>.

As the size of the alkene increases, the trend in the soot/PAH formation can be best understood through the comparison between 1-butene and 1-pentene, as the largest difference in

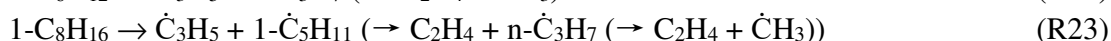
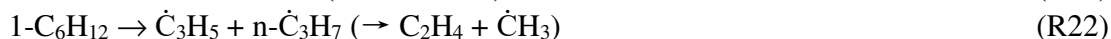
the C<sub>4</sub>-C<sub>8</sub> alkene series was observed between C<sub>4</sub> and C<sub>5</sub>. Since R2 gives the largest contribution to benzene formation, the decrease in the PAH formation in the 1-C<sub>5</sub>H<sub>10</sub> is attributed to a much lower concentration of  $\dot{C}_3H_3$ . The 1-C<sub>4</sub>H<sub>8</sub> flame produces more  $\dot{C}_3H_3$  because the dominant formation channels of propargyl in the region important for aromatic species formation involve H abstraction reactions from C<sub>3</sub>H<sub>4</sub> isomers:



While propyne was found to be mostly produced from allene, according to the kinetic model, allene forms via the reaction of allyl and methyl radicals:

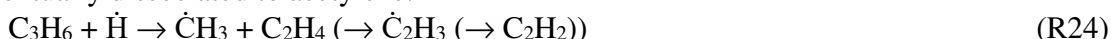


In turn, the concentration profiles of methyl are highly dependent on the fuel decomposition pattern. The rate of production analysis carried out by the authors identified the following fuel decomposition pathways:



Thus, CH<sub>3</sub> is produced directly in the decomposition of 1-butene, through secondary  $\beta$ -scission reactions from 1-hexene and 1-octene, and is not produced at all from 1-pentene. This consideration explains the observed ranking of  $\dot{C}H_3$  concentrations and further rationalizes the highest concentration of benzene in 1-C<sub>4</sub>H<sub>8</sub> flames among C<sub>4</sub>-C<sub>8</sub> fuels. The only caveat here is that  $\dot{C}H_3$  concentration in the 1-octene flame is higher than that in 1-pentene, but this is offset by the lower concentration of allyl in the case of C<sub>8</sub>H<sub>16</sub>.

For the formation of larger aromatics, the analysis by the authors has shown an important role of R10-R14 and hence,  $\dot{C}_3H_5$ , C<sub>6</sub>H<sub>5</sub> $\dot{C}H_2$ , and C<sub>2</sub>H<sub>2</sub> are the key species. Cyclopentadienyl radical is mostly produced by H abstraction from cyclopentadiene, whereas indenyl is formed by H abstraction from indene, which by itself is the product of the C<sub>6</sub>H<sub>5</sub> $\dot{C}H_2$  + C<sub>2</sub>H<sub>2</sub> reaction. The 1-C<sub>4</sub>H<sub>8</sub> flame exhibits the highest concentrations of  $\dot{C}_3H_5$ , C<sub>6</sub>H<sub>5</sub> $\dot{C}H_2$ , and C<sub>2</sub>H<sub>2</sub> and, as a result, has the highest level of larger PAHs. The propene flame has a higher concentration of C<sub>2</sub>H<sub>2</sub> as compared to the 1-hexene flame because H-initiated decomposition produces ethylene, which in turn eventually dissociated to acetylene:



While the quantitative details of the kinetic mechanism developed by Wang et al. may need further quantitative improvements, this work nicely illuminated the indirect role of alkenes as suppliers of RSFR, which are the main precursors of monocyclic aromatics and PAH.

A similar main conclusion can be drawn from a series of works by Ruwe et al. who investigated the PAH growth depending on the fuel structure using various fuels from linear alkanes to methyl substituted alkenes. In 2016 [376], this group studied a premixed fuel-rich flame of 2-methyl-2-butene (2M2B) employing flame-sampling high-resolution molecular-beam mass spectrometry with single-photon ionization via synchrotron-generated vacuum-ultraviolet radiation (MP-PIMS). The advantage of this modern technique is that not only masses of various molecules and radicals can be identified but different isomers can be also distinguished. The experiments presented by Ruwe et al. allowed for the determination of isomer-resolved species mole fraction profiles as a function of height above the burner. The authors first looked at the initial fuel consumption pathways and concluded that they mainly proceed via H abstraction reactions mostly at one of the three allylic carbon atoms – there are totally nine allylic C-H bonds in 2M2B – and by H addition to the double-bond. According to the experimental data, the

fuel consumption pathways, which alternate C-H or C-C  $\beta$ -scissions with H abstractions on allylic carbons, eventually form the RSFR propargyl and *i*-C<sub>4</sub>H<sub>5</sub>. These radicals then contribute to the formation of benzene via the  $\dot{C}_3H_3 + \dot{C}_3H_3$  and *i*- $\dot{C}_4H_5 + C_2H_2$  reactions. There are two more RSFR that are formed at the fuel consumption stage due to the branched structure of 2M2B and the position of the double-bond,  $\dot{C}_4H_5-1$  ( $\dot{C}H_2-C\equiv C-CH_3$ ) and  $\dot{C}_5H_7-1$  ( $\dot{C}H_2-C(CH_3)=C=CH_2$ ). These species can be considered as methyl-substituted  $\dot{C}_3H_3$  and *i*- $\dot{C}_4H_5$  radicals and may therefore undergo analogous reactions forming directly methyl-substituted first aromatic rings, toluene and *o*-xylene:



The authors argue that these reactions forming toluene and *o*-xylene bypass the formation of benzene and support their argument by the unusually high ratio of the toluene-to-benzene concentrations observed experimentally. In addition to the (methyl-substituted) benzenes, Ruwe et al. also observed the formation of styrene via the *i*- $\dot{C}_4H_5 + C_4H_4$  reaction and naphthalene via recombination of two cyclopentadienyl radicals. Because of the specifics of the fuel consumption, i.e., the production of a large amount of RSFR in decomposition of 2M2B, the study revealed an intense formation of soot precursors and PAHs.

Ruwe et al. continued investigating the correlation between the initial fuel structure and the formation of soot precursors in 2018 [377], when they studied n-pentane, 1-pentene, and 2M2B flames using the same experimental technique. They found the formation of PAH increases in the row n-pentane – 1-pentene – 2M2B and explored the chemical reasons causing this differences, which appeared to originate from the fuel consumption patterns, i.e. from the pool of RSFR produced when different fuels decompose. Despite that different PAH formation trends were observed from the three different fuels, the authors concluded that PAH formation generally follows the same mechanism beginning from the decomposition of fuel molecules producing a variety of stable intermediate species including molecules and radicals, mostly RSFR. Although the decomposition mechanisms are generally similar and involve repetitive consecutive H abstraction and  $\beta$ -scission elementary steps, the fragmentation products vastly differ and are controlled by fuel-specific bond strengths, statistical probabilities, and resonance radical stabilization. Considering these differences, one can explain the difference in the formation tendency of typical growth species. While n-pentane as a typical n-alkane mostly decomposes to C<sub>2</sub>H<sub>4</sub>,  $\dot{H}$ , and  $\dot{C}H_3$  through a string of  $\beta$ -scissions following the initial H abstraction, decomposition pathways in the 1-pentene and 2M2B flames produce a large pool of C<sub>4</sub> and C<sub>5</sub> species, especially via the C<sub>4</sub>H<sub>6</sub> and C<sub>5</sub>H<sub>8</sub> dienes, which in turn are traced back to the allylic radicals – the predominant products of the initial fuel decomposition due to the fact that allylic C-H and C-C bonds are the weakest. The 1-pentene and 2M2B flames generate different main C<sub>5</sub> isomers, 1,3- and 1,4-pentadienes for 1-pentene vs. 2-methyl-1,3-butadiene and 3-methyl-1,2-butadiene for 2M2B. The latter flame produces significantly higher concentrations of C<sub>4</sub>H<sub>6</sub> and C<sub>5</sub>H<sub>8</sub> owing to the fuel RSFR that can accumulate in high concentrations and do not break to C<sub>2</sub> and C<sub>3</sub> species via C–C  $\beta$ -scission. The different molecular structures of these small intermediates influence the amount of species available for the aromatic growth and are responsible for the different PAH formation trends in the respective fuels. For 2M2B, toluene can form directly via the  $\dot{C}_4H_5 + \dot{C}_3H_3$  (R25) and  $\dot{C}_5H_7 + C_2H_2$  (R26) reactions discussed above, without passing through benzene. Alternatively, for the two linear fuels n-pentane and 1-pentene, toluene can form only via the addition of methyl and phenyl radicals, because the formation of

the required  $\dot{C}_4H_5$  and  $\dot{C}_5H_7$  radicals is not favored. As a result, the concentration of toluene is much higher in the 2M2B flame. Since toluene can significantly contribute to the formation of indene and naphthalene (in particular, via the reactions of its benzyl radical with  $\dot{C}_3H_3$  and  $C_2H_2$ , respectively), the 2M2B flame shows a higher tendency to form PAHs. The authors conclude that for alkenes, the chemistry of their allylic fuel radicals and their decomposition products strongly affects the initial formation reactions to the first aromatic ring and hence the PAH formation tendency.

In their latest paper, Ruwe et al. [378] improved existing kinetic models for the decomposition of various  $C_5$  fuels followed by the formation of PAHs and used the experimental isomer-specific MB-PIMS data from this group on the pentane, 1-pentene, and 2M2B flames to validate their numerical simulations. They began from the literature models by Wang et al. [379] (JetSurF version 2.0) and Healy et al. [380] developed for different fuels but including 1-pentene as an intermediate, and by Narayanaswamy et al. [381] related to the small PAH chemistry and containing the  $C_0$ - $C_4$  base mechanism [382]. Considering discrepancies between experiment and simulations, the authors developed a new  $C_5$  chemistry mechanism incorporating PAH formation pathways, with a special emphasis on the initial fuel consumption of 1-pentene providing RSFR and the formation of small aromatics involving these RSFR (the ITV mechanism). Overall, the simulations with the ITV mechanism satisfactorily described the peak experimental mole fractions and their profile shapes. The authors reaffirmed that the  $C_5$  chemistry plays an important role in the subsequent growth reactions. They highlighted, for instance, one critical reaction channel converting 1,3-pentadiene to the cyclopentadienyl radical:



for its great importance for the formation of the aromatics. The authors noted however that their new ITV model needs to be further improved for reaction pathways to large PAH molecules and in terms of pressure dependence of rate constants for most sensitive reactions, including, as mentioned by the authors,  $\dot{H}$  recombination with propargyl and  $\dot{H}$  additions to propyne or allene to propenyl isomers at various pressures, which are important for the formation of benzene.

While relatively small alkenes considered so far maintain a similar pattern of cracking to small species, typically to  $C_3$ - $C_5$  RSFR,  $C_2H_2$ , and  $\dot{C}H_3$ , followed by their reactions leading to the aromatic growth, a recent shock-tube and kinetic modeling work by Brezinsky's and Green's groups [118] on oxidation of decene isomers portrays a different picture. According to their results, decenes are predicted to decompose only to  $C_6$  and then cyclize and aromatize on their path to benzene. The observed yield of benzene was ranked in the following order: 5-decenes > cis-2-decene > 1-decene and the models developed in the paper employing the automatic reaction mechanism generator (RMG) were able to account for this ranking. For all considered decenes, benzene was shown to be mostly produced via the cyclization of a hex-2,5-dien-1-yl followed by loss of H atoms. In the reactions of 1-decene and 2-decene, hexadienyl radical originates from a 1,5-hexadiene and 1,4-hexadiene, respectively, but the former is expected to preferentially dissociate into two allyl radicals [318, 319], whereas the latter is more prone to H abstraction. This explains the larger production of benzene from 2-decene as compared to 1-decene. Additionally, for 2-decene, there is also an extra contribution from the pathway of heptadienyl cyclization, not available for 1-decene. For 5-decene, the hexadienyl radical formed by cracking 1,4-nonadiene molecule, which itself is produced through the  $\beta$ -scission of the dec-5-en-3-yl radical. Due to the symmetry of 5-decene, there are four H atoms which can be abstracted to form this decenyl radical, as compared to only two H atoms which can be abstracted to form the appropriate decenyl radicals from 1- and 2-decenes. The multiple H

abstraction sites and a small contribution from cyclization of the dec-5-en-1-yl giving cyclic C<sub>6</sub> and C<sub>5</sub> radicals explain the highest yield of benzene from 5-decene compared to the other decenes. The authors noted that their proposed mechanism for the formation of aromatics is not comprehensive but since a relatively small amount of benzene was formed they did not pursue further improvement of their model. Nevertheless, this study provides a peculiar example of the formation of an aromatic ring via cyclization of an allylic C<sub>6</sub> radical.

Even larger alkenes can contribute to the formation of PAH according Zhang et al. [383] who reported an experimental and modeling study on thermal tracking of n-dodecane at supercritical pressure. The authors identified three stage of cracking: at the first one, alkanes and alkenes were formed up to C<sub>8</sub>, at the second, alkanes and alkenes gave rise to monocyclic aromatics and cycloalkenes, and at the third stage designated as severe cracking PAH molecules were produced. Although the mechanism used by the authors was not detailed and included ‘overall’ rather than elementary reactions, this experiment combined with crude modeling provided yet another evidence that alkenes represent unavoidable intermediates on the path from saturated hydrocarbons to PAHs.

Summarizing the contribution of alkenes into the formation of benzene and larger PAH by the supply of RSFRs via their pyrolysis, one can conclude that alkenes represent a ready source of such radicals, especially of propargyl  $\dot{C}_3H_3$ , its methyl-substituted analogs  $\dot{C}_4H_5-1$  and  $\dot{C}_5H_7-1$ , allyl  $\dot{C}_3H_5$ , and cyclopentadienyl  $\dot{C}_5H_5$ , which then recombine with one another or with  $\dot{C}H_3$ , or react with acetylene to produce (substituted) aromatic rings. The contribution of a particular alkene is ultimately determined by the relative yield of RSFRs and C<sub>2</sub>H<sub>2</sub> produced in their decomposition and the rate of their formation under given combustion conditions. In this view, the position of the double bond in a linear and especially in a branched alkene is particularly important because it determines the number of the allylic C-C and C-H bonds, which are the weakest bonds in alkenes and hence can be cleaved more easily and faster than any other bonds during the pyrolysis. As compared to alkenes, the decomposition of alkanes does not form RSFRs directly. The main pyrolysis products of n-alkanes typically include ethylene C<sub>2</sub>H<sub>4</sub> and  $\dot{C}H_3$  [384, 385] and the former eventually dissociates to acetylene. However, acetylene needs a RSFR counterpart to form the first aromatic ring. The yield of higher alkenes like C<sub>3</sub>H<sub>6</sub>, 1-C<sub>4</sub>H<sub>8</sub>, etc., which are the RSFR precursors, is usually lower than that of C<sub>2</sub>H<sub>4</sub>. Thus, the pathway from alkanes to benzene and PAH formation involves an extra step as compared to alkenes: alkanes → alkenes/C<sub>2</sub>H<sub>2</sub>/ $\dot{C}H_3$  → RSFRs/C<sub>2</sub>H<sub>2</sub>/ $\dot{C}H_3$  → aromatic rings, making the formation of PAHs from alkane fuels slower (and less competitive with oxidation) than from alkene fuels.

## 4.2 Direct involvement of alkenes in PAH growth reactions

Next, we consider observed and proposed PAH growth mechanisms where alkenes play a direct role, immediately participating in the elementary reactions. In a series of works, Wornat and co-workers considered reaction pathways of PAH growth in the supercritical pyrolysis of large hydrocarbons, such as n-decane and 1-octene with various dopants, which facilitated the growth reactions. For instance, they added 1- and 2-methylnaphthalene in pyrolysis of n-decane and observed PAH products using high-pressure liquid chromatography with ultraviolet–visible absorbance and mass-spectrometric detection [386]. The experiment was performed in a flow reactor at supercritical 570° C and 94.6 atm for 133 s – the conditions of incipient solids formation, with a small amount of the dopants. The authors observed a large variety of PAHs from C<sub>12</sub> to C<sub>28</sub>, both purely benzenoid and containing five-member rings, and analyzed the

enhancement of the peaks for individual species when either 1- or 2-methylnaphthalene were added in separate experiments. They deduced a peculiar mechanism of the PAH growth in their system based upon this analysis. The process begins with facile formation of benzylic naphthylmethyl radicals and moves forward by additions of alkene molecules. Due to the position of its methyl group, the growth starting from 2-methylnaphthyl via additions of  $C_2H_4$  or  $C_3H_6$  virtually terminates with the formation of three-ring PAHs, particularly benzoidenes (from  $C_2H_4$ ), anthracene and the very stable phenanthrene (from  $C_3H_6$ ) (Figure 56 (a)). Alternatively, 1-methylnaphthalene has its methyl group of the zigzag edge, adjacent to a valley carbon of the naphthalene core and hence, the reaction of ethylene (or other 1-alkene) with 1-naphthylmethyl forms the relatively unstable three-ring PAH phenalene, which readily loses an H atom from the  $CH_2$  group and gives rise to phenalenyl radical (Figure 56 (b)). Consequently, reactions of arylmethyl, phenalenyl, and higher-ring number phenalenyl-type radicals with the  $C_2$ – $C_4$  1-alkenes, together with phenalenyl/arylmethyl recombinations can explain the formation of the most abundant observed four- to eight-ring benzenoid PAHs. Recombination reactions of different arylmethyl radicals and reactions of arylmethyl radicals with methylaromatic molecules account for most of the remaining minor four- to seven-ring benzenoids. The authors concluded that the typical arylmethyl/alkene/phenalenyl reaction mechanism displayed in Figure 56 should be common for alkane and alkane-rich fuels under the conditions of the supercritical pyrolysis because the main reactants, 1-alkenes and methylated aromatics, should be abundant. Later [387], similar reactions of resonantly-stabilized arylmethyl (benzylic) and phenalenyl-type radicals with  $C_2$ – $C_4$  1-alkenes were also found to be important for the sequential PAH growth up to nine rings in the supercritical pyrolysis of 1-octene. The authors inferred that all necessary conditions for these reactions to occur, such as high pressure, fuel molecules containing a weak allylic C–C bond,  $C_2$ – $C_4$  1-alkenes originating from higher-temperature decomposition of larger *n*-alkanes and 1-alkenes, and methylated PAHs that readily give rise to resonance-stabilized arylmethyl and phenalenyl-type radicals via unimolecular decomposition or direct H abstraction. The reaction mechanisms of the aromatic RSFR with 1-alkenes allowed Wornat et al. to account for the large variety of PAHs experimentally observed in 1-octene pyrolysis.

Wornat et al. further reinforced the role of the reactions of alkenes with highly resonantly stabilized aromatic radicals in the PAH growth in the supercritical pyrolysis by studying *n*-decane with two other dopants, fluorene and 1-methylphenanthrene [388]. These molecules were chosen for two reasons, first, they represent two major three-ring products of *n*-decane pyrolysis and second, they directly dissociate to two aromatic RSFR, 9-fluorenyl and 1-phenanthrylmethyl and eventually give rise to two other radicals, 9-phenanthrylmethyl and fulvalenyl-like benz[*de*]anthracenyl. The former stems from the fluorene dopant's production of 9-methylphenanthrene and 9-ethylphenanthrene (Figure 57 (a)). The pathway to benz[*de*]anthracenyl is more complex and involves the formation of four- to six-ring cata-condensed benzenoid PAH in the reactions with 1- and 9-phenanthrylmethyl radicals followed by their reaction with ethylene. The four important RSFR can react with  $CH_3$ , principal alkenes ( $C_2H_4$ ,  $C_3H_6$ , and 1- $C_4H_8$ ) and aromatic radicals to carry the PAH growth forward. While the reactions of the benzylic and fulvalenyl-like radicals followed the patterns described in the previous work of this group (Figure 56), Wornat et al. additionally proposed reaction mechanisms for fluorenyl-like radicals. For instance, the reactions of 9-fluorenyl radical can either preserve the five-member ring and form substituted fluorenes – fluoranthene, 3-methylfluoranthene (Figure 57 (b)), and several fluoranthene benzologues, or incorporate a reactant's C atom to expand the five-member ring of 9-fluorenyl to a six-member ring producing

phenanthrene, 9-methylphenanthrene, 9-ethylphenanthrene (Figure 57 (a)), and fluoranthene benzologues. Overall, the reactions of the four RSFR were hypothesized to be responsible for the formation of numerous three- to seven-ring PAHs in the supercritical pyrolysis of n-decane, especially the fluoranthene benzologues. The authors concluded that the PAH-growth pathways deduced in their work have widespread applicability to larger PAH.

While the mechanisms proposed by Wornat et al. may be plausible, they still require verification through either direct experimental studies of the proposed elementary reactions or via theoretical calculations of the potential energy surfaces combined with computation of reaction rate constants and product branching ratios under the conditions of the supercritical pyrolysis. The calculations would also allow one to delineate the conditions, such as temperature and pressure, under which the proposed mechanisms may be operational. The idea that sequential additions of alkenes to aryl radicals (or additions of alkenyl radicals to the aromatics) lead to PAH growth can be found in the literature. For example, van Spreybroeck et al. reported a DFT modeling of the mechanism of naphthalene formation from benzene via H abstraction followed by addition of two C<sub>2</sub>H<sub>4</sub> molecules [389]. According to their proposed mechanism, ethylene adds to phenyl producing a C<sub>6</sub>H<sub>5</sub>Ċ<sub>2</sub>H<sub>4</sub> radical, which in turn adds one more C<sub>2</sub>H<sub>4</sub> unit to the side chain, then undergoes a ring closure and an H atom loss forming benzocyclohexene C<sub>10</sub>H<sub>12</sub>. The formation of naphthalene is then completed by sequential abstraction of four extra H atoms in benzocyclohexene by ca. ĊH<sub>3</sub> radicals. However, this mechanism does not seem plausible for a number of reasons. First, there is a strong competition between collisional stabilization of the initial C<sub>6</sub>H<sub>5</sub>Ċ<sub>2</sub>H<sub>4</sub> complex and its decomposition to styrene + Ĥ depending on temperature and pressure. According to earlier kinetic calculations by Tokmakov and Lin [390] and recent by our group [391], the complex stabilization prevails over the formation of styrene + Ĥ only at relatively low temperatures and high pressures, below 1250, 1500, and ~2000 K at 1, 10, and 100 atm, respectively, based on our results. Thus, unless the pressure is very high, the stabilization of C<sub>6</sub>H<sub>5</sub>Ċ<sub>2</sub>H<sub>4</sub> and hence, addition of a second ethylene molecule, is possible only at low combustion temperatures. Second, a removal of four H atoms is required from benzocyclohexene. While H abstraction reactions by other radicals abundant in flames, e.g. Ĥ, ĊH<sub>3</sub>, and ĖH, and H losses from the radical intermediates benzocyclohexyl Ċ<sub>10</sub>H<sub>11</sub> and benzocyclohexadienyl Ċ<sub>10</sub>H<sub>9</sub> are plausible under combustion temperatures [392, 393], this requirement makes the ethylene addition mechanism clearly inferior as compared to HACA where only one initial H abstraction from benzene (Bittner-Howard route) or only one more intermediate one from phenylacetylene (Frenklach route) are needed [394]. The potential barriers for ethylene and acetylene addition to phenyl radical are within 1.3 kcal/mol from one another and consequently, the total rate constants for these reactions at combustion temperatures are relatively close, with the Ċ<sub>6</sub>H<sub>5</sub> + C<sub>2</sub>H<sub>2</sub> reaction being somewhat faster [390, 391, 394-398].

Shukla and Koshi [399] proposed a mechanism they called HAVA (Hydrogen-Abstraction-Vinyl-Addition) as an alternative to HACA where the vinyl radical serves as the main addition reagent to benzene or larger PAHs. This hypothesis was put forward based on their study of gas-phase products of the pyrolysis of acetylene and ethylene using VUV single photon ionization time-of-flight mass spectrometry. According to their mechanism, Ċ<sub>2</sub>H<sub>3</sub> adds to benzene and then the reaction proceeds to styrene by the H loss. Next, H<sub>2</sub> elimination from styrene produces phenylacetylene and the reaction sequence continues by addition of another Ċ<sub>2</sub>H<sub>3</sub> unit to the *ortho* C atom in phenylacetylene, ring closure, and H atom elimination producing naphthalene. A similar reaction sequence was proposed starting from naphthalene to form acenaphthalene after first vinyl radical addition and H and H<sub>2</sub> losses and then to eventually produce fluoranthene

when two more  $\dot{\text{C}}_2\text{H}_3$  radicals are added and two H atoms and one  $\text{H}_2$  molecule are eliminated. However, there are several issues with the plausibility of this mechanism. First, the  $\text{C}_6\text{H}_6 + \dot{\text{C}}_2\text{H}_3$  reaction is significantly slower than  $\dot{\text{C}}_6\text{H}_5 + \text{C}_2\text{H}_4$ , with the rate constant for the former being approximately by a factor of 3.5 lower than that for the latter at combustion temperatures [365, 372, 373]. Second, molecular hydrogen elimination from alkenes (like styrene) usually requires a very high barrier. For example, barriers for  $\text{H}_2$  loss from the simplest alkene,  $\text{C}_2\text{H}_4$ , range from 94 to 107 kcal/mol [400] making this reaction slow even at combustion temperatures. More likely, under flame conditions where the radicals like  $\dot{\text{H}}$ ,  $\dot{\text{C}}\text{H}_3$ , and  $\dot{\text{O}}\text{H}$  are plentiful, at least the first extra H atom from styrene can be removed via a bimolecular H abstraction reaction. We anticipate that the requirement of two additional H atoms to be eliminated in Shukla and Koshi's HAVA as well as in the ethylene addition mechanism discussed above makes these mechanisms less important than HACA. Shukla and Koshi argued their case for HAVA based on the observation of more aromatic species including PAHs, with higher concentrations in the ethylene pyrolysis as compared to the acetylene pyrolysis. However, this argument does not take into account the fact that pyrolysis of alkenes produces RSFR, which greatly contribute to the PAH growth as shown by Wang et al. [361] and Ruwe et al. [376-378] and discussed above. For example, for ethylene, Shukla and Koshi themselves noted the importance of the  $\dot{\text{C}}_2\text{H}_3 + \dot{\text{C}}_2\text{H}_3 \rightarrow \dot{\text{C}}\text{H}_3 + \dot{\text{C}}_3\text{H}_3$  reaction producing the propargyl radical – a precursor of benzene and phenyl radical. Although further kinetic modeling taking into account the vinyl radical addition pathways may be needed, it is unlikely that the mechanism proposed by Shukla and Koshi would be competitive with HACA.

Theoretical calculations by Mebel's group together with experimental studies of the elementary reaction mechanisms in crossed molecular beams and in high temperature chemical reactors provided evidence that alkenes and dienes may indeed directly participate in the PAH growth reactions. Two experimental groups explored the reaction of the phenyl radical with propene in crossed beams. Kaiser and co-workers conducted their experiment [401] at collision energies of  $\sim 45 \text{ kJ mol}^{-1}$  and identified the formation of styrene via methyl loss from  $\dot{\text{C}}_9\text{H}_{11}$  intermediates and of 3-phenylpropene ( $\text{C}_6\text{H}_5\text{CH}_2\text{C}_2\text{H}_3$ ) and 1-phenylpropene ( $\text{CH}_3\text{CHCHC}_6\text{H}_5$ ) via H loss channels (Figure 58). Fractions of the methyl vs. hydrogen loss channels of  $68 \pm 16\%$  :  $32 \pm 10\%$  derived experimentally were corroborated by theoretical calculations using energy-dependent RRKM theory, which clearly demonstrated that 3-phenylpropene is the predominant H loss product. According to the RRKM results, an increase of collision energy to  $200 \text{ kJ mol}^{-1}$  results in a sharp decrease of the contribution of the methyl loss channel to  $\sim 25\%$ ; the decreased importance of the methyl group loss channel was also demonstrated experimentally at elevated collision energies of  $130\text{--}193 \text{ kJ mol}^{-1}$  [402]. Davis and co-workers found a similar trend of a decrease of the methyl loss branching ratio with collision energy, but their experiments gave a higher yield of styrene +  $\dot{\text{C}}\text{H}_3$  [403]. Kislov et al. [404] reported RRKM/ME calculations of the reaction rate constants and product branching ratios at different temperatures and pressures and showed that under combustion conditions the  $\dot{\text{C}}_6\text{H}_5 + \text{C}_3\text{H}_6$  reaction mostly forms benzene + allyl radical via the H abstraction channel followed by styrene plus methyl and 3-phenylpropene +  $\dot{\text{H}}$ . Experiments in a high-temperature chemical microreactor by Zhang et al. at  $1200\text{--}1500 \text{ K}$  confirmed the formation of styrene +  $\dot{\text{C}}\text{H}_3$  as well as 3-phenylpropene as the dominant H loss product [405]. A recent flow-reactor study by Green's group [406] employing flash photolysis combined with time-resolved molecular beam mass spectrometry (MBMS) and visible laser absorbance detected five major product channels of  $\dot{\text{C}}_6\text{H}_5 + \text{C}_3\text{H}_6$  at 600 and 700 K, H abstraction producing benzene,  $\text{CH}_3$  loss forming styrene, H-loss giving phenylpropene isomers

(although those were not distinguished), radical adduct stabilization, and a new unexpected channel forming benzyl radical + C<sub>2</sub>H<sub>4</sub>. While the formation of RSFR like allyl and benzyl as well as styrene, which may form styrenyl and *ortho*-vinylphenyl radicals by H abstraction, can contribute to the PAH growth via various mechanisms, the formation of 3-phenylpropene is of special significance. The calculations by Kislov et al. [404] showed that an H atom from the side-chain CH<sub>2</sub> group (Figure 58) can be preferably and easily abstracted forming a resonantly stabilized 1-phenylallyl radical; the computed barrier for the H abstraction by an  $\dot{\text{H}}$  atom is only ~5 kcal/mol. Next, 1-phenylallyl undergoes a facile ring closure and eliminates an H atom producing indene. RRKM/ME calculations of the rate constant for the 1-phenylallyl  $\rightarrow$  indene +  $\dot{\text{H}}$  reaction gave values from  $6 \times 10^3$  to  $2 \times 10^7$  s<sup>-1</sup> in the 1000-2250 K temperature range at 1 atm [407]. Thus, the addition of propene to phenyl can lead to indene in the series of three consecutive reactions. Similarly, one can expect that the addition of propene to an aryl radical can lead to a growth of PAH by an extra five-member ring.

The simplest diene – 1,3-butadiene C<sub>4</sub>H<sub>6</sub>, has been shown to directly partake in the PAH growth in combined experimental and theoretical studies addressing the reaction mechanism of 1,3-butadiene addition to phenyl and 1-naphthyl radicals. For instance, the crossed beam reaction of the phenyl radical with 1,3-butadiene was carried out under single collision conditions at collision energies of about 55 kJ mol<sup>-1</sup> and the bicyclic 1,4-dihydronaphthalene molecule was experimentally identified as a major reaction product (58±15%) with the 1-phenyl-1,3-butadiene contributing 34±10% [408]. Ab initio calculations of the potential energy surface showed the reaction to be initiated by a barrierless addition of the phenyl radical to the terminal carbon atom of the 1,3-butadiene to form a bound  $\dot{\text{C}}_{10}\text{H}_{11}$  intermediate; the latter undergoes an H atom elimination from the terminal CH<sub>2</sub> group of 1,3-butadiene leading to 1-phenyl-trans-1,3-butadiene. Alternatively, the dominant product, 1,4-dihydronaphthalene, is formed via an isomerization of the adduct by ring closure and elimination of the hydrogen atom from the phenyl moiety at the bridging carbon atom (Figure 58 (b)). Interestingly, the de facto barrierless formation of the 1,4-dihydronaphthalene molecule involving a single collision between  $\dot{\text{C}}_6\text{H}_5$  and 1,3-C<sub>4</sub>H<sub>6</sub> can represent an important step in the PAH growth not only at high temperatures in combustion but also at low or very low temperatures characteristic for interstellar chemistry. The same reaction was also explored in a high temperature chemical reactor under combustion-like conditions at 873 K, where the reaction products were probed utilizing MB-PIMS with VUV radiation from the Advanced Light Source [409]. The authors detected C<sub>10</sub>H<sub>10</sub>, C<sub>9</sub>H<sub>8</sub>, and C<sub>8</sub>H<sub>8</sub> molecular products and assigned C<sub>10</sub>H<sub>10</sub> isomers as 1-phenyl-1,3-butadiene, 1,4-dihydronaphthalene, 1-methylindene, C<sub>9</sub>H<sub>8</sub> isomers as indene, phenylallene, 1-phenyl-1-methylacetylene, and a C<sub>8</sub>H<sub>8</sub> isomer as styrene. By comparing these observations with the crossed molecular beam study and with the computed potential energy surface they identified 1-phenyl-1,3-butadiene, 1,4-dihydronaphthalene, and styrene as the primary reaction products between the phenyl radical and 1,3-butadiene. The other molecules observed in this experiment were assigned as products of secondary reactions. The generality of the butadiene addition mechanism was reinforced by another crossed beams study of the reaction of 1-naphthyl radical with 1,3-butadiene [410]. This experiment showed prevailing formation of 1,4-dihydrophenanthrene and the calculated potential energy surface revealed a similar mechanism in which 1,3-C<sub>4</sub>H<sub>6</sub> adds to the 1-naphthyl radical via a submerged barrier following the formation of a van der Waals complex and then ring closure occurs producing the third six-member ring and an H loss completes the reaction. Thus, the addition of 1,3-butadiene to an aryl

radical was concluded to be a facile pathway to the formation of a dihydrogenated PAH with an extra six-member ring, which can be aromatized by removal of two extra hydrogen atoms.

In summary, alkenes can directly contribute to the PAH growth through reactions of aryl radicals with propene  $C_3H_6$  and 1,3-butadiene  $C_4H_6$  forming an extra five- and six-membered ring, respectively, as directly confirmed experimentally and by theoretical calculations. Also, reactions of highly resonantly stabilized aromatic radicals, such as arylmethyl, phenalenyl, fluorenyl and their higher-ring number analogs with the  $C_2$ – $C_4$  1-alkenes, were deduced (from experimental observations) to play a significant role in the PAH growth. However, further theoretical calculations of the reaction rate constants and kinetic modeling are required to evaluate the particular contributions of these mechanisms depending on the fuel type and combustion conditions.

### 4.3 Alkenes and flame sooting tendencies

In their work, Wang et al. [361] compared PAH and soot formation in different pure alkene flames from propene to 1-octene and, surprisingly, found that the trend in soot formation,  $1-C_4H_8 > C_3H_6 > 1-C_5H_{10} > 1-C_6H_{12} > 1-C_8H_{16} > C_2H_4$ , did not exactly reproduce that for PAH,  $1-C_4H_8 > 1-C_5H_{10} \sim 1-C_6H_{12} > C_3H_6 > 1-C_8H_{16} > C_2H_4$ . A peculiar result is that while the  $1-C_6H_{12}$  flame showed a higher tendency to form PAHs, it produced less soot than the  $C_3H_6$  flame. Wang et al. attributed this observation to the role of acetylene in the soot growth via the HACA mechanism after the nucleation of incipient particle from PAHs [368, 369]. However, overall the study has shown that it is not valid to evaluate sooting tendency only based upon  $C_2H_2$  concentration, as was done in earlier soot models that treated  $C_2H_2$  as one and only soot precursor [411]. The  $C_2H_4$  flame has the highest  $C_2H_2$  concentration among all the considered 1-alkene flames but produced the soot volume fraction of at least an order of magnitude lower compared to the other fuels. The main conclusion of the work is that PAH and sooting tendencies are mostly determined by the levels of RSFR, especially, propargyl, allyl, cyclopentadienyl, benzyl, and indenyl, as well as of methyl and acetylene formed via fuel decomposition reactions. The differences in the concentrations of RSFR, which are determined by the decomposition pattern of the parent fuel molecules, in particular alkenes, appears to be responsible for the differences in soot and PAH formation tendencies.

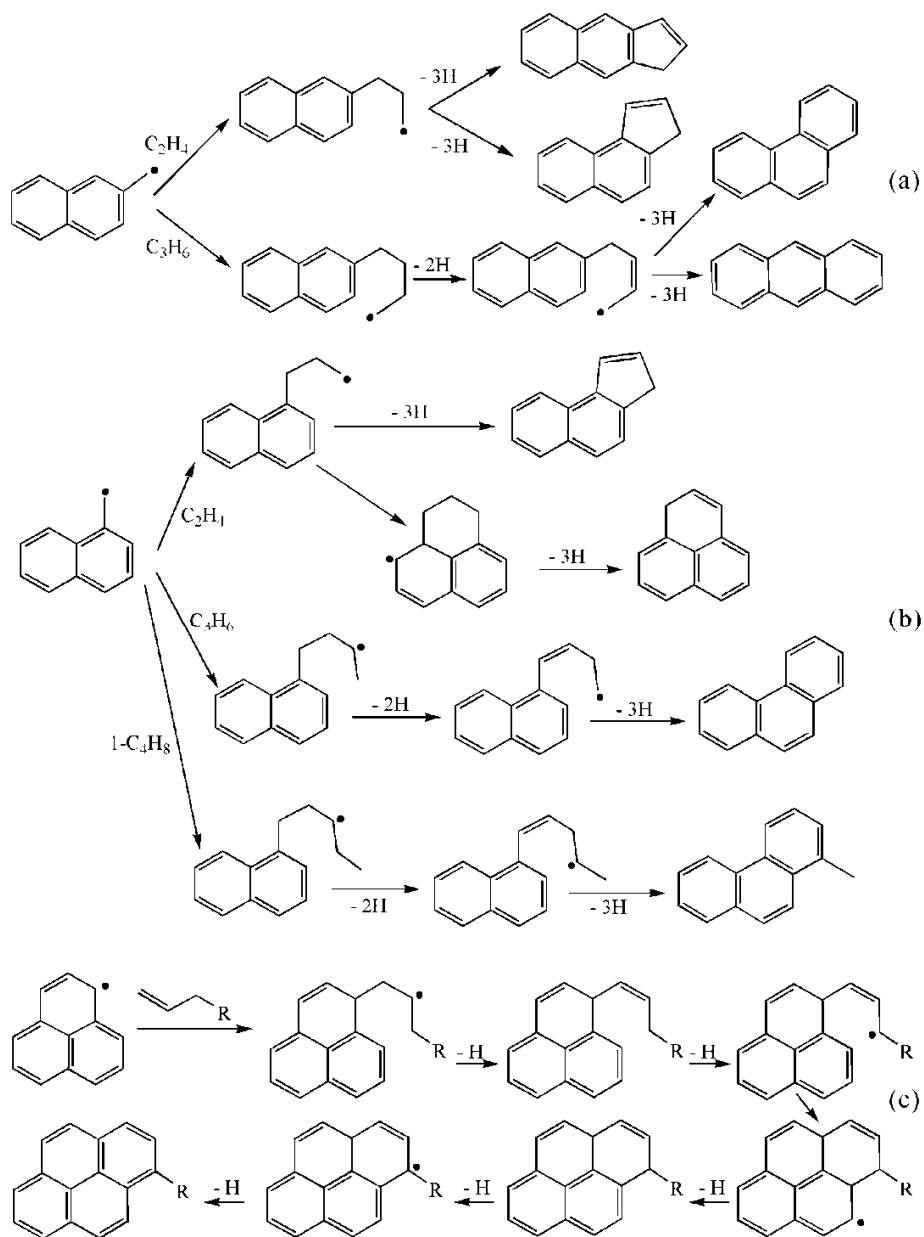


Figure 56. Reaction mechanisms proposed by Wornat and co-workers (Ref. [386]): (a) 2-methylnaphthyl +  $C_2H_4/C_3H_6$ ; (b) 1-methylnaphthyl +  $C_2H_4/C_3H_6/1-C_4H_8$ ; (c) phenalenyl + 1-alkene.

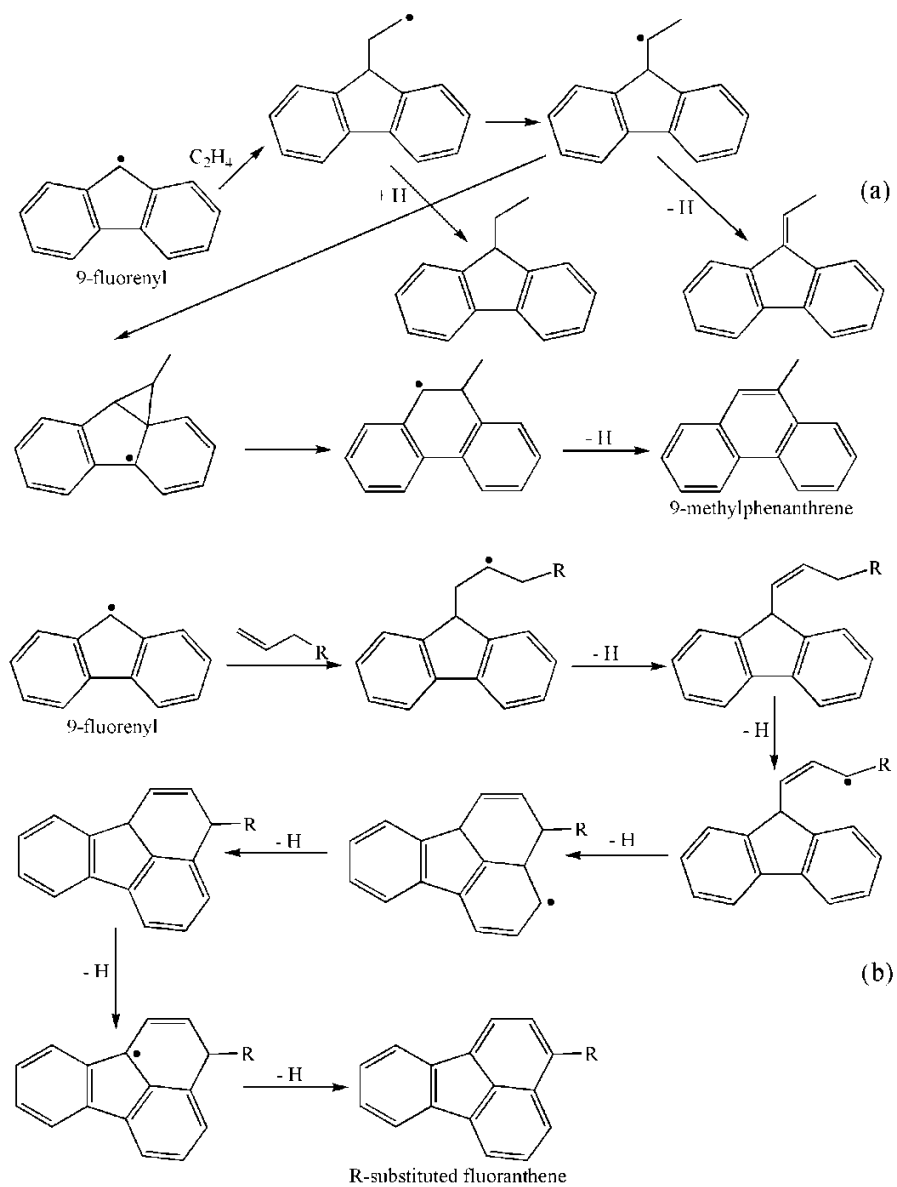


Figure 57. Reaction mechanisms proposed by Wornat and co-workers (Ref. [388]): (a) 9-fluorenyl +  $C_2H_4$ ; (b) 9-fluorenyl + 1-alkene.

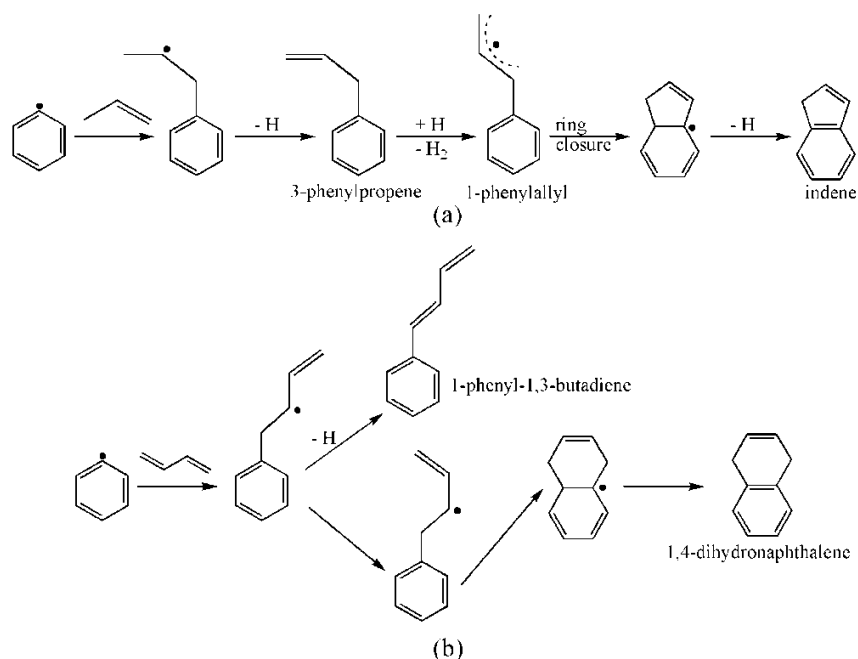


Figure 58. Reaction mechanism of phenyl radical  $\dot{\text{C}}_6\text{H}_5$  with propene  $\text{C}_3\text{H}_6$  (a) and 1,3-butadiene  $\text{C}_4\text{H}_6$  (b). Only PAH growth channels forming indene and 1,4-dihydronaphthalene are shown.

## 5. Conclusions and research outlook

This review has assessed the recent progress in gas-phase detailed kinetic model development for species with  $\text{C}=\text{C}$  double bond. This compiled knowledge of alkene combustion chemistry would be highly useful for a better understanding of the number and the position of the  $\text{C}=\text{C}$  double bond on the oxidation and pyrolysis characteristics of olefinic species. Engine-relevant combustion features were analyzed by the fundamental combustion experiments carried out in different facilities, including STs and RCMs to measuring IDTs, flame burners to measuring laminar flame speeds, and JSRs and FRs to measure the speciation data.

This manuscript highlighted the progress made toward understanding detailed chemistry for the low-, intermediate- and high-temperature alkene oxidation. With the availability of new experimental data and new theoretical insights, it is now possible to develop and assess semi-predictive models for alkene fuels. In addition, the detailed understanding of alkene combustion chemistry presented in this article provides a fundamental explanation of the reactivity of fuels when  $\text{C}=\text{C}$  double bond is present within the molecule. In summary, the presence of the  $\text{C}=\text{C}$  will react with important radicals like  $\dot{\text{O}}\text{H}$ ,  $\text{H}\dot{\text{O}}_2$ ,  $\dot{\text{H}}$ ,  $\dot{\text{O}}$  etc., through different temperature ranges. Moreover, the easily formed unreactive resonance stabilized allylic radical also inhibits the reactivity of unsaturated hydrocarbon. Hence, the more allylic hydrogen atoms in the molecule, the less reactive the fuel is. This is also the main reason of the difference of reactivity between alkenes and alkanes.

Key points and features of the combustion chemistry of alkenes that derived from careful analyses of a number of current state-of-the-art detailed kinetic mechanisms, as well as prospects for future experimental or theoretical studies are summarized as follows:

- (1) At low temperatures (600–850 K), the reactivity of different type of fuels is determined by the formation of KHP. Two types of KHP, including hydroxyketohydroperoxides and alkenylketohydroperoxides, can be formed in the oxidation of unsaturated hydrocarbons. The formation of hydroxyketohydroperoxides initially starts from the molecular oxygen addition to the hydroxylalkyl radical, and competes with the chain propagation reaction through Waddington mechanism. When the chain carbon number of the molecule is larger than three, the formation of hydroxyketohydroperoxides could be competitive. The formation of alkenylketohydroperoxides initially starts from the molecular oxygen addition to alkenyl radicals followed by isomerization and second molecular oxygen addition. When the number of the chain carbon atoms in the molecule is larger than five, the formation of alkenylketohydroperoxides can be competitive. Further refinements of the rate constants for important low-temperature reaction classes, especially  $\dot{\text{O}}\text{H}$  adding to and abstracting H-atom from alkenes, and first and second  $\text{O}_2$  addition reactions to hydroxyalkyl ( $\dot{\text{R}}\text{OH}$ ) or alkenyl ( $\dot{\text{R}}_{\text{AEN}}$ ) radicals, are recommended. Since the available rate constants for butene and higher species for these reaction classes are scarce, either calculated or measured kinetics data would be valuable and is expected to improve model predictions at low temperature regimes.
- (2) At intermediate temperatures (850–1200 K), resonance stabilized allylic radical chemistry is important in determining the reactivity of the unsaturated hydrocarbons. The radical-radical recombination and the subsequent decomposition reaction classes should be taken into consideration when developing the kinetic models for these molecules. Specifically, the recombination between allylic radicals themselves and their recombination with important radicals such as  $\text{H}\dot{\text{O}}_2$ ,  $\dot{\text{C}}\text{H}_3$ , and the subsequent reactions need to be paid special attention to. When the carbon number of the olefin is larger, alkenyl radical chemistry is also important; for example, its reaction with molecular oxygen to form diene and  $\text{H}\dot{\text{O}}_2$  radical is important in promoting the reactivity at intermediate temperatures. Apart from that,  $\text{H}\dot{\text{O}}_2$  radical addition to the double bond in alkenes is also important in fuel consumption with favored formation of a cyclic ether and  $\dot{\text{O}}\text{H}$  radical. We recommend further investigations to be conducted on the kinetics of the aforementioned important intermediate-temperature reaction classes, namely,  $\text{H}\dot{\text{O}}_2$  addition reactions to allylic radicals ( $\dot{\text{R}}_{\text{A}}$ ),  $\dot{\text{R}}_{\text{A}}$  recombination reactions and  $\text{H}\dot{\text{O}}_2$  addition reactions to alkenes. Special emphasis is placed on C4 and higher species, for which available rate constants are quite limited.
- (3) At high temperatures (>1200 K), additions of  $\dot{\text{H}}$  and  $\ddot{\text{O}}$  atom to the double bond are important reaction classes to open the double bond. Apart from the addition reactions, pyrolysis of fuel molecules becomes important when temperature increases. The formation of vinylic radicals through H-atom abstraction by important radicals such as  $\dot{\text{O}}\text{H}$ ,  $\ddot{\text{O}}$ ,  $\dot{\text{H}}$ , and  $\dot{\text{C}}\text{H}_3$  is competitive when temperature increases. Vinylic radicals can further react with molecular oxygen to form oxygenated radicals and  $\ddot{\text{O}}$  atom, which is a very important chain branching reaction pathway to promote the reactivity of unsaturated hydrocarbons at high temperatures. Given that few kinetics data for the important high-temperature reaction classes highlighted here, viz.  $\dot{\text{H}}$  addition reactions to alkenes,  $\ddot{\text{O}}$  addition reactions to alkenes

and O<sub>2</sub> addition reactions to vinylic radicals ( $\dot{R}_{VT}/\dot{R}_{VS}$ ), is available for butene or larger alkenes, further theoretical or experimental investigations on the rate constants of these reactions will be helpful in improving the accuracy of the kinetic models.

- (4) Undoubtedly, there is a large demand for the elementary kinetic investigations on key reactions involved in alkene chemistry from low to high temperatures, both theoretically and experimentally. Experimental rate coefficient measurements at combustion relevant temperatures (600 – 2000 K) are needed to ensure the accuracy of the reaction kinetics data used in chemical kinetic models. As discussed in this paper, theoretical estimates/analogy of some reaction rate constants can be adopted to develop chemical kinetic models, but theoretical calculations for these reactions are needed to provide improved model predictions. Theoretical studies exploring reaction pathways and generating reliable potential energy surfaces is a very valuable tool to identify the importance of the reaction classes over different temperature ranges. Moreover, based on the PES, we may solve RRKM/ME to obtain accurate temperature- and pressure-dependent rate constants which can be used in chemical kinetic model development. As implied in Sections 2 and 3, comprehensive kinetic modeling studies of the oxidation of C5 and higher alkenes are scarce, due in part to the lack of available accurate rate constants for C4 and higher species. In addition, extensive experiments on the global combustion properties as well as the speciation of C5 and higher alkenes will be valuable in aiding the development and validation of the comprehensive chemical kinetic models.

## 6. Acknowledgements

Chong-Wen Zhou gratefully acknowledges Philippe Dagaut (CNRS, France), Henry Curran (NUI Galway, Ireland) and Stephen Klippenstein (Argonne National Laboratory, USA) for their valuable and helpful comments to improve this work. She also acknowledges the funding support from National Science and Technology Major Project (2017-III0004-0028). Aamir Farooq acknowledges the support from the Office of Sponsored Research at King Abdullah University of Science and Technology (KAUST). Alexander M. Mebel acknowledges support from the US Department of Energy, Basic Energy Sciences via the grant DE-FG02-04ER15570.

## 7. References

- [1] Energy and climate change. World energy outlook special report, <https://www.iea.org/publications/freepublications/publication/WEO2015SpecialReportonEnergyandClimateChange.pdf>; 2015 [accessed 18.09.23].
- [2] Façanha C, Blumberg K, Miller J. Global Transportation Energy and Climate Roadmap, <https://www.theicct.org/sites/default/files/publications/ICCT%20Roadmap%20Energy%20Report.pdf>; 2012 [accessed 18.09.23].
- [3] Clais P, Canadell P, Le Quere C, Peylin P, Andres R, Peters G, et al. Global carbon atlas, <http://www.globalcarbonatlas.org/en/CO2-emissions>; 2016 [accessed 18.09.23].
- [4] Blunden J, Arndt D. State of the Climate in 2019. *Bull Am Meteorol Soc.* 2020;101:S1-S429.
- [5] Friedlingstein P, Jones MW, O'sullivan M, Andrew RM, Hauck J, Peters GP, et al. Global carbon budget 2019. *Earth Syst Sci Data.* 2019;11:1783-838.
- [6] Bond TC, Doherty SJ, Fahey DW, Forster PM, Berntsen T, DeAngelo BJ, et al. Bounding the role of black carbon in the climate system: A scientific assessment. *J Geophys Res-Atmos.* 2013;118:5380-552.
- [7] Lim SS, Vos T, Flaxman AD, Danaei G, Shibuya K, Adair-Rohani H, et al. A comparative risk assessment of burden of disease and injury attributable to 67 risk factors and risk factor clusters in 21 regions, 1990-2010: a systematic analysis for the Global Burden of Disease Study 2010. *Lancet.* 2012;380:2224-60.
- [8] Anenberg SC, Schwartz J, Shindell D, Amann M, Faluvegi G, Klimont Z, et al. Global Air Quality and Health Co-benefits of Mitigating Near-Term Climate Change through Methane and Black Carbon Emission Controls. *Environ Health Perspect.* 2012;120:831-9.
- [9] Silva RA, West JJ, Zhang Y, Anenberg SC, Lamarque J-F, Shindell DT, et al. Global premature mortality due to anthropogenic outdoor air pollution and the contribution of past climate change. *Environ Res Lett.* 2013;8.
- [10] Mehl M, Pitz WJ, Westbrook CK, Yasunaga K, Conroy C, Curran HJ. Autoignition behavior of unsaturated hydrocarbons in the low and high temperature regions. *Proc Combust Inst.* 2011;33:201-8.
- [11] Pitz WJ, Cernansky NP, Dryer FL, Egolfopoulos F, Farrell J, Friend DG, et al. Development of an experimental database and chemical kinetic models for surrogate gasoline fuels. *SAE Trans.* 2007:195-216.
- [12] Sarathy SM, Farooq A, Kalghatgi GT. Recent progress in gasoline surrogate fuels. *Prog Energy Combust Sci.* 2018;65:67-108.
- [13] Mehl M, Faravelli T, Giavazzi F, Ranzi E, Scorletti P, Tardani A, et al. Detailed chemistry promotes understanding of octane numbers and gasoline sensitivity. *Energy Fuels.* 2006;20:2391-8.
- [14] Pio G, Ricca A, Palma V, Salzano E. Low temperature combustion of methane/alkenes mixtures. *Fuel.* 2019;254:115567.
- [15] Razus D, Mitu M, Giurcan V, Movileanu C, Oancea D. Additive influence on maximum experimental safe gap of ethylene-air mixtures. *Fuel.* 2019;237:888-94.
- [16] Colket MB, Spadaccini LJ. Scramjet fuels autoignition study. *J Propul Power.* 2001;17:315-23.
- [17] Liu Q, Passaro A, Baccarella D, Do H. Ethylene flame dynamics and inlet unstart in a model scramjet. *J Propul Power.* 2014;30:1577-85.
- [18] Seleznev R, Surzhikov S, Shang J. A review of the scramjet experimental data base. *Prog Aeronaut Sci.* 2019;106:43-70.
- [19] Liu C, Sun M, Wang H, Yang L, An B, Pan Y. Ignition and flame stabilization characteristics in an ethylene-fueled scramjet combustor. *Aerosp Sci Technol.* 2020;106:106186.
- [20] Rankin BA, Fotia ML, Naples AG, Stevens CA, Hoke JL, Kaemming TA, et al. Overview of performance, application, and analysis of rotating detonation engine technologies. *J Propul Power.* 2017;33:131-43.

- [21] Anand V, Gutmark E. Rotating detonation combustors and their similarities to rocket instabilities. *Prog Energy Combust Sci.* 2019;73:182-234.
- [22] Wang Y, Le J, Wang C, Zheng Y. A non-premixed rotating detonation engine using ethylene and air. *Appl Therm Eng.* 2018;137:749-57.
- [23] Edwards T, Colket M, Cernansky N, Dryer F, Egolfopoulos F, Friend D, et al. Development of an experimental database and kinetic models for surrogate jet fuels. 45th AIAA. 2007:770.
- [24] Farrell J, Cernansky N, Dryer F, Law CK, Friend D, Hergart C, et al. Development of an experimental database and kinetic models for surrogate diesel fuels. SAE Tech Pap. 2007.
- [25] Metcalfe WK, Burke SM, Ahmed SS, Curran HJ. A Hierarchical and Comparative Kinetic Modeling Study of C-1 - C-2 Hydrocarbon and Oxygenated Fuels. *Int J Chem Kinet.* 2013;45:638-75.
- [26] Xu C, Konnov AA. Validation and analysis of detailed kinetic models for ethylene combustion. *Energy.* 2012;43:19-29.
- [27] Konnov AA. Implementation of the NCN pathway of prompt-NO formation in the detailed reaction mechanism. *Combust Flame.* 2009;156:2093-105.
- [28] Center for Energy research. Chemical Kinetic Mechanism for Combustion Application, University of California at San Diego, <http://combustion.ucsd.edu>; [accessed 19.10.01].
- [29] Wang Hai, You Xiaoqing, Joshi Ameya V, Davis Scott G, Laskin Alexander, Egolfopoulos Fokion, et al. USC mech version II. High-temperature combustion reaction model of H<sub>2</sub>/CO/C<sub>1</sub>-C<sub>4</sub> compounds, [http://ignis.usc.edu/USC\\_Mech\\_II.htm](http://ignis.usc.edu/USC_Mech_II.htm); 2007 [accessed 19.10.01].
- [30] Kikui S, Nakamura H, Tezuka T, Hasegawa S, Maruta K. Study on combustion and ignition characteristics of ethylene, propylene, 1-butene and 1-pentene in a micro flow reactor with a controlled temperature profile. *Combust Flame.* 2016;163:209-19.
- [31] Kopp MM, Petersen EL, Metcalfe WK, Burke SM, Curran HJ. Oxidation of Ethylene-Air Mixtures at Elevated Pressures, Part 2: Chemical Kinetics. *J Propul Power.* 2014;30:799-811.
- [32] Kopp MM, Donato NS, Petersen EL, Metcalfe WK, Burke SM, Curran HJ. Oxidation of Ethylene-Air Mixtures at Elevated Pressures, Part 1: Experimental Results. *J Propul Power.* 2014;30:790-8.
- [33] Saxena S, Kahandawala MSP, Sidhu SS. A shock tube study of ignition delay in the combustion of ethylene. *Combust Flame.* 2011;158:1019-31.
- [34] Penyazkov OG, Sevrouk KL, Tangirala V, Joshi N. High-pressure ethylene oxidation behind reflected shock waves. *Proc Combust Inst.* 2009;32:2421-8.
- [35] Dagaut P, Boettner J-C, Cathonnet M. Ethylene pyrolysis and oxidation: A kinetic modeling study. *Int J Chem Kinet.* 1990;22:641-64.
- [36] Jallais S, Bonneau L, Auzanneau M, Naudet V, Bockel-Macal S. An experimental and kinetic study of ethene oxidation at a high equivalence ratio. *Ind Eng Chem Res.* 2002;41:5659-67.
- [37] Le Cong T, Bedjanian E, Dagaut P. Oxidation of ethylene and propene in the presence of CO<sub>2</sub> and H<sub>2</sub>O: Experimental and detailed kinetic modeling study. *Combust Sci Technol.* 2010;182:333-49.
- [38] Carriere T, Westmoreland PR, Kazakov A, Stein YS, Dryer FL. Modeling ethylene combustion from low to high pressure. *Proc Combust Inst.* 2002;29:1257-66.
- [39] Lopez JG, Rasmussen CL, Alzueta MU, Gao Y, Marshall P, Glarborg P. Experimental and kinetic modeling study of C<sub>2</sub>H<sub>4</sub> oxidation at high pressure. *Proc Combust Inst.* 2009;32:367-75.
- [40] Hassan MI, Aung KT, Faeth GM. Measured and predicted properties of laminar premixed methane/air flames at various pressures. *Combust Flame.* 1998;115:539-50.
- [41] Egolfopoulos FN, Zhu DL, Law CK. Experimental and numerical determination of laminar flame speeds: Mixtures of C<sub>2</sub>-hydrocarbons with oxygen and nitrogen. *Symp (Int) Combust.* 1991;23:471-8.
- [42] Jomaas G, Zheng XL, Zhu DL, Law CK. Experimental determination of counterflow ignition temperatures and laminar flame speeds of C-2-C-3 hydrocarbons at atmospheric and elevated pressures. *Proc Combust Inst.* 2005;30:193-200.
- [43] Kumar K, Mittal G, Sung CJ, Law CK. An experimental investigation of ethylene/O<sub>2</sub>/diluent mixtures: Laminar flame speeds with preheat and ignition delays at high pressures. *Combust Flame.* 2008;153:343-54.

- [44] Bhargava A, Westmoreland PR. Measured Flame Structure and Kinetics in a Fuel-Rich Ethylene Flame. *Combust Flame*. 1998;113:333-47.
- [45] Dagaut P, Cathonnet M, Boettner JC. Experimental study and kinetic modeling of propene oxidation in a jet stirred flow reactor. *J Phys Chem*. 1988;92:661-71.
- [46] Davis S, Law C, Wang H. Propene pyrolysis and oxidation kinetics in a flow reactor and laminar flames. *Combust Flame*. 1999;119:375-99.
- [47] Westbrook CK, Pitz WJ. A Comprehensive Chemical Kinetic Reaction Mechanism for Oxidation and Pyrolysis of Propane and Propene. *Combust Sci Technol*. 1984;37:117-52.
- [48] Wilk RD, Cernansky NP, Pitz WJ, Westbrook CK. Propene oxidation at low and intermediate temperatures: A detailed chemical kinetic study. *Combust Flame*. 1989;77:145-70.
- [49] Heyberger B, Battin-Leclerc F, Warth V, Fournet R, Côme GM, Scacchi G. Comprehensive mechanism for the gas-phase oxidation of propene. *Combust Flame*. 2001;126:1780-802.
- [50] Braun-Unkshoff M, Slavinskaya N, Aigner M. Enhancement of a Detailed Mechanism of Propene. *ASME Turbo Expo 2010*. 2010:1037-47.
- [51] Burke SM, Burke U, Mc Donagh R, Mathieu O, Osorio I, Keesee C, et al. An experimental and modeling study of propene oxidation. Part 2: Ignition delay time and flame speed measurements. *Combust Flame*. 2015;162:296-314.
- [52] Burke SM, Metcalfe W, Herbinet O, Battin-Leclerc F, Haas FM, Santner J, et al. An experimental and modeling study of propene oxidation. Part 1: Speciation measurements in jet-stirred and flow reactors. *Combust Flame*. 2014;161:2765-84.
- [53] Brezinsky K, Burke EJ, Glassman I. The high temperature oxidation of butadiene. *Symp (Int) Combust*. 1985;20:613-22.
- [54] Laskin A, Wang H, Law CK. Detailed kinetic modeling of 1,3-butadiene oxidation at high temperatures. *Int J Chem Kinet*. 2000;32:589-614.
- [55] Tsang W, Mokrushin V. Mechanism and rate constants for 1,5-butadiene decomposition. *Proc Combust Inst*. 2000;28:1717-23.
- [56] Hidaka Y, Higashihara T, Ninomiya N, Masaoka H, Nakamura T, Kawano H. Shock tube and modeling study of 1,3-butadiene pyrolysis. *Int J Chem Kinet*. 1996;28:137-51.
- [57] Chambreau SA, Lemieux J, Wang LM, Zhang JS. Mechanistic studies of the pyrolysis of 1,3-butadiene, 1,3-butadiene-1,1,4,4d(4), 1,2-butadiene, and 2-butyne by supersonic jet/photoionization mass spectrometry. *J Phys Chem A*. 2005;109:2190-6.
- [58] Libby C, Davidson DF, Hanson RK. A shock tube study of the oxidation of 1, 3-butadiene. *42nd AIAA*. 2004:1322.
- [59] Zheng XL, Lu TF, Law CK. Experimental counterflow ignition temperatures and reaction mechanisms of 1,3-butadiene. *Proc Combust Inst*. 2007;31:367-75.
- [60] Peukert S, Naumann C, Braun-Unkshoff M. Formation of H-atoms in the Pyrolysis of 1,3-butadiene and 2-butyne: A Shock Tube and Modelling Study. *Z Phys Chem*. 2009;223:427-46.
- [61] Cole JA, Bittner JD, Longwell JP, Howard JB. Formation Mechanisms Of Aromatic-Compounds In Aliphatic Flames. *Combust Flame*. 1984;56:51-70.
- [62] Granata S, Faravelli T, Ranzi E, Olten N, Senkan S. Kinetic modeling of counterflow diffusion flames of butadiene. *Combust Flame*. 2002;131:273-84.
- [63] Newby JJ, Stearns JA, Liu C-P, Zwier TS. Photochemical and discharge-driven pathways to aromatic products from 1,3-butadiene. *J Phys Chem A*. 2007;111:10914-27.
- [64] Hansen N, Miller JA, Kasper T, Kohse-Hoinghaus K, Westmoreland PR, Wang J, et al. Benzene formation in premixed fuel-rich 1,3-butadiene flames. *Proc Combust Inst*. 2009;32:623-30.
- [65] Moshhammer K, Seidel L, Wang Y, Selim H, Sarathy SM, Mauss F, et al. Aromatic ring formation in opposed-flow diffusive 1,3-butadiene flames. *Proc Combust Inst*. 2017;36:947-55.
- [66] Goldaniga A, Faravelli T, Ranzi E. The kinetic modeling of soot precursors in a butadiene flame. *Combust Flame*. 2000;122:350-8.

- [67] Zhou C-W, Li Y, Burke U, Banyon C, Somers KP, Ding S, et al. An experimental and chemical kinetic modeling study of 1,3-butadiene combustion: Ignition delay time and laminar flame speed measurements. *Combust Flame*. 2018;197:423-38.
- [68] de Goey LPH, van Maaren A, Quax RM. Stabilization of Adiabatic Premixed Laminar Flames on a Flat Flame Burner. *Combust Sci Technol*. 1993;92:201-7.
- [69] Bradley JN, West KO. Single-pulse shock tube studies of hydrocarbon pyrolysis. Part 6.—The pyrolysis of isobutene. *J Chem Soc, Faraday Trans 1*. 1976;72:558-67.
- [70] Curran HJ, Dunphy MP, Simmie JM, Westbrook CK, Pitz WJ. Shock tube ignition of ethanol, isobutene and MTBE: Experiments and modeling. *Symp (Int) Combust*. 1992;24:769-76.
- [71] Santhanam S, Kiefer JH, Tranter RS, Srinivasan NK. A shock tube, laser-schlieren study of the pyrolysis of isobutene: Relaxation, incubation, and dissociation rates. *Int J Chem Kinet*. 2003;35:381-90.
- [72] Tsang W, Walker JA. Mechanism and rate constants for the reactions of hydrogen atoms with isobutene at high temperatures. *Symp (Int) Combust*. 1989;22:1015-22.
- [73] Yasunaga K, Kuraguchi Y, Ikeuchi R, Masaoka H, Takahashi O, Koike T, et al. Shock tube and modeling study of isobutene pyrolysis and oxidation. *Proc Combust Inst*. 2009;32:453-60.
- [74] Curran HJ. The combustion of isobutene and related compounds. PhD Thesis, Department of Chemistry, University College, Galway. 1994.
- [75] Brezinsky K, Dryer FL. A Flow Reactor Study of the Oxidation of Iso-butylene and an Iso-butylene/n-octane Mixture. *Combust Sci Technol*. 1986;45:225-32.
- [76] Dagaut P, Cathonnet M. Isobutene Oxidation and Ignition: Experimental and Detailed Kinetic Modeling Study. *Combust Sci Technol*. 1998;137:237-75.
- [77] Dias V, Vandooren J. Experimental and modeling study of a lean premixed isobutene/hydrogen/oxygen/argon flame. *Fuel*. 2010;89:2633-9.
- [78] Schenk M, Leon L, Moshhammer K, Oßwald P, Zeuch T, Seidel L, et al. Detailed mass spectrometric and modeling study of isomeric butene flames. *Combust Flame*. 2013;160:487-503.
- [79] Zhao P, Yuan W, Sun H, Li Y, Kelley AP, Zheng X, et al. Laminar flame speeds, counterflow ignition, and kinetic modeling of the butene isomers. *Proc Combust Inst*. 2015;35:309-16.
- [80] Zhang YJ, Cai JH, Zhao L, Yang JZ, Jin HF, Cheng ZJ, et al. An experimental and kinetic modeling study of three butene isomers pyrolysis at low pressure. *Combust Flame*. 2012;159:905-17.
- [81] Cai J, Zhang L, Zhang F, Wang Z, Cheng Z, Yuan W, et al. Experimental and Kinetic Modeling Study of n-Butanol Pyrolysis and Combustion. *Energy Fuels*. 2012;26:5550-68.
- [82] Pan L, Hu E, Zhang J, Tian Z, Li X, Huang Z. A high pressure shock tube study of 1-butene oxidation and its comparison with n-butane and alkenes. *Fuel*. 2015;157:21-7.
- [83] Fenard Y, Dayma G, Halter F, Foucher F, Serinyel Z, Dagaut P. Experimental and Modeling Study of the Oxidation of 1-Butene and cis-2-Butene in a Jet-Stirred Reactor and a Combustion Vessel. *Energy Fuels*. 2015;29:1107-18.
- [84] Chakir A, Cathonnet M, Boettner JC, Gaillard F. Kinetic study of 1-butene oxidation in a jet-stirred flow reactor. *Symp (Int) Combust*. 1989;22:873-81.
- [85] Fenard Y, Dagaut P, Dayma G, Halter F, Foucher F. Experimental and kinetic modeling study of trans-2-butene oxidation in a jet-stirred reactor and a combustion bomb. *Proc Combust Inst*. 2015;35:317-24.
- [86] Li Y, Zhou CW, Curran HJ. An extensive experimental and modeling study of 1-butene oxidation. *Combust Flame*. 2017;181:198-213.
- [87] Li Y, Zhou C-W, Somers KP, Zhang K, Curran HJ. The oxidation of 2-butene: A high pressure ignition delay, kinetic modeling study and reactivity comparison with isobutene and 1-butene. *Proc Combust Inst*. 2017;36:403-11.
- [88] Zhou C-W, Li Y, O'Connor E, Somers KP, Thion S, Keese C, et al. A comprehensive experimental and modeling study of isobutene oxidation. *Combust Flame*. 2016;167:353-79.
- [89] Minetti R, Roubaud A, Therssen E, Ribaucour M, Sochet LR. The chemistry of pre-ignition of n-pentane and 1-pentene. *Combust Flame*. 1999;118:213-20.

- [90] Ribaucour M, Minetti R, Sochet LR. Autoignition of n-pentane and 1-pentene: Experimental data and kinetic modeling. *Symp (Int) Combust.* 1998;27:345-51.
- [91] Westbrook CK, Pitz WJ, Mehl M, Glaude PA, Herbinet O, Bax S, et al. Experimental and Kinetic Modeling Study of 2-Methyl-2-Butene: Allylic Hydrocarbon Kinetics. *J Phys Chem A.* 2015;119:7462-80.
- [92] Cheng Y, Hu E, Lu X, Li X, Gong J, Li Q, et al. Experimental and kinetic study of pentene isomers and n-pentane in laminar flames. *Proc Combust Inst.* 2017;36:1279-86.
- [93] Cheng Y, Hu EJ, Deng FQ, Yang FY, Zhang YJ, Tang CL, et al. Experimental and kinetic comparative study on ignition characteristics of 1-pentene and n-pentane. *Fuel.* 2016;172:263-72.
- [94] Zhong B-J, Peng H-S. Measurement of Laminar Flame Speed and Chemical Kinetic Model of 1-Pentene/Air Mixtures. *Combust Sci Technol.* 2017;189:1698-712.
- [95] Prabhu SK, Bhat RK, Miller DL, Cernansky NP. 1-Pentene oxidation and its interaction with nitric oxide in the low and negative temperature coefficient regions. *Combust Flame.* 1996;104:377-90.
- [96] Alatorre GG, Bohm H, Atakan B, Kohse-Hoinghaus K. Experimental and modelling study of 1-pentene combustion at fuel-rich conditions. *Z Phys Chem.* 2001;215:981-95.
- [97] Kukkadapu G, Kumar K, Sung C-J, Mehl M, Pitz WJ. Autoignition of gasoline and its surrogates in a rapid compression machine. *Proc Combust Inst.* 2013;34:345-52.
- [98] Touchard S, Fournet R, Glaude PA, Warth V, Battin-Leclerc F, Vanhove G, et al. Modeling of the oxidation of large alkenes at low temperature. *Proc Combust Inst.* 2005;30:1073-81.
- [99] Touchard S, Buda F, Dayma G, Glaude PA, Fournet R, Battin-Leclerc F. Experimental and modeling study of the oxidation of 1-pentene at high temperature. *Int J Chem Kinet.* 2005;37:451-63.
- [100] Dong S, Zhang K, Ninnemann EM, Najjar A, Kukkadapu G, Baker J, et al. A comprehensive experimental and kinetic modeling study of 1-and 2-pentene. *Combust Flame.* 2021;223:166-80.
- [101] Battin-Leclerc F, Rodriguez A, Husson B, Herbinet O, Glaude PA, Wang ZD, et al. Products from the Oxidation of Linear Isomers of Hexene. *J Phys Chem A.* 2014;118:673-83.
- [102] Vanhove G, Ribaucour M, Minetti R. On the influence of the position of the double bond on the low-temperature chemistry of hexenes. *Proc Combust Inst.* 2005;30:1065-72.
- [103] Bounaceur R, Warth V, Sirjean B, Glaude PA, Fournet R, Battin-Leclerc F. Influence of the position of the double bond on the autoignition of linear alkenes at low temperature. *Proc Combust Inst.* 2009;32:387-94.
- [104] Mehl M, Vanhove G, Pitz WJ, Ranzi E. Oxidation and combustion of the n-hexene isomers: A wide range kinetic modeling study. *Combust Flame.* 2008;155:756-72.
- [105] Yahyaoui M, Djebaili-Chaumeix N, Dagaut P, Paillard CE, Gail S. Kinetics of 1-hexene oxidation in a JSR and a shock tube: Experimental and modelin study. *Combust Flame.* 2006;147:67-78.
- [106] Battin-Leclerc F. Detailed chemical kinetic models for the low-temperature combustion of hydrocarbons with application to gasoline and diesel fuel surrogates. *Prog Energy Combust Sci.* 2008;34:440-98.
- [107] Yahyaoui M, Djebaili-Chaumeix N, Paillard CE, Touchard S, Fournet R, Glaude PA, et al. Experimental and modeling study of 1-hexene oxidation behind reflected shock waves. *Proc Combust Inst.* 2005;30:1137-45.
- [108] Vanhove G, Minetti R, Touchard S, Fournet R, Glaude PA, Battin-Leclerc F. Experimental and modeling study of the autoignition of 1-hexene/isooctane mixtures at low temperatures. *Combust Flame.* 2006;145:272-81.
- [109] Meng X, Rodriguez A, Herbinet O, Wang T, Battin-Leclerc F. Revisiting 1-hexene low-temperature oxidation. *Combust Flame.* 2017;181:283-99.
- [110] Fan X, Wang G, Li Y, Wang Z, Yuan W, Zhao L. Experimental and kinetic modeling study of 1-hexene combustion at various pressures. *Combust Flame.* 2016;173:151-60.
- [111] Yang F, Deng F, Zhang P, Tian Z, Tang C, Huang Z. Experimental and Kinetic Modeling Study on trans-3-Hexene Ignition behind Reflected Shock Waves. *Energy Fuels.* 2016;30:706-16.
- [112] Wu Y, Liu Y, Tang C, Huang Z. Ignition delay times measurement and kinetic modeling studies of 1-heptene, 2-heptene and n-heptane at low to intermediate temperatures by using a rapid compression machine. *Combust Flame.* 2018;197:30-40.

- [113] Tanaka S, Ayala F, Keck JC, Heywood JB. Two-stage ignition in HCCI combustion and HCCI control by fuels and additives. *Combust Flame*. 2003;132:219-39.
- [114] Mei BW, Li W, Ma SY, Wang HY, Pan HQ, Qi F, et al. Investigation on 1-Heptene/Air Laminar Flame Propagation under Elevated Pressures. *Chin J Chem Phys*. 2019;32:99-106.
- [115] Hellier P, Ladommatos N, Allan R, Rogerson J. Combustion and emissions characteristics of toluene/n-heptane and 1-octene/n-octane binary mixtures in a direct injection compression ignition engine. *Combust Flame*. 2013;160:2141-58.
- [116] Hellier P, Ladommatos N, Allan R, Filip S, Rogerson J. The importance of double bond position and cis-trans isomerisation in diesel combustion and emissions. *Fuel*. 2013;105:477-89.
- [117] Meng XZ, Herbinet O, Wang TY, Battin-Leclerc F. Experimental and modeling study of 1-octene jet-stirred reactor oxidation. *Fuel*. 2017;207:763-75.
- [118] Fridlyand A, Goldsborough SS, Brezinsky K, Merchant SS, Green WH. Influence of the double bond position on the oxidation of decene isomers at high pressures and temperatures. *Proc Combust Inst*. 2015;35:333-40.
- [119] Tekawade A, Xie TB, Oehlschlaeger MA. Comparative Study of the Ignition of 1-Decene, trans-5-Decene, and n-Decane: Constant-Volume Spray and Shock-Tube Experiments. *Energy Fuels*. 2017;31:6493-500.
- [120] Hu EJ, Yin GY, Ku JF, Gao ZH, Huang ZH. Experimental and kinetic study of 2,4,4-trimethyl-1-pentene and iso-octane in laminar flames. *Proc Combust Inst*. 2019;37:1709-16.
- [121] Hu EJ, Yin GY, Gao ZH, Liu Y, Ku JF, Huang ZH. Experimental and kinetic modeling study on 2,4,4-trimethyl-1-pentene ignition behind reflected shock waves. *Fuel*. 2017;195:97-104.
- [122] Yin GY, Hu EJ, Huang SH, Ku JF, Li XJ, Xu ZH, et al. Experimental and kinetic study of diisobutylene isomers in laminar flames. *Energy*. 2019;170:537-45.
- [123] Metcalfe WK, Pitz WJ, Curran HJ, Simmie JM, Westbrook CK. The development of a detailed chemical kinetic mechanism for diisobutylene and comparison to shock tube ignition times. *Proc Combust Inst*. 2007;31:377-84.
- [124] Zheng D, Zhong BJ, Xiong PF. Experimental study on laminar flame speeds and chemical kinetic model of 2,4,4-trimethyl-1-pentene. *Fuel*. 2018;229:95-104.
- [125] Kohse-Hoinghaus K. Clean combustion: Chemistry and diagnostics for a systems approach in transportation and energy conversion. *Prog Energy Combust Sci*. 2018;65:1-5.
- [126] Agarwal AK. Biofuels (alcohols and biodiesel) applications as fuels for internal combustion engines. *Prog Energy Combust Sci*. 2007;33:233-71.
- [127] Demirbas A. Importance of biodiesel as transportation fuel. *Energy Policy*. 2007;35:4661-70.
- [128] Hanson RK. Applications of quantitative laser sensors to kinetics, propulsion and practical energy systems. *Proc Combust Inst*. 2011;33:1-40.
- [129] Hanson RK, Davidson DF. Recent advances in laser absorption and shock tube methods for studies of combustion chemistry. *Prog Energy Combust Sci*. 2014;44:103-14.
- [130] Goldsborough SS, Hochgreb S, Vanhove G, Wooldridge MS, Curran HJ, Sung CJ. Advances in rapid compression machine studies of low- and intermediate-temperature autoignition phenomena. *Prog Energy Combust Sci*. 2017;63:1-78.
- [131] Sung CJ, Curran HJ. Using rapid compression machines for chemical kinetics studies. *Prog Energy Combust Sci*. 2014;44:1-18.
- [132] Baker JA, Skinner GB. Shock-tube studies on the ignition of ethylene-oxygen-argon mixtures. *Combust Flame*. 1972;19:347-50.
- [133] Wang K, Xu R, Parise T, Shao J, Movaghar A, Lee DJ, et al. A physics-based approach to modeling real-fuel combustion chemistry – IV. HyChem modeling of combustion kinetics of a bio-derived jet fuel and its blends with a conventional Jet A. *Combust Flame*. 2018;198:477-89.
- [134] Hidaka Y, Kataoka T, Suga M. A shock-tube investigation of ignition in ethylene–oxygen–argon mixtures. *Bull Chem Soc Jpn*. 1974;47:2166-70.
- [135] Hidaka Y, Nishimori T, Sato K, Henmi Y, Okuda R, Inami K, et al. Shock-tube and modeling study of ethylene pyrolysis and oxidation. *Combust Flame*. 1999;117:755-76.

- [136] Brown C, Thomas G. Experimental studies of shock-induced ignition and transition to detonation in ethylene and propane mixtures. *Combust Flame*. 1999;117:861-70.
- [137] Cadman P, Bambrey R, Box S, Thomas G. Ethylene combustion studied over a wide temperature range in high-temperature shock waves. *Combust Sci Technol*. 2002;174:111-27.
- [138] Kalitan DM, Hall JM, Petersen EL. Ignition and oxidation of ethylene-oxygen-diluent mixtures with and without silane. *J Propul Power*. 2005;21:1045-56.
- [139] Wang H, Laskin A. A comprehensive kinetic model of ethylene and acetylene oxidation at high temperatures. Progress Report for an AFOSR New World Vista Program. 1998.
- [140] Shao J, Davidson DF, Hanson RK. A shock tube study of ignition delay times in diluted methane, ethylene, propene and their blends at elevated pressures. *Fuel*. 2018;225:370-80.
- [141] Burcat A, Radhakrishnan K. High temperature oxidation of propene. *Combust Flame*. 1985;60:157-69.
- [142] Qin Z, Yang H, Gardiner WC. Measurement and modeling of shock-tube ignition delay for propene. *Combust Flame*. 2001;124:246-54.
- [143] Curran H, Simmie JM, Dagaut P, Voisin D, Cathonnet M. The ignition and oxidation of allene and propyne: Experiments and kinetic modeling. *Symp (Int) Combust*. 1996;26:613-20.
- [144] Fournet R, Bauge J, Battin - Leclerc F. Experimental and modeling of oxidation of acetylene, propyne, allene and 1, 3 - butadiene. *Int J Chem Kinet*. 1999;31:361-79.
- [145] Heyberger B, Belmekki N, Conraud V, Glaude PA, Fournet R, Battin-Leclerc F. Oxidation of small alkenes at high temperature. *Int J Chem Kinet*. 2002;34:666-77.
- [146] Horning DC, Davidson D, Hanson R. Study of the high-temperature autoignition of n-alkane/O/Ar mixtures. *J Propul Power*. 2002;18:363-71.
- [147] Shen H-PS, Vanderover J, Oehlschlaeger MA. A shock tube study of iso-octane ignition at elevated pressures: The influence of diluent gases. *Combust Flame*. 2008;155:739-55.
- [148] Yang F, Deng F, Zhang P, Hu E, Cheng Y, Huang Z. Comparative study on ignition characteristics of 1-hexene and 2-hexene behind reflected shock waves. *Energy Fuels*. 2016;30:5130-7.
- [149] Wagon SW, Barraza-Botet CL, Wooldridge MS. Effects of bond location on the ignition and reaction pathways of trans-hexene isomers. *J Phys Chem A*. 2015;119:7695-703.
- [150] Garner S, Dubois T, Togbe C, Chaumeix N, Dagaut P, Brezinsky K. Biologically derived diesel fuel and NO formation: Part 2: Model development and extended validation. *Combust Flame*. 2011;158:2302-13.
- [151] Konnov AA, Mohammad A, Kishore VR, Kim NI, Prathap C, Kumar S. A comprehensive review of measurements and data analysis of laminar burning velocities for various fuel+ air mixtures. *Prog Energy Combust Sci*. 2018;68:197-267.
- [152] Egolfopoulos FN, Hansen N, Ju Y, Kohse-Höinghaus K, Law CK, Qi F. Advances and challenges in laminar flame experiments and implications for combustion chemistry. *Prog Energy Combust Sci*. 2014;43:36-67.
- [153] Linnett J, Hoare M. Burning velocities in ethylene-air-nitrogen mixtures. *Symposium on Combustion and Flame, and Explosion Phenomena*. 1948;3:195-204.
- [154] Gerstein M, Levine O, Wong EL. Flame propagation. II. The determination of fundamental burning velocities of hydrocarbons by a revised tube method. *J Am Chem Soc*. 1951;73:418-22.
- [155] Huo J, Shu T, Ren Z, Law CK. Extrapolation of Laminar Ethylene/Air Flame Speeds at Elevated Pressures with Flame Chemistry Analysis. *J Propul Power*. 2018:1-8.
- [156] Davis S, Law C. Determination of and fuel structure effects on laminar flame speeds of C1 to C8 hydrocarbons. *Combust Sci Technol*. 1998;140:427-49.
- [157] Movaghar A, Lawson R, Egolfopoulos FN. Confined spherically expanding flame method for measuring laminar flame speeds: Revisiting the assumptions and application to C1-C4 hydrocarbon flames. *Combust Flame*. 2020;212:79-92.
- [158] Homann KH, Mochizuki M, Wagner HG. *Phys Chem N F*. 1963;37:299.

- [159] Peeters J, Mahnen G. STRUCTURE OF ETHYLENE-OXYGEN FLAMES. REACTION MECHANISM AND RATE CONSTANTS OF ELEMENTARY REACTIONS. *Combust Inst European Symp.* 1973;1:53-8.
- [160] Peeters J, Vinckier C. Production of chemi-ions and formation of CH and CH<sub>2</sub> radicals in methane-oxygen and ethylene-oxygen flames. *Symp (Int) Combust.* 1975;15:969-77.
- [161] Harris SJ, Weiner AM, Cleveland Ashcraft C. Soot particle inception kinetics in a premixed ethylene flame. *Combust Flame.* 1986;64:65-81.
- [162] Cool TA, Bernstein JS, Song XM, Goodwin PM. Profiles of HCO and CH<sub>3</sub> in CH<sub>4</sub>/O<sub>2</sub> and C<sub>2</sub>H<sub>4</sub>/O<sub>2</sub> flames by resonance ionization. *Symp (Int) Combust.* 1989:1421.
- [163] Marinov NM, Malte PC. Ethylene oxidation in a well - stirred reactor. *Int J Chem Kinet.* 1995;27:957-86.
- [164] Wilk RD, Pitz WJ, Westbrook CK, Cernansky NP. Chemical kinetic modeling of ethene oxidation at low and intermediate temperatures. *Symp (Int) Combust.* 1991;23:203-10.
- [165] Westbrook CK, Dryer FL, Schug KP. A comprehensive mechanism for the pyrolysis and oxidation of ethylene. *Symp (Int) Combust.* 1982;19:153-66.
- [166] Bhargava A, Westmoreland PR. MBMS analysis of a fuel-lean ethylene flame. *Combust Flame.* 1998;115:456-67.
- [167] Dagaut P, Cathonnet M, Boettner J, Gaillard F. Kinetic modeling of ethylene oxidation. *Combust Flame.* 1988;71:295-312.
- [168] Westbrook CK, Thornton MM, Pitz WJ, Malte PC. A kinetic study of ethylene oxidation in a well-stirred reactor. *Symp (Int) Combust.* 1989;22:863-71.
- [169] Dagaut P, Luche J, Cathonnet M. Experimental and kinetic modeling of the reduction of NO by propene at 1 atm. *Combust Flame.* 2000;121:651-61.
- [170] Pauwels J-F, Volponi JV, Miller JA. The Oxidation of Allene in a Low-Pressure H<sub>2</sub>/O<sub>2</sub>/Ar-C<sub>3</sub> H<sub>4</sub> Flame. *Combust Sci Technol.* 1995;110:249-76.
- [171] Faravelli T, Goldaniga A, Zappella L, Ranzi E, Dagaut P, Cathonnet M. An experimental and kinetic modeling study of propyne and allene oxidation. *Proc Combust Inst.* 2000;28:2601-8.
- [172] Hansen N, Miller JA, Westmoreland PR, Kasper T, Kohse-Höinghaus K, Wang J, et al. Isomer-specific combustion chemistry in allene and propyne flames. *Combust Flame.* 2009;156:2153-64.
- [173] Zhang X, Zou J, Cao C, Chen W, Yang J, Qi F, et al. Exploring the low-temperature oxidation chemistry of 1-butene and i-butene triggered by dimethyl ether. *Proc Combust Inst.* 2021;38:289-98.
- [174] Cao C, Li W, Chen W, Ahmad H, Yang J, Li Y. Exploring combustion chemistry of 1 - pentene: Flow reactor pyrolysis at various pressures and development of a detailed combustion model. *Int J Chem Kinet.* 2021;53:514-26.
- [175] Hansen N, Li W, Law ME, Kasper T, Westmoreland PR, Yang B, et al. The importance of fuel dissociation and propargyl+ allyl association for the formation of benzene in a fuel-rich 1-hexene flame. *Phys Chem Chem Phys.* 2010;12:12112-22.
- [176] Cao C, Zhang X, Zhang Y, Zou J, Li Y, Yang J, et al. Probing the fuel-specific intermediates in the low-temperature oxidation of 1-heptene and modeling interpretation. *Proc Combust Inst.* 2021;38:385-94.
- [177] Piperel A, Dagaut P, Montagne X. Impact of acetaldehyde and NO addition on the 1-octene oxidation under simulated HCCI conditions. *Proc Combust Inst.* 2009;32:2861-8.
- [178] Fridlyand A, Goldsborough SS, Brezinsky K. Chemical Kinetic Influences of Alkyl Chain Structure on the High Pressure and Temperature Oxidation of a Representative Unsaturated Biodiesel: Methyl Nonenoate. *J Phys Chem A.* 2015;119:7559-77.
- [179] Dagaut P, Cathonnet M. The Oxidation of 1,3-Butadiene: Experimental Results and Kinetic Modeling. *Combust Sci Technol.* 1998;140:225-57.
- [180] Hirasawa T, Sung C, Joshi A, Yang Z, Wang H, Law C. Determination of laminar flame speeds using digital particle image velocimetry: binary fuel blends of ethylene, n-butane, and toluene. *Proc Combust Inst.* 2002;29:1427-34.

- [181] Ravi S, Sikes T, Morones A, Keesee C, Petersen E. Comparative study on the laminar flame speed enhancement of methane with ethane and ethylene addition. *Proc Combust Inst.* 2015;35:679-86.
- [182] Curtiss LA, Redfern PC, Raghavachari K. Gaussian-4 theory. *J Chem Phys.* 2007;126:12.
- [183] Montgomery JA, Frisch MJ, Ochterski JW, Petersson GA. A complete basis set model chemistry. VI. Use of density functional geometries and frequencies. *J Chem Phys.* 1999;110:2822-7.
- [184] Frisch MJ, et al. Gaussian 09, Gaussian, Inc., Wallingford. 2009.
- [185] Klippenstein SJ. From theoretical reaction dynamics to chemical modeling of combustion. *Proc Combust Inst.* 2017;36:77-111.
- [186] Klippenstein SJ, Harding LB, Ruscic B. Ab initio computations and active thermochemical tables hand in hand: Heats of formation of core combustion species. *J Phys Chem A.* 2017;121:6580-602.
- [187] Simmie JM, Somers KP. Benchmarking compound methods (CBS-QB3, CBS-APNO, G3, G4, W1BD) against the active thermochemical tables: a litmus test for cost-effective molecular formation enthalpies. *J Phys Chem A.* 2015;119:7235-46.
- [188] Somers KP, Simmie JM. Benchmarking compound methods (CBS-QB3, CBS-APNO, G3, G4, W1BD) against the active thermochemical tables: formation enthalpies of radicals. *J Phys Chem A.* 2015;119:8922-33.
- [189] Luo Y-R. Comprehensive handbook of chemical bond energies. CRC press; 2007.
- [190] Westbrook CK, Mizobuchi Y, Poinot TJ, Smith PJ, Warnatz J. Computational combustion. *Proc Combust Inst.* 2005;30:125-57.
- [191] Westbrook CK, Dryer FL. Chemical kinetics and modeling of combustion processes. *Symp (Int) Combust.* 1981;18:749-67.
- [192] Westbrook C. K., F.L. D. Chemical kinetic modeling of hydrocarbon combustion. *Prog Energy Combust Sci.* 1984;10:1-57.
- [193] Simmie JM. Detailed chemical kinetic models for the combustion of hydrocarbon fuels. *Prog Energy Combust Sci.* 2003;29:599-634.
- [194] Curran HJ. Developing detailed chemical kinetic mechanisms for fuel combustion. *Proc Combust Inst.* 2019;37:57-81.
- [195] Burke U, Metcalfe WK, Burke SM, Heufer KA, Dagaut P, Curran HJ. A detailed chemical kinetic modeling, ignition delay time and jet-stirred reactor study of methanol oxidation. *Combust Flame.* 2016;165:125-36.
- [196] Keromnes A, Metcalfe WK, Heufer KA, Donohoe N, Das AK, Sung CJ, et al. An experimental and detailed chemical kinetic modeling study of hydrogen and syngas mixture oxidation at elevated pressures. *Combust Flame.* 2013;160:995-1011.
- [197] Wang H, Sheen DA. Combustion kinetic model uncertainty quantification, propagation and minimization. *Prog Energy Combust Sci.* 2015;47:1-31.
- [198] Miller JA, Sivaramakrishnan R, Tao Y, Goldsmith CF, Burke MP, Jasper AW, et al. Combustion chemistry in the twenty-first century: developing theory-informed chemical kinetics models. *Prog Energy Combust Sci.* 2021;83:100886.
- [199] Goldsmith CF, Tomlin AS, Klippenstein SJ. Uncertainty propagation in the derivation of phenomenological rate coefficients from theory: A case study of n-propyl radical oxidation. *Proc Combust Inst.* 2013;34:177-85.
- [200] Xing L, Li S, Wang Z, Yang B, Klippenstein SJ, Zhang F. Global uncertainty analysis for RRKM/master equation based kinetic predictions: A case study of ethanol decomposition. *Combust Flame.* 2015;162:3427-36.
- [201] Prager J, Najm HN, Zádor J. Uncertainty quantification in the ab initio rate-coefficient calculation for the  $\text{CH}_3\text{CH}(\text{OH})\text{CH}_3 + \text{OH} \rightarrow \text{CH}_3\text{C}(\text{OH})\text{CH}_3 + \text{H}_2\text{O}$  reaction. *Proc Combust Inst.* 2013;34:583-90.
- [202] Tsang W. Chemical Kinetic Data Base for Combustion Chemistry. Part V. Propene. *J Phys Chem Ref Data.* 1991;20.
- [203] Badra J, Khaled F, Giri BR, Farooq A. A shock tube study of the branching ratios of propene+ OH reaction. *Phys Chem Chem Phys.* 2014;17:2421-31.

- [204] Elwardany A, Badra J, Farooq A. High-temperature rate constant measurements for OH plus xylenes. *Combust Flame*. 2015;162:2348-53.
- [205] Khaled F, Giri BR, Farooq A. A high-temperature shock tube kinetic study for the branching ratios of isobutene+ OH reaction. *Proc Combust Inst*. 2017;36:265-72.
- [206] Stothard ND, Walker RW. DETERMINATION OF THE ARRHENIUS PARAMETERS FOR THE INITIATION REACTION  $C_3H_6 + O_2 \rightarrow CH_2CHCH_2 + HO_2$ . *J Chem Soc, Faraday Trans*. 1991;87:241-7.
- [207] Ingham T, Walker RW, Woolford RE. Kinetic parameters for the initiation reaction  $RH+O_2 \rightarrow R+HO_2$ . *Symp (Int) Combust*. 1994;25:767-74.
- [208] Zhou CW, Simmie JM, Somers KP, Goldsmith CF, Curran HJ. Chemical Kinetics of Hydrogen Atom Abstraction from Allylic Sites by O-3(2); Implications for Combustion Modeling and Simulation. *J Phys Chem A*. 2017;121:1890-9.
- [209] Li XH, Jasper AW, Zador J, Miller JA, Klippenstein SJ. Theoretical kinetics of O + C<sub>2</sub>H<sub>4</sub>. *Proc Combust Inst*. 2017;36:219-27.
- [210] Cavallotti C, Leonori F, Balucani N, Nevrlly V, Bergeat A, Falcinelli S, et al. Relevance of the Channel Leading to Formaldehyde plus Triplet Ethylidene in the O(P-3) + Propene Reaction under Combustion Conditions. *J Phys Chem Lett*. 2014;5:4213-8.
- [211] Leonori F, Balucani N, Nevrlly V, Bergeat A, Falcinelli S, Vanuzzo G, et al. Experimental and Theoretical Studies on the Dynamics of the O(P-3) + Propene Reaction: Primary Products, Branching Ratios, and Role of Intersystem Crossing. *J Phys Chem C*. 2015;119:14632-52.
- [212] Bedjanian Y, Morin J. Reaction of O(3P) with C<sub>3</sub>H<sub>6</sub>: Yield of the Reaction Products as a Function of Temperature. *J Phys Chem A*. 2017;121:1553-62.
- [213] Goldsmith CF, Harding LB, Georgievskii Y, Miller JA, Klippenstein SJ. Temperature and Pressure-Dependent Rate Coefficients for the Reaction of Vinyl Radical with Molecular Oxygen. *J Phys Chem A*. 2015;119:7766-79.
- [214] Krueger H, Weitz E. Diode-Laser Probes of Vinyl Radical Kinetics – The Reaction of C<sub>2</sub>H<sub>3</sub> with HCl and DCl. *J Chem Phys*. 1988;88:1608-16.
- [215] Fahr A, Laufer AH. Ultraviolet-Absorption of the Vinyl Radical and Reaction with Oxygen. *J Phys Chem*. 1988;92:7229-32.
- [216] Knyazev VD, Slagle IR. Kinetics of the Reaction of Vinyl Radical with Molecular Oxygen. *J Phys Chem*. 1995;99:2247-9.
- [217] Cooke DF, Williams A. Shock-Tube Studies of the Ignition and Combustion of Ethane and Slightly Rich Methane Mixtures with Oxygen. *Symp Combust, [Proc]*. 1971;13:757-66.
- [218] Baldwin RR, Walker RW. Elementary Reactions in the Oxidation of Alkenes. *Symp Combust, [Proc]*. 1981;18:819-29.
- [219] Park J-Y, Heaven MC, Gutman D. Kinetics and Mechanism of the Reaction of Vinyl Radical with Molecular-Oxygen. *Chem Phys Lett*. 1984;104:469-74.
- [220] Slagle IR, Park J-Y, Heaven MC, Gutman D. Kinetics of Polyatomic Free-Radicals Produced by Laser Photolysis. 3. Reaction of Vinyl Radicals with Molecular Oxygen. *J Am Chem Soc*. 1984;106:4356-61.
- [221] Matsugi A, Miyoshi A. Yield of Formyl Radical from the Vinyl + O-2 Reaction. *Int J Chem Kinet*. 2014;46:260-74.
- [222] Eskola AJ, Timonen RS. Kinetics of the reactions of vinyl radicals with molecular oxygen and chlorine at temperatures 200-362 K. *Phys Chem Chem Phys*. 2003;5:2557-61.
- [223] Oguchi T, Sato Y, Matsui H. The CH<sub>2</sub>CHO + O channel of the reaction of vinyl radical with O<sub>2</sub>. *Chem Phys Lett*. 2009;472:181-4.
- [224] Chishima H, Koshi M, Tonokura K. Pressure Dependence of Vinylperoxyl Radical Formation in the Reaction of Vinyl Radical with Molecular Oxygen. *Chem Lett*. 2009;38:1150-1.
- [225] Westmoreland PR. Thermochemistry and Kinetics of C<sub>2</sub>H<sub>3</sub> + O<sub>2</sub> Reactions. *Combust Sci Technol*. 1992;82:151-68.

- [226] Bozzelli JW, Dean AM. Hydrocarbon Radical Reactions with O<sub>2</sub> – Comparison of Allyl, Formyl, and Vinyl to Ethyl. *J Phys Chem.* 1993;97:4427-41.
- [227] Carpenter BK. Computational prediction of new mechanisms for the reactions of vinyl and phenyl radicals with molecular oxygen. *J Am Chem Soc.* 1993;115:9806-7.
- [228] Mebel AM, Diau EWG, Lin MC, Morokuma K. Ab Initio and RRKM Calculations for Multichannel Rate Constants of the C<sub>2</sub>H<sub>3</sub> + O<sub>2</sub> Reaction. *J Am Chem Soc.* 1996;118:9759-71.
- [229] Carpenter BK. Ab Initio Computation of Combustion Kinetics. 1. Vinyl Radical + O<sub>2</sub>. *J Phys Chem.* 1995;99:9801-10.
- [230] Klippenstein SJ, Georgievskii Y, Miller JA, Nummela JA, Carpenter BK, Westmoreland PR. Vinyl + O<sub>2</sub>: A Complete Theoretical Treatment. 3rd Joint Meeting of the US Sections of The Combustion Institute, Chicago, IL. 2003.
- [231] Goldsmith CF, Klippenstein SJ, Green WH. Theoretical rate coefficients for allyl + HO<sub>2</sub> and allyloxy decomposition. *Proc Combust Inst.* 2011;33:273-82.
- [232] Zador J, Klippenstein SJ, Miller JA. Pressure-Dependent OH Yields in Alkene plus HO<sub>2</sub> Reactions: A Theoretical Study. *J Phys Chem A.* 2011;115:10218-25.
- [233] Zador J, Taatjes CA, Fernandes RX. Kinetics of elementary reactions in low-temperature autoignition chemistry. *Prog Energy Combust Sci.* 2011;37:371-421.
- [234] Savee JD, Papajak E, Rotavera B, Huang H, Eskola AJ, Welz O, et al. Direct observation and kinetics of a hydroperoxyalkyl radical (QOOH). *Science.* 2015;347:643-6.
- [235] Goldsmith CF, Green WH, Klippenstein SJ. Role of O-2 + QOOH in Low-Temperature Ignition of Propane. 1. Temperature and Pressure Dependent Rate Coefficients. *J Phys Chem A.* 2012;116:3325-46.
- [236] Zador J, Jasper AW, Miller JA. The reaction between propene and hydroxyl. *Phys Chem Chem Phys.* 2009;11:11040-53.
- [237] Loison J-C, Daranlot J, Bergeat A, Caralp F, Mereau R, Hickson KM. Gas-Phase Kinetics of Hydroxyl Radical Reactions with C<sub>3</sub>H<sub>6</sub> and C<sub>4</sub>H<sub>8</sub>: Product Branching Ratios and OH Addition Site-Specificity. *J Phys Chem A.* 2010;114:13326-36.
- [238] Zhou CW, Li ZR, Li XY. Kinetics and Mechanism for Formation of Enols in Reaction of Hydroxide Radical with Propene. *J Phys Chem A.* 2009;113:2372-82.
- [239] Dibble TS. Mechanism and dynamics of the CH<sub>2</sub>OH+O-2 reaction. *Chem Phys Lett.* 2002;355:193-200.
- [240] Hermans I, Muller JF, Nguyen TL, Jacobs PA, Peeters J. Kinetics of alpha-hydroxy-alkylperoxyl radicals in oxidation processes. HO<sub>2</sub> center dot-initiated oxidation of ketones/aldehydes near the tropopause. *J Phys Chem A.* 2005;109:4303-11.
- [241] Schocker A, Uetake M, Kanno N, Koshi M, Tonokura K. Kinetics and rate constants of the reaction CH<sub>2</sub>OH+O-2 -> CH<sub>2</sub>O+HO<sub>2</sub> in the temperature range of 236-600 K. *J Phys Chem A.* 2007;111:6622-7.
- [242] Zador J, Fernandes RX, Georgievskii Y, Meloni G, Taatjes CA, Miller JA. The reaction of hydroxyethyl radicals with O-2: A theoretical analysis and experimental product study. *Proc Combust Inst.* 2009;32:271-7.
- [243] da Silva G, Bozzelli JW, Liang L, Farrell JT. Ethanol Oxidation: Kinetics of the alpha-Hydroxyethyl Radical + O-2 Reaction. *J Phys Chem A.* 2009;113:8923-33.
- [244] Sun HY, Bozzelli JW, Law CK. Thermochemical and kinetic analysis on the reactions of O-2 with products from OH addition to isobutene, 2-hydroxy-1,1-dimethylethyl, and 2-hydroxy-2-methylpropyl radicals: HO<sub>2</sub> formation from oxidation of neopentane, part II. *J Phys Chem A.* 2007;111:4974-86.
- [245] Cavalli F, Geiger H, Barnes I, Becker KH. FTIR kinetic, product, and modeling study of the OH-initiated oxidation of 1-butanol in air. *Environ Sci Technol.* 2002;36:1263-70.
- [246] Hurley MD, Wallington TJ, Lairsen L, Javadi MS, Nielsen OJ, Yamanaka T, et al. Atmospheric Chemistry of n-Butanol: Kinetics, Mechanisms, and Products of Cl Atom and OH Radical Initiated Oxidation in the Presence and Absence of NO<sub>x</sub>. *J Phys Chem A.* 2009;113:7011-20.
- [247] Andersen VF, Wallington TJ, Nielsen OJ. Atmospheric Chemistry of i-Butanol. *J Phys Chem A.* 2010;114:12462-9.

- [248] Ray DJ, Redfearn A, Waddington DJ. Gas-phase oxidation of alkenes: decomposition of hydroxy-substituted peroxy radicals. *J Chem Soc, Perkin Trans 2*. 1973;540-3.
- [249] Sarathy SM, Vranckx S, Yasunaga K, Mehl M, Oßwald P, Metcalfe WK, et al. A comprehensive chemical kinetic combustion model for the four butanol isomers. *Combust Flame*. 2012;159:2028-55.
- [250] Sarathy SM, Osswald P, Hansen N, Kohse-Hoinghaus K. Alcohol combustion chemistry. *Prog Energy Combust Sci*. 2014;44:40-102.
- [251] Zhou C-W, Simmie JM, Curran HJ. Rate constants for hydrogen abstraction by HO<sub>2</sub> from n-butanol. *Int J Chem Kinet*. 2012;44:155-64.
- [252] I. SM, J. WD. Reactions of Oxygenated Radicals in the Gas Phase. Part 12. The Reactions of Isopropylperoxy Radicals and Alkenes. *J Chem Soc Perkin Trans II*. 1983;2:139-43.
- [253] M. RDJ, J. WD. Gas Phase Oxidation of Alkenes-Part II. The Oxidation of 2-Methylbutene-2 and 2,3-Dimethylbutene-2. *Combust Flame*. 1973;21:327-34.
- [254] Welz O, Savee JD, Eskola AJ, Sheps L, Osborn DL, Taatjes CA. Low-temperature combustion chemistry of biofuels: Pathways in the low-temperature (550-700 K) oxidation chemistry of isobutanol and tert-butanol. *Proc Combust Inst*. 2013;34:493-500.
- [255] Welz O, Zador J, Savee JD, Ng MY, Meloni G, Fernandes RX, et al. Low-temperature combustion chemistry of biofuels: pathways in the initial low-temperature (550 K-750 K) oxidation chemistry of isopentanol. *Phys Chem Chem Phys*. 2012;14:3112-27.
- [256] Welz O, Zador J, Savee JD, Sheps L, Osborn DL, Taatjes CA. Low-Temperature Combustion Chemistry of n-Butanol: Principal Oxidation Pathways of Hydroxybutyl Radicals. *J Phys Chem A*. 2013;117:11983-2001.
- [257] Olivella S, Solé A. Unimolecular Decomposition of  $\beta$ -Hydroxyethylperoxy Radicals in the HO $\bullet$ -Initiated Oxidation of Ethene: A Theoretical Study. *J Phys Chem A*. 2004;108:11651-63.
- [258] Kuwata KT, Dibble TS, Sliz E, Petersen EB. Computational studies of intramolecular hydrogen atom transfers in the  $\beta$ -hydroxyethylperoxy and  $\beta$ -hydroxyethoxy radicals. *J Phys Chem A*. 2007;111:5032-42.
- [259] Lizardo-Huerta J, Sirjean B, Bounaceur R, Fournet R. Intramolecular effects on the kinetics of unimolecular reactions of  $\beta$ -HORO $\bullet$  and HOQ' OOH radicals. *Phys Chem Chem Phys*. 2016;18:12231-51.
- [260] CHEMKIN-PRO 15101, Reaction Design, San Diego, 2013.
- [261] Slagle IR, Park JY, Heaven MC, Gutman D. Kinetics of polyatomic free radicals produced by laser photolysis. 3. Reaction of vinyl radicals with molecular oxygen. *J Am Chem Soc*. 1984;106:4356-61.
- [262] Hanning-Lee MA, Green NJB, Pilling MJ, Robertson SH. Direct observation of equilibration in the system H + C<sub>2</sub>H<sub>4</sub> = C<sub>2</sub>H<sub>5</sub>: standard enthalpy of formation of the ethyl radical. *J Phys Chem*. 1993;97:860-70.
- [263] Brouard M, Lightfoot P, Pilling M. Observations of equilibration in the system H + C<sub>2</sub>H<sub>4</sub>  $\rightarrow$  C<sub>2</sub>H<sub>5</sub>. The determination of the heat of formation of C<sub>2</sub>H<sub>5</sub>. *J Phys Chem*. 1986;90:445-50.
- [264] Lightfoot PD, Pilling MJ. Temperature and pressure dependence of the rate constant for the addition of hydrogen atoms to ethylene. *J Phys Chem*. 1987;91:3373-9.
- [265] Kurylo MJ, Peterson NC, Braun W. Absolute rates of the reactions H + C<sub>2</sub>H<sub>4</sub> and H + C<sub>2</sub>H<sub>5</sub>. *J Chem Phys*. 1970;53:2776-83.
- [266] Michael J, Osborne D, Suess G. Reaction H + C<sub>2</sub>H<sub>4</sub>: Investigation into the effects of pressure, stoichiometry, and the nature of the third body species. *J Chem Phys*. 1973;58:2800-6.
- [267] Sugawara K-i, Okazaki K, Sato S. Temperature dependence of the rate constants of H and D-atom additions to C<sub>2</sub>H<sub>4</sub>, C<sub>2</sub>H<sub>3</sub>D, C<sub>2</sub>D<sub>4</sub>, C<sub>2</sub>H<sub>2</sub>, and C<sub>2</sub>D<sub>2</sub>. *Bull Chem Soc Jpn*. 1981;54:2872-7.
- [268] Lee J, Michael J, Payne W, Stief L. Absolute rate of the reaction of atomic hydrogen with ethylene from 198 to 320 K at high pressure. *J Chem Phys*. 1978;68:1817-20.
- [269] Bott J, Cohen N. A shock tube study of the reactions of the hydroxyl radical with several combustion species. *Int J Chem Kinet*. 1991;23:1075-94.
- [270] Smith GP. Laser pyrolysis studies of OH reaction rates with several butenes at 1200 K. *Int J Chem Kinet*. 1987;19:269-76.

- [271] Bradley J, Capey W, Fair R, Pritchard D. A shock - tube study of the kinetics of reaction of hydroxyl radicals with H<sub>2</sub>, CO, CH<sub>4</sub>, CF<sub>3</sub>H, C<sub>2</sub>H<sub>4</sub>, and C<sub>2</sub>H<sub>6</sub>. *Int J Chem Kinet.* 1976;8:549-61.
- [272] Baldwin RR, Simmons R, Walker R. Inhibition of the hydrogen+ oxygen reaction by ethylene. Part 2.—Discussion and evaluation of velocity constants. *Trans Faraday Soc.* 1966;62:2486-98.
- [273] Westenberg A, Fristrom R. H and O atom profiles measured by ESR in C<sub>2</sub> hydrocarbon-O<sub>2</sub> flames. *Symp (Int) Combust.* 1965;10:473-87.
- [274] Tully FP. Laser photolysis/laser-induced fluorescence study of the reaction of hydroxyl radical with ethylene. *Chem Phys Lett.* 1983;96:148-53.
- [275] Tully FP. Hydrogen-atom abstraction from alkenes by OH, ethene and 1-butene. *Chem Phys Lett.* 1988;143:510-4.
- [276] Liu AD, Mulac WA, Jonah CD. Pulse radiolysis study of the reaction of OH radicals with C<sub>2</sub>H<sub>4</sub> over the temperature range 343–1173 K. *Int J Chem Kinet.* 1987;19:25-34.
- [277] Liu A, Mulac WA, Jonah CD. Kinetic isotope effects in the gas-phase reaction of hydroxyl radicals with ethylene in the temperature range 343-1173 K and 1-atm pressure. *J Phys Chem.* 1988;92:3828-33.
- [278] Greiner N. Hydroxyl Radical Kinetics by Kinetic Spectroscopy. VII. The Reaction with Ethylene in the Range 300–500° K. *J Chem Phys.* 1970;53:1284-5.
- [279] Fulle D, Hamann H, Hippler H, Jansch C. The High Pressure Range of the Addition of OH to C<sub>2</sub>H<sub>2</sub> and C<sub>2</sub>H<sub>4</sub>. *Berichte der Bunsengesellschaft für physikalische Chemie.* 1997;101:1433-42.
- [280] Srinivasan N, Su M-C, Michael J. Reflected shock tube studies of high-temperature rate constants for OH + C<sub>2</sub>H<sub>2</sub> and OH + C<sub>2</sub>H<sub>4</sub>. *Phys Chem Chem Phys.* 2007;9:4155-63.
- [281] Diau EWG, Lee YP. Detailed rate coefficients and the enthalpy change of the equilibrium reaction OH+ C<sub>2</sub>H<sub>4</sub>= MHOC<sub>2</sub>H<sub>4</sub> over the temperature range 544–673 K. *J Chem Phys.* 1992;96:377-86.
- [282] Zellner R, Lorenz K. Laser photolysis/resonance fluorescence study of the rate constants for the reactions of hydroxyl radicals with ethene and propene. *J Phys Chem.* 1984;88:984-9.
- [283] Hoare D, Patel M. Role of OH and HO<sub>2</sub> radicals in the slow combustion of mixtures of methane, ethane and ethylene. *Trans Faraday Soc.* 1969;65:1325-33.
- [284] Avramenko L, Lorentso R. REAKTSII SVOBODNOGO GIDROKSILA S ALDEGIDAMI. DOKLADY AKADEMII NAUK SSSR. 1949;69:205-7.
- [285] Vasu SS, Hong Z, Davidson DF, Hanson RK, Golden DM. Shock Tube/Laser Absorption Measurements of the Reaction Rates of OH with Ethylene and Propene. *J Phys Chem A.* 2010;114:11529-37.
- [286] Senosiain JP, Klippenstein SJ, Miller JA. Reaction of ethylene with hydroxyl radicals: A theoretical study. *J Phys Chem A.* 2006;110:6960-70.
- [287] Khaled F, Giri BR, Farooq A. On the reaction of OH radicals with C<sub>2</sub> hydrocarbons. *Proc Combust Inst.* 2019;37:213-9.
- [288] Chen CJ, Bozzelli JW. Kinetic analysis for HO<sub>2</sub> addition to ethylene, propene, and isobutene, and thermochemical parameters of alkyl hydroperoxides and hydroperoxide alkyl radicals. *J Phys Chem A.* 2000;104:4997-5012.
- [289] Miller JA, Klippenstein SJ, Robertson SH. A theoretical analysis of the reaction between ethyl and molecular oxygen. *Proc Combust Inst.* 2000;28:1479-86.
- [290] Baldwin RR, Dean CE, Walker RW. *J Chem Soc, Faraday Trans 2.* 1986;82:1445.
- [291] Baldwin RR, Stout DR, Walker RW. *J Chem Soc, Faraday Trans.* 1991:2147.
- [292] DeSain JD, Klippenstein SJ, Miller JA, Taatjes CA. Measurements, theory, and modeling of OH formation in ethyl plus O<sub>2</sub> and propyl plus O<sub>2</sub> reactions. *J Phys Chem A.* 2003;107:4415-27.
- [293] Utsav KC, Beshir M, Farooq A. Simultaneous measurements of acetylene and soot during the pyrolysis of ethylene and benzene in a shock tube. *Proc Combust Inst.* 2017;36:833-40.
- [294] Georgievskii Y, Klippenstein SJ. Variable reaction coordinate transition state theory: Analytic results and application to the C<sub>2</sub>H<sub>3</sub>+H → C<sub>2</sub>H<sub>4</sub> reaction. *J Chem Phys.* 2003;118:5442-55.
- [295] Nguyen TL, Vereecken L, Hou XJ, Nguyen MT, Peeters J. Potential energy surfaces, product distributions and thermal rate coefficients of the reaction of O(P-3) with C<sub>2</sub>H<sub>4</sub>(X(1)A(g)): A comprehensive theoretical study. *J Phys Chem A.* 2005;109:7489-99.

- [296] Miyoshi A, Yoshida J, Shiki N, Koshi M, Matsui H. Product branching fractions for the reaction of O(P-3) with ethene. *Phys Chem Chem Phys*. 2009;11:7318-23.
- [297] Smalley JF, Nesbitt FL, Klemm RB. Branching Ratio for the Hydrogen Atom Product Channel in the Reaction of Ground-State Atomic Oxygen with Ethylene. *J Phys Chem*. 1986;90:491-7.
- [298] Morton ML, Szpunar DE, Butler LJ. Photodissociating methyl vinyl ether to calibrate O+ethylene product branching and to test propensity rules for product channel electronic accessibility. *J Chem Phys*. 2001;115:204-16.
- [299] Casavecchia P, Capozza G, Segoloni E, Leonori F, Balucani N, Volpi GG. Dynamics of the O(3P)+C<sub>2</sub>H<sub>4</sub> reaction: Identification of five primary product channels (vinoxy, acetyl, methyl, methylene, and ketene) and branching ratios by the crossed molecular beam technique with soft electron ionization. *J Phys Chem A*. 2005;109:3527-30.
- [300] Schmoltner AM, Chu PM, Brudzynski RJ, Lee YT. Crossed molecular beam study of the reaction O(3P)+C<sub>2</sub>H<sub>4</sub>. *J Chem Phys*. 1989;91:6926-36.
- [301] Fu B, Han Y-C, Bowman JM, Leonori F, Balucani N, Angelucci L, et al. Experimental and theoretical studies of the O(P-3)+C<sub>2</sub>H<sub>4</sub> reaction dynamics: Collision energy dependence of branching ratios and extent of intersystem crossing. *J Chem Phys*. 2012;137.
- [302] Balucani N, Leonori F, Casavecchia P, Fu BN, Bowman JM. Crossed Molecular Beams and Quasiclassical Trajectory Surface Hopping Studies of the Multichannel Nonadiabatic O(P-3) + Ethylene Reaction at High Collision Energy. *J Phys Chem A*. 2015;119:12498-511.
- [303] Miller JA, Klippenstein SJ. The H+C<sub>2</sub>H<sub>2</sub> (+M)reversible arrow C<sub>2</sub>H<sub>3</sub> (+M) and H+C<sub>2</sub>H<sub>2</sub> (+M)reversible arrow C<sub>2</sub>H<sub>5</sub> (+M) reactions: Electronic structure, variational transition-state theory, and solutions to a two-dimensional master equation. *Phys Chem Chem Phys*. 2004;6:1192-202.
- [304] Knyazev VD, Slagle IR. Experimental and Theoretical Study of the C<sub>2</sub>H<sub>3</sub> ⇌ H + C<sub>2</sub>H<sub>2</sub> Reaction. Tunneling and the Shape of Falloff Curves. *J Phys Chem*. 1996;100:16899-911.
- [305] Y. Feng, J. T. Niiranen, Á. Bencsura, V. D. Knyazev, D. Gutman, Tseng W. Weak Collision Effects in the Reaction C<sub>2</sub>H<sub>5</sub> ⇌ C<sub>2</sub>H<sub>4</sub> + H. *J Phys Chem*. 1993;97:871-80.
- [306] Yang XL, Tranter RS. High-temperature dissociation of ethyl radicals and ethyl iodide. *Int J Chem Kinet*. 2012;44:433-43.
- [307] Wang H, Xu R, Wang K, Bowman CT, Hanson RK, Davidson DF, et al. A physics-based approach to modeling real-fuel combustion chemistry - I. Evidence from experiments, and thermodynamic, chemical kinetic and statistical considerations. *Combust Flame*. 2018;193:502-19.
- [308] Wang K, Villano SM, Dean AM. Fundamentally-based kinetic model for propene pyrolysis. *Combust Flame*. 2015;162:4456-70.
- [309] Ye LL, Georgievskii Y, Klippenstein SJ. Pressure-dependent branching in the reaction of <sup>1</sup>CH<sub>2</sub> with C<sub>2</sub>H<sub>4</sub> and other reactions on the C<sub>3</sub>H<sub>6</sub> potential energy surface. *Proc Combust Inst*. 2015;35:223-30.
- [310] Hung W-C, Tsai C-Y, Matsui H, Wang N-S, Miyoshi A. Experimental and Theoretical Study on the Thermal Decomposition of C<sub>3</sub>H<sub>6</sub> (Propene). *J Phys Chem A*. 2015;119:1229-37.
- [311] Szori M, Fittschen C, Csizmadia IG, Viskolcz B. Allylic H-abstraction mechanism: The potential energy surface of the reaction of propene with OH radical. *J Chem Theory Comput*. 2006;2:1575-86.
- [312] Díaz-Acosta I, Alvarez-Idaboy JR, Vivier-Bunge A. Mechanism of the OH-propene-O<sub>2</sub> reaction: An ab initio study. *Int J Chem Kinet*. 1999;31:29-36.
- [313] Alvarez-Idaboy JR, Díaz-Acosta I, Vivier-Bunge A. Energetics of mechanism of OH-propene reaction at low pressures in inert atmosphere. *J Comput Chem*. 1998;19:811-9.
- [314] Huynh LK, Zhang HR, Zhang S, Eddings E, Sarofim A, Law ME, et al. Kinetics of Enol Formation from Reaction of OH with Propene. *J Phys Chem A*. 2009;113:3177-85.
- [315] El-Nahas AM, Uchimaru T, Sugie M, Tokuhashi K, Sekiya A. Relative reactivity and regioselectivity of halogen-substituted ethenes and propene toward addition of an OH radical or O (P-3) atom: An ab initio study. *J Mol Struct: THEOCHEM*. 2006;770:59-65.
- [316] Izsák R, Szőri M, Knowles PJ, Viskolcz B. High Accuracy ab Initio Calculations on Reactions of OH with 1-Alkenes. The Case of Propene. *J Chem Theory Comput*. 2009;5:2313-21.

- [317] Miller JA, Klippenstein SJ. Dissociation of Propyl Radicals and Other Reactions on a  $C_3H_7$  Potential. *J Phys Chem A*. 2013;117:2718-27.
- [318] Fridlyand A, Lynch PT, Tranter RS, Brezinsky K. Single Pulse Shock Tube Study of Allyl Radical Recombination. *J Phys Chem A*. 2013;117:4762-76.
- [319] Lynch PT, Annesley CJ, Aul CJ, Yang X, Tranter RS. Recombination of allyl radicals in the high temperature fall-off regime. *J Phys Chem A*. 2013;117:4750-61.
- [320] Georgievskii Y, Miller JA, Klippenstein SJ. Association rate constants for reactions between resonance-stabilized radicals:  $C_3H_3+C_3H_3$ ,  $C_3H_3+C_3H_5$ , and  $C_3H_5+C_3H_5$ . *Phys Chem Chem Phys*. 2007;9:4259-68.
- [321] Xu R, Wang K, Banerjee S, Shao J, Parise T, Zhu Y, et al. A physics-based approach to modeling real-fuel combustion chemistry - II. Reaction kinetic models of jet and rocket fuels. *Combust Flame*. 2018;193:520-37.
- [322] Held T. The oxidation of methanol, isobutene and methyl tertiary-butyl ether. PhD Thesis, Department of Mechanical and Aerospace Engineering, Princeton University. 1993.
- [323] Tsang W, Hampson RF. Chemical Kinetic Data Base for Combustion Chemistry. Part I. Methane and Related Compounds. *J Phys Chem Ref Data*. 1986;15:1087-279.
- [324] Sun HY, Law CK. Kinetics of Hydrogen Abstraction Reactions of Butene Isomers by OH Radical. *J Phys Chem A*. 2010;114:12088-98.
- [325] Vasu SS, Huynh LK, Davidson DF, Hanson RK, Golden DM. Reactions of OH with Butene Isomers: Measurements of the Overall Rates and a Theoretical Study. *J Phys Chem A*. 2011;115:2549-56.
- [326] Chen CJ, Bozzelli JW. Thermochemical property, pathway and kinetic analysis on the reactions of allylic isobutenyl radical with O-2: an elementary reaction mechanism for isobutene oxidation. *J Phys Chem A*. 2000;104:9715-32.
- [327] Martin JML. Ab initio total atomization energies of small molecules - Towards the basis set limit. *Chem Phys Lett*. 1996;259:669-78.
- [328] Feller D, Dixon DA. Extended benchmark studies of coupled cluster theory through triple excitations. *J Chem Phys*. 2001;115:3484-96.
- [329] Miyoshi A. Systematic Computational Study on the Unimolecular Reactions of Alkylperoxy (RO<sub>2</sub>), Hydroperoxyalkyl (QOOH), and Hydroperoxyalkylperoxy (O<sub>2</sub>QOOH) Radicals. *J Phys Chem A*. 2011;115:3301-25.
- [330] Villano SM, Carstensen HH, Dean AM. Rate Rules, Branching Ratios, and Pressure Dependence of the HO<sub>2</sub> + Olefin Addition Channels. *J Phys Chem A*. 2013;117:6458-73.
- [331] Sharma S, Raman S, Green WH. Intramolecular Hydrogen Migration in Alkylperoxy and Hydroperoxyalkylperoxy Radicals: Accurate Treatment of Hindered Rotors. *J Phys Chem A*. 2010;114:5689-701.
- [332] Villano SM, Huynh LK, Carstensen HH, Dean AM. High-Pressure Rate Rules for Alkyl + O-2 Reactions. 1. The Dissociation, Concerted Elimination, and Isomerization Channels of the Alkyl Peroxy Radical. *J Phys Chem A*. 2011;115:13425-42.
- [333] Villano SM, Huynh LK, Carstensen HH, Dean AM. High-Pressure Rate Rules for Alkyl + O-2 Reactions. 2. The Isomerization, Cyclic Ether Formation, and beta-Scission Reactions of Hydroperoxy Alkyl Radicals. *J Phys Chem A*. 2012;116:5068-89.
- [334] Miyoshi A. Molecular size dependent falloff rate constants for the recombination reactions of alkyl radicals with O<sub>2</sub> and implications for simplified kinetics of alkylperoxy radicals. *Int J Chem Kinet*. 2012;44:59-74.
- [335] Somers KP, Simmie JM, Gillespie F, Conroy C, Black G, Metcalfe WK, et al. A comprehensive experimental and detailed chemical kinetic modelling study of 2,5-dimethylfuran pyrolysis and oxidation. *Combust Flame*. 2013;160:2291-318.
- [336] Bugler J, Marks B, Mathieu O, Archuleta R, Camou A, Gregoire C, et al. An ignition delay time and chemical kinetic modeling study of the pentane isomers. *Combust Flame*. 2016;163:138-56.
- [337] Wang WJ, Gowdagiri S, Oehlschlaeger MA. Comparative Study of the Autoignition of Methyl Decenoates, Unsaturated Biodiesel Fuel Surrogates. *Energy Fuels*. 2013;27:5527-32.

- [338] Zhang Y, Yang Y, Boehman AL. Premixed ignition behavior of C-9 fatty acid esters: A motored engine study. *Combust Flame*. 2009;156:1202-13.
- [339] Curran HJ, Gaffuri P, Pitz WJ, Westbrook CK. A Comprehensive Modeling Study of n-Heptane Oxidation. *Combust Flame*. 1998;114:149-77.
- [340] Westbrook CK, Pitz WJ, Sarathy SM, Mehl M. Detailed chemical kinetic modeling of the effects of C=C double bonds on the ignition of biodiesel fuels. *Proc Combust Inst*. 2013;34:3049-56.
- [341] Senosiain JP, Miller JA. The reaction of n- and i-C<sub>4</sub>H<sub>5</sub> radicals with acetylene. *J Phys Chem A*. 2007;111:3740-7.
- [342] Goldsmith CF, Magoon GR, Green WH. Database of Small Molecule Thermochemistry for Combustion. *J Phys Chem A*. 2012;116:9033-57.
- [343] Zhao Y, Truhlar DG. The M06 suite of density functionals for main group thermochemistry, thermochemical kinetics, noncovalent interactions, excited states, and transition elements: two new functionals and systematic testing of four M06-class functionals and 12 other functionals. *Theor Chem Acc*. 2008;120:215-41.
- [344] Kiefer JH, Wei HC, Kern RD, Wu CH. The High Temperature Pyrolysis of 1,3-Butadiene: Heat of Formation and Rate of Dissociation of Vinyl Radical. *Int J Chem Kinet*. 1985;17:225-53.
- [345] Rao VS, Takeda K, Skinner GB. Formation of H and D Atoms in Pyrolysis of 1,3-Butadiene and 1,3-Butadiene-1,1,4,4-d<sub>4</sub> behind Shock Waves. *Int J Chem Kinet*. 1988;20:153.
- [346] Lockhart JPA, Goldsmith CF, Randazzo JB, Ruscic B, Tranter RS. An Experimental and Theoretical Study of the Thermal Decomposition of C<sub>4</sub>H<sub>6</sub> Isomers. *J Phys Chem A*. 2017;121:3827-50.
- [347] Miller JL. Theoretical study of the straight-chain C<sub>4</sub>H<sub>7</sub> radical isomers and their dissociation and isomerization transition states. *J Phys Chem A*. 2004;108:2268-77.
- [348] Miyoshi A. Computational Studies on the Reactions of 3-Butenyl and 3-Butenylperoxy Radicals. *Int J Chem Kinet*. 2010;42:273-88.
- [349] Xu C, Al Shoaibi AS, Wang C, Carstensen H-H, Deant AM. Kinetic Modeling of Ethane Pyrolysis at High Conversion. *J Phys Chem A*. 2011;115:10470-90.
- [350] Huang C, Yang B, Zhang F. Pressure-dependent kinetics on the C<sub>4</sub>H<sub>7</sub> potential energy surface and its effect on combustion model predictions. *Combust Flame*. 2017;181:100-9.
- [351] Shestov AA, Popov KV, Slagle IR, Knyazev VD. Kinetics of the reaction between vinyl radical and ethylene. *Chem Phys Lett*. 2005;408:339-43.
- [352] Ismail H, Goldsmith CF, Abel PR, Howe P-T, Fahr A, Halpern JB, et al. Pressure and temperature dependence of the reaction of vinyl radical with Ethylene. *J Phys Chem A*. 2007;111:6843-51.
- [353] Fahr A, Stein SE. Reactions of Vinyl and Phenyl Radicals with Ethyne, Ethene and Benzene. *Symp (Int) Combust, [Proc]*. 1989;22:1022-9.
- [354] Li Y, Klippenstein SJ, Zhou CW, Curran HJ. Theoretical Kinetics Analysis for H Atom Addition to 1,3-Butadiene and Related Reactions on the C<sub>4</sub>H<sub>7</sub> Potential Energy Surface. *J Phys Chem A*. 2017;121:7433-45.
- [355] Vasu SS, Zador J, Davidson DF, Hanson RK, Golden DM, Miller JA. High-Temperature Measurements and a Theoretical Study of the Reaction of OH with 1,3-Butadiene. *J Phys Chem A*. 2010;114:8312-8.
- [356] Slagle IR, Bencsura Á, Xing S-B, Gutman D. Kinetics and thermochemistry of the oxidation of unsaturated radicals: C<sub>4</sub>H<sub>5</sub>+O<sub>2</sub>. *Symp (Int) Combust*. 1992;24:653-60.
- [357] Dagaut P, Cathonnet M. A Comparative Study of the Kinetics of Benzene Formation from Unsaturated C<sub>2</sub> to C<sub>4</sub> Hydrocarbons. *Combust Flame*. 1998;113:620-3.
- [358] Moskaleva LV, Lin M-C. Unimolecular isomerization/decomposition of cyclopentadienyl and related bimolecular reverse process: ab initio MO/statistical theory study. *J Comput Chem*. 2000;21:415-25.
- [359] da Silva G. Mystery of 1-vinylpropargyl formation from acetylene addition to the propargyl radical: an open-and-shut case. *J Phys Chem A*. 2017;121:2086-95.
- [360] Shapero M, Ramphal IA, Neumark DM. Photodissociation of the Cyclopentadienyl Radical at 248 nm. *J Phys Chem A*. 2018;122:4265-72.

- [361] Wang Y, Park S, Sarathy SM, Chung SH. A comparative study on the sooting tendencies of various 1-alkene fuels in counterflow diffusion flames. *Combust Flame*. 2018;192:71-85.
- [362] Selvaraj P, Arias PG, Lee BJ, Im HG, Wang Y, Gao Y, et al. A computational study of ethylene-air sooting flames: Effects of large polycyclic aromatic hydrocarbons. *Combust Flame*. 2016;163:427-36.
- [363] Darcy D, Nakamura H, Tobin CJ, Mehl M, Metcalfe WK, Pitz WJ, et al. A high-pressure rapid compression machine study of n-propylbenzene ignition. *Combust Flame*. 2014;161:65-74.
- [364] Raj A, Prada IDC, Amer AA, Chung SH. A reaction mechanism for gasoline surrogate fuels for large polycyclic aromatic hydrocarbons. *Combust Flame*. 2012;159:500-15.
- [365] Wang Y, Raj A, Chung SH. A PAH growth mechanism and synergistic effect on PAH formation in counterflow diffusion flames. *Combust Flame*. 2013;160:1667-76.
- [366] Mehl M, Pitz WJ, Westbrook CK, Curran HJ. Kinetic modeling of gasoline surrogate components and mixtures under engine conditions. *Proc Combust Inst*. 2011;33:193-200.
- [367] Raj A, Al Rashidi MJ, Chung SH, Sarathy SM. PAH growth initiated by propargyl addition: mechanism development and computational kinetics. *J Phys Chem A*. 2014;118:2865-85.
- [368] Wang H, Frenklach M. A detailed kinetic modeling study of aromatics formation in laminar premixed acetylene and ethylene flames. *Combust Flame*. 1997;110:173-221.
- [369] Frenklach M. Reaction mechanism of soot formation in flames. *Phys Chem Chem Phys*. 2002;4:2028-37.
- [370] Moskaleva L, Mebel A, Lin M. The CH<sub>3</sub>+ C<sub>5</sub>H<sub>5</sub> reaction: A potential source of benene at high temperatures. *Symp (Int) Combust*. 1996;26:521-6.
- [371] Sharma S, Green WH. Computed rate coefficients and product yields for c-C<sub>5</sub>H<sub>5</sub>+ CH<sub>3</sub>→ products. *J Phys Chem A*. 2009;113:8871-82.
- [372] Jasper AW, Hansen N. Hydrogen-assisted isomerizations of fulvene to benzene and of larger cyclic aromatic hydrocarbons. *Proc Combust Inst*. 2013;34:279-87.
- [373] Krasnoukhov VS, Porfiriev DP, Zavershinskiy IP, Azyazov VN, Mebel AM. Kinetics of the CH<sub>3</sub>+ C<sub>5</sub>H<sub>5</sub> Reaction: A Theoretical Study. *J Phys Chem A*. 2017;121:9191-200.
- [374] Hwang J, Lee W, Kang H, Chung S. Synergistic effect of ethylene-propane mixture on soot formation in laminar diffusion flames. *Combust Flame*. 1998;114:370-80.
- [375] Yoon S, Lee S, Chung S. Effect of mixing methane, ethane, propane, and propene on the synergistic effect of PAH and soot formation in ethylene-base counterflow diffusion flames. *Proc Combust Inst*. 2005;30:1417-24.
- [376] Ruwe L, Moshhammer K, Hansen N, Kohse-Höinghaus K. Consumption and hydrocarbon growth processes in a 2-methyl-2-butene flame. *Combust Flame*. 2017;175:34-46.
- [377] Ruwe L, Moshhammer K, Hansen N, Kohse-Höinghaus K. Influences of the molecular fuel structure on combustion reactions towards soot precursors in selected alkane and alkene flames. *Phys Chem Chem Phys*. 2018;20:10780-95.
- [378] Ruwe L, Cai L, Moshhammer K, Hansen N, Pitsch H, Kohse-Höinghaus K. The C<sub>5</sub> chemistry preceding the formation of polycyclic aromatic hydrocarbons in a premixed 1-pentene flame. *Combust Flame*. 2019;206:411-23.
- [379] Wang H, Dames E, Sirjean B, Sheen DA, Tango R, Violi A, et al. A high-temperature chemical kinetic model of n-alkane (up to n-dodecane), cyclohexane, and methyl-, ethyl-, n-propyl and n-butyl-cyclohexane oxidation at high temperatures, JetSurF version 2.0, <http://web.stanford.edu/group/haiwanglab/JetSurF/JetSurF2.0/index.html>; 2010 [accessed 20.05.16].
- [380] Healy D, Kalitan D, Aul C, Petersen E, Bourque G, Curran H. Oxidation of C<sub>1</sub>- C<sub>5</sub> alkane quaternary natural gas mixtures at high pressures. *Energy Fuels*. 2010;24:1521-8.
- [381] Narayanaswamy K, Blanquart G, Pitsch H. A consistent chemical mechanism for oxidation of substituted aromatic species. *Combust Flame*. 2010;157:1879-98.
- [382] Blanquart G, Pepiot-Desjardins P, Pitsch H. Chemical mechanism for high temperature combustion of engine relevant fuels with emphasis on soot precursors. *Combust Flame*. 2009;156:588-607.
- [383] Zhang D, Hou L, Gao M, Zhang X. Experiment and Modeling on Thermal Cracking of n-Dodecane at Supercritical Pressure. *Energy Fuels*. 2018;32:12426-34.

- [384] Zhao L, Yang T, Kaiser RI, Troy TP, Ahmed M, Belisario-Lara D, et al. Combined Experimental and Computational Study on the Unimolecular Decomposition of JP-8 Jet Fuel Surrogates. I. n-Decane (n-C<sub>10</sub>H<sub>22</sub>). *J Phys Chem A*. 2017;121:1261-80.
- [385] Zhao L, Yang T, Kaiser RI, Troy TP, Ahmed M, Ribeiro JM, et al. Combined Experimental and Computational Study on the Unimolecular Decomposition of JP-8 Jet Fuel Surrogates. II: n-Dodecane (n-C<sub>12</sub>H<sub>26</sub>). *J Phys Chem A*. 2017;121:1281-97.
- [386] Kalpathy SV, Poddar NB, Bagley SP, Wornat MJ. Reaction pathways for the growth of polycyclic aromatic hydrocarbons during the supercritical pyrolysis of n-decane, as determined from doping experiments with 1-and 2-methylnaphthalene. *Proc Combust Inst*. 2015;35:1833-41.
- [387] Hurst EA, Poddar NB, Vutukuru K, Kalpathy SV, Wornat MJ. Polycyclic aromatic hydrocarbons formation and growth during the supercritical pyrolysis of 1-octene. *Proc Combust Inst*. 2019;37:1107-15.
- [388] Kalpathy SV, Poddar NB, Hurst EA, Caspary EC, Wornat MJ. Growth reactions of polycyclic aromatic hydrocarbons during the supercritical pyrolysis of n-decane, as determined from doping experiments with 1-methylphenanthrene and fluorene. *Proc Combust Inst*. 2017;36:965-73.
- [389] Van Speybroeck V, Hemelsoet K, Minner B, Marin GB, Waroquier M. Modeling elementary reactions in coke formation from first principles. *Mol Simul*. 2007;33:879-87.
- [390] Tokmakov I, Lin M. Combined quantum chemical/RRKM-ME computational study of the phenyl+ethylene, vinyl+ benzene, and H+ styrene reactions. *J Phys Chem A*. 2004;108:9697-714.
- [391] Belisario-Lara D, Mebel AM, Kaiser RI. Computational Study on the Unimolecular Decomposition of JP-8 Jet Fuel Surrogates III: Butylbenzene Isomers (n-, s-, and t-C<sub>14</sub>H<sub>10</sub>). *J Phys Chem A*. 2018;122:3980-4001.
- [392] Sebree JA, Kislov VV, Mebel AM, Zwier TS. Spectroscopic and Thermochemical Consequences of site-specific H-atom addition to Naphthalene. *J Phys Chem A*. 2010;114:6255-62.
- [393] Sebree JA, Kislov VV, Mebel AM, Zwier TS. Isomer specific spectroscopy of C<sub>10</sub>H<sub>n</sub>, n= 8–12: Exploring pathways to naphthalene in Titan's atmosphere. *Faraday Discuss*. 2010;147:231-49.
- [394] Mebel AM, Georgievskii Y, Jasper AW, Klippenstein SJ. Temperature- and pressure-dependent rate coefficients for the HACA pathways from benzene to naphthalene. *Proc Combust Inst*. 2017;36:919-26.
- [395] Fahr A, Mallard W, Stein S. *Symp (Int) Combust*. 1986:825.
- [396] Fahr A, Stein S. *Symp (Int) Combust*. 1988:1023.
- [397] Yu T, Lin M. Kinetics of the phenyl radical reaction with ethylene: An RRKM theoretical analysis of low and high temperature data. *Combust Flame*. 1995;100:169-76.
- [398] Heckmann E, Hippler H, Troe J. High-temperature reactions and thermodynamic properties of phenyl radicals. *Symp (Int) Combust*. 1996;26:543-50.
- [399] Shukla B, Koshi M. A novel route for PAH growth in HACA based mechanisms. *Combust Flame*. 2012;159:3589-96.
- [400] Chang AH, Mebel A, Yang X-M, Lin S, Lee Y. Ab initio/RRKM approach toward the understanding of ethylene photodissociation. *J Chem Phys*. 1998;109:2748-61.
- [401] Kaiser R, Parker D, Goswami M, Zhang F, Kislov V, Mebel A, et al. Crossed beam reaction of phenyl and D5-phenyl radicals with propene and deuterated counterparts—competing atomic hydrogen and methyl loss pathways. *Phys Chem Chem Phys*. 2012;14:720-9.
- [402] Zhang F, Gu X, Guo Y, Kaiser RI. Reaction dynamics of phenyl radicals (C<sub>6</sub>H<sub>5</sub>) with propylene (CH<sub>3</sub>CHCH<sub>2</sub>) and its deuterated isotopologues. *J Phys Chem A*. 2008;112:3284-90.
- [403] Albert DR, Todt MA, Davis HF. Crossed molecular beams studies of phenyl radical reactions with propene and trans-2-butene. *J Phys Chem A*. 2013;117:13967-75.
- [404] Kislov V, Mebel A, Aguilera-Iparraguirre J, Green WH. Reaction of phenyl radical with propylene as a possible source of indene and other polycyclic aromatic hydrocarbons: An ab initio/RRKM-ME study. *J Phys Chem A*. 2012;116:4176-91.
- [405] Zhang F, Kaiser RI, Golan A, Ahmed M, Hansen N. A VUV photoionization study of the combustion-relevant reaction of the phenyl radical (C<sub>6</sub>H<sub>5</sub>) with propylene (C<sub>3</sub>H<sub>6</sub>) in a high temperature chemical reactor. *J Phys Chem A*. 2012;116:3541-6.

- [406] Buras ZJ, Chu T-C, Jamal A, Yee NW, Middaugh JE, Green WH. Phenyl radical+ propene: a prototypical reaction surface for aromatic-catalyzed 1, 2-hydrogen-migration and subsequent resonance-stabilized radical formation. *Phys Chem Chem Phys*. 2018;20:13191-214.
- [407] Mebel AM, Georgievskii Y, Jasper AW, Klippenstein SJ. Pressure-dependent rate constants for PAH growth: formation of indene and its conversion to naphthalene. *Faraday Discuss*. 2017;195:637-70.
- [408] Kaiser RI, Parker DS, Zhang F, Landera A, Kislov VV, Mebel AM. PAH formation under single collision conditions: reaction of phenyl radical and 1,3-butadiene to form 1,4-dihydronaphthalene. *J Phys Chem A*. 2012;116:4248-58.
- [409] Golan A, Ahmed M, Mebel AM, Kaiser RI. A VUV photoionization study of the multichannel reaction of phenyl radicals with 1, 3-butadiene under combustion relevant conditions. *Phys Chem Chem Phys*. 2013;15:341-7.
- [410] Thomas AM, Lucas M, Yang T, Kaiser RI, Fuentes L, Belisario - Lara D, et al. A Free - Radical Pathway to Hydrogenated Phenanthrene in Molecular Clouds—Low Temperature Growth of Polycyclic Aromatic Hydrocarbons. *Chem PhysChem*. 2017;18:1971-6.
- [411] Leung KM, Lindstedt RP, Jones W. A simplified reaction mechanism for soot formation in nonpremixed flames. *Combust Flame*. 1991;87:289-305.